

Politecnico di Torino

Politecnico di Torino

Master's Degree in Aerospace Engineering

Thermal Analysis and Preliminary Thermal Control System Design for a Rechargeable Lunar Mini Rover

Supervisor:
Prof. Paolo Maggiore

Co-supervisor:
Ing. Enrico Sacchi

Candidate
Fabrizio Letterio Cartella

Academic Year 2025–2026

Abstract

This thesis presents the thermal analysis and preliminary thermal-control-system design of a rechargeable mini rover operating on the lunar surface. The study addresses the main thermal challenges associated with lunar surface operations, including the absence of atmospheric convection, the large variation of surface temperature with illumination and latitude, the radiative interaction with the lunar regolith, and the limited thermal inertia and heat-rejection capability of a compact robotic platform.
A transient numerical model is developed using Thermal Desktop, RadCAD and SINDA/FLUINT. The lunar surface is represented through a layered regolith model with temperature-dependent thermo-physical properties in order to reproduce the variation of the thermal environment with latitude and illumination conditions. The rover is represented by a simplified protected internal compartment surrounded by an MLI-like insulating shell and subjected to distributed internal heat dissipation. Conductive and radiative heat-transfer paths between the rover, the radiator, the wheels and the lunar surface are progressively included in the thermal model.
The parametric analyses show that insulation alone cannot simultaneously provide sufficient heat retention in cold conditions and heat rejection at higher internal power levels. A dedicated radiator is therefore introduced, and the results indicate the need for a variable thermal connection between the protected internal region and the heat-rejection surface. This behaviour is represented at preliminary level by the equivalent action of a Loop Heat Pipe combined with a Thermal Control Valve.
The influence of the wheel–hub–body and wheel–regolith conductive paths is also investigated. The results show that ground contact can become a significant heat-loss path during cold conditions. A combined thermal and structural trade-off is therefore performed to investigate an alternative support strategy based on low-conductance deployable rods, leading to the selection of a hollow Ti-6Al-4V configuration.
For the analysed high-latitude cases at 70°, 80° and 85°, the proposed preliminary architecture maintains the internal rover temperature within the adopted system-level design range of 253.15–323.15 K for the considered heat-load combinations. The work demonstrates that the thermal behaviour of a compact lunar rover is governed by the combined interaction of the lunar environment, insulation, internal power dissipation, radiator coupling and conductive contact with the regolith. The thesis therefore provides a consistent preliminary thermal-analysis framework and identifies the principal design parameters that should be refined during the subsequent development of a rechargeable lunar mini rover.

Contents

1 Introduction **7**
- 1.1 Motivation . . . 8
- 1.2 Scope of the Work . . . 9

2 Lunar Exploration Context **11**
- 2.1 The Moon as a Strategic Exploration Target . . . 11
- 2.2 NASA Moon Base and Distributed Robotic Mobility . . . 12
- 2.3 Lava Tubes and Lunar Pits . . . 13
- 2.4 Mare Tranquillitatis and Marius Hills . . . 14
- 2.5 The Lunar South Pole . . . 15
- 2.6 Thermal Implications of Lunar Locations . . . 16

3 Mini Rover Mission and System Overview **18**
- 3.1 Mission Concept . . . 18
- 3.2 Mission Objectives . . . 19
- 3.3 Concept of Operations . . . 20
- 3.4 Main Subsystems . . . 21
  - 3.4.1 Mobility System . . . 21
  - 3.4.2 Guidance, Navigation and Control . . . 21
  - 3.4.3 Communication System . . . 22
  - 3.4.4 Electrical Power System and Recharge Interface . . . 22
  - 3.4.5 Structure and Payload . . . 22
  - 3.4.6 Thermal Control Elements . . . 23
- 3.5 Thermal Requirements . . . 23

4 State of the Art of Thermal Control Systems for Small Spacecraft and Lunar Mini Rovers **25**
- 4.1 Role of the Thermal Control System . . . 25
- 4.2 Passive Thermal Control . . . 26
  - 4.2.1 Coatings, Paints and Surface Finishes . . . 26
  - 4.2.2 Multi-Layer Insulation . . . 27
  - 4.2.3 Thermal Straps and Conductive Path Management . . . 27
  - 4.2.4 Radiators . . . 28
  - 4.2.5 Heat Pipes, Loop Heat Pipes and Phase-Change Devices . . . 29
- 4.3 Adaptive and Active Thermal Control . . . 30
  - 4.3.1 Heaters . . . 30
  - 4.3.2 Louvers and Variable-Emittance Devices . . . 31

4.3.3 Thermal Switches and Variable Conductance Links 32
4.3.4 Fluid Loops 32
4.4 TCS Selection Criteria 33
4.5 Chapter Summary 34

5 Thermal Analysis **35**
5.1 Purpose and Scope of the Chapter 35
5.2 Thermal Control as an Iterative Spacecraft Design Process 36
5.3 Thermal Requirements, Temperature Definitions and Margins 37
5.4 ECSS-Oriented Thermal Modelling Process 38
5.4.1 Conduction 40
5.4.2 Contact Conduction 42
5.4.3 Convection 42
5.4.4 Radiation 43
5.5 Thermo-Optical Properties and Semi-Grey Modelling 45
5.6 View Factors, Grey-Body Exchange and Radiative Coupling 46
5.7 General Nodal Heat Balance 47
5.8 Thermal Mathematical Networks 47
5.8.1 Linear Conductors 48
5.8.2 Radiation Conductors 49
5.9 Types of Thermal Analysis 49
5.9.1 Steady-State Analysis 49
5.9.2 Transient Analysis 50
5.9.3 Hot and Cold Cases 50
5.9.4 Sensitivity Analysis 50
5.10 Numerical Methods for Thermal Analysis 51
5.10.1 Finite Difference Method 51
5.10.2 Explicit, Implicit and Crank–Nicolson Schemes 52
5.10.3 Numerical Errors in FDM 53
5.10.4 Finite Element Method 54
5.10.5 Comparison Between FDM and FEM 55
5.11 Chapter Summary 55

6 Thermal Model and Thermal Desktop **57**
6.1 Geometrical Mathematical Model and Thermal Mathematical Model . 57
6.1.1 Geometrical Mathematical Model 57
6.1.2 Thermal Mathematical Model 58
6.2 Integrated Thermal Analysis Codes 58
6.3 Thermal Desktop 59
6.4 SINDA/FLUINT 60
6.5 RadCAD and Radiation Analysis 60
6.6 Modelling Thermal Conduction in Thermal Desktop 61
6.7 Modelling Thermal Radiation in Thermal Desktop 61
6.8 RadK and Radiation Conductors 62
6.9 Heating Rate Functions 63
6.10 Monte Carlo Ray Tracing 63
6.11 Thermal Desktop Workflow Applied to a Lunar Rover 64

6.11.1 Definition of Environment and Mission Cases 64
6.11.2 Construction of the Lunar Surface Model 64
6.11.3 Rover Geometry and Nodalisation 65
6.11.4 Assignment of Material and Optical Properties 65
6.11.5 Definition of Conductors and Contactors 65
6.11.6 Internal Heat Loads 65
6.11.7 Radiation Analysis and Thermal Solution 66
6.12 Thermal Analysis of a Latitude-Parametric Lunar Rover Environment 66
6.13 Verification, Validation and Correlation 67
6.14 Practical Modelling Assumptions and Limitations 67
6.15 Summary Tables for Numerical Thermal Modelling 68
6.16 Implementation Considerations for the Thermal Model 69
6.16.1 Choice of Node Size 70
6.16.2 Boundary Nodes and Sink Temperatures 70
6.16.3 Internal Dissipation Modelling 70
6.16.4 Radiation Case Convergence 70
6.16.5 Interpretation of Results 71
6.17 Physical Interpretation for Lunar Applications 71
6.18 Model Verification Checks 71
6.19 Thermal Network Formulation 72
6.19.1 Criteria for Node Size, Position and Shape 73
6.19.2 Conductors in the Thermal Network 73
6.19.3 Radiation-Conductor Linearisation 74
6.20 Grey-Diffuse and Monte Carlo Radiation Methods 74
6.20.1 Grey-Diffuse View-Factor Method 75
6.20.2 Monte Carlo Ray-Tracing Method 75
6.21 Thermal Desktop Modelling Procedure 76
6.21.1 Geometry Creation 76
6.21.2 Nodalisation and Submodels 76
6.21.3 Material Properties 76
6.21.4 Optical Properties 76
6.21.5 Conductive Interfaces 77
6.21.6 Radiation Cases 77
6.21.7 SINDA/FLUINT Solution Settings 77
6.21.8 Post-Processing 77
6.22 Thermal Design Consequences for the Rechargeable Rover 77
6.23 Validation Logic for the Latitude-Parametric Lunar Surface Model . . 78
6.24 Chapter Summary 78

7 Lunar Thermal Environment **80**
7.1 Introduction 80
7.2 Mission Thermal Environments 81
7.3 Ground Environment 83
7.4 Launch Environment 83
7.5 General Space Radiative Environment 84
7.6 Direct Solar Radiation 84

7.7 Albedo Radiation . . . 86
7.8 Planetary and Lunar Infrared Radiation . . . 86
7.9 Earth On-Orbit Environment . . . 87
7.10 Lunar Transfer Environment . . . 87
7.11 Lunar Orbit and Descent Environment . . . 88
7.11.1 Direct Solar Radiation at the Moon . . . 88
7.11.2 Lunar Albedo . . . 88
7.11.3 Lunar Infrared Radiation . . . 89
7.11.4 Comments on Lunar Orbit and Descent . . . 89
7.12 Lunar Surface Thermal Environment . . . 90
7.13 Heat Sources and Sinks on the Lunar Surface . . . 91
7.14 Lunar Orbital Features Relevant to the Thermal Environment . . . 92
7.14.1 Orbital Parameters and Motion . . . 92
7.14.2 Precession and Perturbations . . . 93
7.14.3 Effects on Mission Design . . . 93
7.15 Apollo 17 Landing Site as Thermal Reference . . . 94
7.16 Lunar South Pole Thermal Environment . . . 94
7.16.1 Topography and Illumination . . . 95
7.16.2 Temperature Conditions . . . 95
7.16.3 Cold Traps and Volatiles . . . 96
7.16.4 South Pole Mission Implications . . . 96
7.17 Lunar Pits and Cave Thermal Environment . . . 97
7.18 Comparison Between Equatorial, Mid-Latitude and Polar Environments 98
7.19 Thermal Environment Requirements for the Rover Model . . . 99
7.20 Chapter Summary . . . 100

8 Lunar Surface Thermal Model 101
8.1 Objective and Modelling Logic . . . 101
8.2 General Thermal Balance . . . 103
8.3 Why the Lunar Soil Must Be Modelled . . . 103
8.4 Lunar Soil Geometry Adopted for the Analysis . . . 104
8.5 Subsurface Heat Flux . . . 105
8.6 Thermo-Physical Properties of the Regolith . . . 105
8.6.1 Specific Heat . . . 106
8.6.2 Thermal Conductivity . . . 107
8.7 Conductance Between Dust and Soil . . . 108
8.8 Two Regolith Optical Models . . . 109
8.8.1 Equatorial and Mid-Latitude Optical Model . . . 110
8.8.2 Polar Optical Model . . . 110
8.9 Latitude-Dependent Model Selection . . . 111
8.10 Pseudo-Orbit Implementation . . . 112
8.11 Validation of the Soil Model . . . 113
8.12 Chapter Summary . . . 114

9 Rover and Thermal Control System Model 116
9.1 Modelling Philosophy and Chapter Logic . . . 116
9.2 Temperature Limits and Result Classification . . . 117

9.3 Simplified Internal Rover Box . . . 118
9.3.1 Purpose of the Simplified Rover Geometry . . . 118
9.3.2 Internal Box Geometry and Nodalisation . . . 118
9.3.3 Conductive Coupling Between Panels . . . 120
9.4 Face Temperature Behaviour Before the MLI Shell . . . 121
9.4.1 Extreme Latitude Cases . . . 121
9.4.2 Intermediate Latitude Cases . . . 122
9.5 MLI Shell Model . . . 125
9.5.1 Purpose of the MLI-Like Shell . . . 125
9.5.2 MLI Geometry and Equivalent Representation . . . 126
9.5.3 Effective Conductance Between Internal Box and MLI . . . 127
9.6 Soil–Rover Radiative Coupling . . . 128
9.7 Internal Heat Load . . . 129
9.8 Sensitivity to MLI Coupling and Internal Power . . . 130
9.8.1 Extreme MLI Coupling Cases . . . 131
9.8.2 Intermediate MLI Coupling Cases . . . 132
9.9 Need for a Dedicated Radiator . . . 135
9.9.1 Radiator Geometry and Coupling . . . 135
9.9.2 Radiator Heat Balance . . . 136
9.10 Fixed Radiator Coupling Trade-Off . . . 136
9.10.1 Weak Radiator Link: $G_{\mathrm{rad}} = 0.02\,\mathrm{W/K}$ . . . 137
9.10.2 Strong Radiator Link: $G_{\mathrm{rad}} = 0.08\,\mathrm{W/K}$ . . . 138
9.10.3 Intermediate Radiator Link: $G_{\mathrm{rad}} = 0.05\,\mathrm{W/K}$ . . . 139
9.11 Hot and Cold Case Definitions . . . 140
9.12 Cold-Case Results With Fixed Radiator . . . 141
9.13 Hot-Case Results With Fixed Radiator . . . 142
9.14 Combined Interpretation of Hot and Cold Cases . . . 144
9.15 Physical Interpretation of the Results . . . 144
9.16 Loop Heat Pipe as a Variable Radiator Link . . . 145
9.16.1 Need for Variable Conductance . . . 145
9.16.2 General Function of a Loop Heat Pipe . . . 145
9.16.3 Difference Between Heat Pipe and Loop Heat Pipe . . . 146
9.16.4 Thermal Control Valve and Variable Conductance Logic . . . 147
9.16.5 Physical Meaning of the Conductance Reduction . . . 147
9.16.6 Variable Radiator Example . . . 148
9.17 Design Implications . . . 148
9.18 Possible Improvements to the Model . . . 149
9.19 Baseline Modelling Architecture Before Wheel-System Extension . . . 150
9.20 Chapter Summary . . . 151

10 Thermal Modelling and Thermo-Structural Design of the Wheel and Support System 152
10.1 Modelling Rationale and Design Sequence . . . 152
10.2 Construction of the Wheel Assembly . . . 154
10.2.1 Wheel geometry and material definition . . . 154
10.2.2 Hub and conductive connections . . . 156

10.3 Hub-to-Body Conductance Sensitivity Analysis 158
10.3.1 Case $G_{\mathrm{hub-body}} = 0.03$ W/K 159
10.3.2 Case $G_{\mathrm{hub-body}} = 0.01$ W/K 160
10.3.3 Case $G_{\mathrm{hub-body}} = 0.003$ W/K 161
10.3.4 Interpretation of the sensitivity study 162
10.4 Design Decision: Thermal Switch or Alternative Support Strategy . . . 162
10.5 Thermo-Structural Selection of the Deployable Support Rods 164
10.5.1 Design requirements and MATLAB search 164
10.5.2 Material and geometry trade-off 165
10.5.3 Thermal Desktop implementation of the selected rod 166
10.6 Operational Wheel–Ground and Rod–Ground Contact Strategy 168
10.6.1 Wheel–regolith contact 168
10.6.2 Rod–regolith contact 170
10.7 Thermo-Optical Properties of Wheels and Rods 172
10.8 Final High-Latitude Thermal Verification 173
10.8.1 Result at 70° 173
10.8.2 Result at 80° 174
10.8.3 Result at 85° 175
10.8.4 Interpretation of the final cases 175
10.9 Model Limitations and Required Refinements 176
10.10 Chapter Summary 176

11 Conclusions **178**
11.1 Overall Conclusions 178
11.2 Limitations and Future Development 180

Chapter 1

Introduction

"A journey of a thousand miles
starts under one's feet."

— Laozi
Tao Te Ching, Chapter 64

The renewed international interest in lunar exploration has transformed the Moon from a destination for short scientific visits into a proving ground for increasingly sustained surface operations. Current exploration architectures consider the lunar surface as an environment in which robotic systems, autonomous surface vehicles, scientific payloads, power and communication infrastructure and, in the longer term, human surface systems must operate together. This evolution is consistent with NASA's Moon to Mars Architecture and with the progressive development of lunar surface infrastructure and mobility systems envisioned for future Moon Base operations [1, 2].
Within this context, the lunar surface combines high scientific value with severe engineering constraints. Its ancient crust preserves information about the early evolution of the Solar System, while the regolith, permanently shadowed regions, volcanic formations and polar resources are important targets for future exploration. At the same time, the absence of a dense atmosphere, the lack of external convective heat exchange, the large variation of surface temperature with illumination and latitude, the radiation environment, abrasive dust and the limited availability of power and communications make lunar surface missions particularly demanding from a thermal and systems-engineering point of view.
A rechargeable mini rover represents a suitable platform for local lunar exploration and support activities. Compared with large surface vehicles, a mini rover can be designed with lower mass, reduced launch and deployment constraints and a compact mechanical architecture. It can be used as a precursor or support system to investigate local terrain, validate mobility and autonomy technologies, characterise illumination and thermal conditions, acquire close-range scientific data and perform repeated inspection or reconnaissance tasks around a lander or surface base. The use of compact rovers is therefore relevant not only from a scientific perspective, but also as part of a future distributed robotic infrastructure in which different classes of vehicles cooperate with larger crewed and uncrewed systems.
The small size of the rover, however, makes the thermal problem particularly critical. A compact vehicle has limited thermal inertia, limited radiator area, restricted internal

volume and reduced power availability for active thermal control. In addition, the proximity between structural panels, insulation, wheel assemblies, mechanical supports and external surfaces creates strong coupling between the mechanical configuration and the thermal response of the system. For this reason, even a preliminary thermal analysis must consider the lunar environment, the regolith temperature, the rover geometry, the conductive paths, the radiative exchanges, the internal heat dissipation and the possible need for variable or active thermal-control elements.
The mission concept adopted in this thesis is based on repeated surface sorties of approximately three hours followed by return to a charging station. This nominal duration defines the operational exposure of a single sortie. The longer simulations used later in the work, including cases extended over a complete lunar day, have a different purpose: they are used as an environmental and thermal-design envelope to expose the model to the complete range of local illumination and regolith-temperature conditions and to identify bounding hot and cold cases. They must therefore not be interpreted as a single continuous rover sortie.
The objective of this thesis is to develop a coherent preliminary thermal-analysis framework for a rechargeable mini rover operating on the lunar surface. The work combines the mission context, the lunar thermal environment, the state of the art of spacecraft thermal-control technologies, the theoretical foundations of thermal modelling and a numerical model implemented with Thermal Desktop, RadCAD and SINDA/FLUINT [3, 4]. The analysis is performed at system level: the internal equipment architecture is not yet defined component by component, and the thermal requirement is therefore expressed through a preliminary temperature envelope for the protected internal region rather than through final qualification limits for specific hardware.
The numerical investigation progressively introduces the main physical elements of the problem: a layered lunar regolith model, a simplified internal rover box, an MLI-like external shell, distributed internal heat loads, a top radiator, a variable thermal link and, finally, the wheel–hub–body and wheel–ground thermal paths. The wheel analysis is extended to a combined thermo-structural trade-off in which deployable low-conductance support rods are selected using a MATLAB sizing procedure. The final purpose is not to define a flight-qualified thermal-control system, but to identify a physically consistent preliminary architecture and the parameters that most strongly control its hot- and cold-case behaviour.

1.1 Motivation

Mini rovers are particularly attractive for lunar exploration because they can operate close to the surface, acquire local measurements and inspect areas that cannot be fully characterised from orbit. Orbital data are fundamental for global mapping and landing-site selection, but they cannot always provide the local level of detail required to assess small-scale roughness, slopes, obstacles, illumination conditions, wheel–soil interaction, dust accumulation or the thermal behaviour of a specific operating area. A compact rover can therefore act as a mobile scientific and engineering scout.
From an exploration point of view, mini rovers can support several mission objectives. They can investigate the mechanical and thermal behaviour of the regolith, image rocks and surface features at close range, evaluate traversability, explore the surroundings

of a lander or base, inspect shadowed or partially illuminated regions and collect local environmental data relevant to future missions. In polar regions, they may help characterise strong spatial variations in illumination and temperature. At low and intermediate latitudes, they can provide information on the response of surface systems to the regular lunar day–night environmental cycle.
From a technology-demonstration point of view, mini rovers are useful because they allow mobility, autonomy, communication, power-management and thermal-control strategies to be tested on a reduced platform. This is particularly relevant to future lunar architectures in which multiple robotic systems may support larger landers, habitats, scientific stations, logistics operations or in-situ resource-utilisation activities. Cooperative concepts such as NASA's CADRE project illustrate the broader interest in distributed small-robot operations on the lunar surface [5].
Thermal control is one of the enabling aspects of this type of system. The lunar surface does not provide atmospheric convection, and the rover exchanges heat mainly through radiation, solid conduction and direct contact paths. During illuminated conditions, the vehicle can absorb direct solar radiation, reflected solar radiation from the regolith and infrared radiation emitted by the warm ground. During shadowed or cold conditions, the same vehicle can lose heat toward deep space and toward a cold surrounding environment. The thermal design must therefore reject heat efficiently in hot cases while limiting heat loss in cold cases.
For small spacecraft and compact robotic systems, thermal control is strongly constrained by mass and power. Passive solutions such as coatings, multi-layer insulation, conductive decoupling and radiators are attractive because they require little or no electrical power. However, the same passive configuration cannot always satisfy both hot and cold conditions. Active or adaptive solutions, such as electrical heaters, thermal switches or variable-conductance heat-rejection paths, can increase controllability but introduce additional power consumption, mass and complexity. The rover considered in this thesis therefore represents a typical early-phase thermal-design problem: the environment is severe, the geometry is compact, the available resources are limited and the optimum solution must balance insulation, heat rejection, internal dissipation and mechanical thermal paths.

1.2 Scope of the Work

The work developed in this document is organised around five main questions:

1. Why is the Moon a relevant target for future robotic and human exploration?
2. Which characteristics of a rechargeable lunar mini rover drive the thermal problem?
3. Which passive, active and adaptive thermal-control technologies are suitable for a compact rover operating on the lunar surface?
4. Which heat-transfer mechanisms govern the thermal behaviour of the rover, the lunar soil, the radiator and the wheel–ground interfaces?

5. How can these mechanisms be translated into a numerical thermal model suitable for Thermal Desktop, RadCAD and SINDA/FLUINT and used to guide preliminary thermo-structural design decisions?

The scope of the work is focused on the thermal analysis and preliminary thermal-control design of a mini rover on the lunar surface. The main elements considered are the lunar thermal environment, the layered regolith model, the simplified rover geometry, the conductive and radiative couplings, the internal heat loads, the insulation concept, the radiator, the possible use of a variable thermal link such as a Loop Heat Pipe combined with a Thermal Control Valve, and the thermal interaction of the wheel assembly with the rover body and the regolith.
The final part of the work extends the thermal analysis to the wheel and support system. The hub–body conductance is investigated through a sensitivity study, while alternative support rods are selected by combining thermal conductance, structural strength, Euler buckling, deflection and mass constraints. This extension links the thermal model directly to a preliminary mechanical design choice and shows how the external ground-contact condition can become part of the thermal-control strategy.
The objective is not to finalise a flight-ready thermal-control system or to qualify specific internal components. Instead, the thesis develops a consistent preliminary model, adopts a system-level internal temperature envelope for comparison of the analysed configurations, identifies the dominant thermal design drivers and evaluates a thermal-control architecture suitable for refinement in a later component-level design phase.

Chapter 2

Lunar Exploration Context

"We are all in the gutter,
but some of us are looking at the stars."

— Oscar Wilde
Lady Windermere's Fan

2.1 The Moon as a Strategic Exploration Target

The Moon is both a scientific archive and an engineering testbed. From a scientific perspective, its surface preserves information about impact history, volcanic evolution, crustal differentiation and space-weathering processes. From an engineering perspective, it provides a nearby planetary environment in which technologies for surface mobility, autonomous operations, in-situ resource utilisation, power management, thermal control and long-duration habitation can be tested before being transferred to more distant destinations.

The renewed interest in the Moon is also linked to its possible role as a logistics and operational node for future exploration architectures. NASA's Moon to Mars Architecture explicitly treats the lunar surface as part of a progressive exploration framework in which mobility, logistics, power, habitation, infrastructure and robotic systems are developed together to support increasingly sustained operations [1]. Polar volatiles, if accessible and economically usable, could support life-support systems and propellant production. Surface infrastructure could support communication relays, navigation beacons, scientific observatories, power stations and logistics nodes. These objectives require robotic precursors capable of mapping local hazards, identifying resources and characterising environmental conditions with high spatial resolution.

In this framework, small and rechargeable robotic vehicles are particularly attractive. A mini rover can be transported by a relatively small lander, deployed with limited mechanical complexity and used to explore the area surrounding the landing site. Its reduced size and mass make it suitable for precursor missions, technology-demonstration activities and local scientific investigations. At the same time, the use of rechargeable batteries and solar energy allows the rover to perform repeated operational cycles, provided that the power and thermal conditions remain compatible with the mission profile.

For a rechargeable mini rover, the lunar environment directly affects both mobility and survivability. The rover must operate on a surface characterised by dust, rocks, slopes, variable illumination and large thermal gradients. It must also manage limited electrical energy, because the battery must supply mobility, avionics, communication, payloads and, when needed, thermal-control devices. The thermal design is therefore strongly linked to the power subsystem: during illuminated periods the rover can recharge its batteries and dissipate operational heat, while during shadowed periods or lunar night it may need to reduce activity, preserve heat and protect temperature-sensitive components.



Figure 2.1: Example of a compact lunar rover concept. Credits: [6]

2.2 NASA Moon Base and Distributed Robotic Mobility

The role of surface mobility becomes even clearer in NASA's current Moon Base development concept. The Moon Base is planned as a phased infrastructure at the lunar South Pole, in continuity with the broader Moon to Mars exploration architecture. Mobility is not represented by a single rover type: NASA describes an evolving set of crewed and uncrewed vehicles intended to support exploration, logistics, site preparation, resource-related activities and infrastructure operations [2, 7].
In the first phase, NASA explicitly refers to a *fleet* of Lunar Terrain Vehicles. These vehicles are intended to support both crewed and uncrewed operations, and current concepts include remote operation and autonomous functions. Later phases add dedicated site-preparation and logistics rovers for cargo transport, regolith handling, excavation and soil-compaction tasks, followed by more advanced crewed and uncrewed mobility systems for long-duration operations, robotic manipulation and exploration of difficult regions [2, 7].
This architecture provides an important context for the mini rover considered in this thesis. The present vehicle is not intended to reproduce the capability of a crew-carrying Lunar Terrain Vehicle. Instead, it represents the smaller end of a possible distributed robotic mobility architecture, in which compact vehicles can perform local reconnaissance, environmental monitoring, inspection and support activities around a base while larger vehicles provide crew and cargo transportation.

NASA is also developing cooperative multi-rover autonomy through the Cooperative Autonomous Distributed Robotic Exploration project, or CADRE. The technology demonstration uses three small rovers that communicate and operate as a team, with the objective of demonstrating autonomous cooperative exploration, mapping and distributed measurements without continuous commands from Earth [5]. This concept is particularly relevant to future lunar infrastructure because several small robots can distribute sensing tasks, inspect different areas simultaneously and access terrain that may be inefficient or risky for a larger crewed vehicle.
From a thermal-design perspective, distributed robotic operations strengthen the motivation for lightweight and energy-efficient thermal-control solutions. A fleet architecture favours vehicles that can tolerate repeated exposure to the lunar environment, return to a support or charging station, and operate with limited heater power and limited thermal-control mass. These requirements are consistent with the rechargeable mini-rover concept analysed in the following chapters.

2.3 Lava Tubes and Lunar Pits

Lava tubes are subsurface conduits associated with fluid basaltic lava flows. Terrestrial analogues and lunar volcanic morphology have long supported the interpretation of some lunar channels and collapsed structures as lava tubes, while Lunar Reconnaissance Orbiter observations have identified pits that may represent skylights into subsurface voids [8, 9]. On Earth, the exterior of a lava stream can solidify while the interior remains molten and continues to flow. When the lava drains away, a hollow tunnel remains. On the Moon, the preservation of volcanic structures and the scale of mare volcanism make such subsurface cavities important targets for exploration. The roof of a tube can collapse locally, producing a vertical opening known as a skylight or pit. The interest in lunar lava tubes and pits is driven by several potential advantages:

- protection from micrometeoroids and direct solar radiation;
- natural shielding against galactic cosmic rays and solar energetic particles;
- reduced thermal cycling compared with the exposed surface;
- possible preservation of pristine geological materials;
- potential use as sheltered volumes for future infrastructure.

A pit does not automatically prove the existence of an accessible lava tube, but it is a strong candidate target for robotic reconnaissance. For a mini rover, the direct descent into a vertical pit is generally not a realistic baseline mission mode unless a dedicated mobility or deployment system is added. However, a rover can still provide important support to pit and lava-tube exploration by approaching the rim, mapping the surrounding terrain, acquiring images from different viewpoints, measuring local illumination and temperature conditions, and identifying possible safe access paths for future robotic or human missions.

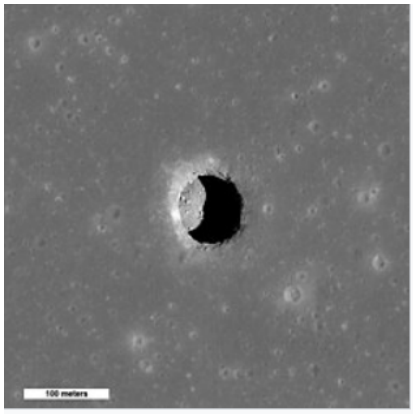


Figure 2.2: Representative lunar pit associated with possible subsurface lava-tube structures. Credits: [10]

From a thermal point of view, pits and skylights are important because they create strong local variations in radiative boundary conditions. Illuminated surfaces, shadowed walls, cold floors and possible subsurface voids may coexist within a small area. A rover operating near a pit would therefore experience a thermal environment that can change significantly with position, local slope, solar elevation and time of day. Even if the rover does not enter the pit, the surrounding terrain can influence the absorbed solar radiation, the infrared radiation received from the ground and the view factor toward cold space.

2.4 Mare Tranquillitatis and Marius Hills

Mare regions are particularly relevant because their basaltic origin is compatible with the formation of lava tubes. Mare Tranquillitatis and Marius Hills are among the most cited regions in the context of lunar pit and skylight exploration. Mare Tranquillitatis is also historically important because of the Apollo 11 landing site, while the Marius Hills volcanic region contains a well-known pit imaged by the Lunar Reconnaissance Orbiter and interpreted as a possible lava-tube skylight [9]. These regions provide a useful exploration context for missions aimed at understanding whether pits may be connected to larger subsurface cavities.

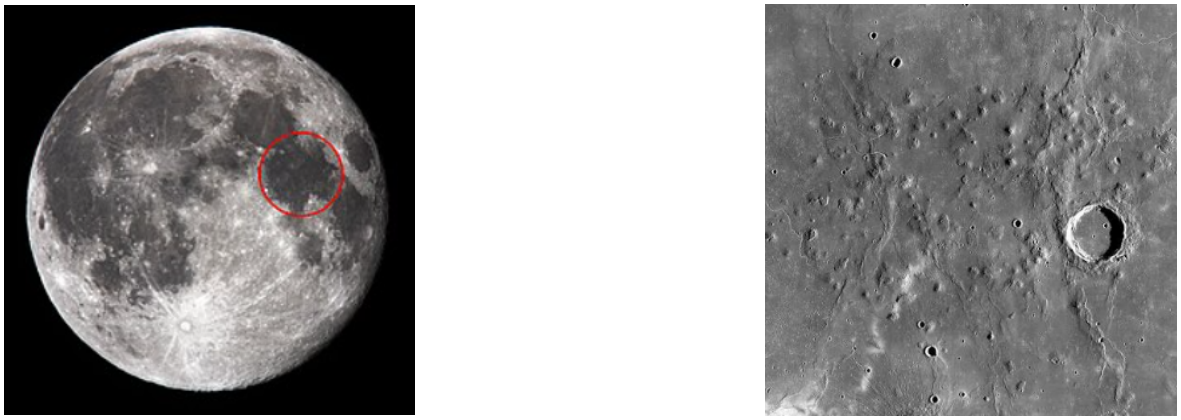


Figure 2.3: Mare Tranquillitatis and Marius Hills. Credits: [11] (left); [12] (right).

For a mini rover, mare regions can represent scientifically valuable and technically challenging operating environments. The terrain may include basaltic regolith, rocks, local slopes, rough surfaces and illumination conditions that vary with local topography. A small rechargeable rover could be used to investigate the area surrounding a lander, perform close-range imaging, support geological interpretation and collect local environmental measurements that cannot be obtained with the same resolution from orbit.
For thermal analysis, mare pits and mare terrains are interesting because they combine direct solar illumination, reflected solar radiation from the surrounding regolith, infrared emission from the ground and shadowed surfaces with much lower temperatures. The rover thermal environment can therefore depend strongly on the local geometry. A radiator or external panel that has a favourable view to cold space in an open flat region may receive additional infrared radiation when the rover is close to a warm wall, a sunlit slope or a pit rim. Consequently, the thermal model must be able to represent not only the rover itself, but also the interaction between the rover and the lunar surface.

2.5 The Lunar South Pole

The lunar south pole has become a priority region for sustained lunar exploration and is the target region of NASA's Moon Base concept [13, 14]. It combines scientific interest, possible volatile deposits and favourable illumination conditions in selected elevated areas. Permanently shadowed regions can maintain extremely low temperatures and preserve volatile compounds such as water ice, while nearby ridges or crater rims can receive sunlight for long fractions of the year. This close spatial proximity between illuminated and permanently shadowed terrain is attractive for science and power generation but creates a particularly demanding environment for rechargeable robotic systems.
From a thermal-design perspective, however, the south pole is especially challenging. The Sun remains close to the horizon, so illumination is strongly affected by local topography. A small change in position can move a rover from direct sunlight to partial shadow or deep shadow. The surface temperature is therefore highly heterogeneous. Unlike a simplified equatorial case, where the thermal forcing is dominated by a relatively regular day–night cycle, polar operations require careful modelling of slope, azimuth, shadowing, local terrain properties and infrared exchange with the surrounding surface.
For a rechargeable mini rover, the south-pole environment is particularly relevant because the power and thermal problems are coupled. Long illumination periods on selected ridges may allow battery recharge and repeated operations, while nearby shadowed regions may contain scientifically interesting volatiles but expose the rover to severe cold conditions. The rover must therefore balance mobility, power availability and thermal survival. It may need to plan traverses according to illumination windows, avoid remaining too long in cold traps, maintain the battery within its allowable temperature range and use passive or active thermal-control strategies during standby periods.



Figure 2.4: Lunar south-pole region, characterised by low solar elevation and strong illumination contrasts. Credits: [15].

2.6 Thermal Implications of Lunar Locations

The thermal environment relevant to a rechargeable mini rover depends strongly on the mission site. An equatorial or mare scenario emphasises the contrast between illuminated daytime conditions and cold nighttime conditions. A pit or skylight scenario emphasises the local contrast between sunlit terrain, shadowed walls, cold surfaces and possible subsurface voids. A south-pole scenario emphasises low-angle illumination, terrain-induced shadowing, cold traps and spatially non-uniform infrared exchange. In all cases, the absence of atmosphere eliminates external aerodynamic convection as a heat-transfer mechanism, leaving conduction through contacts and internal structures, radiation with the environment and internal dissipation as the dominant terms.

The thermal design must therefore account for both hot and cold cases. Hot cases are driven by direct solar flux, reflected solar radiation, warm regolith infrared emission and internal heat generation from avionics, mobility systems, communication units, payloads and battery charging or discharging. Cold cases are driven by shadow, low environmental infrared flux, limited internal dissipation and poor conductive coupling to external heat sources. For a small rover, the limited thermal inertia makes these transitions more critical, because the temperature of internal components can change relatively quickly.

The rechargeable nature of the rover introduces an additional design constraint. During sunlit phases, the solar panels and power electronics can generate heat while recharging the battery. During eclipse, shadow or survival phases, the battery may become both the main energy source and one of the most temperature-sensitive components. The thermal-control system must therefore protect the battery from excessive cooling, avoid overheating during charge and discharge, and maintain the electronics and payload within their allowable operating and survival limits.

For this reason, the lunar surface cannot be treated as a simple fixed-temperature boundary. The regolith absorbs solar radiation, emits infrared radiation, stores heat and conducts heat toward the subsurface. Its temperature changes with latitude, local

time, optical properties, thermal conductivity, density and heat capacity. A realistic preliminary thermal model of the rover must therefore include a representation of the lunar ground, the rover–ground radiative coupling, the conductive contacts through the wheels or supports, and the changing environmental heat fluxes over the selected mission case.

The final objective of the thermal analysis is to identify a configuration able to reject heat during hot conditions and preserve heat during cold conditions. This may require a combination of surface optical properties, multi-layer insulation, controlled conductive paths, thermal straps, radiators, heaters and possibly a variable thermal link between the rover body and the radiator. The selected thermal-control strategy must be compatible with the limited mass, power and volume of a mini rover. At the preliminary level adopted in this thesis, this requirement is first assessed through a system-level internal temperature envelope; component-specific operational and survival limits can be introduced once the final equipment is selected.

Chapter 3

Mini Rover Mission and System Overview

"Great things are done by a series of small things brought together."

— Vincent van Gogh

3.1 Mission Concept

The mission concept considered in this thesis is based on a rechargeable mini rover designed for local exploration on the lunar surface. The rover is intended to operate in the proximity of a crewed lunar base or surface outpost, where it can be deployed, commanded, monitored and periodically recharged. Unlike a large long-range rover, the vehicle considered here is a compact robotic platform with limited mass, limited internal volume and limited energy storage. Its main purpose is to perform short-duration exploration, inspection and environmental-characterisation tasks around the base.

The general mission architecture assumes that the mini rover is transported to the Moon as part of a larger surface mission and is deployed after landing. Once on the surface, the rover operates in repeated cycles. Each cycle starts from a charging station located at the astronaut base, where the rover battery is recharged and the vehicle can remain in a thermally safer standby condition. After charging, the rover leaves the station and performs a local traverse lasting approximately three hours. At the end of the operational period, or when the battery state of charge reaches a predefined limit, the rover returns to the charging station to download data, recharge the battery and prepare for the next mission cycle.

The approximately three-hour interval represents the *nominal operational sortie duration*. The longer transients used later in the thesis, including simulations extended over a complete lunar day, do not represent a single continuous rover sortie. They are used as an environmental and thermal-design envelope to expose the model to the full range of illumination and regolith-temperature conditions and to identify hot- and cold-case sensitivities. The operational three-hour mission cases should therefore be interpreted as shorter time windows extracted from, or bounded by, this broader environmental envelope.

This operational concept is particularly suitable for a small lunar vehicle. The presence of a nearby base reduces the need for very long autonomous survival periods, because the rover can periodically return to a controlled or semi-controlled location. At the same time, the rover must still be able to withstand the external lunar surface environment during its sorties. It is exposed to direct solar radiation, reflected solar radiation from the regolith, infrared radiation emitted by the ground, shadowed regions, highly variable surface temperatures and conductive contact through the wheels. For this reason, even a short-range rechargeable rover requires a dedicated thermal analysis.
The concept follows the logic of compact robotic system design: reduced mass, reduced volume, high subsystem integration, limited power availability and strong coupling between mechanical, electrical and thermal design. In a small rover, components are close to each other, thermal capacitances are limited and the internal heat paths may be dominated by local details such as brackets, screws, electronic boards, battery supports, harnesses, wheel interfaces, structural panels and insulation layers. These aspects make early thermal modelling essential, because small changes in geometry, material selection or conductive coupling can significantly affect the predicted component temperatures.

3.2 Mission Objectives

The mission objectives can be grouped into three main categories: scientific, technological and operational. The scientific objective is to acquire local information about the lunar surface near the base. The mini rover can collect close-range images, inspect rocks and regolith, characterise local terrain features, observe shadowed or partially illuminated areas, and measure environmental quantities such as temperature or illumination conditions. These measurements are useful because orbital data provide global coverage but cannot always resolve local hazards, small-scale roughness, wheel–soil interaction, dust accumulation or the thermal conditions experienced by a surface vehicle.
The technological objective is to demonstrate the operation of a compact rechargeable rover in the lunar environment. This includes surface mobility, autonomous or semi-autonomous navigation, energy management, communication with the base, repeated charging cycles and thermal control of a small robotic platform. The mission therefore acts as a technology demonstrator for future networks of small robotic vehicles that may support astronauts, inspect infrastructure or perform scientific tasks around a lunar outpost.
The operational objective is to support surface activities around the astronaut base. The rover can be used as a scout to inspect the terrain before crewed extravehicular activities, monitor the surroundings of the base, support local mapping, check the condition of surface equipment and collect data from locations that are inconvenient or time-consuming for astronauts to reach directly. In this sense, the rover is not designed as an independent long-duration exploration system, but as a reusable robotic asset integrated into a larger surface infrastructure.
For thermal design, these objectives translate into system-level requirements. The rover must remain functional during a nominal sortie of approximately three hours, survive temporary non-operational periods on the surface, return safely to the charging station and tolerate repeated thermal cycles associated with charging, standby and external

operations. At the present stage, the detailed internal equipment is not yet defined; consequently, the thermal-control problem is formulated for the protected internal region rather than for a fixed list of component nodes. Once selected, temperature-sensitive equipment such as the battery, avionics, communication electronics, sensors and payload units will require dedicated limits and local verification. The preliminary model must nevertheless avoid both excessive cooling and overheating over the considered operating envelope.

3.3 Concept of Operations

A representative sequence of operations is as follows:

1. launch and transfer as part of a larger lunar surface mission;
2. lunar descent and landing of the host lander or surface element;
3. deployment of the mini rover near the astronaut base;
4. connection to, or placement inside, the charging station;
5. battery recharge, health check and thermal conditioning before the sortie;
6. release from the charging station and start of surface operations;
7. local traverse around the base for exploration, inspection or environmental measurements;
8. acquisition of images, housekeeping data and payload measurements;
9. communication with the astronaut base, lander or local relay;
10. return to the charging station before the end of the approximately three-hour autonomy window;
11. data download, battery recharge and possible thermal recovery;
12. repetition of the operational cycle if power, thermal conditions and mission planning allow it.

The thermal criticality of each phase is different. During charging and standby at the base, the rover may benefit from a more favourable thermal boundary condition, especially if the charging station provides partial shielding, conductive interfaces or local thermal support. During the traverse, the rover is directly exposed to the lunar surface environment. It can experience heating due to solar radiation and internal power dissipation, or cooling if it enters shadowed regions or operates when the surrounding regolith is cold. During communication or payload operation, electronic units may create short-duration heat-load peaks. During return and recharge, the battery may require particular attention because charging efficiency, safety and lifetime depend strongly on temperature.

The nominal autonomy of approximately three hours is an important operational design driver. It limits the duration of each individual open-surface exposure and constrains the available energy for mobility, computation, communication, payload operation and thermal control. The parametric simulations developed later over much longer intervals serve a different purpose: they characterise the environmental envelope and determine the combinations of latitude, illumination and internal power that can become hot- or cold-critical. A future mission-level thermal timeline should then apply realistic time-dependent dissipation to the approximately three-hour sortie and to the subsequent recharge or recovery phase.

3.4 Main Subsystems

3.4.1 Mobility System

The mobility system enables the rover to move on the lunar surface. It typically includes wheels, motors, gearboxes, suspension elements, structural supports and motor-control electronics. From a thermal point of view, the mobility system is important for two reasons. First, motors and motor drivers dissipate heat during traverses, especially when the rover moves on slopes, rough terrain or high-resistance regolith. Second, the wheels represent conductive and radiative interfaces with the lunar ground. Heat can be exchanged through the wheel–soil contact areas and through radiation between the wheels, the rover body and the surrounding surface.
The thermal model should therefore include the mobility system at least in simplified form. The wheels can be represented as external elements with their own thermal capacitance, optical properties and conductive links to the rover body. The motor units and motor drivers can be represented as internal or semi-internal dissipating components. The conductive coupling between wheels, axles, suspension and internal structure should be treated carefully, because it can either introduce unwanted heat losses during cold cases or provide a useful path for heat rejection during hot cases.

3.4.2 Guidance, Navigation and Control

The guidance, navigation and control subsystem includes the sensors, processors and algorithms required to move safely on the lunar surface. Possible elements include cameras, inertial sensors, wheel encoders, proximity sensors, LiDAR or range sensors, an on-board computer and motor-control electronics. Unlike a flying vehicle, the rover does not require propulsion control for take-off or hovering, but it does require reliable surface navigation, obstacle avoidance and attitude or slope awareness.
These elements generally have narrower temperature limits than structural parts. Their heat dissipation is moderate but may be continuous during active traverses. Since they are often placed inside the main rover body, their temperature is controlled indirectly through the thermal behaviour of the structure, insulation, conductive paths and internal heat distribution. For this reason, the on-board computer and navigation sensors are among the most important units to monitor in the thermal model.

3.4.3 Communication System

The communication subsystem transfers scientific data, images and housekeeping information to the astronaut base, lander or local relay. Its thermal relevance is associated with radio-frequency electronics, antennas and data-handling units. Depending on the duty cycle, communication can represent a significant heat-load case, especially during high-data-rate transmission after a traverse or during real-time teleoperation.
Antenna surfaces may be externally exposed and must therefore be included in the radiative model if their area or optical properties are not negligible. Communication electronics, on the other hand, are usually internal dissipating units and should be thermally connected to the structure or to a dedicated heat-spreading element. If communication is concentrated at the end of the sortie, the thermal model should include this phase as a possible local temperature peak.

3.4.4 Electrical Power System and Recharge Interface

The electrical power system includes the battery, power-conditioning electronics, harnesses, protection circuits and the recharge interface with the station at the astronaut base. The battery is one of the most temperature-sensitive components of the rover. Its capacity, internal resistance, charge acceptance, discharge performance, lifetime and safety depend strongly on temperature. For this reason, the battery thermal environment is a primary design driver.
The rechargeable nature of the rover changes the mission thermal problem. During external operations, the battery supplies power to mobility, avionics, communication, payloads and possible heaters. During recharge at the base station, electrical energy is transferred back to the battery, and part of this energy is dissipated as heat inside the battery and power electronics. The charging station may also provide a more controlled environment than the open lunar surface, for example through a shaded parking location, a conductive docking interface, local heaters or a thermally protective enclosure. These possibilities should be considered in the system-level thermal design, even if the first numerical model uses simplified boundary conditions.
The three-hour autonomy requirement introduces a direct link between the energy budget and the thermal budget. A larger battery increases available energy and thermal inertia, but also increases mass and may require additional thermal control during charging. A smaller battery reduces mass but may be more sensitive to temperature variations and may leave less power available for heaters. Therefore, the power subsystem and the thermal control system must be designed together.

3.4.5 Structure and Payload

The structure provides mechanical support and defines the main heat paths inside the rover. In a compact mini rover, panels, frames, brackets and internal supports are not only mechanical elements, but also thermal conductors, heat spreaders and radiating surfaces. The material choice, wall thickness, contact conductance and mechanical interfaces can significantly influence the internal temperature distribution.
The payload may include cameras, environmental sensors, thermal sensors or other scientific instruments. These units may require a controlled temperature to ensure

measurement quality and reliability. Optical payloads may need external apertures or windows, which can create direct radiative coupling with the lunar environment. Therefore, the payload must be included in the thermal model either as a dissipating internal unit or as an externally exposed element, depending on its final configuration.

3.4.6 Thermal Control Elements

The preliminary thermal control system of a rechargeable mini rover can include both passive and active elements. Passive elements may include surface coatings, multi-layer insulation, low-conductance mounts, thermal straps, conductive heat spreaders and radiators. Active elements may include electrical heaters, thermostatic control of the battery, operational constraints and possible thermal conditioning at the charging station.

The radiator design is particularly important because the rover must reject heat during active and sunlit phases while avoiding excessive heat loss during cold cases. If a fixed conductive link to the radiator is too strong, the radiator may overcool the internal box during shadow or standby conditions. If the link is too weak, the rover may overheat during active operation. For this reason, a variable thermal link, a controlled conductive interface or a loop-heat-pipe-like concept can be considered in later design iterations, depending on the complexity allowed by the mission.

3.5 Thermal Requirements

At the present stage of the study, the internal architecture of the rover is not defined at component level. The final battery type, on-board computer, sensors, communication electronics, motor drivers and payload have not yet been selected. For this reason, component-specific operational and survival temperature limits are not introduced in this chapter. Assigning numerical limits to equipment that has not yet been selected would give the model a level of detail that is not supported by the present mission definition.

The thermal requirement used in the numerical analysis is therefore formulated at system level. The protected internal region of the rover is required to remain within the preliminary temperature interval

$$253.15\ \mathrm{K} \leq T_{\mathrm{internal}} \leq 323.15\ \mathrm{K}, \tag{3.1}$$

corresponding approximately to

$$-20^{\circ}\mathrm{C} \leq T_{\mathrm{internal}} \leq +50^{\circ}\mathrm{C}. \tag{3.2}$$

This interval is not intended to represent the qualification range of a specific battery or electronic unit. It is used as a preliminary design envelope for comparing the different thermal configurations analysed in the thesis and for identifying conditions that are clearly too cold or too hot for the internal rover compartment.

The purpose of the thermal analysis is therefore to determine whether the combination of lunar environment, internal heat dissipation, insulation, radiator coupling and conductive paths can maintain the rover inside this preliminary envelope during the

relevant operating conditions. Particular attention is given to the variation with latitude and internal power, because these parameters strongly affect both the hot and cold cases. The full-lunar-cycle simulations used in the following chapters are design-envelope analyses rather than a representation of one three-hour sortie; they are used to identify the thermal states from which realistic operational windows can subsequently be defined.

Once the actual rover equipment is selected, this system-level interval must be replaced or complemented by component-specific limits taken from the corresponding datasheets and mission requirements. The final thermal verification would then be performed on separate thermal nodes representing, for example, the battery, avionics, communication electronics, sensors, payload and mobility electronics, each with its own operational and survival limits.

In accordance with the preliminary nature of the present work, the temperature interval adopted here is therefore used as a design and comparison criterion rather than as a final qualification requirement. The objective of the following analyses is to identify a thermal-control architecture capable of keeping the internal rover environment within a reasonable range before a detailed equipment-level design is available.

Chapter 4

State of the Art of Thermal Control Systems for Small Spacecraft and Lunar Mini Rovers

"Non est ad astra mollis e terris via."

— Seneca
Hercules Furens

4.1 Role of the Thermal Control System

The thermal control system maintains spacecraft hardware within its allowable temperature limits throughout the mission [4, 16]. It must reject excess heat in hot cases and preserve heat in cold cases. In small spacecraft and compact lunar rovers, this function is particularly difficult because the available surface area, mass, power and internal volume are limited. For the preliminary rover considered in this thesis, the detailed equipment list and component-specific temperature limits are not yet fixed. The thermal-control problem is therefore first treated at system level, while the lunar environment, local terrain temperature, shadowing, regolith properties and conductive wheel–ground paths are included as the principal external drivers.
The thermal control system is not an isolated subsystem. It is strongly coupled with the mechanical configuration, the electrical power subsystem and the operational profile of the rover. Future equipment such as a battery, avionics, communication electronics, mobility drives and payload units will introduce component-specific dissipation and temperature limits once the detailed architecture is defined. In the present work, these contributions are represented at system level through distributed internal heat loads. Recharge, standby and shadowed conditions remain important because the amount of internal dissipation and the available electrical power for active thermal control can change substantially between operating modes.
Thermal control technologies are commonly grouped into passive and active solutions, although some adaptive devices lie between these categories. Passive solutions require no commanded electrical power and are generally preferred when simplicity and reliability are priorities. Active solutions use electrical power, commanded actuation or

control logic to modify the thermal state. Thermostatic louvers, variable-emittance surfaces and thermal switches may behave passively or actively depending on the implementation. For a small rechargeable lunar rover, passive heat management should be used wherever possible, while active or adaptive control is introduced when the hot–cold trade-off cannot be satisfied by a fixed passive architecture.

4.2 Passive Thermal Control

4.2.1 Coatings, Paints and Surface Finishes

Surface finishes control the balance between absorbed solar radiation and emitted infrared radiation. The two key properties are solar absorptivity α and hemispherical infrared emissivity ε. A surface with high α and low ε tends to heat up under solar illumination, while a surface with low α and high ε tends to remain cooler. White paints, second-surface mirrors, black paints, metallic finishes and optical solar reflectors are common examples.

For a lunar mini rover, coatings can be used to tune the thermal behaviour of external panels, radiator surfaces, solar-panel backsides, antenna supports, wheel covers and exposed payload surfaces. The choice of coating is especially important because the same surface may experience very different conditions during a mission cycle. A coating that is beneficial during a hot illuminated traverse may be penalising during a cold shadowed phase. Conversely, a surface that helps the rover retain heat in a cold case may increase the risk of overheating during battery charging, communication or payload operation.

The ratio α/ε is often used as a first indicator of the thermal tendency of a surface under solar illumination. Low values of α/ε are generally preferred for surfaces that must remain cool in sunlight, while high values may be useful when solar heating is desired. However, on the lunar surface the problem is more complex than in deep space because the rover also exchanges infrared radiation with the regolith and may receive reflected solar radiation from the ground. Therefore, the final coating selection must be verified in the complete thermal model.

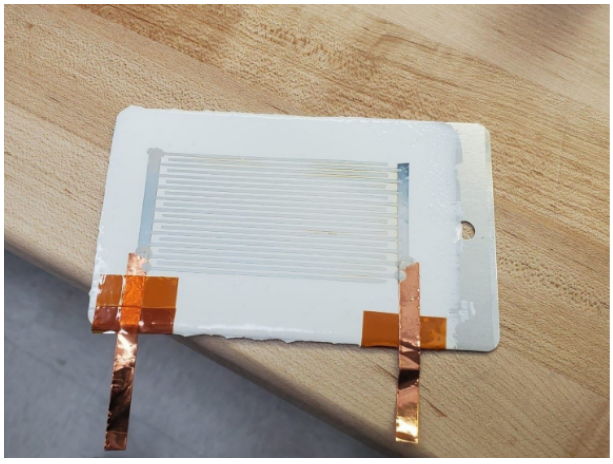


Figure 4.1: Examples of spacecraft thermal-control surface coatings and finishes. Credits: [17]

4.2.2 Multi-Layer Insulation

Multi-layer insulation (MLI) reduces [4] radiative heat exchange by using several low-emissivity reflective layers separated by low-conductivity spacers. It is highly effective in vacuum when properly installed, but its performance can be degraded by compression, seams, penetrations, edges, mounting points and conductive contact paths. In a compact lunar rover, MLI can reduce heat loss from the internal compartment during cold phases, but excessive insulation may also cause overheating during active or sunlit phases.
For the mini rover considered in this thesis, MLI can be used around the internal equipment box or around selected temperature-sensitive units. Its purpose is to reduce the radiative coupling between the internal structure and the external lunar environment. This is especially useful for protecting the battery and electronics during shadowed phases or low-temperature conditions. However, the insulation must be designed together with the heat-rejection system. If the rover is too well insulated and the radiator coupling is too weak, internal heat generated by the electronics and mobility subsystem may accumulate and lead to excessive temperatures.

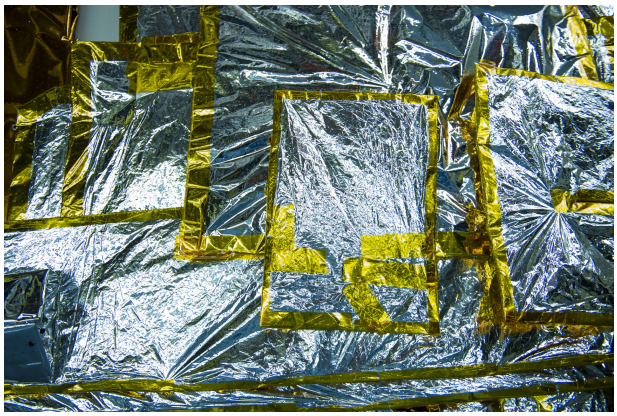


Figure 4.2: Representative multi-layer insulation blankets used to reduce radiative heat exchange in vacuum. Credits: [18]

4.2.3 Thermal Straps and Conductive Path Management

Thermal straps are flexible conductive links, often made of copper or aluminium, used to transfer heat from a component to a radiator, structural panel or heat spreader while accommodating mechanical tolerances and vibration. In a compact lunar rover, straps can couple hot electronics to external panels or distribute heat from local sources to larger thermal masses. They may also be used to connect the battery or on-board computer to a controlled thermal node, provided that the resulting heat path does not produce excessive cooling during cold phases.
Conductive path management is a fundamental aspect of rover thermal design. It includes the choice of bracket materials, contact areas, interface materials, screw patterns, structural connections, harness routing and mechanical supports. In small vehicles, apparently secondary mechanical details may become dominant thermal paths. For example, a metallic bracket connecting the internal equipment box to an external

panel may create a significant conductive leak during lunar night or shadowed operation. Conversely, a poorly designed interface may prevent heat generated by electronics from reaching the radiator during hot cases.
For the wheels and mobility subsystem, conductive path management is also important because the wheel–ground contact creates a possible heat-transfer path between the rover and the lunar regolith. The effectiveness of this path depends on the contact area, wheel material, regolith properties and contact conductance. In many preliminary models, this effect is simplified, but it should not be ignored when assessing hot and cold cases on the lunar surface.

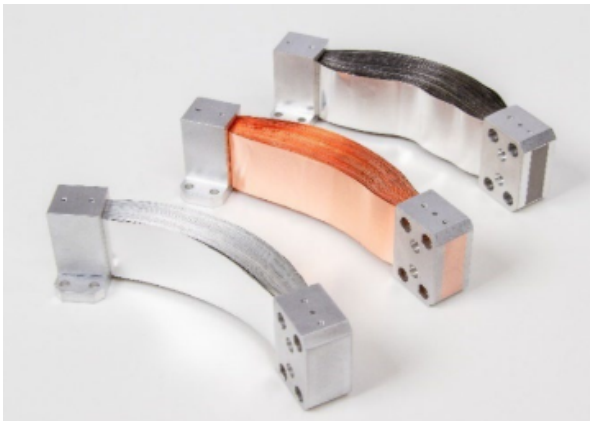


Figure 4.3: Representative flexible thermal straps used to control conductive heat paths. Credits: [19]

4.2.4 Radiators

A radiator is a surface designed to reject heat by infrared emission. Its effectiveness depends on area, emissivity, view factor to cold space and incident environmental fluxes. On the lunar surface, a radiator may not always see only deep space. It may also see warm regolith, illuminated slopes, the rover body, nearby structures or the charging station. Therefore, radiator placement is a key design variable.
For a rechargeable mini rover, the radiator must be sized and coupled carefully. During active operation, it must reject heat generated by the on-board computer, communication electronics, payload, mobility subsystem and power electronics. During recharge, it may also need to reject heat generated by the battery and power-conditioning unit. During cold phases, however, the same radiator can become an excessive heat-loss path. If the conductive link between the internal compartment and the radiator is too strong, the radiator may overcool the battery and electronics when the rover is in shadow or when the external environment is cold.
This trade-off is one of the main reasons why a fixed radiator conductance may not be sufficient for a lunar mini rover. The hot case requires effective heat rejection, while the cold case requires thermal isolation. A preliminary design can start with a fixed conductance between the internal box and the radiator, but later iterations may require a variable-conductance device, a thermal switch, a loop heat pipe or an operational strategy in which the rover uses the charging station as a thermally safer location.

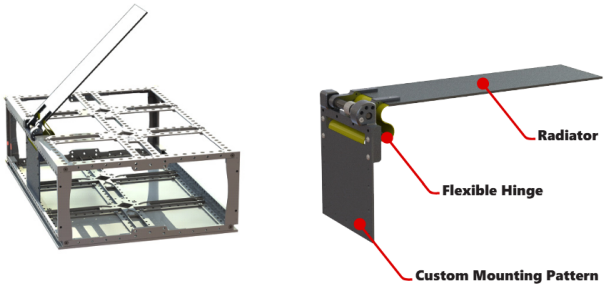


Figure 4.4: Representative spacecraft radiator used for heat rejection by infrared emission. Credits: [20]

4.2.5 Heat Pipes, Loop Heat Pipes and Phase-Change Devices

Heat pipes transfer heat with high effective conductance through evaporation and condensation of a working fluid. They are widely used in spacecraft because they can transport heat with small temperature differences and without mechanical pumping. For lunar-surface applications, however, miniaturisation, integration constraints, orientation relative to the local gravity field, capillary performance, freeze–thaw behaviour and compatibility with the expected temperature range must be considered.
Loop heat pipes are related two-phase devices in which capillary forces drive circulation between the evaporator, compensation chamber and condenser. They can transport heat over longer distances and offer greater integration flexibility than a conventional heat pipe. A standard LHP is primarily a passive heat-transport device and should not automatically be described as a thermal switch. In the architecture investigated later in this thesis, the required hot–cold modulation is represented by the equivalent behaviour of an LHP combined with a Thermal Control Valve or another controlled variable-conductance interface. The objective is to provide a high effective conductance when heat rejection is required and a much lower conductance when heat must be conserved.
Phase-change materials store thermal energy during melting and release it during solidification. They can reduce peak temperatures during short high-power events, such as communication peaks, payload operation or battery charging. Their drawback is added mass and limited energy capacity. They are useful only if the mission profile includes temperature peaks of limited duration and if the material can be fully regenerated during the following cold or recovery phase.

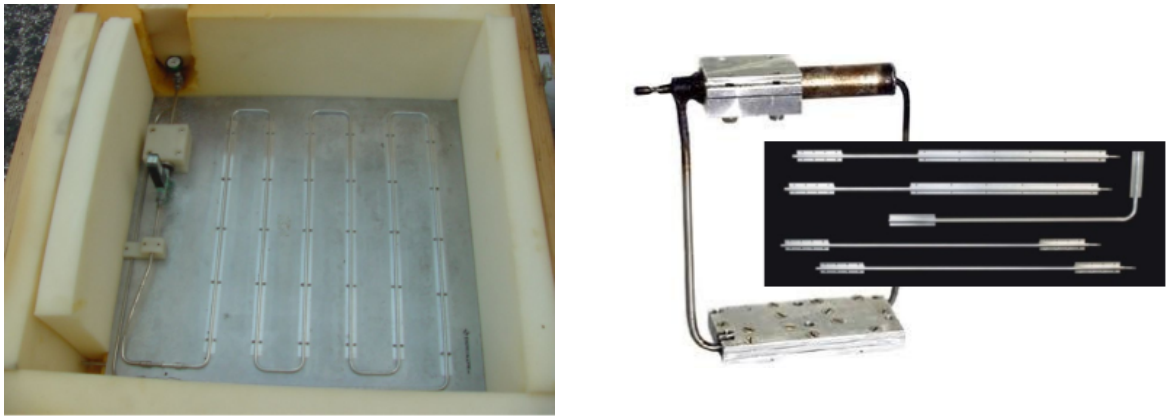


Figure 4.5: Representative heat-pipe and loop-heat-pipe configurations. Credits: [21]

4.3 Adaptive and Active Thermal Control

4.3.1 Heaters

Electrical heaters are among the simplest active thermal-control elements. They are used to maintain batteries, sensors, electronics, mechanisms and payload units above minimum allowable temperatures. They require thermostats or software control and consume power, which may be scarce during shadowed operations or when the rover is far from the charging station.

For a rechargeable mini rover, heaters are expected to be particularly relevant for the future battery subsystem because electrochemical performance, charge acceptance and safety are temperature dependent. The actual heater requirement cannot be fixed until the cell chemistry and battery architecture are selected. In a later design phase, a local battery heater or a thermally controlled battery compartment may therefore be introduced if the component-specific limits require it.

Heaters may also be required for avionics, sensors or other equipment once their specific survival limits are known. Heater power must be included in the rover energy budget because any active thermal-control power used during the approximately three-hour nominal sortie reduces the energy available for the primary mission functions. The complete-lunar-cycle simulations used later in the thesis are design-envelope analyses and do not imply continuous heater operation over an entire lunar day.



Figure 4.6: Representative electrical heater used for active thermal control. Credits: [21]

4.3.2 Louvers and Variable-Emittance Devices

Louvers regulate heat rejection by changing the effective radiating area or view to space. Variable-emittance devices change optical properties electrically or thermally. These technologies can provide adaptive behaviour, allowing the thermal control system to reject heat in hot cases and retain heat in cold cases. For a small lunar rover, these devices may be attractive from a thermal point of view but challenging from a system point of view. Mechanical louvers introduce moving parts, mass, volume and potential dust-related issues. Variable-emittance surfaces may require electrical control, dedicated materials and qualification effort.
Therefore, they are usually considered only if simpler solutions such as coatings, MLI, heaters, radiator sizing and conductive path tuning cannot satisfy the thermal requirements with sufficient.



Figure 4.7: Example of spacecraft thermal louvers used to modulate heat rejection. Credits: [22]

4.3.3 Thermal Switches and Variable Conductance Links

A thermal switch is a device or interface that changes its effective conductance depending on temperature, command state or mechanical configuration. The purpose is to connect a heat source to a sink when heat rejection is required and to isolate it when heat preservation is required. This concept is highly relevant for lunar surface systems because the thermal environment can alternate between very hot and very cold conditions.
For the mini rover, a thermal switch or variable-conductance link can be placed between the protected internal region and the radiator. During heat-rejection conditions, the conductance should be high enough to transfer heat to the radiator, whereas in cold conditions it should be reduced to limit parasitic heat loss. In a preliminary numerical model this behaviour can be represented by two or more equivalent conductance states. A similar design question also arises later for the wheel–body thermal path, where a dedicated thermal switch is compared with an alternative mechanical strategy based on low-conductance deployable supports.

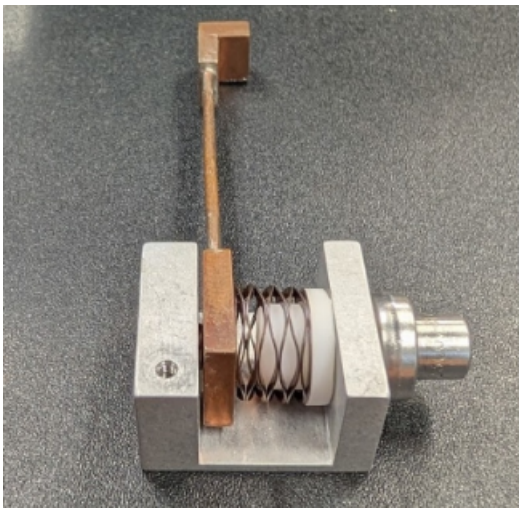


Figure 4.8: Representative thermal switch used to change the effective conductance between thermal nodes. Credits: [23]

4.3.4 Fluid Loops

Fluid loops can transport heat between components and radiators. They are powerful solutions for large spacecraft or high-power systems, but they are usually too complex for very small rovers unless the mission requires significant heat transport. A mechanically pumped fluid loop would introduce pumps, lines, valves, control electronics, working fluid, additional mass and possible reliability concerns.
For the rechargeable mini rover considered in this work, a mechanically pumped thermal loop is not expected to be the first design choice because of its mass, complexity and power requirements. Two-phase passive transport devices such as heat pipes or loop heat pipes remain more relevant candidates. At preliminary level, their system effect can be represented through equivalent thermal links, provided that the distinction between passive heat transport and actively controlled conductance is maintained.

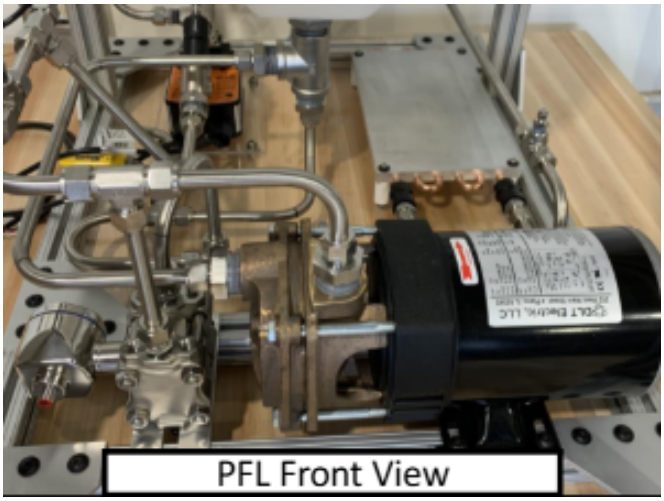


Figure 4.9: Schematic example of a mechanically pumped fluid loop for spacecraft thermal control. Credits: [24]

4.4 TCS Selection Criteria

The selection of the preliminary thermal control system should consider the following criteria:

- thermal effectiveness in hot and cold cases;
- compatibility with the temperature needs of the future battery and avionics once their component-specific limits are defined;
- compatibility with the approximately three-hour nominal sortie and with the broader environmental design envelope used for hot–cold analysis;
- mass, volume and power impact;
- integration feasibility with the rover mechanical layout;
- compatibility with wheels, mobility mechanisms and surface operations;
- robustness to uncertainty in the lunar environment and regolith properties;
- compatibility with the charging station at the astronaut base;
- manufacturability and testability in an academic or early industrial context.

For the first design iterations, coatings, MLI, conductive-path management, thermal straps, radiator sizing and provision for local heaters are among the most realistic options. These technologies are relatively simple, compatible with compact systems and suitable for preliminary numerical modelling. The future battery subsystem is expected to be thermally important because it is directly linked to autonomy and recharge capability, but its specific temperature limits are deliberately left open until a real battery architecture is selected.
More complex adaptive systems, such as louvers, variable-emittance surfaces, thermal switches or controlled two-phase heat-transport devices, should be introduced only if

the analysis shows that a fixed passive architecture cannot satisfy the hot and cold requirements with adequate margin. In particular, the numerical results developed later in the thesis show that the radiator requires a variable effective conductance: a stronger thermal link is beneficial for heat rejection, while a weaker link is required to conserve heat in cold conditions. This motivates the LHP/TCV-type equivalent architecture adopted in the preliminary model.
The final thermal-control architecture must therefore be selected as a compromise between heat rejection, heat preservation, power consumption, mechanical simplicity and reliability. For a rechargeable lunar mini rover operating near an astronaut base, the charging station can also become part of the thermal strategy by providing a protected parking condition, recharge capability or a dedicated thermal interface. In the present thesis, however, the station itself is not modelled in detail; the numerical work focuses on the open-surface rover, the variable radiator link and the additional thermal paths introduced by the wheel and support system.

4.5 Chapter Summary

This chapter reviewed the thermal-control technologies most relevant to a compact lunar rover. Passive solutions such as surface coatings, MLI, conductive-path management, thermal straps and radiators provide the first level of thermal control because they require little or no electrical power. Their limitation is that a fixed passive architecture may not satisfy both hot and cold operating conditions.
Adaptive and active solutions can extend the usable thermal range. Electrical heaters provide local cold protection, while louvers, variable-emittance devices and thermal switches can modify heat rejection or conductive coupling. Heat pipes and loop heat pipes provide efficient passive heat transport, but a standard LHP should not be confused with a thermal switch; the variable behaviour required later in this thesis is represented by an LHP combined with a Thermal Control Valve or another controlled equivalent interface.
For the preliminary rover considered here, the detailed equipment architecture is not yet defined. The technologies are therefore assessed at system level, with emphasis on the trade-off between insulation, heat rejection, internal dissipation and parasitic conductive paths. This review provides the technological basis for the numerical architecture developed in the following chapters, where an MLI-like shell, a top radiator with variable effective conductance and a dedicated wheel/support thermal strategy are investigated.

Chapter 5

Thermal Analysis

"Heat, like gravity, penetrates every substance of the universe."

— Joseph Fourier
The Analytical Theory of Heat

5.1 Purpose and Scope of the Chapter

This chapter provides the theoretical, methodological and numerical background required for the thermal analysis of the rechargeable lunar mini rover. It introduces the heat-transfer mechanisms, the ECSS-oriented modelling process, the construction of the Geometrical Mathematical Model (GMM) and Thermal Mathematical Model (TMM), the thermal-network approach, the main numerical methods used in spacecraft thermal solvers, and the role of Thermal Desktop, RadCAD and SINDA/FLUINT in the present work.

A lunar rover is subjected to a particularly severe thermal environment. The absence of a dense atmosphere eliminates external convection and makes the external thermal balance almost completely governed by radiation and surface contact conduction. The vehicle receives direct solar radiation, reflected solar radiation from the lunar regolith, infrared radiation emitted by the lunar ground, and it rejects heat by infrared emission toward deep space and toward the surrounding terrain. At the same time, internal components dissipate electrical power and exchange heat with the structure through conductive interfaces. Therefore, the thermal problem is intrinsically coupled, time-dependent and strongly dependent on latitude, local solar time and surface properties. In a complete spacecraft programme, the objective of thermal analysis is to verify that each thermally relevant unit remains within its allowable operating and survival temperature ranges during the applicable mission phases. The operating range applies while a unit performs its function, whereas the survival range defines temperatures that must not be exceeded even when the unit is inactive. In the present thesis, however, the detailed rover equipment has not yet been selected and separate component limits are therefore not available. The numerical verification is consequently performed first at system level, using the preliminary temperature envelope defined for the protected internal region. Component-level limits would be introduced in a later design phase

once the battery, avionics, sensors, communication hardware, mobility electronics and payload are selected.
Thermal control is not a generic design accessory, but a mission-enabling subsystem. Without a suitable thermal control strategy, temperature excursions may cause degradation of materials, structural deformations, changes in optical properties, loss of electronic performance, battery degradation or failure, payload malfunction, mobility-system thermal issues or irreversible damage to sensitive units. For this reason, the thermal design must be introduced early in the project and refined iteratively as the physical design becomes more mature.

5.2 Thermal Control as an Iterative Spacecraft Design Process

Thermal control design is a transversal and iterative activity that accompanies all phases of a space project. In the earliest phases, the available information about geometry, materials, dissipations, mission profile and interfaces may be incomplete. Nevertheless, preliminary thermal analyses are necessary to identify the main thermal drivers and to define the first thermal-control concept. In later phases, the model is progressively improved using more accurate geometries, detailed component data, thermal-balance-test results and correlated interface conductances.
The thermal engineer does not normally design a thermal control system able to satisfy every possible space environment. Such a solution would usually be excessively massive, expensive and over-designed. A more effective approach is to tailor the TCS to the mission-specific hot and cold environments, the spacecraft configuration and the actual operational modes. This mission-oriented philosophy allows the thermal design to remain lighter, cheaper and more consistent with modern spacecraft-design practice [25]. The typical thermal design sequence can be summarised as follows:

1. definition of the mission phases and mission thermal requirements;
2. definition of system-level or component-level temperature limits, depending on the maturity of the design;
3. definition of the external environment and environmental heat fluxes;
4. construction of a first simplified thermal model;
5. analysis of extreme hot and cold cases;
6. identification of thermal criticalities;
7. preliminary design of the thermal control system;
8. refinement of the model and repetition of the analyses;
9. verification of the design against the applicable limits and uncertainty margins;
10. correlation with test data when thermal-balance or thermal-vacuum tests become available.

In early design stages, thermal analysis can be the only practical verification tool for some requirements. Reproducing the real space or lunar environment experimentally on Earth is expensive and sometimes not feasible at system level. Thermal-vacuum and thermal-balance tests are extremely valuable, but they generally occur only after a significant part of the design is already fixed. Computational thermal analysis therefore reduces cost and risk by allowing problems to be detected before hardware manufacturing.

5.3 Thermal Requirements, Temperature Definitions and Margins

At component level, spacecraft thermal requirements define the temperature intervals within which each item of equipment must remain. Two categories are normally distinguished:

- **operational temperature range**: the range within which the component must remain when it is performing its function;
- **survival or non-operational temperature range**: the wider range within which the component must remain throughout its lifetime to avoid irreversible damage, even when not operating.

The thermal budget is the organised collection of these limits, together with the associated dissipations, operational modes and environmental assumptions. It is used to compare predicted temperatures against the allowable ranges. A component may be acceptable in survival mode but not in operating mode, depending on its functional requirements and thermal inertia. In the present preliminary rover study, this component-level budget is not yet available; the adopted 253.15–323.15 K internal interval is instead used as a system-level design and comparison criterion.
The calculated temperature range is the direct output of the thermal analysis. Since the model contains uncertainties, the calculated range must be expanded by appropriate uncertainty margins before comparison with design limits. The result is the predicted temperature range. This predicted range must remain inside the design temperature range and, with the appropriate test margins, inside qualification and acceptance limits. The sources of uncertainty include:

- environmental flux uncertainties;
- uncertain material properties;
- thermo-optical property degradation;
- contact conductance uncertainty;
- simplified geometry and nodalisation;
- internal power dissipation uncertainty;
- boundary-condition approximations;

- numerical discretisation and solver tolerances.

The ECSS thermal-analysis handbook gives phase-dependent uncertainty values that decrease as the project matures. The values are normally applied to calculated temperatures in the range between approximately 200 K and 470 K. Below cryogenic temperatures or above high-temperature ranges, mission-specific considerations may be required [3, 26].

Table 5.1: Typical ECSS temperature uncertainties as a function of project phase.

Project phase	**Temperature uncertainty**
A	± 15 K
B	± 10 K
C/D before TB test	± 8 K
C/D after TB test and correlation	± 5 K

For an early-phase rover model, a Phase-A-level temperature uncertainty can materially reduce the apparent thermal margin and therefore influence the selection of insulation, radiator coupling and heater provision. In this thesis the nominal maps are primarily used to compare design alternatives; they should not be interpreted as qualification evidence. A later verification step should apply the appropriate project-phase uncertainty and component-specific limits before judging the final TCS acceptable.

5.4 ECSS-Oriented Thermal Modelling Process

The European Cooperation for Space Standardization provides requirements and guidelines for thermal control and thermal analysis of space systems. The ECSS thermal-control standard defines the requirements that the thermal control subsystem must satisfy, while the ECSS thermal-analysis handbook provides recommendations for modelling, analysis, verification, validation, model management and uncertainty treatment [3, 26]. The thermal-control requirements can be grouped into three main classes:

- **mission requirements**: requirements applicable to all mission phases, from ground and pre-launch operations to the end of the operating lifetime;
- **thermal-performance requirements**: requirements that must be satisfied in worst-case hot and cold environments, using accepted margins and temperature limits defined by the system authority;
- **interface requirements**: requirements associated with thermal, mechanical, electrical, data-handling and monitoring interfaces between the TCS and other subsystems.

The ECSS-oriented thermal modelling process can be described as an iterative workflow:

1. **Mission requirements**. Define mission constraints, operational modes, allowable temperature ranges, thermal budget, environmental requirements and functional requirements.

2. **Spacecraft or rover design**. Define the geometry, physical configuration, mass distribution, materials, thermo-physical properties and thermo-optical properties.

3. **Thermal and radiative modelling**. Define the radiative environment, the active radiating surfaces, the conductive paths, the heat-load cases and the dissipations.

4. **GMM and TMM construction**. Build the GMM for radiative outputs and the TMM for thermal solution.

5. **Radiative solution**. Use the GMM to compute view factors, interchange factors, radiative couplings and environmental heating rates.

6. **Thermal solution**. Combine radiative results with the TMM and solve the heat-balance equations.

7. **Thermal results**. Extract temperatures, heat fluxes, absorbed powers and interface heat flows.

8. **Post-processing**. Verify requirements, identify critical nodes and define design modifications.

This process must be documented and controlled. Model configuration, version control, assumptions, verification status and analysis-case definitions must remain traceable. Verification and validation are fundamental parts of the modelling process: topology checks, convergence analyses and sensitivity studies are used to ensure that the model behaves physically and that its outputs are reliable. Heat transfer is the physical process by which thermal energy is exchanged between regions at different temperatures. For spacecraft and lunar vehicles, the three relevant mechanisms are conduction, convection and radiation. Their relative importance depends on the environment. On the lunar surface, external convection is absent, whereas conduction and radiation dominate.
Internal convection may still occur only in specific enclosed or fluid-based devices, such as heat pipes, thermal-control loops or other sealed components. For the present mini rover, external convection is neglected in the lunar surface environment.

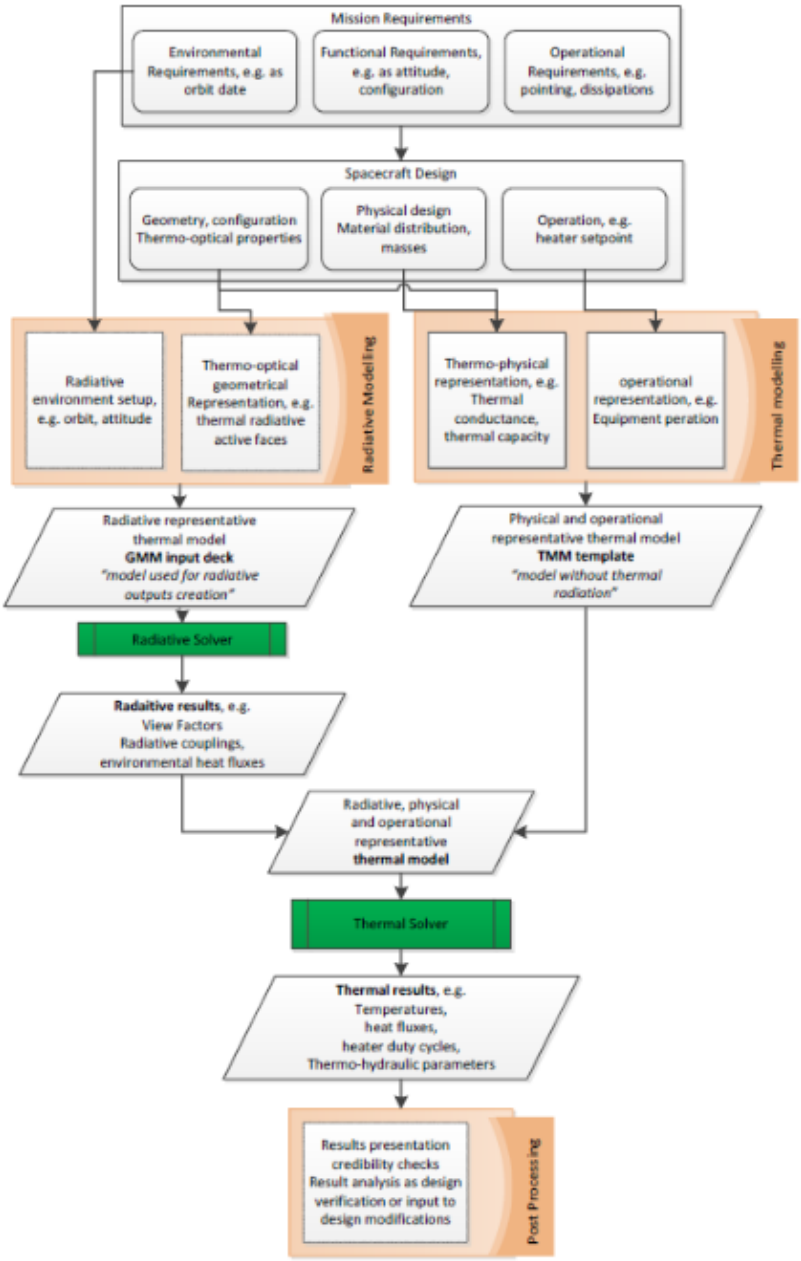


Figure 5.1: Thermal-analysis workflow from mission requirements to model verification and post-processing. Credits: [26]

5.4.1 Conduction

Conduction is the transfer of thermal energy through matter due to a temperature gradient. The microscopic mechanisms include lattice vibration and, in conductive materials, the motion of free electrons. Since matter is required, heat conduction cannot occur through a perfect vacuum.
For a plane wall of area A, thickness Δx and temperature difference ΔT, the heat-flow rate is proportional to the area and temperature difference and inversely proportional

to the path length:

$$\dot{Q} \propto A\frac{\Delta T}{\Delta x}. \tag{5.1}$$

Introducing the thermal conductivity k, measured in $\mathrm{W\,m^{-1}\,K^{-1}}$, Fourier's law for one-dimensional conduction becomes:

$$\dot{Q} = kA\frac{\Delta T}{\Delta x}. \tag{5.2}$$

In differential form:

$$\dot{Q} = -kA\frac{dT}{dx}. \tag{5.3}$$

The minus sign indicates that heat flows from higher to lower temperature. The heat flux per unit area is:

$$q = -k\frac{dT}{dx}. \tag{5.4}$$

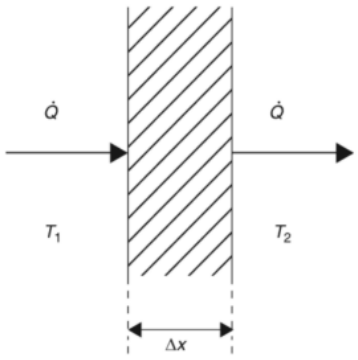


Figure 5.2: One-dimensional heat conduction across a solid wall with surfaces at different temperatures. Credits: [16]

For three-dimensional conduction in Cartesian coordinates:

$$\vec{q} = -k\nabla T = -k\left(\frac{\partial T}{\partial x}\vec{u}_x + \frac{\partial T}{\partial y}\vec{u}_y + \frac{\partial T}{\partial z}\vec{u}_z\right). \tag{5.5}$$

In thermal-network form, conduction is often expressed using a thermal resistance:

$$R_{cond} = \frac{L}{kA} \tag{5.6}$$

or a thermal conductance:

$$G = \frac{kA}{L}. \tag{5.7}$$

The heat flow between two nodes is then:

$$\dot{Q} = G\left(T_1 - T_2\right). \tag{5.8}$$

For a lunar rover, conduction is relevant inside structural panels, between electronic units and their mounting interfaces, between internal and external shells, through insulation supports, and at the contact between wheels and regolith.

5.4.2 Contact Conduction

In real assemblies, the thermal path between two parts is not determined only by the bulk material. Contact surfaces are rough at microscopic scale, so the real contact area is smaller than the apparent area. The contact conductance depends on surface roughness, contact pressure, material hardness, coatings, fasteners, washers, thermal interface materials and possible gaps. The heat transfer through a contact interface can be represented by:

$$\dot{Q}_{contact} = h_c A_c \left(T_1 - T_2\right) \tag{5.9}$$

where h_c is the contact conductance per unit area and A_c is the contact area. During preliminary design, contact conductance is frequently uncertain; therefore it should be treated as a sensitivity parameter. This is especially important for rover wheel–ground contact and for internal component mounting interfaces.

5.4.3 Convection

Convection is the exchange of energy between a solid surface and a moving fluid. It combines conduction in the fluid close to the wall with the macroscopic motion of the fluid. Convection can be classified into:

- **natural or free convection**, driven by buoyancy forces generated by temperature-dependent density variations;
- **forced convection**, driven by external mechanisms such as pumps, fans or imposed flow.

The convective heat-flow rate is described by Newton's law of cooling:

$$\dot{Q} = hA \left(T_a - T_s\right) \tag{5.10}$$

where T_s is the surface temperature, T_a is the fluid temperature, A is the surface area and h is the average convective heat-transfer coefficient. The coefficient h is not a pure material property; it depends on geometry, fluid state, laminar or turbulent regime and boundary conditions.
The Rayleigh number relates the time scale of thermal transport by diffusion to the time scale of transport by convection:

$$Ra = Gr\, Pr = \frac{g\beta \left(T_s - T_a\right) L^3}{\alpha\nu} \tag{5.11}$$

where g is gravitational acceleration, β is the thermal expansion coefficient, L is a characteristic length, α is thermal diffusivity and ν is kinematic viscosity.
The Grashof and Prandtl numbers are:

$$Gr = \frac{g\beta \left(T_s - T_a\right) L^3}{\nu^2} \tag{5.12}$$

$$Pr = \frac{\nu}{\alpha} \tag{5.13}$$

The thermal diffusivity is:

$$\alpha = \frac{k}{\rho c_p}. \tag{5.14}$$

The Nusselt number, which relates convective to conductive heat transfer in the fluid, is:

$$Nu = \frac{hL}{k}. \tag{5.15}$$

For simple geometries, the Nusselt number may be correlated with dimensionless parameters. For natural convection:

$$Nu = c\, Gr^a Pr^b \tag{5.16}$$

whereas for forced convection:

$$Re = \frac{VL}{\nu} \tag{5.17}$$

$$Nu = c\, Re^a Pr^b. \tag{5.18}$$

For the lunar rover external environment, convection is neglected because there is no significant atmosphere. However, it can still be relevant inside sealed fluidic components, heat pipes or internal thermal-control devices [27].

5.4.4 Radiation

All bodies at non-zero absolute temperature emit electromagnetic radiation. Thermal radiation is the portion of electromagnetic radiation able to affect the thermal state of matter. It includes wavelengths approximately from 0.1 µm to 100 µm, covering part of the ultraviolet, the visible range and the infrared range [16].
Unlike conduction and convection, radiation does not require matter to propagate; therefore it is the dominant heat-transfer mode in vacuum. Radiation is complex because it is spectral and directional. A surface receiving incident radiation can absorb, reflect and transmit fractions of the incident energy, while also emitting its own radiation. For an incident radiant flux Φ_i:

$$\Phi_i = \Phi_a + \Phi_r + \Phi_t \tag{5.19}$$

where Φ_a, Φ_r and Φ_t are the absorbed, reflected and transmitted contributions. The spectral intensity of emitted radiation is defined as the rate at which radiant energy is emitted at wavelength λ in a given direction, per unit projected area, solid angle and wavelength interval:

$$I_{\lambda,e}\left(\lambda, \theta, \phi, T\right) = \frac{\partial \dot{Q}}{dA \cos\theta \, d\omega \, d\lambda}. \tag{5.20}$$

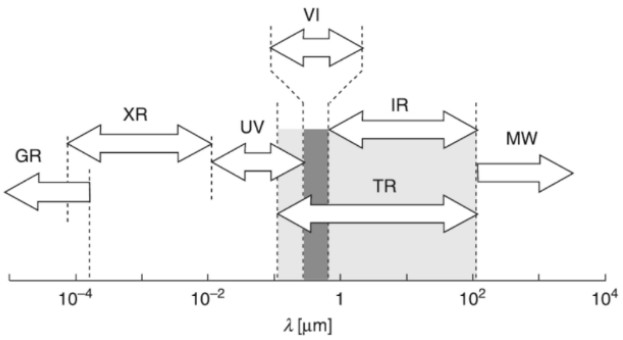


Figure 5.3: Electromagnetic-spectrum classification highlighting the wavelength range relevant to thermal radiation. Credits: [16]

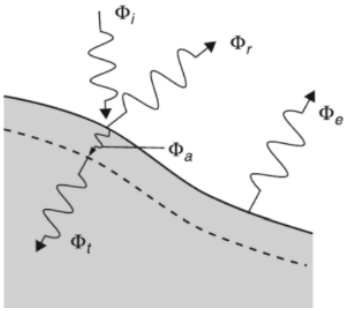


Figure 5.4: Absorption, reflection and transmission of incident radiation at a surface. Credits: [16]

The solid angle in spherical coordinates is:

$$d\omega = \sin\theta \, d\theta \, d\phi. \tag{5.21}$$

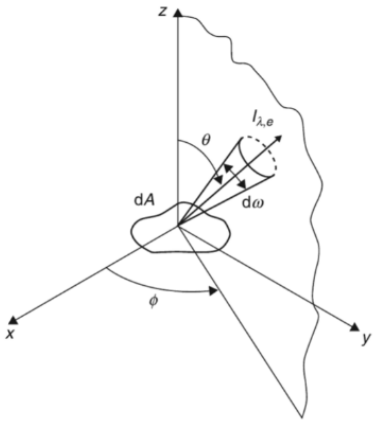


Figure 5.5: Directional definition used for emitted radiative intensity. Credits: [16]

The spectral hemispherical emissive power is:

$$E_\lambda(\lambda, T) = \int_0^{2\pi} \int_0^{\pi/2} I_{\lambda,e}(\lambda, \theta, \phi, T) \cos\theta \sin\theta \, d\theta \, d\phi. \tag{5.22}$$

The total emissive power is obtained by integrating over the whole spectrum:

$$E(T) = \int_0^\infty E_\lambda(\lambda, T)\, d\lambda. \tag{5.23}$$

An ideal blackbody absorbs all incident radiation and is the maximum possible emitter at a given temperature and wavelength. It is diffuse and, in vacuum, its emission depends only on its temperature. The total emissive power of a blackbody is given by the Stefan–Boltzmann law:

$$E_b(T) = \sigma T^4 \tag{5.24}$$

with:

$$\sigma = 5.67 \times 10^{-8}\ \mathrm{W\,m^{-2}\,K^{-4}}. \tag{5.25}$$

Real surfaces emit only a fraction of the blackbody emission. The spectral emissivity is defined as:

$$\varepsilon(\lambda, T) = \frac{E_\lambda(\lambda, T)}{E_{b,\lambda}(\lambda, T)}. \tag{5.26}$$

For a grey diffuse surface, the emitted power is:

$$E = \varepsilon \sigma T^4. \tag{5.27}$$

The radiative heat exchange between a surface and an environment at temperature T_{env} can be approximated as:

$$\dot{Q}_{rad} = \varepsilon \sigma A \left(T^4 - T_{env}^4\right). \tag{5.28}$$

5.5 Thermo-Optical Properties and Semi-Grey Modelling

The optical response of a spacecraft surface depends on wavelength. For this reason, spacecraft thermal analysis usually adopts a semi-grey approximation. The spectrum is divided into a solar range and an infrared thermal range. In the solar range, the relevant property is the solar absorptivity α. In the infrared range, the relevant property is the emissivity ε. For an opaque surface in the solar range:

$$\alpha + \rho = 1 \tag{5.29}$$

where ρ is reflectivity. In the infrared range:

$$\varepsilon + \rho_{IR} = 1. \tag{5.30}$$

Thermo-optical properties are functions of the material, surface finish, temperature, contamination state and degradation history. Polishing, painting, coating or applying films can significantly modify emissivity and absorptivity. This is why coatings and surface finishes are among the simplest and most powerful passive thermal-control tools.

The ratio α/ε gives an immediate qualitative indication of the surface equilibrium tendency under solar illumination. A high value of α/ε leads to high equilibrium

temperatures, because the surface absorbs solar energy efficiently but emits thermal infrared radiation less efficiently. A low value of α/ε is useful for radiator-like behaviour because the surface absorbs relatively little solar radiation and emits infrared radiation efficiently.
For a lunar rover, the correct choice of external thermo-optical properties is particularly important. The same surface may be exposed to direct solar radiation, reflected radiation from the lunar ground and infrared exchange with regolith at a temperature varying over the lunar day. Dust deposition can also modify optical properties and reduce the effectiveness of coatings and MLI external layers.

5.6 View Factors, Grey-Body Exchange and Radiative Coupling

Radiative heat exchange depends on geometry. The geometrical or configuration factor F_{i-j} is defined as the fraction of energy leaving surface i that directly reaches surface j. For finite diffuse surfaces, the view factor is:

$$F_{A-B} = \frac{1}{A_A} \int_{A_A} \int_{A_B} \frac{\cos\theta_A \cos\theta_B}{\pi L^2} \, dA_B \, dA_A \tag{5.31}$$

where A_A and A_B are the areas, θ_A and θ_B are the angles between surface normals and the connecting line, and L is the distance between the differential areas [28].

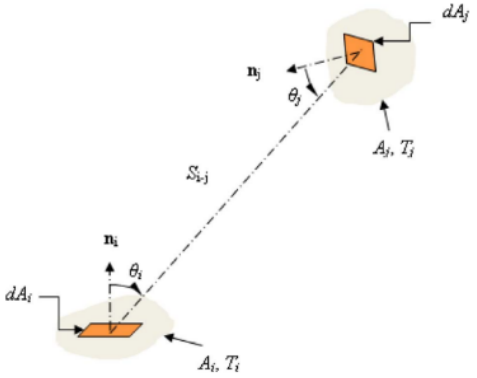


Figure 5.6: Radiative exchange geometry between two differential surface elements. Credits: [29]

View factors satisfy several properties:

$$0 \leq F_{i,j} \leq 1, \tag{5.32}$$

$$\sum_j F_{i,j} = 1 \quad \text{for a closed enclosure,} \tag{5.33}$$

$$A_i F_{i,j} = A_j F_{j,i}, \tag{5.34}$$

$$F_{i,j+k} = F_{i,j} + F_{i,k}, \tag{5.35}$$

$$F_{i+j,k} = \frac{A_i F_{i,k} + A_j F_{j,k}}{A_i + A_j}. \tag{5.36}$$

For two black surfaces, the net radiative heat exchange can be written as:

$$\dot{Q}_{i-j} = \sigma A_i F_{i,j} \left(T_i^4 - T_j^4\right). \tag{5.37}$$

Real surfaces are not black. Grey-body radiation factors or interchange factors are therefore introduced to include emissivity, reflectivity and multiple reflections. In a simple blackbody-to-grey-surface approximation, one may write an effective radiative conductance-like quantity. In a complete grey-diffuse enclosure, methods such as Gebhart's method can be used to account for reflections and absorption among multiple surfaces [28, 30].
For complex rover geometry, hand calculation of view factors is not practical. The rover contains wheels, panels, internal and external surfaces, insulation layers and a surrounding ground plane. Modern thermal software therefore computes radiative coupling automatically using ray-tracing or Monte Carlo methods.

5.7 General Nodal Heat Balance

The thermal behaviour of a spacecraft or rover can be represented by a set of nodal heat-balance equations. For a generic node i, the transient heat balance is:

$$C_i \frac{dT_i}{dt} = \dot{Q}_{int,i} + \dot{Q}_{env,i} + \sum_j G_{ij}(T_j - T_i) + \sum_j \sigma K_{ij}(T_j^4 - T_i^4) \tag{5.38}$$

where C_i is the thermal capacitance, $\dot{Q}_{int,i}$ is the internal dissipation, $\dot{Q}_{env,i}$ is the external environmental load, G_{ij} are conductive conductances and K_{ij} are radiative coupling coefficients. The thermal capacitance of node i is:

$$C_i = m_i c_{p,i}. \tag{5.39}$$

For a differential volume:

$$C = \rho c_p \Delta V. \tag{5.40}$$

For a rechargeable lunar mini rover, the external load can be decomposed into:

$$\dot{Q}_{env} = \dot{Q}_{solar} + \dot{Q}_{albedo} + \dot{Q}_{IR,lunar} - \dot{Q}_{deep\,space} \tag{5.41}$$

where the signs depend on the adopted convention. Direct solar radiation is driven by surface orientation and solar incidence angle; albedo depends on the lunar reflectivity and geometric coupling with the ground; lunar infrared depends on regolith temperature and view factor; and deep-space emission depends on exposed surface emissivity and sink temperature.

5.8 Thermal Mathematical Networks

A thermal network is a discrete representation of the thermal system. Nodes represent thermal capacitances and conductors represent heat-transfer paths. The analogy with electrical circuits is useful:
Thermal networks may include:

Table 5.2: Analogy between thermal and electrical quantities.

Thermal quantity	**Electrical analogue**
Temperature	Voltage
Heat-flow rate	Current
Thermal resistance	Electrical resistance
Thermal conductance	Electrical conductance
Thermal capacitance	Electrical capacitance
Internal heat generation	Current source
Boundary temperature	Voltage source

- diffusion nodes, which have thermal capacitance and temperature time history;
- arithmetic nodes, used to impose algebraic relations or boundary conditions;
- boundary nodes, whose temperature is prescribed;
- linear conductors, representing conduction or convection;
- radiation conductors, representing nonlinear radiative exchange;
- heat loads, representing internal dissipations or absorbed environmental fluxes.

The challenge for the thermal engineer is to build a network accurate enough to capture relevant thermal gradients but simple enough to remain computationally efficient. Too few nodes may hide critical gradients, while too many nodes increase computational cost and may introduce unnecessarily small time constants. A good nodalisation therefore depends on the physics of the problem, the expected gradients, the project phase and the required accuracy.

5.8.1 Linear Conductors

A linear conductor between nodes i and j has the form:

$$\dot{Q}_{ij} = G_{ij}(T_i - T_j). \tag{5.42}$$

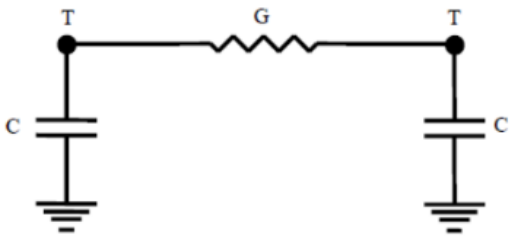


Figure 5.7: Schematic representation of a lumped thermal network. Credits: [30].

Several conductive paths can be connected in series or parallel. In series, the equivalent resistance is:

$$R_{eq} = \sum_{n} R_n \tag{5.43}$$

whereas in parallel:

$$G_{eq} = \sum_{n} G_n. \tag{5.44}$$

These relations are useful for simplified modelling of stacked insulation layers, mounting interfaces, straps, brackets and equivalent paths through mechanical supports.

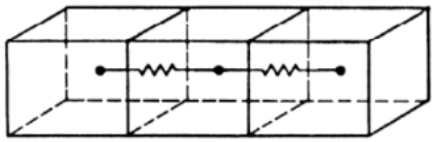


Figure 5.8: Linear conductive link between thermal nodes. Credits: [30]

5.8.2 Radiation Conductors

A radiation conductor represents radiative exchange between surfaces. Since radiation depends on the fourth power of temperature, the exchange is nonlinear:

$$\dot{Q}_{rad,ij} = \sigma K_{ij}(T_i^4 - T_j^4). \tag{5.45}$$

For numerical solution, radiation terms may be linearised around a reference temperature at each iteration. The effective linearised conductance is proportional to the derivative of the fourth-power term and depends on the current temperature estimate.

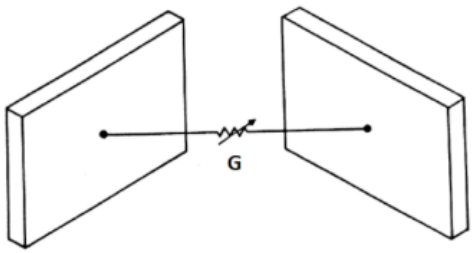


Figure 5.9: Nonlinear radiative link between thermal nodes. Credits: [30]

5.9 Types of Thermal Analysis

5.9.1 Steady-State Analysis

In steady-state analysis, temperatures are assumed constant in time:

$$\frac{dT_i}{dt} = 0. \tag{5.46}$$

The nodal energy balance reduces to:

$$\sum \dot{Q}_i = 0. \tag{5.47}$$

Steady-state analysis is useful for preliminary hot and cold equilibrium estimates. However, the lunar surface problem is rarely purely steady because the lunar day-night cycle is long and the regolith thermal inertia strongly affects the surface temperature evolution.

5.9.2 Transient Analysis

Transient analysis retains thermal capacitance and solves the time evolution of node temperatures. It is essential when boundary conditions or internal dissipations vary with time. For a lunar rover, transient analysis is required to evaluate changes in illumination, regolith temperature, internal dissipation and thermal lag between external surfaces and the protected internal region. In the present work, simulations extended over a complete lunar day are used as an environmental design envelope; they do not represent one continuous rover sortie. The nominal operational concept remains based on approximately three-hour surface traverses followed by return to the charging station.

5.9.3 Hot and Cold Cases

Hot and cold cases are used to evaluate thermal extremes. A hot case combines high solar input, high internal dissipation, unfavourable attitude or geometry, degraded radiator performance and high environmental infrared load. A cold case combines minimum solar input, low internal dissipation, high radiative loss to deep space and low ground infrared emission.
For a rechargeable lunar mini rover, the hot and cold cases depend strongly on latitude, illumination conditions and the operational phase. At equatorial latitudes, local noon and lunar midnight are natural hot and cold drivers. At high latitudes, grazing solar incidence and local shadowing become dominant. Near the poles, areas of near-continuous illumination may coexist with permanently shadowed regions. This makes latitude parametrisation a crucial feature of the lunar surface model.

5.9.4 Sensitivity Analysis

Sensitivity analysis evaluates how model outputs vary when uncertain inputs are changed. Important parameters include:

- solar absorptivity and infrared emissivity;
- material conductivity, density and specific heat;
- contact conductance;
- internal dissipation;
- heater set points, when heaters are included;
- MLI effective emissivity;
- lunar soil properties;

- regolith albedo and infrared emissivity;
- latitude and solar incidence angle;
- nodal resolution and time step.

Sensitivity analysis is important during preliminary design because many parameters are not known with high confidence.

5.10 Numerical Methods for Thermal Analysis

Real spacecraft thermal problems cannot generally be solved analytically. They include complex geometry, nonlinear radiation, time-dependent boundary conditions, temperature-dependent properties and many conductive interfaces. Numerical methods are therefore used. The two principal methods are the Finite Difference Method and the Finite Element Method.

5.10.1 Finite Difference Method

The Finite Difference Method approximates derivatives in differential equations by finite differences. The physical domain is divided into nodes, and the continuous heat-transfer equation is transformed into a system of finite-difference equations. Two assumptions are fundamental:

- physical properties are constant within each node;
- each node is isothermal.

Nodes are linked by conductive, convective or radiative conductors representing real heat paths. For a one-dimensional mesh, Taylor expansion around x_0 gives:

$$T(x_0 + \Delta x) = T(x_0) + \left.\frac{\partial T}{\partial x}\right|_{x_0} \Delta x + \left.\frac{\partial^2 T}{\partial x^2}\right|_{x_0} \frac{\Delta x^2}{2!} + \left.\frac{\partial^3 T}{\partial x^3}\right|_{x_0} \frac{\Delta x^3}{3!} + \dots \tag{5.48}$$

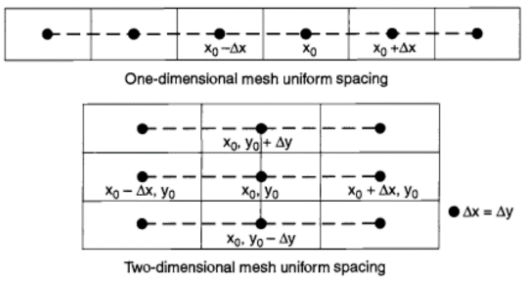


Figure 5.10: Examples of one- and two-dimensional finite-difference discretisation. Credits: [4]

The first derivative can be approximated as:

$$\left.\frac{\partial T}{\partial x}\right|_{x_0} \approx \frac{T(x_0 + \Delta x) - T(x_0)}{\Delta x} + o(\Delta x) \tag{5.49}$$

and the second derivative as:

$$\left.\frac{\partial^2 T}{\partial x^2}\right|_{x_0} \approx \frac{T(x_0+\Delta x) - 2T(x_0) + T(x_0-\Delta x)}{\Delta x^2} + o(\Delta x^2). \tag{5.50}$$

The general transient heat-transfer equation with temperature-dependent conductivity can be written as:

$$\rho c_p \frac{\partial T}{\partial t} = \frac{\partial}{\partial x}\left(k_x(T)\frac{\partial T}{\partial x}\right) + \frac{\partial}{\partial y}\left(k_y(T)\frac{\partial T}{\partial y}\right) + \frac{\partial}{\partial z}\left(k_z(T)\frac{\partial T}{\partial z}\right) + \dot{Q}(T,t). \tag{5.51}$$

For a node n and adjacent nodes $n+1$ and $n-1$, the conductive term in the x direction can be rewritten in terms of conductances:

$$G_{n+1,n}\left(T_{n+1} - T_n\right) - G_{n,n-1}\left(T_n - T_{n-1}\right). \tag{5.52}$$

The nodal capacitance is:

$$C_n = \rho c_p \Delta x A. \tag{5.53}$$

The nodal radiative term between two grey surfaces can be written as:

$$\sigma A \zeta_{n,n+1}\left(T_n^4 - T_{n+1}^4\right) \tag{5.54}$$

where $\zeta_{n,n+1}$ is the grey-body radiative exchange factor. The time derivative can be approximated using a variable implicit weighting factor θ:

$$T(t^* + \Delta t) = T(t^*) + \theta \left.\frac{\partial T}{\partial t}\right|_{t^*+\Delta t} \Delta t + (1-\theta)\left.\frac{\partial T}{\partial t}\right|_{t^*} \Delta t. \tag{5.55}$$

Combining conductors, radiative exchange and source terms leads to the general finite-difference nodal equation:

$$C_n \frac{T_n(t+\Delta t) - T_n(t)}{\Delta t} = \theta \left[\sum_{j=1}^{N} G_{jn}(T_j - T_n) + \sigma \sum_{j=1}^{N} \zeta_{jn} A_n (T_j^4 - T_n^4) + \dot{Q}_n(T_n, t)\right]_{t^*+\Delta t} \tag{5.56}$$

$$+ (1-\theta)\left[\sum_{j=1}^{N} G_{jn}(T_j - T_n) + \sigma \sum_{j=1}^{N} \zeta_{jn} A_n (T_j^4 - T_n^4) + \dot{Q}_n(T_n, t)\right]_{t^*}. \tag{5.57}$$

The number of algebraic equations is equal to the number of non-boundary nodes. Boundary nodes have prescribed temperature histories and are not unknowns in the same way as diffusion nodes.

5.10.2 Explicit, Implicit and Crank–Nicolson Schemes

The value of θ determines the integration scheme:

- $\theta = 0$: Euler forward explicit method;

- $\theta = 1/2$: Crank–Nicolson method;
- $\theta = 1$: Euler backward implicit method.

For $\theta = 0$, each unknown temperature at time $t + \Delta t$ is computed directly from known temperatures at time t. This is simple but conditionally stable. The stability of the explicit method is limited by the smallest thermal time constant in the network:

$$\tau_n = \frac{C_n}{\sum_j G_{nj}}. \tag{5.58}$$

Radiation conductances can be linearised as:

$$G_{nj} = \sigma \zeta_{nj} A_j \left(T_n^2 + T_j^2\right)\left(T_n + T_j\right). \tag{5.59}$$

The explicit solution is stable only if the time step is lower than the minimum time constant of the thermal network. In SINDA terminology, the minimum time constant is referred to as CSGMIN. The default time-step logic may be expressed as:

$$\Delta t = 0.95 \frac{CSGMIN}{CSGFAC} \tag{5.60}$$

with $CSGFAC$ equal to one by default. For $\theta = 1$, the scheme is implicit. Temperatures at $t + \Delta t$ appear in a coupled system of equations. For the linear diffusion problem, the backward-Euler scheme is unconditionally stable with respect to the time step; this does not mean that arbitrarily large steps are accurate. In nonlinear thermal networks, large time steps may increase truncation error and the number of iterations required for convergence.
SINDA uses convergence criteria such as DRLXCA and ARLXCA for diffusion and arithmetic nodes. In practice, implicit methods are often faster for large models, but excessively large time steps may become inefficient because each step requires more iterations. The stability behaviour can be summarised as follows [4]:

- $\theta = 0$ is stable only for time steps below the minimum time constant;
- $\theta < 1/2$ has conditional stability;
- $\theta \geq 1/2$ provides unconditional stability in the usual linear sense.

5.10.3 Numerical Errors in FDM

Three main types of numerical errors may occur in finite-difference thermal analysis:

- **truncation error**: caused by replacing the differential equation with a finite-difference approximation. It depends on mesh size and time step. Uniform meshes are preferred because the truncation error can be of second order, while non-uniform meshes may introduce first-order errors;
- **stability error**: associated with unstable numerical integration schemes, especially explicit methods when the time step exceeds the stability limit;

- **round-off error**: caused by finite computer precision. On modern 64-bit computers, this is rarely the dominant source of error.

Reducing truncation error requires finer meshes and smaller time steps, but this increases computational cost. Therefore, thermal modelling always involves a compromise between accuracy and execution time. For a parametric lunar rover model, this compromise is particularly important because many latitudes, configurations and sensitivity cases may need to be simulated.

5.10.4 Finite Element Method

The Finite Element Method is another numerical approach for solving heat-transfer problems. It originated in structural analysis and is widely used when complex geometries and coupled thermo-structural behaviour are important. In FEM, the geometry is discretised into finite elements. Temperature values are computed at element nodes, and the temperature distribution inside each element is approximated by interpolation or basis functions. A finite-element approximation can be written as:

$$T(t, a_i) = \sum_{i=0}^{N} a_i \Phi_i(t) \tag{5.61}$$

where a_i are degrees of freedom, equal to nodal temperatures in a thermal problem, and Φ_i are basis functions. A simple linear basis function can vary from zero to one across an element, although higher-order functions may be quadratic, cubic or quartic. Typical finite elements include:

- one-dimensional bar elements;
- two-dimensional rectangular or triangular elements;
- three-dimensional tetrahedral or hexahedral elements.

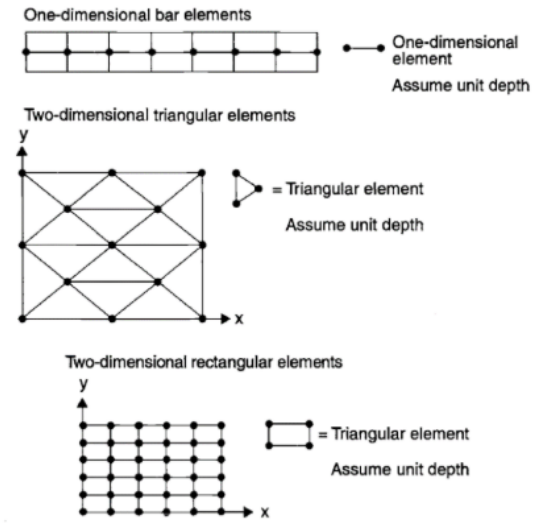


Figure 5.11: Examples of one- and two-dimensional finite-element discretisation. Credits: [4]

Accuracy can be improved either by refining the mesh or by increasing the order of the basis functions. Unlike FDM, the magnitude of the error is not always directly predictable before the analysis. Therefore, convergence studies or initially fine meshes are often required.

5.10.5 Comparison Between FDM and FEM

FDM and FEM can both solve heat-transfer problems, but their advantages differ. Finite-difference and lumped-parameter network methods are particularly effective for spacecraft thermal analysis because many system-level models are built from thermal nodes connected by equivalent conductive and radiative paths. Simple geometric primitives are also convenient for radiation analysis and Monte Carlo ray tracing. Small components or equipment groups can therefore be represented by one or a few thermal nodes when detailed internal gradients are not required. FEM is instead more naturally suited to resolving spatial temperature fields in geometrically detailed solids.
FEM is more flexible for irregular geometries and detailed thermo-structural problems. It is often more appropriate when the exact geometry strongly affects conduction paths or when the thermal model must be coupled to stress and deformation analysis. For the present type of system-level radiation-driven problem, a detailed FEM model would generally require more geometric degrees of freedom than a lumped thermal network and would not necessarily improve the accuracy of uncertain interface and environmental parameters. FEM becomes more attractive when detailed local conduction, stress or deformation fields are required.
For radiation-driven space-environment problems, FDM is often preferred because:

- it is computationally efficient;
- it integrates naturally with thermal networks;
- it supports lumped modelling of small components;
- it is compatible with Monte Carlo radiation analysis;
- it allows the analyst to focus on the dominant physics rather than unnecessary geometrical detail.

For the present lunar rover, a finite-difference lumped-parameter approach is appropriate because the dominant external exchange is radiative and the lunar surface can be discretised into layers.

5.11 Chapter Summary

This chapter established the theoretical and numerical framework used in the subsequent lunar-surface and rover models. The principal external heat-transfer mechanisms for the rover are radiation and solid/contact conduction, while external convection is neglected in the lunar vacuum. The system is represented through a transient thermal network in which nodal capacitances, conductive links, radiative exchange and time-dependent environmental or internal heat loads are solved together.

The chapter also distinguished the general component-level ECSS thermal-verification process from the preliminary system-level approach adopted in this thesis. Since the final rover equipment has not yet been selected, the numerical results are compared first with the internal design envelope defined for the protected rover region. Component-specific operating and survival limits, together with the appropriate project-phase uncertainty margins, belong to a later verification stage.
Finally, the finite-difference/lumped-parameter approach was identified as appropriate for the present radiation-dominated preliminary model. It provides the numerical basis for the regolith model, rover thermal network and parametric sensitivity analyses developed in the following chapters with Thermal Desktop, RadCAD and SINDA/FLUINT.

Chapter 6

Thermal Model and Thermal Desktop

"All models are wrong,
but some are useful."

— George E. P. Box
Empirical Model-Building and Response Surfaces

6.1 Geometrical Mathematical Model and Thermal Mathematical Model

A complete thermal model is usually divided into two coupled parts: the Geometrical Mathematical Model and the Thermal Mathematical Model.

6.1.1 Geometrical Mathematical Model

The GMM is the geometrical representation used for radiation calculations and environmental heating. It contains the radiating surfaces, their location, their orientation and their thermo-optical properties. Surfaces may be represented as thin shells or solid shapes. The analyst can activate or deactivate surfaces for radiative participation depending on whether they contribute to the radiative problem. The GMM is used to compute:

- interchange factors and view factors between surfaces;
- direct solar absorption;
- reflected radiation absorption;
- infrared radiation exchange;
- shadowing and self-shadowing;
- planetary or lunar environmental heating rates.

For a lunar rover, the GMM must represent both the rover external geometry and the surrounding lunar ground. The relative orientation of panels, wheels and ground surfaces affects solar absorption, albedo absorption and infrared exchange. If the rover is close to the ground, the view factor toward the lunar surface may be comparable to or larger than the view factor toward deep space for downward-facing and lateral surfaces.

6.1.2 Thermal Mathematical Model

The TMM is the thermal network solved by the thermal solver. It consists of nodes, capacitances, conductors, radiation conductors, boundary nodes and heat loads. It is used to compute temperatures and heat flows. The TMM receives inputs from the GMM after radiative analysis. These inputs include radiation coupling coefficients and heating-rate functions. The TMM also includes conductive paths and internal heat dissipations that are not purely geometrical radiative quantities.
The distinction between GMM and TMM is important. A surface can be part of the GMM for radiation, but its corresponding thermal node must be correctly connected in the TMM to the rest of the system. Conversely, a lumped internal component may be thermally important in the TMM even if it has no direct participation in the GMM because it is not externally radiating.

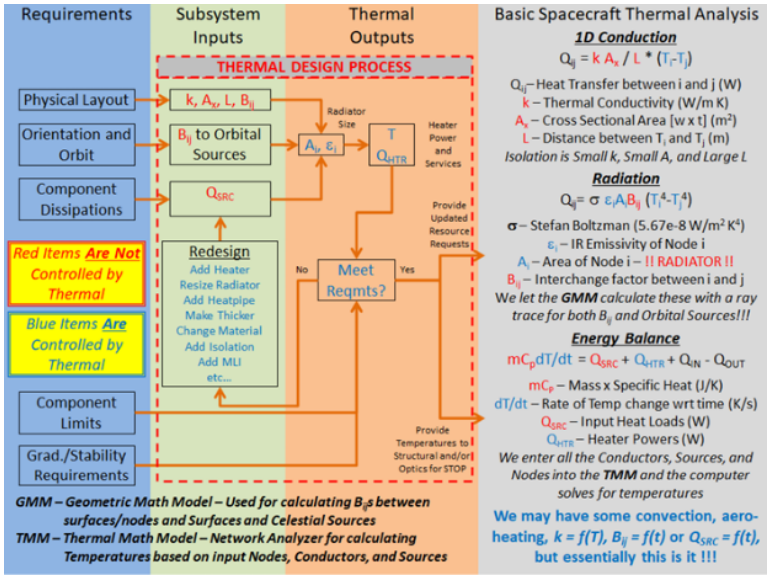


Figure 6.1: Thermal Analysis Process. Credits: [31]

6.2 Integrated Thermal Analysis Codes

Since the 1990s, integrated thermal-analysis software tools have been widely used in spacecraft design. Their objective is to help the analyst build thermal models efficiently and to let the computer perform repetitive calculations, while the engineer focuses on the physical interpretation of the problem [32].
The main elements of an integrated thermal-analysis tool are:

- geometrical and thermal model builder;
- radiation analyser, either grey-diffuse or Monte Carlo based;
- thermal analyser, often FDM based;
- orbital or environmental analyser;
- pre-processing and post-processing tools;
- CAD import capability or CAD-based interface.

Thermal Desktop belongs to this class of tools. It supports model construction, radiative analysis, thermal solution and post-processing in an integrated environment.

6.3 Thermal Desktop

Thermal Desktop is the thermal modelling tool used for the analyses in this thesis. It is based on an AutoCAD interface and integrates with SINDA/FLUINT for thermal and fluid solution. It is widely used in the space industry because it can model conduction, radiation and fluid thermal interactions with high precision [31]. Thermal Desktop allows the analyst to:

- build surface and solid geometries;
- assign materials, thicknesses and optical properties;
- define nodalisation;
- define conductive conductors and contactors;
- create internal heat loads;
- define radiation cases;
- compute environmental heating rates;
- export thermal networks to SINDA/FLUINT;
- visualise temperature maps, heat flows and time histories.

Two principal modules are used in the Thermal Desktop workflow:

- **RadCAD**, for radiation analysis;
- **SINDA/FLUINT**, for thermal and fluid solution.

Thermal Desktop operates by connecting the GMM and TMM. The GMM is used to compute radiative quantities, while the TMM is solved to obtain node temperatures. This is the workflow adopted for the lunar rover and for the latitude-parametric lunar surface model.

6.4 SINDA/FLUINT

SINDA/FLUINT is the solver associated with Thermal Desktop. It solves thermal and fluid networks using a lumped-parameter finite-difference formulation. Historically developed for NASA applications, SINDA includes a processor and execution library. The preprocessor reads an input file and builds the executable thermal model, while library routines are selected to evaluate temperatures and heat flows [4, 32].
SINDA/FLUINT can manage:

- steady-state thermal analyses;
- transient thermal analyses;
- nonlinear radiation;
- temperature-dependent properties;
- user-defined heat loads and conductors;
- fluid networks, including incompressible, compressible and two-phase flows;
- complex models assembled from simpler submodels.

The generic nodal equation solved by SINDA/FLUINT can be represented as:

$$C_i \frac{dT_i}{dt} = \sum_j G_{ij}(T_j - T_i) + \sum_j \sigma K_{ij}(T_j^4 - T_i^4) + \dot{Q}_i. \tag{6.1}$$

The ability to combine submodels is important for spacecraft and rover applications. A lunar rover thermal model may include a regolith submodel, external shell submodel, internal equipment submodel, wheels, payload, batteries and possible battery, mobility and possible fluidic thermal-control subsystems.

6.5 RadCAD and Radiation Analysis

RadCAD is the radiation module associated with Thermal Desktop. Its role is to compute radiation exchange factors and heating rates. In a lunar analysis, this module is essential because the external heat exchange is dominated by radiation. RadCAD can compute:

- surface-to-surface radiation couplings;
- view factors and interchange factors;
- direct solar heating;
- albedo heating;
- planetary or lunar infrared heating;
- shadowing and occultation;

- diffuse and specular reflection effects;
- heating-rate functions for time-dependent analyses.

Radiation analysis requires correct thermo-optical properties. In Thermal Desktop, the software distinguishes between solar optical properties and infrared optical properties depending on the type of radiation being modelled. Direct solar radiation, albedo, diffuse sky solar and diffuse sky albedo use solar optical properties. Planetshine, lunar infrared and diffuse sky infrared use infrared optical properties.

6.6 Modelling Thermal Conduction in Thermal Desktop

In Thermal Desktop, conduction is modelled using thermal nodes connected by conductors. Conductors are TMM elements representing heat-flow paths between nodes. The basic relation is:

$$Q = G\Delta T \tag{6.2}$$

where:

$$G = \frac{kA}{L}. \tag{6.3}$$

Here k is the thermal conductivity, A is the cross-sectional area crossed by heat flow and L is the distance between nodes [4]. The software allows complex conductive pathways to be defined through nodal networks. Large components can be treated as lumped nodes with equivalent thermal resistance, while detailed regions can be discretised more finely. Manual conductors can represent component mounting, harnesses, brackets, contact interfaces and equivalent paths not explicitly represented by geometry.
For the lunar rover, the most important conductive paths are:

- internal conduction through structural panels;
- conductive coupling between electronic boxes and their supports;
- panel-to-panel conduction;
- shell-to-insulation support conduction;
- wheel-to-ground contact conduction;
- conduction through possible thermal straps;
- conduction through battery or payload mounting interfaces.

6.7 Modelling Thermal Radiation in Thermal Desktop

Radiation modelling in Thermal Desktop is performed by assigning optical properties to surfaces and running a RadCAD radiation case. The software computes radiative

exchange factors and heating rates using Monte Carlo Ray Tracing. Surfaces may be diffuse or specular, and shadowing effects are automatically detected. For radiation to a blackbody sink, a simplified radiative conductance-like coefficient can be written as:

$$G_{ij} = \sigma \varepsilon F_{ij} A_i. \tag{6.4}$$

For grey-body radiation, an interchange factor is used instead of a simple view factor, because reflections and emissivities must be included. In lunar rover analysis, the software must consider:

- radiation from external rover surfaces to deep space;
- radiation between rover surfaces;
- radiation between rover and lunar ground;
- reflected solar flux from the ground;
- infrared emission from the ground;
- self-shadowing by wheels or structural elements;
- time-dependent solar incidence.

6.8 RadK and Radiation Conductors

RadK represents surface-to-surface radiative exchange in Thermal Desktop. It is a radiative coupling parameter used as a radiation conductor in the thermal model. The radiative heat transfer between surfaces i and j is:

$$Q_{rad} = \sigma RadK_{ij} \left(T_i^4 - T_j^4 \right). \tag{6.5}$$

For a simple diffuse case, one may write:

$$RadK_{ij} = \varepsilon_i A_i F_{ij} \tag{6.6}$$

while for grey bodies the interchange factor replaces the simple view-factor treatment. RadK depends on geometry, area, view factors or interchange factors, and thermo-optical properties.
In Thermal Desktop, RadK values are computed by RadCAD using Monte Carlo ray tracing. The values are then introduced as radiative conductors in the TMM and solved by SINDA/FLUINT. Radiation is nonlinear, SINDA/FLUINT handles these conductors iteratively, often by linearising the fourth-power relation around the current temperature estimate.

6.9 Heating Rate Functions

Heating rates are environmental heat loads absorbed, emitted or transferred by a surface per unit time. In Thermal Desktop, heating-rate calculations are controlled by the selected radiation sources. By activating or deactivating checkboxes, the analyst can include or exclude specific contributions from the heating-rate output. For a Moon-centred or lunar surface problem, the relevant sources include:

- direct solar radiation;
- reflected solar radiation from the lunar surface;
- lunar infrared emission;
- diffuse sky solar contribution, if applicable in the model setting;
- diffuse sky albedo contribution, if applicable;
- diffuse sky infrared contribution, if applicable;
- internal heat generation applied separately in the TMM.

The direct solar power absorbed by a surface can be written as:

$$\dot{Q}_{solar} = \alpha A S \cos\theta \tag{6.7}$$

where S is the solar flux at the Moon and θ is the incidence angle between the solar direction and the surface normal. If the surface is shadowed or $\cos\theta < 0$, the direct contribution is zero. The albedo contribution depends on the lunar ground reflectivity, the solar incidence on the ground and the view factor between the rover surface and the illuminated regolith. The lunar infrared contribution depends on ground temperature, emissivity and radiative coupling.
Since regolith temperature changes with local time and depth, the infrared environment is transient. Heating rates are crucial because they transform the external environment into node-level heat loads for the thermal solution. In the rover model, they allow the same geometry to be simulated under different latitudes and illumination conditions.

6.10 Monte Carlo Ray Tracing

Monte Carlo Ray Tracing is a stochastic technique used to compute radiative exchange for complex geometries. The method treats radiation as a large number of rays representing photon paths. Rays are emitted from surfaces, traced through the geometry and followed until they are absorbed, reflected, transmitted or terminated. If N rays are emitted from surface i and m rays reach surface j, the view factor can be estimated as:

$$F_{i-j} \approx \frac{m}{N}. \tag{6.8}$$

When a ray strikes a surface, a fraction of its energy is absorbed and the remaining energy may be reflected or transmitted according to the surface optical properties. If

all ray energy is absorbed, the ray path terminates. If partial absorption occurs, the ray continues until its energy is dissipated or a termination criterion is met [29].
The accuracy of Monte Carlo methods improves as the number of rays increases, but computational time also increases. Therefore, the analyst must choose an appropriate trade-off between precision and computational cost. Thermal Desktop allows the number of rays and other ray-tracing settings to be adjusted according to the required accuracy.
Monte Carlo ray tracing is useful for:

- complex geometries;
- partial visibility between surfaces;
- shadowing and self-shadowing;
- multiple reflections;
- specular and diffuse reflections;
- radiation exchange in non-enclosed configurations.

For a lunar rover, Monte Carlo analysis is particularly appropriate because wheels, panels, local ground, possible terrain features and insulation surfaces create a complex radiation enclosure that is difficult to treat analytically.

6.11 Thermal Desktop Workflow Applied to a Lunar Rover

The Thermal Desktop workflow for a lunar rover can be organised in several steps.

6.11.1 Definition of Environment and Mission Cases

The first step is the definition of the mission cases. For a rover, this includes the latitude, local time, surface properties, operational phase and internal power mode. The lunar environment must include solar flux, albedo, infrared emission from the regolith and deep-space sink. Unlike a spacecraft in orbit, the rover exchanges heat with a nearby ground surface that has its own thermal inertia and temperature evolution.

6.11.2 Construction of the Lunar Surface Model

The lunar surface should be represented as an active thermal body. A simple constant-temperature boundary condition would not capture the transient nature of the regolith. The surface is therefore discretised into layers, with finer resolution near the top where the diurnal thermal wave produces the strongest gradients. Deeper layers may be coarser because temperature oscillations are damped with depth.
In the present thesis, the important modelling objective is the construction of a parametric lunar surface model valid for all latitudes. This means that the same model

structure can be used at the equator, mid-latitudes, high latitudes and near-polar regions by changing the latitude and the corresponding illumination conditions. This approach is more flexible than a model built only for a single landing site.

6.11.3 Rover Geometry and Nodalisation

The rover geometry is then introduced. The rover geometry is represented through the main structural surfaces, the internal equipment compartment, the wheels, the possible external insulation and the conductive interfaces. The level of detail is selected according to the thermal objective of the analysis rather than to reproduce every mechanical feature of the CAD geometry.
The nodalisation must reflect the expected thermal gradients. External panels exposed to different radiative environments may require several nodes. Small components with high internal conductivity can be lumped into single nodes. Wheels and ground-contact regions require particular attention because they combine contact conduction and radiation with the regolith.

6.11.4 Assignment of Material and Optical Properties

Each node or surface is assigned thermo-physical and thermo-optical properties. Thermo-physical properties include density, specific heat and thermal conductivity. Thermo-optical properties include absorptivity, emissivity and, where needed, reflectivity.
For external surfaces, optical properties are critical. A dark, high-absorptivity surface may reach high daytime temperatures. A high-emissivity low-absorptivity surface can act as a radiator. MLI can reduce radiative exchange but may also limit heat rejection. Therefore, coatings, MLI and conductive paths must be selected consistently.

6.11.5 Definition of Conductors and Contactors

Conductive paths are introduced through automatically generated conductors or manual conductors. Contactors represent interfaces whose conductance is not determined only by the geometry. In preliminary design, contact conductances may be uncertain and should be varied in sensitivity studies.
Typical contactors for the rover include component-to-panel interfaces, panel joints, wheel-to-ground contacts and possible support points between an internal box and an external shell or insulation layer.

6.11.6 Internal Heat Loads

Internal heat loads are assigned according to operating modes. A rechargeable rover may have different dissipations during standby, driving, communication, payload operation, heating, survival mode and battery recharge at the base station. These dissipations are applied as nodal heat loads in the TMM.
The thermal model must therefore be able to change heat loads between analysis cases. For example, a nominal sortie may include mobility, avionics and payload dissipation

for approximately three hours, while a recharge case may include battery and power-conditioning losses at the base station. A cold survival case may include only heaters and essential electronics.

6.11.7 Radiation Analysis and Thermal Solution

RadCAD computes radiation couplings and heating rates. SINDA/FLUINT then solves the thermal network. The outputs include node temperatures, temperature maps, heat flows, absorbed powers and radiative/conductive balances.
The results are compared with operational and survival limits, including uncertainty margins. If limits are violated, the thermal design is modified. Possible modifications include changes in coating, MLI, insulation thickness, contact conductance, radiator area, heater power, power profile or operational timeline.

6.12 Thermal Analysis of a Latitude-Parametric Lunar Rover Environment

A key contribution of the present work is the development of a lunar surface thermal model valid over a range of latitudes. The same environmental model can be adapted by changing the latitude parameter. This allows the rover thermal behaviour to be evaluated at equatorial, mid-latitude, high-latitude and near-polar conditions.
Latitude changes the thermal environment through several mechanisms:

- the maximum solar elevation changes;
- the local incidence angle on the ground changes;
- the absorbed solar heat flux changes;
- the ground temperature cycle changes;
- the lunar infrared load changes;
- shadowing becomes more important at high latitude;
- the hot and cold cases may shift with respect to local time.

At low latitudes, the lunar surface can experience very high daytime temperatures and very low night-time temperatures. At high latitudes, the Sun remains close to the horizon, producing lower maximum solar input but greater sensitivity to local topography and long-duration shadows. Near polar regions, permanently shadowed areas can remain extremely cold, while nearby illuminated ridges may receive long periods of low-angle sunlight.
For rover design, this means that the thermal-control strategy cannot be assessed at one latitude only. The same insulation that is beneficial in a cold high-latitude case can cause overheating in a lower-latitude hot case. Conversely, a configuration designed to reject heat efficiently during the day may require significant heating during cold phases. A parametric model therefore supports trade-offs on landing site, operational schedule and thermal-control architecture.

6.13 Verification, Validation and Correlation

Verification and validation are essential to ensure that a thermal model is reliable. Verification checks that the model has been implemented correctly: geometry, nodes, conductors, material properties, boundary conditions, heat loads and solver settings must be consistent with the modelling assumptions. Validation checks whether the model reproduces real physical behaviour, using experimental data or reference measurements.
For spacecraft, validation is often performed through thermal-balance and thermal-vacuum tests. For a lunar surface model, full-scale validation is more difficult. Therefore, comparison with available lunar measurements and literature data becomes essential.
A validated lunar surface model should reproduce:

- realistic maximum daytime surface temperatures;
- realistic minimum night-time temperatures;
- damping of temperature oscillations with depth;
- phase lag of subsurface temperatures;
- latitude-dependent trends;
- reasonable infrared emission from the ground.

After validation, the model can be used as an environmental boundary for the rover. Nevertheless, limitations must be clearly stated. Local roughness, small-scale shadowing, uncertain regolith properties, dust deposition and simplified contact conditions may still introduce discrepancies.

6.14 Practical Modelling Assumptions and Limitations

In preliminary thermal analysis, some simplifications are necessary. The following assumptions are commonly adopted:

- external convection is neglected on the lunar surface;
- surfaces are approximated as diffuse-grey unless more detailed optical data are available;
- small internal components can be represented as lumped nodes;
- contact conductances are approximated or treated parametrically;
- lunar regolith is represented by layered homogeneous properties;
- local micro-topography is simplified or neglected unless explicitly modelled;

- dust degradation is not included unless specific degradation factors are available;
- numerical ray-tracing convergence is controlled by selecting an adequate number of rays.

These assumptions are acceptable for preliminary design if they are documented and if sensitivity analyses are performed on the most uncertain parameters. As the project develops, the model should be refined and correlated with tests or higher-fidelity simulations.

6.15 Summary Tables for Numerical Thermal Modelling

The following tables summarise two elements that are useful for the interpretation of the numerical model: the comparison between finite-difference and finite-element approaches, and the main outputs produced by Thermal Desktop, RadCAD and SINDA/FLUINT.

Table 6.1: Qualitative comparison between FDM and FEM for spacecraft thermal analysis.

Aspect	**FDM / lumped network**	**FEM**
Geometry	Efficient for primitives and simplified spacecraft geometry	Better for irregular and detailed geometries
Radiation compatibility	Very suitable for radiation-driven spacecraft models	Requires surface discretisation that may complicate radiation exchange
Small components	Can be lumped into single nodes	Less natural if internal geometry is not needed
Computational cost	Generally lower for preliminary models	Generally higher for equivalent system-level models
Thermo-structural coupling	Less direct	Strong advantage in coupled thermo-structural analyses
Preliminary design	Very suitable	Often unnecessarily detailed

Table 6.2: Main Thermal Desktop / RadCAD / SINDA outputs used in thermal analysis.

Output	**Use in the analysis**
View factors / interchange factors	Quantify radiative coupling between surfaces
RadK values	Radiation conductors passed to SINDA/FLUINT
Heating rates	Environmental heat loads applied to thermal nodes
Node temperatures	Main requirement-verification output
Heat flows	Identification of dominant heat paths
Temperature maps	Visual inspection of hot and cold regions
Time histories	Transient verification of components and operational phases

6.16 Implementation Considerations for the Thermal Model

The theoretical formulation must be translated into practical modelling choices before the numerical analysis can be performed. When the model is implemented in Thermal Desktop, each ideal concept becomes a modelling object. A physical panel becomes a shell or solid. A surface finish becomes an optical-property definition. A screw or bracket can become a manual conductor. A payload box can become either a detailed set of surfaces or a lumped mass connected to a panel through a contact conductance. A radiation case becomes a RadCAD analysis that produces RadK and heating rates. The thermal solution then becomes a SINDA/FLUINT run.
For a lunar rover, this translation must be performed carefully because the same object can participate in several thermal paths. For example, an external lower panel may conduct heat to internal units, radiate to the lunar ground, receive infrared emission from the regolith, absorb reflected sunlight, and also exchange heat with adjacent side panels. If it is represented as a single node, local gradients may be lost. If it is over-discretised, the model may become unnecessarily expensive. The correct compromise depends on the objective of the analysis.
The adopted modelling hierarchy is organised as follows:

1. define the environmental model independently from the rover;
2. verify that the lunar surface model produces realistic temperature cycles;
3. introduce a simplified rover geometry and verify absorbed heat loads;
4. replace simplified boxes with subsystem-level equivalent models;
5. add conductive interfaces and contactors;
6. introduce operational heat loads;
7. perform hot, cold and transient cases;

8. perform sensitivity analyses on uncertain parameters;

9. refine only the regions that affect requirement compliance.

This approach avoids building an unnecessarily detailed model before the dominant heat paths are understood. It also makes the model easier to debug, because the environmental model, the radiative model and the internal conductive model can be checked separately.

6.16.1 Choice of Node Size

The choice of node size is driven by the expected thermal gradients. Regions with high conductivity and low gradients can be coarse. Regions with low conductivity, large heat loads, external exposure or contact uncertainty should be more detailed. In the regolith, the upper layers require finer discretisation because the thermal wave creates strong gradients near the surface. In deeper layers, the diurnal oscillation is attenuated and a coarser discretisation is acceptable.
For rover panels, finer nodalisation is useful when different parts of the same panel have different view factors, different solar exposure or different attached components. For small electronic units, a lumped node is often sufficient in preliminary design, provided that the objective is the unit-average temperature rather than internal board-level gradients.

6.16.2 Boundary Nodes and Sink Temperatures

Boundary nodes should be used only when the temperature history is known or intentionally imposed. Deep space is often treated as a radiative sink with a very low effective temperature. The lunar ground, however, should not be reduced to a constant boundary temperature if the purpose is to study latitude-dependent thermal behaviour. The ground must be thermally active, because its temperature controls infrared emission and conductive contact.

6.16.3 Internal Dissipation Modelling

Internal dissipations must be associated with operational phases. A component that is off during survival mode should not dissipate the same power as during active operation. Conversely, heaters may be active only in cold phases and controlled by temperature thresholds. In preliminary design, stepwise heat-load profiles are acceptable. In refined models, time-dependent functions can be used.

6.16.4 Radiation Case Convergence

Monte Carlo radiation results contain statistical uncertainty. Increasing the number of rays improves convergence but increases computational time. For early studies, lower ray counts may be acceptable to compare trends. For final verification, radiation cases should be repeated with higher accuracy and checked for convergence of key temperatures and absorbed powers.

6.16.5 Interpretation of Results

Temperature results should not be interpreted only by reading maxima and minima. The analyst should also inspect heat-flow paths. A high temperature may be caused by too much absorbed solar power, insufficient radiative emission, weak conduction to a radiator, excessive internal dissipation or insufficient contact with a heat sink. Similarly, a cold component may result from excessive radiative exposure, weak coupling to internal heat sources, excessive insulation from warm components or a low-duty-cycle operational mode.

6.17 Physical Interpretation for Lunar Applications

The lunar environment differs from the orbital environment in a fundamental way: the nearby surface is not merely a background source but a thermally active participant. In orbit, a spacecraft exchanges heat with the Sun, planetary albedo, planetary infrared radiation and deep space. On the lunar surface, the rover is close to regolith, which receives solar radiation, conducts heat into the subsurface, stores heat, emits infrared radiation and can also conduct heat through contact interfaces.

The regolith thermal inertia determines how quickly the ground heats and cools. During daytime, the upper surface can reach high temperatures while deeper layers remain cooler. During night, the surface cools rapidly by radiation to space, while deeper layers release stored heat. Therefore, the ground temperature experienced by the rover depends on time and depth. The lower surfaces and wheels of the rover are particularly sensitive to this effect.

Latitude modifies the balance between absorbed solar power and emitted infrared power. Near the equator, solar incidence can be close to normal and the peak daytime heat input is high. Near the poles, solar incidence is grazing, reducing direct absorption on horizontal surfaces but increasing the importance of vertical and tilted surfaces. A rover at high latitude can therefore have strong asymmetry between sides depending on orientation.

The thermal engineer must not consider only the maximum environmental temperature. A low solar elevation can reduce global absorbed power but create long shadows and cold traps. Conversely, a low incidence angle can illuminate vertical surfaces for long durations. These competing effects explain why a latitude-parametric model is more useful than a single-site model.

6.18 Model Verification Checks

Before running the final thermal analyses, the model must be checked for consistency. The main verification items are:

- verify all units of material properties;
- verify density, specific heat and conductivity assignments;
- verify absorptivity and emissivity assignments for each external surface;

- verify that radiative surfaces are active only when intended;
- verify nodalisation and node numbering;
- verify that internal components have realistic masses and capacitances;
- verify conductive interfaces and contact conductances;
- verify heat-load values and operating modes;
- verify boundary temperatures and sink definitions;
- verify radiation case settings and ray count;
- verify that generated RadK and heating rates are updated before thermal solution;
- verify time step, convergence criteria and simulation duration;
- verify post-processing variables and plotted nodes.

A common modelling error is to update the geometry or optical properties without regenerating the radiation data. Another common error is to apply the same heat load to a component in all phases even though its operational duty cycle changes. For a lunar rover, additional attention must be paid to the sign and orientation of surfaces, because incorrect normals can produce wrong solar absorption and radiation exchange.

6.19 Thermal Network Formulation

A thermal network is obtained by dividing a physical system into a finite number of subvolumes. This discretisation process is called nodalisation. Each subvolume is represented by a node whose temperature is the average temperature of the corresponding physical region. The thermal properties of the subvolume are concentrated at the node, giving a lumped-parameter model. This is the same modelling philosophy used by most spacecraft thermal solvers.
The main assumption is that each node is isothermal. This does not mean that the real component has no internal gradients; rather, it means that those gradients are either negligible for the purpose of the model or are represented by splitting the component into more nodes. If the gradient inside a component is important, the component should not be represented by a single lumped node.
The nodal capacitance is:

$$C = \rho V c_p \tag{6.9}$$

where ρ is the density, V is the node volume and c_p is the specific heat. If density or specific heat vary strongly with temperature, these dependencies should be included, especially when the system spans a large temperature interval.
Three types of nodes are commonly used:

- **diffusion nodes**, which have finite non-zero capacitance and represent normal physical material volumes;

- **arithmetic nodes**, which have zero capacitance and are useful for algebraic relationships or low-capacitance approximations;
- **boundary nodes**, which have prescribed temperature histories and can represent fixed-temperature sinks or imposed environmental conditions.

For a diffusion node, the energy equation can be written as:

$$\sum \dot{Q} - C\frac{\Delta T}{\Delta t} = 0. \tag{6.10}$$

For an arithmetic node:

$$\sum \dot{Q} = 0. \tag{6.11}$$

For a boundary node:

$$T = T_{prescribed}. \tag{6.12}$$

Arithmetic nodes can reduce stiffness caused by very low thermal capacitance elements. They are also useful for modelling surfaces that respond almost instantaneously to fast-changing heating rates. However, an excessive number of arithmetic nodes may reduce physical fidelity. Boundary nodes are useful when a known temperature history exists, but they should not be used to hide important physics. For example, treating the entire lunar surface as a fixed-temperature boundary would not be acceptable if the aim is to model latitude-dependent ground temperature.

6.19.1 Criteria for Node Size, Position and Shape

The node size must be selected considering structural design, required accuracy, available computer memory and execution time. In regions with steep gradients, smaller nodes are required. In regions with nearly uniform temperature, larger nodes are acceptable. This is particularly important for the lunar regolith: the upper layers require finer nodes, while deeper layers can be coarser.
The node centre should be placed in a physically meaningful position. Its location should reflect the expected temperature distribution, the desired output point and the computational simplicity of the model. In a plate with one-dimensional heat flow, a centred node may be sufficient. In a panel with asymmetric solar illumination or local heat sources, multiple nodes may be required.
The node shape should be simple and should respect the geometry and symmetries of the component. Rectangular and triangular nodes are common for planar geometries. Rectangular nodes simplify area-to-length conductance calculations, while triangular nodes can better represent some heat-flow patterns. Circular structures may be represented by radial and annular nodes.

6.19.2 Conductors in the Thermal Network

Conductors model heat-flow paths between nodes. The basic linear form is:

$$\dot{Q} = G_{ij}(T_i - T_j). \tag{6.13}$$

For conduction:

$$G = \frac{kA}{L}. \tag{6.14}$$

For convection:

$$G = hA. \tag{6.15}$$

For radiation, the relation is nonlinear:

$$\dot{Q} = G_{ij}(T_i^4 - T_j^4). \tag{6.16}$$

Parallel conductive paths can be combined by summing conductances:

$$G_T = G_1 + G_2 + \ldots + G_n. \tag{6.17}$$

Series conductive paths can be combined by summing resistances, or equivalently:

$$\frac{1}{G_T} = \frac{1}{G_1} + \frac{1}{G_2} + \ldots + \frac{1}{G_n}. \tag{6.18}$$

These combinations are useful for modelling multilayer interfaces, stacked panels, insulation supports and parallel structural heat paths. For example, an internal component may conduct heat through a mounting plate, screws and a thermal interface material. Depending on geometry, these paths may be represented in parallel, in series or as an equivalent conductor.

6.19.3 Radiation-Conductor Linearisation

The radiation term is nonlinear because:

$$T_i^4 - T_j^4 = (T_i - T_j)(T_i + T_j)(T_i^2 + T_j^2). \tag{6.19}$$

This allows a local linearisation around the current temperature estimate. Thermal solvers use this idea to include radiation in iterative solution schemes. Although the final physical law remains nonlinear, the solver can build a locally linear system at each iteration.
For radiation from a grey surface to a blackbody sink:

$$G_{ij} = \sigma \varepsilon_i F_{i-j} A_i. \tag{6.20}$$

For radiation between grey surfaces:

$$G_{ij} = \sigma \zeta_{i-j} A_i. \tag{6.21}$$

where ζ_{i-j} is the grey-body radiation factor. It includes the contribution of view factor, emissivity and multiple reflections in the radiative configuration.

6.20 Grey-Diffuse and Monte Carlo Radiation Methods

Radiation codes in thermal software have two main tasks: computing radiative exchange between surfaces and determining incoming environmental heat fluxes. Two families of methods are commonly used: grey-diffuse view-factor methods and Monte Carlo ray-tracing methods.

6.20.1 Grey-Diffuse View-Factor Method

The grey-diffuse method assumes that surfaces have uniform temperature, diffuse emission, diffuse reflection and uniform energy fluxes. Absorptivity, emissivity and transmittance are not functions of direction or wavelength within the adopted spectral band. This approach extends blackbody view-factor methods to real surfaces by introducing grey-body effects.
The method is efficient for simple radiation enclosures and simple geometries. It is also useful for hand calculations and for developing intuition. However, it becomes difficult for complex three-dimensional geometries, non-enclosed configurations, partial visibility, multiple reflections and shadowing.
The assumptions can be summarised as:

- each surface is isothermal;
- each surface emits diffusely;
- each surface reflects diffusely;
- incoming and outgoing fluxes are uniform over each surface;
- optical properties are constant in the considered band;
- geometry determines the view factors.

For a rover on the lunar surface, these assumptions may be reasonable for first-order understanding, but a ray-tracing approach is preferable because wheels, panels and ground generate complex visibility conditions.

6.20.2 Monte Carlo Ray-Tracing Method

The Monte Carlo method follows the path of a large number of rays. Each ray represents a packet of radiative energy. The ray is emitted from a surface, travels in a straight line, interacts with other surfaces and is then absorbed, reflected or transmitted according to the optical properties.
The strength of the method is its flexibility. It can handle complex geometry, shadowing, partial visibility and multiple reflections. Its weakness is statistical noise. If too few rays are used, view factors and heating rates may fluctuate. If too many rays are used, computational time increases.
In Thermal Desktop, the same principle is used to compute both RadK values and heating-rate functions. Rays can be traced from surfaces to other surfaces for radiative coupling, or from environmental sources to surfaces for absorbed fluxes. This is why the selected ray count affects both surface-to-surface radiation and environmental heating.
For a lunar rover, the analyst should check convergence of the quantities that matter most: maximum component temperature, minimum survival temperature, heat load on critical panels and wheel-ground heat exchange. It is usually unnecessary to force every small surface heat rate to converge to extremely high precision if it has negligible effect on requirements.

6.21 Thermal Desktop Modelling Procedure

The practical construction of the model in Thermal Desktop can be broken down into detailed operations.

6.21.1 Geometry Creation

The geometry can be created directly in the AutoCAD-based interface or imported from CAD and simplified. For thermal purposes, the geometry does not have to reproduce every mechanical detail. It must reproduce the surfaces and masses that matter thermally. Small fillets, bolts or details with negligible thermal role can be removed, while panels, radiators, insulation, wheels and contact regions must be represented.
External surfaces must have correct normals because solar absorption and radiation exchange depend on orientation. If a surface normal is reversed, solar and radiative results may be wrong. For this reason, normal checks are an important part of GMM verification.

6.21.2 Nodalisation and Submodels

Thermal Desktop allows the analyst to assign nodalisation to surfaces and solids. Each subdivided element becomes a set of thermal nodes in the TMM. Submodels can be used to organise the global thermal model into meaningful blocks, such as environment, rover structure, internal equipment, wheels, batteries and payload.
Submodels make the model easier to manage and debug. They also allow parts of the system to be refined without changing the entire model. For example, the lunar surface submodel can be validated first, then the rover can be added.

6.21.3 Material Properties

Thermo-physical properties must be assigned consistently. Density and specific heat determine thermal capacitance, while thermal conductivity determines conduction. Temperature-dependent properties can be included when variations are large. This is relevant for regolith thermal conductivity and for materials operating over wide temperature ranges.

6.21.4 Optical Properties

Solar absorptivity and infrared emissivity must be defined for each radiating surface. The analyst must ensure that the correct properties are used for the correct spectral band. Solar radiation and albedo use solar optical properties. Infrared exchange uses IR properties.
For lunar applications, this distinction is especially important because the ground can be both a reflector of solar radiation and an emitter of infrared radiation. A rover surface may absorb these two contributions differently.

6.21.5 Conductive Interfaces

Conductive connections can be created automatically from shared geometry or manually. Manual conductors are often required for contact interfaces that are not represented geometrically or whose conductance is not a simple kA/L value. These include screws, brackets, harnesses, thermal straps and mechanical mounts.
A preliminary model should explicitly list the assumed contact conductances. These values can later be updated after mechanical design or experimental characterisation.

6.21.6 Radiation Cases

A radiation case defines how RadCAD computes radiative exchange and environmental heating. It includes active surfaces, ray-tracing settings, optical-property sets, environmental sources and shadowing options. If geometry or optical properties change, the radiation case should be regenerated.

6.21.7 SINDA/FLUINT Solution Settings

The thermal solution requires a time grid, convergence criteria and solver options. For transient lunar analyses, the simulation duration must cover the relevant part of the lunar day or multiple cycles if periodic convergence is needed. The time step must be small enough to capture changes in solar incidence and internal power profiles, but large enough to keep run time manageable.

6.21.8 Post-Processing

Post-processing should include both temperatures and heat flows. Temperature maps help identify local hot and cold regions. Time histories show whether a component violates limits only briefly or for long durations. Heat-flow reports reveal dominant paths and guide design modifications.

6.22 Thermal Design Consequences for the Rechargeable Rover

The theoretical framework has direct consequences for the thermal design of the rover. Since external convection is absent, increasing exposed radiator area or increasing emissivity is the main way to reject heat externally. However, the same high-emissivity surface can become a strong heat-loss path during cold phases. MLI can reduce losses during cold conditions but can also trap heat during hot conditions. Conductive coupling to the ground can be useful or harmful depending on ground temperature.
At low latitudes, the hot case may be driven by direct solar absorption and high ground infrared emission. At night, the cold case may be driven by radiative cooling to space and low ground temperature. At high latitudes, the low solar elevation reduces horizontal solar input but increases the importance of vertical surfaces and shadowing. Therefore, surface orientation becomes more important.
The rover thermal-control concept must balance several competing needs:

- reject internally generated heat during operation;
- avoid excessive daytime solar absorption;
- retain heat during cold phases;
- protect batteries and electronics from low temperatures;
- avoid overheating of external surfaces;
- avoid excessive gradients between external shell and internal components;
- maintain acceptable temperatures for all latitudes considered.

6.23 Validation Logic for the Latitude-Parametric Lunar Surface Model

A model valid for all latitudes must be validated at more than one environmental condition. A single comparison at the equator is not sufficient to guarantee polar validity.
The validation logic should therefore include:

- comparison of equatorial temperature trends against Apollo or literature data;
- comparison of high-latitude trends against Diviner or literature polar data;
- verification of the decrease of maximum temperature with latitude;
- verification of the behaviour of the night-time minimum temperature;
- verification of the thermal-wave attenuation with regolith depth;
- verification of phase lag between surface and subsurface nodes;
- sensitivity analysis on regolith conductivity, density, heat capacity, albedo and emissivity.

If the model reproduces these behaviours, it can be used as an environmental generator for rover thermal analyses. If discrepancies are found, the first parameters to inspect are surface optical properties, regolith conductivity, layer thickness, boundary condition at the bottom of the soil model, radiation sink definition and time-step resolution.

6.24 Chapter Summary

This chapter introduced the theoretical and numerical framework required to perform the thermal analysis of the rechargeable lunar mini rover. The discussion started from the role of thermal control in space systems, the definition of operational and survival temperature limits, the ECSS treatment of uncertainties and the iterative nature of

thermal-model development. The fundamental heat-transfer mechanisms were then described. Conduction governs the internal heat redistribution and the interfaces between components, contact conduction is important at mechanical joints and wheel–ground interfaces, external convection is absent on the lunar surface, and radiation dominates the exchange with the lunar environment. The chapter also introduced thermo-optical properties, view factors, grey-body radiation and semi-grey modelling, which are essential to evaluate the absorbed and emitted powers of external rover surfaces.
The thermal-network approach was then presented through the distinction between GMM and TMM. The GMM describes the geometry used for radiation and environmental heating, while the TMM describes the nodal network solved to obtain temperatures and heat flows. The Finite Difference Method is particularly suitable for lumped spacecraft and rover thermal networks, while the Finite Element Method is more appropriate for detailed irregular geometries and coupled thermo-structural analyses.
Finally, the workflow adopted in Thermal Desktop was described. RadCAD is used to compute radiative couplings, RadK values and heating-rate functions, while SINDA/FLUINT solves the thermal network in steady-state or transient conditions. This methodology provides the basis for the following chapters, where the lunar surface model is constructed, validated and coupled to the rover thermal model in order to assess hot and cold thermal criticalities and support the preliminary design of the thermal control system.

Chapter 7

Lunar Thermal Environment

"Some say the world will end in fire,
Some say in ice."

— Robert Frost
Fire and Ice

7.1 Introduction

The thermal environment is one of the main design drivers for a rechargeable mini rover operating on the lunar surface. The external environment, together with the heat dissipated internally by the battery, on-board computer, sensors, communication electronics, mobility motors, motor drivers and payload, determines the thermal loads that the thermal control system must manage during the mission. For this reason, the thermal problem cannot be treated only as a final verification activity. It must be considered from the first design iterations, because the size of the rover, the position of the radiator, the insulation concept, the wheel–ground interfaces and the battery location all influence the final temperature distribution.

The rover considered in this thesis is assumed to operate near a crewed lunar base or surface outpost. Its mission concept is based on repeated sorties of approximately three hours, followed by return to a charging station located at the base. This architecture reduces the need for very long independent survival periods, because the rover can periodically recharge and recover thermally in a more favourable location. However, the rover is still exposed to the real lunar surface environment during each traverse. Therefore, the thermal model must reproduce the external heat fluxes acting on the vehicle, the temperature of the surrounding regolith, the radiative exchange with the ground and deep space, and the conductive heat transfer through the wheel–soil contacts.

The approximately three-hour duration defines the nominal operational exposure of one sortie. By contrast, the complete-lunar-day transients introduced in the following chapters are used to construct a broader environmental design envelope. They are not intended to imply that the rover remains continuously away from the charging station for an entire lunar cycle. Their purpose is to sweep the local illumination and regolith-temperature conditions and to identify the hot and cold environmental states that can bound shorter operational cases.

The lunar environment is particularly severe because the Moon has no dense atmosphere able to moderate surface temperature, transport heat by convection or redistribute energy through weather systems. As a consequence, the surface energy balance is controlled mainly by direct solar radiation, reflected solar radiation, thermal infrared emission of the ground, radiation toward deep space and subsurface conduction within the regolith. For a landed rover, an additional contribution is represented by direct or indirect conductive contact with the lunar soil through the wheels, supports or docking interfaces. The Moon also rotates slowly. At low and mid latitudes, this produces approximately two weeks of daylight followed by approximately two weeks of darkness. At the poles, the situation is more complex because the small lunar obliquity causes the Sun to remain close to the horizon. This generates grazing illumination, long shadows, illuminated ridges, cold traps and permanently shadowed regions. The thermal environment is therefore strongly dependent on latitude, local time, terrain properties and local topography. For a mini rover, this variability is critical. The vehicle has limited thermal inertia, limited internal volume, limited radiator area and limited electrical power for active thermal control. In hot cases, the rover must reject the heat generated by its electronics, mobility system and battery operation. In cold cases, it must preserve heat, especially around the battery and other temperature-sensitive units. The charging station can contribute to the overall thermal strategy by providing a protected parking location, a recharge interface and, potentially, a conductive or radiative thermal boundary condition that is less severe than the open surface.
This chapter describes the thermal environments relevant to the rover mission. It first introduces the mission thermal phases, from ground operations to lunar surface operation. It then summarises the general radiative environment, the lunar orbit and descent environment, and the specific thermal conditions encountered on the lunar surface. Particular attention is given to latitude effects, south-pole conditions, regolith properties, surface infrared emission and the requirements that these effects impose on the rover thermal model.

7.2 Mission Thermal Environments

During the full mission lifetime, the rover and the spacecraft or lander that carries it experience a sequence of environments with different dominant heat-transfer mechanisms. The first phases occur on Earth and are characterised by convection, conduction and controlled facility conditions. After launch and fairing jettison, radiative exchange becomes progressively dominant. Once the mission reaches the Moon, the most important external contributions are direct solar radiation, lunar albedo, lunar infrared emission, radiation toward deep space and, after landing, conductive contact with the regolith. For the mission considered in this thesis, the following environments must be considered:

- ground and pre-launch environment;
- launch environment;
- Earth on-orbit environment, if the transfer architecture includes an Earth parking orbit;

- lunar transfer environment;
- lunar orbit and descent environment;
- surface deployment environment;
- nominal lunar surface operation during the approximately three-hour rover sortie;
- return, recharge and standby at the base charging station;
- shadowed or polar surface conditions, if included in the operational scenario.

The distinction between these phases is important because the thermal problem is not solved in the same way during all mission phases. Ground and launch environments are often managed through facility constraints, integration rules and launch-provider requirements. Space and lunar surface environments, instead, require the rover thermal response to be designed through coatings, insulation, conductive paths, radiators, heaters, battery thermal control and operational constraints.

Table 7.1: Main mission thermal environments and dominant thermal effects.

Mission phase	**Dominant thermal aspects**
Ground and pre-launch	Controlled ambient temperature, convection, conduction with ground-support equipment, humidity, cleanliness and contamination constraints.
Launch	Fairing radiative heating, conductive paths through adapters, pressure drop, acoustic and mechanical constraints, thermal conditions imposed by the launcher.
Earth orbit	Direct solar radiation, Earth albedo, Earth infrared radiation, radiation to deep space and possible eclipse cycles.
Lunar transfer	Nearly continuous solar exposure, decreasing Earth albedo and infrared contribution, increasing lunar contribution and attitude-dependent heat rejection.
Lunar orbit and descent	Direct solar radiation, lunar albedo, lunar infrared radiation, changing view factors and descent-dependent thermal fluxes.
Lunar surface sortie	Direct solar radiation, albedo, ground infrared emission, radiation to deep space, conduction with regolith, local shadowing, internal dissipation and dust deposition.
Recharge and standby at the base	Battery recharge heat, power-conditioning dissipation, possible conductive docking interface, possible shielding from the environment and thermal recovery before the next sortie.
South-pole or shadowed operation	Low solar elevation, long shadows, illuminated ridges, permanently shadowed regions, cold traps and strong spatial thermal heterogeneity.

7.3 Ground Environment

The first thermal environment encountered by the rover is the terrestrial ground environment. This phase includes assembly, integration and testing, payload processing, transport to the launch site, integration with the lander or host spacecraft and the pre-launch waiting period. In contrast to space and lunar operation, heat transfer during these phases is dominated by convection and conduction with the surrounding air, ground-support equipment and mechanical interfaces. Radiation may still be relevant in thermal-vacuum testing or inside the launcher fairing, but it is usually not the dominant exchange mechanism during standard ground operations.
In most missions, the ground environment is not controlled by modifying the rover thermal design itself, but by controlling the facility environment and limiting exposure outside the allowed temperature range. The launch or integration provider normally specifies a guaranteed temperature interval. Typical lower limits are close to 0°C, while upper limits are commonly of the order of 35°C. In the Astrobotic payload user's guide, for example, the indicated pre-launch temperature range is between 0°C and 27°C [33]. For a rechargeable mini rover, the most important ground-phase thermal constraints concern the battery, electronics and payload sensors. The battery should not be stored, transported or charged outside the temperature range recommended by the cell manufacturer. Sensitive cameras, optical sensors and electronic boards may also impose cleanliness and humidity constraints. These aspects are not the main subject of the lunar thermal model, but they define the initial condition and the acceptable handling environment before launch.

7.4 Launch Environment

The launch environment is severe because the vehicle is exposed to strong accelerations, vibration, acoustic loads, pressure variations and fairing thermal conditions. The mini rover is not directly exposed to the external aerodynamic environment if it is stowed inside a lander or host spacecraft. Nevertheless, the thermal conditions inside the payload fairing and through the mechanical interfaces can affect the initial temperature of the rover and its battery. Before fairing jettison, aerodynamic heating affects the external fairing surface. The fairing temperature depends on the balance between aerodynamic heating, material heat capacity, convective losses and radiative losses. The payload temperature rise inside the fairing is controlled mainly by radiation from the fairing inner skin and by conduction through mechanical interfaces [34, 35].
Fairing inner surfaces and acoustic blankets are normally designed or treated with surface finishes compatible with typical payload temperature requirements. The fairing is usually jettisoned only after the launcher has reached a sufficiently high altitude. The timing of jettison is a compromise: early jettison reduces mass and improves launcher performance, but jettisoning too early would expose the payload to high dynamic pressure and aerodynamic heating. A representative altitude for fairing jettison is around 100–115 km, depending on launcher and mission design.
After fairing jettison, the thermal environment includes direct solar radiation, Earth albedo, Earth infrared radiation, emitted radiation toward the upper stage and deep space, and conduction through the payload adapter. At altitudes above approximately

200 km, free molecular heating becomes negligible for most preliminary thermal analyses. In operational Earth orbits above about 300 km, the residual pressure is very low and radiative exchange is dominant.
For the mini rover, the launch phase is usually not the sizing case for the surface thermal control system. However, it can influence the initial temperature before transfer and may impose restrictions on the battery state of charge, heater availability and allowable storage conditions.

7.5 General Space Radiative Environment

Once the spacecraft is in orbit or in deep space and no longer conductively coupled to the launcher in a thermally significant way, radiative exchange becomes the dominant external heat-transfer mechanism. The three principal external radiative sources are:

- direct solar radiation;
- solar radiation reflected by a nearby celestial body, usually called albedo;
- thermal infrared radiation emitted by a nearby celestial body.

The spacecraft or rover also rejects heat by emitting infrared radiation toward deep space. This outgoing radiation is fundamental for thermal balance because, in vacuum, there is no external convection. For the rover, this general radiative framework remains valid on the lunar surface, but the surrounding regolith becomes a nearby radiative source and sink. Therefore, the local ground cannot be treated only as a distant planetary background; it must be included explicitly in the thermal model.

7.6 Direct Solar Radiation

Direct solar radiation is usually the most intense external heating source for spacecraft operating within approximately 2 AU from the Sun. The solar spectrum can be approximated, for thermal engineering purposes, by a blackbody curve with an effective temperature of about 5800 K. Most of the solar energy is concentrated at short wavelengths: approximately 99% of the solar energy lies between 150 nm and 10 μm, with a maximum near 450 nm [34].

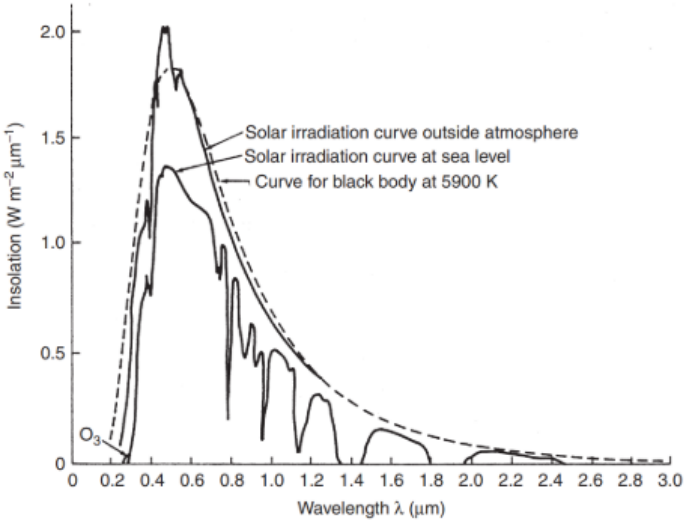


Figure 7.1: Solar spectral radiation curve. Credits: [34]

The solar radiation intensity at a distance d from the Sun can be expressed as:

$$J_S = \frac{P_S}{4\pi d^2} \tag{7.1}$$

where P_S is the total solar power output, approximately 3.856×10^{26} W. At the average Earth–Sun distance, the solar constant is approximately 1371 ± 5 W/m^2. Because Earth's orbit is elliptical, the solar intensity varies during the year, reaching values of about 1418 W/m^2 near the minimum Earth–Sun distance and about 1320 W/m^2 near the maximum distance [34].

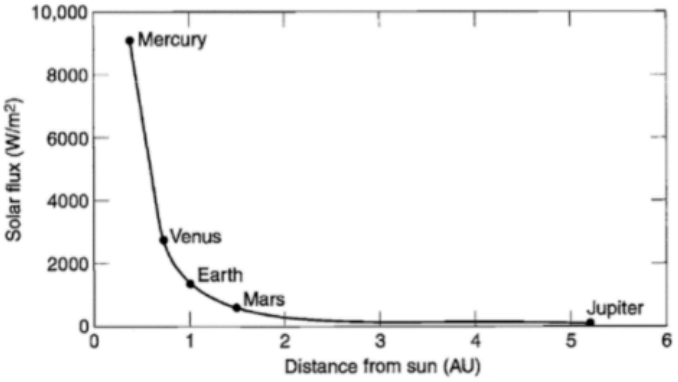


Figure 7.2: Solar flux variation with distance. Credits: [4]

The Sun subtends an angular diameter of about 0.5° at 1 AU. Therefore, for most spacecraft thermal-control applications, sunlight can be considered a parallel beam coming from a point source. This assumption is also appropriate for a lunar surface thermal model.

For a flat surface of area A, with its normal forming an angle θ_S with the solar rays, the absorbed solar power is:

$$\dot{Q}_{Sun} = \alpha J_S A \cos\theta_S \tag{7.2}$$

where α is the solar absorptivity of the surface [16]. This expression is valid when the surface is illuminated and $\cos\theta_S > 0$; otherwise the absorbed direct solar power is zero.

For the rechargeable mini rover, direct solar radiation affects the external panels, the wheels, the radiator, possible solar panels on the charging station, and any exposed payload or antenna surface. It can create a hot-case condition during illuminated sorties, but it can also be used indirectly as a power source if the base charging station relies on solar energy. The short-wavelength nature of solar radiation makes the thermo-optical properties of the external surfaces particularly important.

7.7 Albedo Radiation

Albedo radiation is the part of the incident solar radiation reflected by the surface or atmosphere of a celestial body. The albedo coefficient a is defined as the ratio between reflected solar radiation and incident solar radiation. In a first approximation, albedo radiation can be treated as short-wavelength radiation with a spectral distribution similar to direct solar radiation. This simplification is usually acceptable for thermal engineering because the reflected radiation remains solar-origin radiation.
For Earth, the average albedo is approximately 0.3, although it varies strongly with surface type, cloud coverage, season and latitude. Oceans and forests can have low albedo values, while clouds, polar snow and ice-covered regions can reach much higher values. As a consequence, the average albedo seen by an orbiting spacecraft depends on orbit inclination and altitude. Approximate orbit-averaged albedo coefficients can be around 0.23 for equatorial orbits and around 0.42 for polar orbits [34].
If the planet is approximated as a diffuse reflecting sphere, the albedo intensity incident on a spacecraft can be written as:

$$J_a = J_S a F \tag{7.3}$$

where J_S is the solar radiation intensity at the celestial body, a is the albedo coefficient and F is a visibility factor including the geometrical view factor and the angle between the local vertical and the solar direction.
The absorbed albedo power on a surface can be written in simplified form as:

$$\dot{Q}_{Alb} = \alpha J_a A \tag{7.4}$$

where α is the solar absorptivity of the receiving surface.
On the lunar surface, albedo is not only an orbital background term. It is a local contribution reflected by the regolith surrounding the rover. Downward-facing, lateral and inclined rover surfaces can receive a non-negligible fraction of reflected solar radiation from the ground. The absorbed albedo depends on local terrain reflectivity, solar incidence on the ground, rover orientation and view factor between each rover surface and the illuminated regolith.

7.8 Planetary and Lunar Infrared Radiation

Any body at non-zero temperature emits thermal radiation. Planetary infrared radiation is the thermal radiation emitted by a planet or moon. For Earth, the contribution includes both surface and atmospheric emission. The spectral range is at longer wavelengths than the solar spectrum, typically between about 2 and 50 μm, with a peak

around 10 μm. A global average Earth infrared flux of about 237 W/m^2 is often used for preliminary spacecraft analyses [34].
For a blackbody planetary source at temperature T_P, the infrared radiation absorbed by a spacecraft surface can be approximated by:

$$\dot{Q}_{planet} = \varepsilon A F_{A-P} \sigma T_P^4 \tag{7.5}$$

where ε is the infrared absorptivity/emissivity of the receiving surface, F_{A-P} is the view factor between the surface and the planet, and σ is the Stefan–Boltzmann constant [16].
For the Moon, the infrared radiation comes directly from the regolith because there is no atmosphere. The emitted flux depends on the local surface temperature and emissivity. Lunar regolith emissivity is generally high, typically in the range 0.95 to 0.98 according to soil composition, while other references indicate values close to 0.9–1.0 for lunar surface materials [36, 37].
The rover exchanges infrared radiation with the local ground continuously. During daytime, warm regolith can increase the heat load on the rover, reducing the effectiveness of downward-facing radiators. During the lunar night or in shadowed regions, cold regolith can act as a strong heat sink. This is one of the reasons why the regolith temperature must be calculated or imposed realistically in the thermal model.

7.9 Earth On-Orbit Environment

The Earth on-orbit thermal environment is governed by direct solar radiation, Earth albedo, Earth infrared radiation and radiation to deep space. Eclipse transitions may also be important, depending on the orbit. In Low Earth Orbit, albedo and Earth infrared contributions can be significant because the spacecraft is close to the planet and has a large Earth view factor. At higher altitudes, such as geostationary orbit, albedo becomes much less important and can drop to less than one percent of its Low Earth Orbit contribution.
For a mini rover transported as part of a lunar mission, the Earth on-orbit environment is usually not the final design driver. However, it may influence the thermal state before lunar transfer, especially if the host spacecraft remains in Earth orbit for a significant time. The thermal engineer must therefore verify that the rover, while stowed, remains within survival limits and that battery storage constraints are satisfied.

7.10 Lunar Transfer Environment

During lunar transfer, the spacecraft leaves the Earth environment and progressively enters the Moon-dominated environment. The Earth albedo and Earth infrared contributions decrease with distance, while the lunar reflected and infrared contributions increase as the spacecraft approaches the Moon. Direct solar radiation remains approximately constant because the Earth–Moon distance is small compared with the Earth–Sun distance.
The lunar transfer environment can be modelled with different levels of fidelity. A simple preliminary model may include only direct solar radiation and deep-space radiation.

A more complete model may include time-dependent Earth and Moon albedo and infrared radiation, seasonal variations, spacecraft attitude history and changing view factors. For high-accuracy studies, environmental data and dedicated thermal-analysis tools are required.
For the rover, the transfer phase is mainly a stowed survival condition. The host spacecraft or lander provides mechanical support and may provide thermal protection or heater power. The critical components are again the battery, electronics and payload. The rover thermal model may represent this phase with simplified boundary conditions unless detailed host spacecraft interfaces are available.

7.11 Lunar Orbit and Descent Environment

The lunar orbital environment includes direct solar radiation, lunar albedo and lunar infrared radiation. However, their relative importance and variability differ from Earth because the Moon has no atmosphere, has low near-surface thermal inertia and rotates slowly.

7.11.1 Direct Solar Radiation at the Moon

The average direct solar radiation at the Moon can be considered close to the 1 AU value. However, because the Moon orbits Earth, the Moon–Sun distance has a slightly wider variation than the Earth–Sun distance alone. Considering the maximum Earth–Moon distance, the lunar solar flux can range approximately from 1315 W/m^2 to 1420 W/m^2 [36, 38].

7.11.2 Lunar Albedo

The lunar albedo varies across the surface. Compared with Earth, two aspects are especially important: there is no atmospheric contribution and short-term temporal variations are negligible. The main variations are due to surface composition and geological region. Highlands are brighter because of exposed lunar bedrock and can have albedo values up to about 0.3. Maria are darker basaltic plains and can have albedo values as low as 0.07 [38, 39].
Average normal albedo values were evaluated from Apollo 11 and Apollo 12 samples in the spectral range 0.327 to 1.050 μm. After applying bolometric corrections for a solar spectrum approximated as a 5780 K blackbody, the near-side average bolometric albedo is about 0.12 [40]. For the far side, Clementine UV/Vis imagery at 750 nm indicates a brighter average value around 0.15, consistent with the lower abundance of mare regions on the far side [41].
In low lunar orbit, the albedo seen by a spacecraft is spatially averaged over the visible surface. For surface applications, local albedo becomes much more important. A rover operating on darker mare regolith absorbs and receives a different reflected flux from a rover operating on brighter highland terrain. If the landing site is known, high-resolution albedo data from lunar remote-sensing missions should be used.

7.11.3 Lunar Infrared Radiation

Because the Moon has no atmosphere, lunar infrared radiation comes directly from the surface. The emitted flux depends on surface temperature and emissivity. Surface temperatures are extremely variable. At equatorial latitudes, illuminated regions can exceed 400 K, while night-time temperatures may fall to about 90–100 K. Permanently shadowed polar regions can reach temperatures of only a few tens of kelvin, with reported values around 20 K in the coldest cases or 30–40 K in typical polar cold traps [36, 42].
The local surface temperature is highly sensitive to topography and material properties. Because lunar regolith has low thermal inertia and low thermal conductivity, a shadowed area can be up to 200 K colder than a neighbouring sunlit area. Differences in albedo and composition also generate thermal contrasts: mare regions tend to be warmer than highlands at the same latitude and local time because of their lower reflectivity. Due to thermal inertia, dawn and dusk are not symmetric; near the equator, the dusk terminator can be around 30 K warmer than the dawn terminator [36, 43].

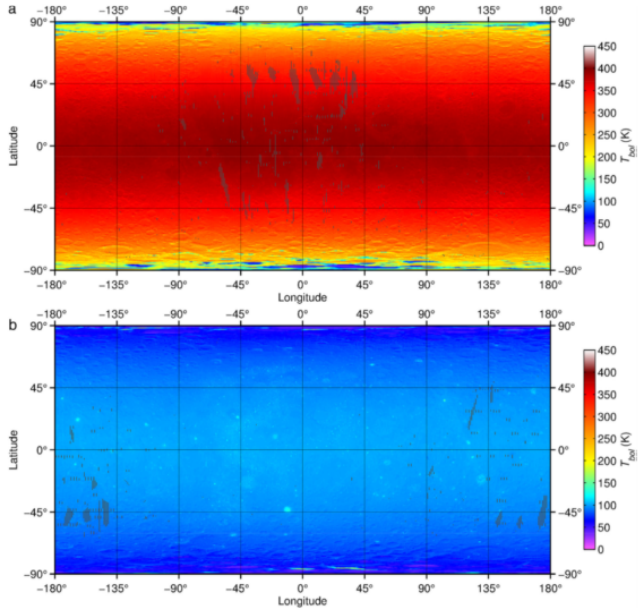


Figure 7.3: Mean global bolometric temperatures for one hour of local time centered on (a) noon and (b) midnight. Credits: [43]

7.11.4 Comments on Lunar Orbit and Descent

The distribution of thermal loads in lunar orbit differs from Earth orbit. In some hot cases, the direct solar contribution can become comparable to the combined albedo and infrared contributions. If a radiator views the subsolar region of the Moon, the lunar infrared radiation can significantly reduce its ability to reject heat. Therefore, the lunar orbit environment can be critical for thermal control, especially for spacecraft with limited radiator placement options.
The descent to the lunar surface introduces a time-dependent and geometry-dependent environment. The spacecraft altitude decreases, the ground view factor increases, the

local terrain becomes more important and the descent attitude determines which surfaces receive solar, albedo and infrared loads. The landing site, local time and descent trajectory therefore strongly influence the thermal environment. If the trajectory is not yet defined, a reasonable preliminary approach is to bound the problem with worst-case hot and cold scenarios [36, 44].
For the rover, descent is normally a stowed phase inside or on the lander. The rover may not directly see the lunar surface until deployment, but the lander thermal environment can still influence its initial temperature. This initial condition must be considered before simulating the first sortie or the first recharge cycle at the base.

7.12 Lunar Surface Thermal Environment

The lunar surface is the most important environment for the rover because it combines all relevant radiative contributions with direct contact with the ground and repeated operational exposure. The long synodic period of the Moon, approximately 29.5 days, produces a slow and deep environmental thermal cycle. At low latitudes, the surface can remain illuminated for about 14 Earth days and then remain in darkness for about 14 Earth days. These durations describe the lunar boundary condition, not the nominal duration of a rover sortie. In this thesis, the full cycle is used to identify bounding hot and cold environmental states, while the operational concept remains based on shorter, approximately three-hour traverses.
Compared with an orbital spacecraft, a rover has an additional thermal path: conduction with the lunar surface through wheels, supports or other contact points. Even if the real contact area may be small and contact conductance uncertain, this path must be considered because the regolith temperature can be very different from the rover temperature. For wheeled systems, the wheel–ground contact also depends on material, pressure, soil compaction and local geometry.
A first characterisation of the operating site is necessary before performing a meaningful surface thermal analysis. The minimum information includes:

- terrain type, such as mare, highland or polar regolith;
- latitude and longitude;
- local time or solar incidence condition;
- local albedo and emissivity;
- expected ground temperature range;
- possible shadowing by rocks, crater walls, slopes, base elements or rover geometry;
- dust deposition risk and its effect on optical properties.

A purely orbital-style approach, in which the ground is represented only by constant infrared and albedo fluxes, is not sufficient for detailed surface analysis. It does not capture the mutual radiative and conductive interaction between rover and ground. A better approach is to develop a lunar surface and subsurface thermal model based

on local thermo-optical and thermo-physical regolith properties. Such a model can reproduce time-dependent surface temperature, subsurface damping and heat exchange with the rover.
Dust deposition is another important factor for long-duration surface missions. Lunar dust can modify the optical properties of radiators, coatings and solar panels. If a radiator becomes covered by dust, its effective absorptivity and emissivity may change, reducing thermal-control performance and possibly increasing absorbed solar heating. For a rover operating near a base, dust raised by mobility, landing events or crew activity may therefore influence both thermal control and power generation.

7.13 Heat Sources and Sinks on the Lunar Surface

The energy balance of the lunar surface is controlled mainly by electromagnetic radiation. Since the Moon lacks a significant atmosphere, there is no atmospheric convection to smooth temperature gradients, no weather-driven redistribution of heat and no atmospheric greenhouse effect comparable to Earth. The intensity and duration of the heat fluxes depend on Sun–Moon geometry, local terrain, surface properties and latitude.
The principal heat sources and sinks are:

- direct solar radiation incident on the surface;
- reflected solar radiation, governed by lunar albedo;
- infrared radiation emitted by the surface;
- radiation exchange with deep space;
- subsurface conduction in the regolith;
- conductive and radiative interaction with landed hardware;
- surface-property changes produced by dust deposition and space weathering.

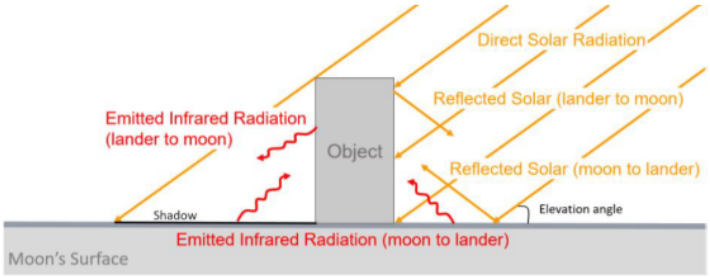


Figure 7.4: Radiation exchange on the lunar surface. Credits: [36]

During the lunar day, solar radiation dominates and heats exposed regolith. During the lunar night, there is no direct solar input and the surface cools by infrared emission to space. Because the regolith has low thermal conductivity, this heat is not efficiently

replenished from deeper layers. Therefore, surface temperature drops rapidly after sunset, while subsurface temperatures are much more stable.
The lunar albedo is low on average, around 0.12, but it varies by geological region. Dark mare basalts may have albedo values around 0.07 and therefore absorb more solar energy, reaching higher daytime temperatures. Highland regions, rich in anorthositic material, have higher albedo and reflect more incident radiation, remaining cooler in daylight [38].
Infrared emission is the primary heat-loss mechanism. Since regolith emissivity is high, the surface radiates efficiently. During the night this causes low temperatures, especially in regions that receive no sunlight for long durations. Equatorial night temperatures can be close to 100 K, while polar permanently shadowed regions may remain at 30–40 K or less [37, 42].
Topography has a strong effect on local thermal conditions. Slopes, craters, boulders and ridges alter the solar incidence angle and may produce partial or permanent shadows. This effect is especially important near the poles because the Sun remains near the horizon and even small terrain elevations can cast long shadows.
Regolith properties also strongly influence heat transfer. Lunar regolith is a fragmented layer of dust, soil and rock. Its low thermal conductivity, often in the range 10^{-3} to 10^{-2} W/(m K) depending on depth and temperature, limits heat penetration into the subsurface [39]. Consequently, the upper surface experiences large temperature excursions, while deeper layers remain more stable.

7.14 Lunar Orbital Features Relevant to the Thermal Environment

The Moon's orbital and rotational characteristics are fundamental for the thermal environment. The Moon is in synchronous rotation with Earth: it rotates once around its axis in approximately the same time required to orbit Earth, so the same hemisphere faces Earth. This does not mean that one side is permanently illuminated; both near side and far side experience the lunar day–night cycle. However, synchronous rotation is important for communication geometry, illumination planning and mission operations.

7.14.1 Orbital Parameters and Motion

The Moon follows an elliptical orbit around Earth with an average semi-major axis of approximately 384,400 km. Its distance varies from about 363,300 km at perigee to about 405,500 km at apogee. The orbital eccentricity is approximately 0.0549 [36, 38].
The sidereal month, corresponding to one orbit relative to the fixed stars, is approximately 27.3 Earth days. The synodic month, corresponding to the cycle of lunar phases relative to the Sun as seen from Earth, is approximately 29.5 days. The difference occurs because Earth moves along its orbit around the Sun while the Moon orbits Earth.
The inclination of the lunar orbit relative to the ecliptic is approximately 5.14°. Because of this inclination, eclipses do not occur every month. They occur only when the Moon crosses the ecliptic plane near the line connecting Earth and Sun.

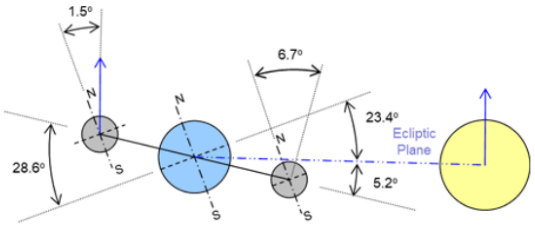


Figure 7.5: Lunar Orbit. Credits: [45]

7.14.2 Precession and Perturbations

The lunar orbit is perturbed mainly by the gravitational interaction with Earth and the Sun. One important long-period effect is the precession of the lunar nodes, the points where the lunar orbit crosses the ecliptic. This nodal precession has a period of about 18.6 years and affects long-term illumination conditions at the poles [38, 46].
Another effect is apsidal precession, the rotation of the major axis of the Moon's elliptical orbit. The line of apsides completes a cycle in approximately 8.85 years. This changes the timing and orientation of perigee and apogee and contributes to long-term variations in lunar geometry.
These orbital perturbations are relevant to polar mission planning because the illumination of ridges, crater rims and permanently shadowed regions depends on the long-term geometry of the Sun relative to the local terrain. For missions at the south pole, illumination maps over long time intervals are necessary to identify candidate locations with high solar availability.

7.14.3 Effects on Mission Design

For surface rovers and landers, lunar orbital and rotational parameters affect:

- duration of daylight and darkness;
- solar incidence angle;
- ground temperature evolution;
- communication availability with Earth or relay spacecraft;
- selection of landing site and operational windows;
- power availability for recharging;
- definition of hot and cold thermal cases.

At the poles, mission planning must account for the combination of slow lunar rotation, small axial tilt, local topography and long-term orbital precession. The same latitude can contain both near-continuously illuminated regions and permanently shadowed cold traps depending on local elevation.

7.15 Apollo 17 Landing Site as Thermal Reference

The Apollo 17 landing site provides an important reference for validating lunar surface thermal models because in-situ temperature data are available. The measured temperature trend at an equatorial or near-equatorial site is commonly used as a benchmark for models of the lunar regolith and surface energy balance.
Apollo and ALSEP data confirmed that daytime lunar surface temperatures can reach approximately 390 K, while nighttime temperatures can drop below 100 K [36, 37]. These values are consistent with the theoretical expectation of rapid heating under solar illumination and strong radiative cooling during the lunar night.
The Apollo experiments also provided information on subsurface thermal behaviour. The low thermal conductivity and low thermal inertia of the upper regolith imply that the diurnal thermal wave penetrates only a limited depth. Surface layers respond rapidly to solar illumination, while deeper layers experience damped and delayed temperature variations.
The Apollo 17 site is therefore useful for a modelling strategy in which an equatorial surface model is first validated against available measurements and then adapted to other latitudes. In this thesis, this reference is relevant because the objective is to develop a lunar surface model that can be parameterised with latitude and used to support rover thermal analyses over a wide range of possible operating locations.

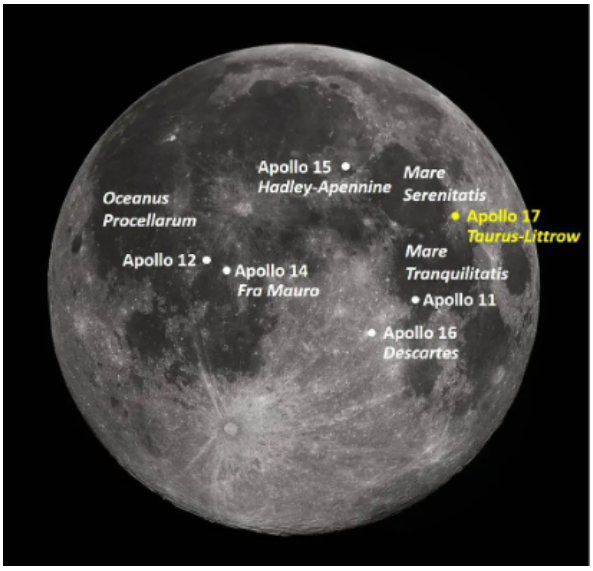


Figure 7.6: Apollo 17 landing site. Credits: [47]

7.16 Lunar South Pole Thermal Environment

The lunar south pole is one of the most important regions for future robotic and human exploration. Its interest is due to the possible presence of water ice and other volatiles in permanently shadowed regions, the existence of elevated areas with high solar illumination, and the relevance of these resources for in-situ resource utilisation. From a thermal point of view, the south pole is not simply a colder version of the equator; it is a highly heterogeneous environment where local topography dominates

illumination and temperature.
At equatorial and mid-latitude regions, the thermal cycle is mainly governed by the regular alternation between lunar day and night. At the south pole, instead, the Sun remains close to the horizon because the Moon's axial tilt is only about 1.54°. This produces grazing illumination, very long shadows and strong temperature differences over short distances.

7.16.1 Topography and Illumination

The south-pole terrain is rugged and dominated by large impact craters, ridges, slopes and depressions. Important craters include Shackleton, Shoemaker, Haworth and Faustini. Many of these craters contain permanently shadowed regions because their floors never receive direct sunlight. At the same time, crater rims and elevated ridges may receive sunlight for a large fraction of the lunar year [42, 46].
Shackleton crater is one of the most studied examples. Its rim can be illuminated for long periods, while its floor remains in permanent darkness. This creates a sharp contrast between regions suitable for solar power generation and regions that act as extremely cold traps.
Illumination maps averaged over long time spans, such as the 18.6-year nodal-precession period, are used to identify candidate sites for polar missions. These maps show that illumination conditions vary strongly with local topography and that spatial resolution is important. Features at scales of tens to hundreds of metres can determine whether a site is sunlit or shadowed.

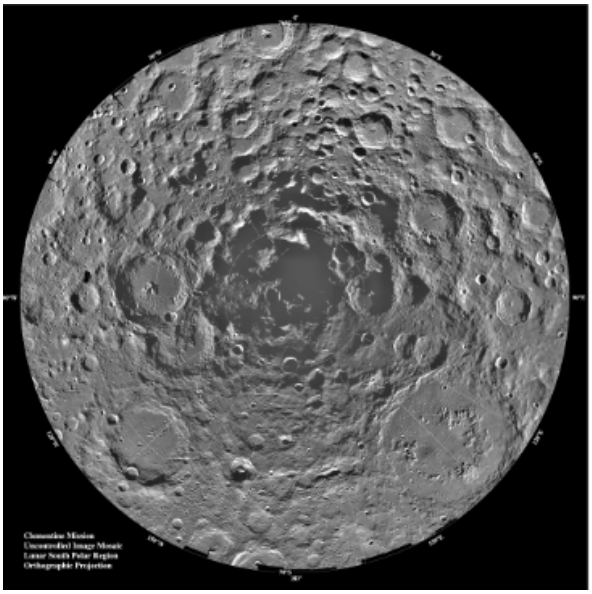


Figure 7.7: Lunar south pole topography. Credits: [48]

7.16.2 Temperature Conditions

South-pole temperatures depend on local illumination. Sunlit areas may maintain relatively moderate temperatures, often around 200–250 K, because they receive continuous

or near-continuous solar input but at low incidence angle. In contrast, permanently shadowed regions can reach extremely low temperatures, around 30–40 K, and in some models or measurements even lower values are reported for the coldest traps [37, 42]. The low thermal conductivity of the regolith amplifies these contrasts. A crater floor can remain extremely cold even when nearby ridges receive sunlight. The result is a highly non-uniform thermal environment that cannot be represented accurately by a single latitude-dependent temperature curve. Local topography must be included when the mission involves polar operation, crater exploration or permanently shadowed regions.

7.16.3 Cold Traps and Volatiles

Cold traps are regions where temperatures remain low enough for water ice and other volatile compounds to remain stable over geological timescales. For water ice in vacuum, temperatures below about 110 K are favourable for long-term stability [42]. Permanently shadowed craters at the lunar south pole therefore represent potential reservoirs of water ice.

Several mechanisms have been proposed for the origin of polar volatiles. Water may have been delivered by cometary or asteroidal impacts, produced by solar wind interactions with oxygen-bearing minerals, or released by volcanic outgassing in the Moon's history and later migrated to cold traps. Once molecules reach regions with sufficiently low temperature, they can freeze and remain trapped.

The LCROSS impact experiment in Cabeus crater provided direct evidence of water in the south-pole region. The ejecta plume analysis indicated water concentrations of approximately 5.6% by mass in the impacted material [42]. Additional evidence comes from LRO instruments and neutron spectrometer measurements, which show hydrogen enhancements and frost signatures in shadowed regions.

For rover thermal design, cold traps are challenging because they combine extremely low environmental temperature, limited or absent solar power, difficult illumination conditions and high uncertainty in local terrain. A rechargeable mini rover operating near a base should therefore avoid long exposure inside such regions unless it is specifically designed for survival in extreme cold.

7.16.4 South Pole Mission Implications

The lunar south pole offers both opportunities and challenges. Near-continuously illuminated ridges are attractive for solar power generation and communication, while nearby permanently shadowed regions are scientifically valuable because they may contain water ice and ancient volatile records. This combination makes the region one of the most promising for long-term human presence.

However, the same characteristics create engineering difficulties. The low Sun angle generates long shadows, which complicate navigation and hazard detection. The terrain is rugged, with craters, slopes and boulders. Temperatures can change drastically over short distances. Rovers must be designed to tolerate cold conditions, manage limited solar input, reject heat when illuminated and survive possible exposure to extremely cold shadowed zones.

For a rechargeable mini rover operating from a base, the south-pole environment also affects the recharge strategy. The charging station should be placed in a location with favourable illumination, thermal conditions and communication geometry. The rover sorties should be planned so that the vehicle can return before the battery state of charge or temperature reaches critical limits.

7.17 Lunar Pits and Cave Thermal Environment

Lunar pits, skylights and possible lava tubes are relevant to the broader context of lunar exploration because they may provide access to subsurface environments that are thermally and radiatively different from the exposed surface. Although direct pit descent is not assumed as the baseline mission for the rechargeable mini rover considered in this thesis, these environments are useful as reference cases because they show how strongly local geometry can affect surface thermal conditions.
A general thermal description valid for all pits is difficult because the environment depends on many parameters:

- latitude and longitude of the pit;
- mare or highland geological context;
- wall material and optical properties;
- pit diameter, depth and shape;
- presence of overhangs or vertical walls;
- possible connection to an underground lava tube;
- local time and solar incidence;
- visibility of the sky and ground surfaces.

Mare Tranquillitatis Pit is one of the most studied examples. Diviner measurements over more than ten years indicate that regolith-covered pit floors at equatorial latitudes can reach peak daylight temperatures around 420 K. During the night, pits can be about 100 K warmer than surrounding surface features because their geometry reduces radiative cooling and allows exchange with warmer walls [49].
If a connected lava tube is present, the interior permanent-shadow temperature could be much more stable and less extreme than the exposed surface, behaving somewhat like a radiative cavity. For Mare Tranquillitatis Pit, constantly shadowed regions have been estimated at approximately 17°C. This value is very favourable compared with the exposed lunar surface. However, thermal measurements alone cannot prove the presence of an underground void; detailed geometry and additional observations are needed [49].
For the mini rover, the main implication is that local terrain features can produce thermal environments that differ strongly from a flat-surface approximation. Even if the rover operates only near a pit rim or near rough terrain, the surrounding geometry can modify view factors, infrared exchange and solar exposure. This reinforces the need

for a thermal model able to include the ground and, when necessary, local geometric features.

7.18 Comparison Between Equatorial, Mid-Latitude and Polar Environments

The thermal environment of the Moon changes significantly with latitude. For rover design, this is one of the most important aspects because it directly affects maximum and minimum temperatures, solar power availability, recharge opportunities and heater requirements.

At equatorial latitudes, the Sun can reach high elevation angles. Daytime surface temperatures can exceed 390–400 K, while nighttime temperatures can fall near 90–100 K. The thermal cycle is strong and regular, with a long day and long night. This environment is critical both for hot-case radiator design and cold-case survival.

At mid latitudes, the solar incidence angle is lower, reducing peak daytime temperatures compared with the equator. However, the long lunar night remains severe. Terrain properties, slopes and local albedo become increasingly important.

At high latitudes, and especially near the poles, solar elevation is low. The direct solar heat input can be reduced, but shadowing becomes dominant. Some areas can receive extended illumination, while nearby crater interiors may remain permanently shadowed. Therefore, the polar environment is not homogeneous. It is a mosaic of illuminated ridges, partially shadowed slopes and extremely cold traps.

Table 7.2: Representative lunar thermal-environment characteristics by region.

Region	**Thermal characteristics**
Equatorial mare	High daytime temperatures, low albedo, strong day–night cycle, night temperatures near 100 K and useful conditions for Apollo-based validation.
Highlands	Higher albedo than maria, generally lower daytime temperatures at equal latitude and local time, strong dependence on local terrain.
Mid latitude	Intermediate solar incidence, relevant for many landing scenarios and still affected by the long lunar night.
South-pole ridges	Low-angle illumination, possible near-continuous sunlight, moderate but variable temperatures and favourable conditions for solar power and recharge stations.
Permanently shadowed regions	No direct solar input, extremely low temperatures, possible water-ice stability and severe rover survival challenge.
Pits and caves	Geometry-dominated environment, possible warmer night conditions and stable temperatures in permanently shadowed internal regions.

7.19 Thermal Environment Requirements for the Rover Model

For the rover considered in this thesis, the lunar thermal environment must be represented in a way that is flexible enough to support different latitudes and mission scenarios. The model should not be restricted to a single landing site. Instead, it should allow the latitude and illumination conditions to be varied, so that the same rover configuration can be assessed under equatorial, mid-latitude, high-latitude and polar cases.
The environmental model should include:

- direct solar radiation with the correct incidence angle;
- lunar albedo depending on region and surface properties;
- lunar infrared emission depending on ground temperature;
- radiation to deep space;
- local ground temperature as a function of latitude and time;
- regolith thermal inertia and low thermal conductivity;
- possible conduction through wheel–ground contact;
- shadowing by terrain, base elements and rover geometry when available;
- dust-deposition effects for long-duration analyses;
- recharge and standby conditions at the base station.

The development of a latitude-parametric lunar surface model is therefore justified by the physics of the environment. It allows the same thermal analysis framework to be applied to multiple locations and helps identify how the rover thermal balance changes with latitude. This is especially useful for a rechargeable mini rover because the thermal design must be compatible with both external sorties and repeated return to the charging station.
The model should ultimately support at least two operational cases. The first is the open-surface sortie, in which the rover operates for approximately three hours while exposed to the lunar environment. The second is the recharge and standby case, in which the rover is located at the charging station and exchanges heat with a different thermal boundary condition. In addition, the present thesis uses complete-lunar-day parametric simulations as an environmental design tool. These longer simulations identify the local-time and latitude combinations that bound the shorter operational cases; they should not be interpreted as the nominal mission timeline.

7.20 Chapter Summary

This chapter described the thermal environments relevant to a rechargeable lunar mini rover. The mission begins in controlled terrestrial conditions, continues through launch and transfer, reaches lunar orbit and descent, and finally enters the surface operational phase. Each environment is characterised by different dominant heat-transfer mechanisms and different modelling needs.

The general space radiative environment is governed by direct solar radiation, albedo radiation and planetary infrared radiation. Around Earth, atmosphere, clouds, seasons and surface types contribute to the variability of albedo and infrared flux. During lunar transfer, Earth contributions decrease and lunar contributions increase, while direct solar radiation remains approximately constant.

The lunar orbit and surface environments are more severe because the Moon has no atmosphere and rotates slowly. Lunar albedo depends on surface composition, with dark maria and brighter highlands producing different thermal responses. Lunar infrared emission is entirely surface-driven and varies strongly with local time, latitude, terrain and regolith properties. Surface temperatures can exceed 400 K in sunlit equatorial regions and fall below 100 K during the lunar night, while permanently shadowed polar regions can reach only a few tens of kelvin.

For a rover, the lunar surface environment adds direct conductive interaction with the ground, local shadowing, dust deposition and mutual radiative coupling between rover and regolith. The south-pole environment is even more heterogeneous because low solar elevation creates near-continuously illuminated ridges and permanently shadowed cold traps. Local terrain features, including pits and rough surfaces, can further modify view factors and infrared exchange.

These considerations motivate the construction of a parametric lunar surface thermal model valid for different latitudes. Such a model is necessary to analyse the rover thermal response consistently, to compare hot and cold cases, and to support the preliminary design of the thermal control system. The complete lunar thermal cycle is used as an environmental design envelope, whereas the nominal rover concept remains based on approximately three hours of surface activity followed by return to the charging station at the astronaut base. This distinction separates the duration of the environmental analysis from the duration of a single operational sortie.

Chapter 8

Lunar Surface Thermal Model

"Pulvis et umbra sumus."

— Horace
Odes, IV, 7

8.1 Objective and Modelling Logic

The objective of this chapter is to describe the lunar surface thermal model used as environmental boundary for the mini rover analysis. The rover does not operate in a generic space environment: it operates close to a surface that absorbs solar radiation, reflects part of the incident flux, emits infrared radiation and stores heat in the subsurface. For this reason, the lunar regolith is not treated as a fixed-temperature boundary. It is modelled as an active thermal system whose temperature evolves during the lunar day and changes with latitude, local time and material properties.

The model is used to evaluate the thermal conditions encountered by a rechargeable mini rover during representative surface operations. The nominal mission concept considers short sorties of approximately three hours followed by return to a charging station located at the astronaut base. The full lunar-day simulations used in this chapter have a different purpose: they are not intended to represent one continuous rover sortie, but to generate the latitude-dependent environmental envelope and the hot and cold boundary conditions that can be encountered at different local times. This distinction is important because the rover operational timeline is much shorter than the environmental cycle used to characterise the regolith.

The complete thermal architecture is divided into two main parts. The first part, presented in this chapter, is the lunar surface model. It calculates the local regolith temperature and the thermal environment generated by the ground. The second part, developed in the following chapter, is the mini rover model, which includes the internal equipment box, insulation, radiator coupling, internal heat loads and the thermal-control strategy. This separation makes the modelling logic clearer: first the lunar environment is defined and validated, then the rover is coupled to it.

The lunar surface model is based on two regolith descriptions. This choice is necessary because the thermal response of the Moon changes significantly with latitude. Up to 60°, the model follows an equatorial and mid-latitude approach, suitable for reproducing the strong day–night thermal cycle of Apollo-like surface conditions. From 70°

to 90°, a polar model is used, because high-latitude cases are dominated by low solar elevation, grazing illumination and lower regolith temperatures. The interval between 60° and 70° is treated as a transition region and is not used as a primary validation range.
The latitude-dependent modelling logic can be written as:

$$\mathcal{M}(\varphi) = \begin{cases} \mathcal{M}_{\text{mid}}, & |\varphi| \leq 60°, \\ \mathcal{M}_{\text{polar}}, & 70° \leq |\varphi| \leq 90°, \end{cases} \tag{8.1}$$

where φ is the latitude, $\mathcal{M}_{\text{mid}}$ is the equatorial/mid-latitude model and $\mathcal{M}_{\text{polar}}$ is the high-latitude polar model.

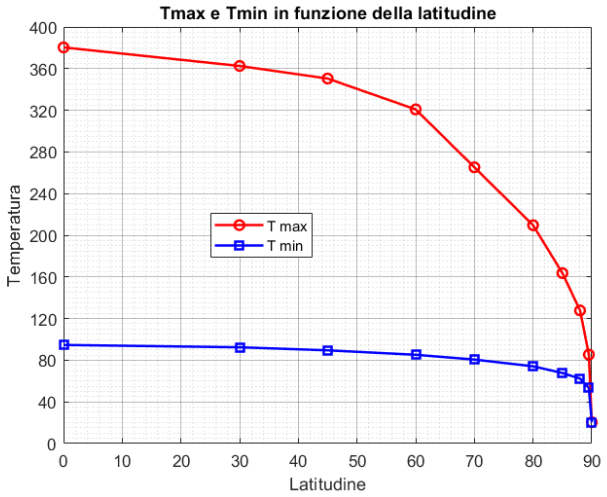


Figure 8.1: Latitude dependence of the lunar-surface temperature extrema used to identify the transition between the equatorial/mid-latitude and polar modelling ranges.

The physical reason for this split is the different solar geometry. At equatorial and mid latitudes, the Sun can reach high elevation during the lunar day. The surface is heated strongly and can reach temperatures comparable with Apollo and Diviner measurements. At high latitudes, the Sun remains close to the horizon, the incidence angle is large and the absorbed solar power is reduced. In this region, the regolith remains colder and the temperature dependence of thermal conductivity and specific heat becomes more important.
The lunar surface model is therefore used to answer the following questions:

- how the surface temperature changes with latitude and local time;
- how much infrared radiation the rover receives from the regolith;
- how the cold and hot environmental cases vary between equatorial, mid-latitude and polar locations;
- whether the ground thermal response is consistent with reference lunar temperature data;
- which environmental boundary conditions must be applied to the rover model.

8.2 General Thermal Balance

The model is implemented as a transient nodal thermal model. Each region of the system is discretised into thermal nodes, and each node is characterised by a thermal capacitance, conductive links, radiative links and possible heat loads. For a generic node i, the energy balance can be written as:

$$C_i \frac{dT_i}{dt} = \dot{Q}_{i,\text{int}} + \sum_j G_{ij}(T_j - T_i) + \sum_j \dot{Q}_{ij,\text{rad}} + \dot{Q}_{i,\text{env}}, \tag{8.2}$$

where $C_i = m_i c_{p,i}$ is the thermal capacitance of the node, $\dot{Q}_{i,\text{int}}$ is the internal heat generated in the node, G_{ij} is the conductive coupling between nodes, $\dot{Q}_{ij,\text{rad}}$ is the radiative exchange and $\dot{Q}_{i,\text{env}}$ is the external environmental heat load.
The conductive heat exchanged between two nodes is:

$$\dot{Q}_{ij,\text{cond}} = G_{ij}(T_j - T_i). \tag{8.3}$$

When an area conductance h is used, the equivalent conductance is:

$$G = hA, \tag{8.4}$$

where A is the coupled area. This form is useful for interfaces represented through an effective conductance rather than through an explicitly meshed solid.
Radiative exchange is nonlinear. For a surface radiating toward an equivalent sink, the heat rejected can be written as:

$$\dot{Q}_{\text{rad}} = \varepsilon \sigma A \left(T^4 - T_{\text{sink}}^4\right), \tag{8.5}$$

where ε is the infrared emissivity, σ is the Stefan–Boltzmann constant, A is the radiating area and T_{sink} is the equivalent sink temperature.
External convection is neglected because the Moon has no significant atmosphere. The external heat balance is therefore governed by radiation and by conduction through the solid paths that are explicitly included in the model. In this chapter the focus is the regolith thermal response and its radiative interaction with the rover environment. Wheel–ground conduction is introduced only when the rover model is coupled to the surface, because it depends on wheel geometry, contact area, material and contact conductance.

8.3 Why the Lunar Soil Must Be Modelled

The lunar soil is a key part of the thermal environment. A rover on the Moon exchanges radiation not only with the Sun and deep space, but also with the surrounding ground. The bottom face, wheels and lower side surfaces can have a significant view factor toward the regolith. As a result, the ground temperature directly affects the infrared load received by the rover and the net heat rejected by its external surfaces.
The lunar regolith has very low thermal conductivity. The superficial dust is particularly insulating because it is porous and weakly compacted. Therefore, the temperature

gradient in the first centimetres of the surface can be very high. During the lunar day, the upper surface can become hot while the deeper layers remain colder. During the lunar night, or in polar regions, the surface can cool down strongly while the subsurface temperature changes more slowly.
This behaviour has two important consequences. First, the surface temperature cannot be imposed as a constant value if the objective is to reproduce the thermal environment over a lunar day. Second, the subsurface must have enough thermal inertia to store and release heat during the cycle. A layered soil model is therefore used. It allows the surface node to respond rapidly to solar and infrared radiation, while deeper nodes represent heat storage and vertical heat conduction.

8.4 Lunar Soil Geometry Adopted for the Analysis

For the simulations, the lunar soil is modelled as two superimposed axisymmetric cylinders. The upper cylinder represents the superficial dust layer, while the lower cylinder represents the deeper regolith. The adopted geometry is:

- deep soil layer thickness: 1 m;
- deep soil vertical discretisation: 4 nodes;
- superficial dust layer thickness: 0.02 m;
- superficial dust vertical discretisation: 3 nodes.

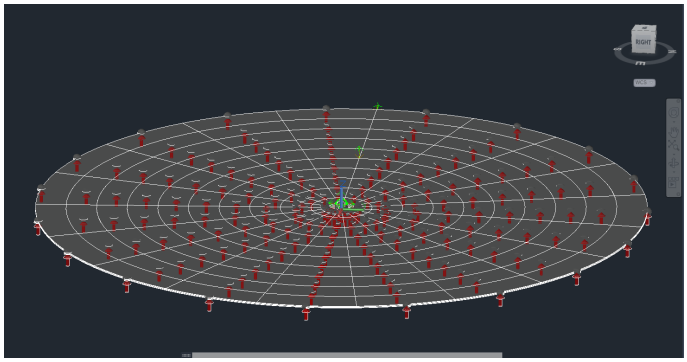


Figure 8.2: Axisymmetric lunar ground geometry used for the regolith thermal model.

This geometry is chosen because it is computationally efficient for repeated parametric analyses. Several cases must be run by varying latitude, internal rover heat load, insulation level and radiator coupling. A complete high-resolution terrain mesh would increase computational cost without being necessary for the first design iteration. The axisymmetric representation keeps the most important physical effect for this phase of the work: the vertical stratification of the regolith.
The dust layer is thinner and more finely discretised because the strongest temperature gradient occurs close to the surface. The deeper soil layer is thicker because it represents the thermal inertia of the subsurface. A depth of 1 m is sufficient for the preliminary model because the diurnal thermal wave is mainly concentrated near the upper regolith. The lower boundary is not treated as a fixed-temperature sink; instead, a heat flux is applied at the base to represent the contribution from deeper lunar layers.

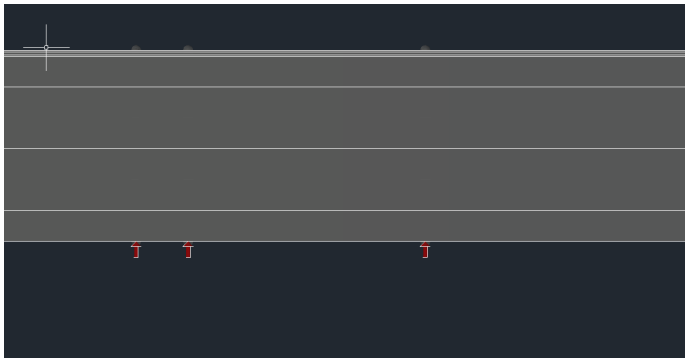


Figure 8.3: Vertical stratification of the superficial dust layer and deeper regolith.

8.5 Subsurface Heat Flux

A constant upward heat flux is applied at the base of the deep soil layer:

$$\dot{q}_{\text{base}} = 0.018\,\text{W/m}^2. \tag{8.6}$$

This value is the reference interior heat flux adopted in the regolith thermal model of Hayne et al. [50]. It is small compared with the daytime solar input, but it is relevant over long cold transients and prevents the lower part of the numerical domain from behaving as an artificial zero-flux thermal reservoir.
The base heat flux is especially relevant when analysing minimum soil temperatures, polar cases with reduced absorbed solar power, long transients over a complete lunar day and the thermal inertia of the soil beneath the superficial dust. Without this contribution, the model would lose part of the slow heat release that occurs from deeper regolith layers. The surface temperature could therefore be underestimated during cold periods, affecting the infrared radiation seen by the rover and producing an overly conservative cold-case environment.

8.6 Thermo-Physical Properties of the Regolith

The thermo-physical properties describe how the regolith stores and conducts heat. The adopted surface and deep-density values are consistent with the Diviner-based regolith model of Hayne et al. [50]:

$$\rho_{\text{soil}} = 1800\,\text{kg/m}^3, \qquad \rho_{\text{dust}} = 1100\,\text{kg/m}^3. \tag{8.7}$$

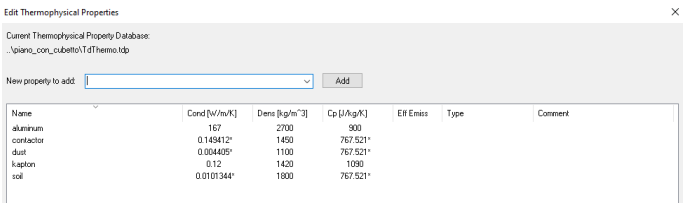


Figure 8.4: Thermo-physical property definition used for the lunar regolith model.

The superficial dust has lower density because it is more porous and less compacted. The deeper soil has higher density because compaction increases with depth. Since the

thermal capacitance is:

$$C = \rho V c_p, \tag{8.8}$$

the lower-density dust layer has lower thermal inertia and responds faster to the external radiative environment.

8.6.1 Specific Heat

The specific heat is modelled as a function of temperature:

$$c_p = c_p(T). \tag{8.9}$$

This is important because the model is used both at equatorial temperatures and at high latitudes, where the regolith can reach much lower temperatures. A constant value of specific heat would be a rough approximation over such a wide temperature range. A temperature-dependent c_p improves the representation of the soil thermal inertia, especially in cold cases.
In the implementation, $c_p(T)$ follows the temperature-dependent polynomial used by Hayne et al. [50]:

$$c_p(T) = c_0 + c_1 T + c_2 T^2 + c_3 T^3 + c_4 T^4, \tag{8.10}$$

with

$$\begin{aligned} c_0 &= -3.6125, \\ c_1 &= 2.7431, \\ c_2 &= 2.3616 \times 10^{-3}, \\ c_3 &= -1.2340 \times 10^{-5}, \\ c_4 &= 8.9093 \times 10^{-9}, \end{aligned} \tag{8.11}$$

where the coefficient units are such that c_p is obtained in $\mathrm{J/(kg\,K)}$ when T is expressed in kelvin.

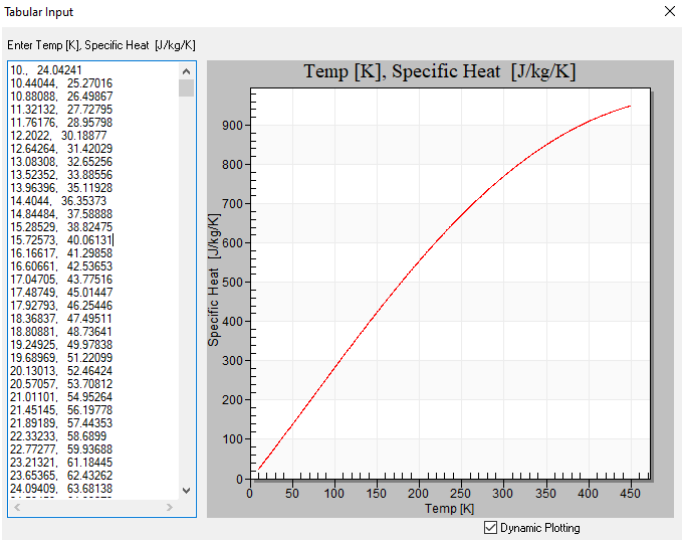


Figure 8.5: Temperature-dependent specific heat implemented for the lunar regolith.

During the transient solution, the solver updates the specific heat according to the current node temperature. The use of this fourth-order relation is consistent with the numerical values shown in Figure 8.5 and avoids treating the regolith thermal inertia as constant over the wide temperature range investigated.

8.6.2 Thermal Conductivity

The thermal conductivity is also modelled as a function of temperature:

$$k = k(T). \tag{8.12}$$

This dependence is physically necessary because lunar regolith is a porous granular material in vacuum. Heat transfer between particles occurs through solid contacts and through radiation between grains. The radiative contribution increases with temperature; therefore, the effective conductivity increases when the material becomes warmer. For the variable-property model, the conductivity follows the density- and temperature-dependent structure used in Diviner-based regolith models [50, 51]:

$$K(T, z) = K_c(z) \left[1 + \chi \left(\frac{T}{350} \right)^3 \right], \tag{8.13}$$

where $K_c(z)$ is the solid phonon conductivity, T is the absolute temperature, z is depth and χ is a dimensionless coefficient.
The density profile with depth can be written as:

$$\rho(z) = \rho_d - (\rho_d - \rho_s)\, e^{-z/H}, \tag{8.14}$$

where ρ_s is the surface density, ρ_d is the deep density and H is the scale height.
The depth-dependent solid conductivity is:

$$K_c(z) = K_d - (K_d - K_s)\, \frac{\rho_d - \rho(z)}{\rho_d - \rho_s}. \tag{8.15}$$

The parameters adopted in the variable regolith conductivity model are reported in Table 8.1. The density bounds and radiative parameter follow the Diviner-based formulation of Hayne et al. [50], while the values $K_s = 8 \times 10^{-4}$ and $K_d = 3.8 \times 10^{-3}$ W/(m K) correspond to the revised conductivity values reported by Feng et al. [51].

Table 8.1: Parameters used for the variable regolith conductivity model.

Parameter	**Value**	**Meaning**
ρ_s	$1100\,\mathrm{kg/m^3}$	surface/dust density
ρ_d	$1800\,\mathrm{kg/m^3}$	deep soil density
K_s	$8 \times 10^{-4}\,\mathrm{W/(m\,K)}$	surface conductivity parameter
K_d	$3.8 \times 10^{-3}\,\mathrm{W/(m\,K)}$	deep conductivity parameter
H	$0.06\,\mathrm{m}$	density scale height
χ	2.7	temperature-radiative conductivity coefficient

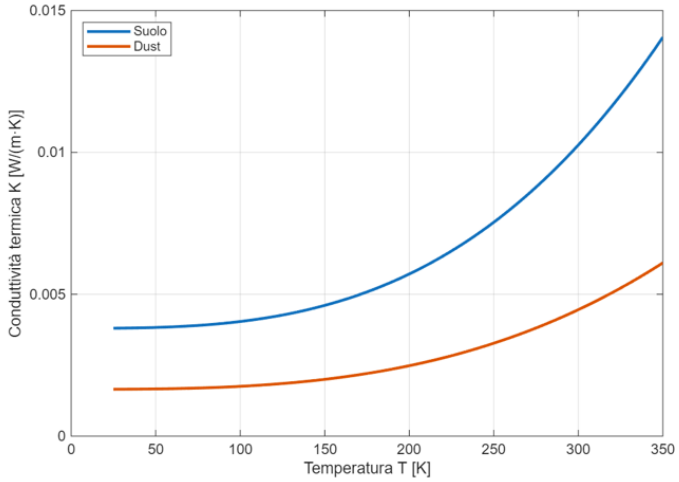


Figure 8.6: Temperature-dependent thermal conductivity of the representative soil and dust regions.

The use of $k(T)$ is one of the reasons why the high-latitude model is suitable for polar conditions. In cold regions, a constant conductivity would not reproduce correctly the reduced heat-transfer capability of the regolith.
Since the minimum rover temperatures depend on the ground infrared radiation, and the ground infrared radiation depends on the soil thermal response, this improvement is important for cold-case analysis.

8.7 Conductance Between Dust and Soil

The thermal connection between the superficial dust and the deeper regolith is represented through an equivalent area conductance. In the numerical implementation, a characteristic conduction length

$$L_{\text{eff}} = 0.01\,\text{m} \tag{8.16}$$

is associated with each side of the interface.

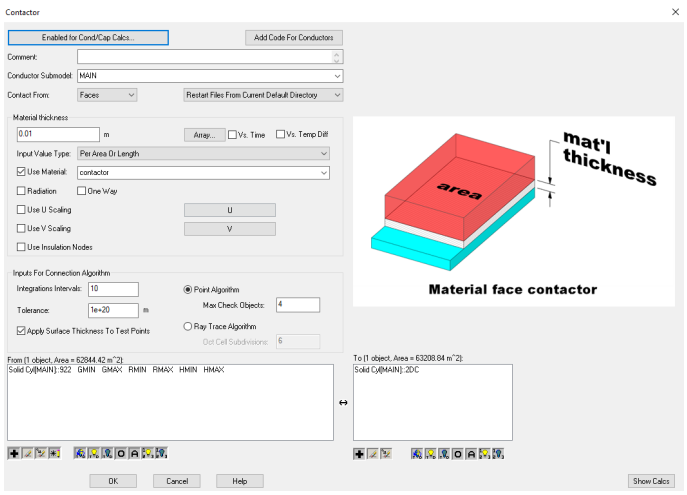


Figure 8.7: Thermal Desktop face contactor used at the dust–soil interface.

For two conductive regions acting in series, it is clearer to write the resistance per unit area directly. With the same characteristic length assigned to the dust and soil sides,

$$R''_{\mathrm{dust-soil}} = \frac{L_{\mathrm{eff}}}{k_{\mathrm{dust}}} + \frac{L_{\mathrm{eff}}}{k_{\mathrm{soil}}}, \tag{8.17}$$

and the corresponding area conductance is

$$h_{\mathrm{dust-soil}} = \frac{1}{R''_{\mathrm{dust-soil}}} = \left[L_{\mathrm{eff}} \left(\frac{1}{k_{\mathrm{dust}}} + \frac{1}{k_{\mathrm{soil}}} \right) \right]^{-1}. \tag{8.18}$$

This form is dimensionally explicit and avoids interpreting the series combination as a material conductivity independent of the adopted path length.

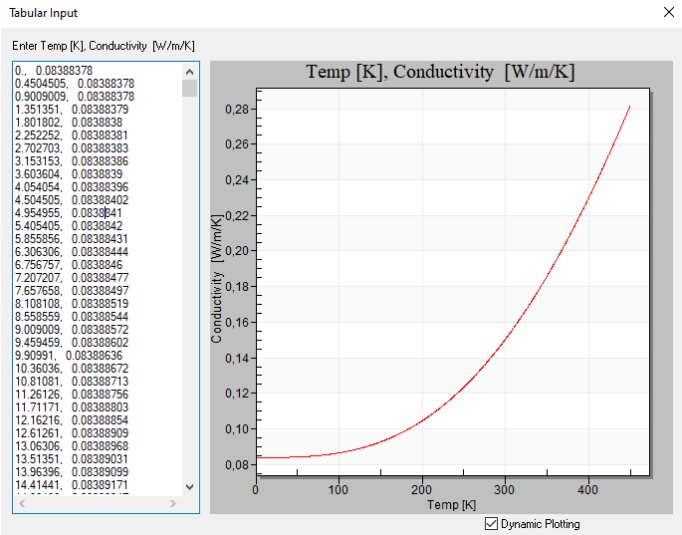


Figure 8.8: Temperature-dependent interface parameter used to define the dust–soil conductive coupling.

This conductance has a direct influence on the surface thermal cycle. If the conductance is high, the superficial dust is strongly coupled to the deeper soil and its temperature variations are damped. If the conductance is low, the dust becomes more isolated and the surface temperature can vary more strongly. Since both k_{dust} and k_{soil} depend on temperature, the equivalent conductance also varies with temperature.
This effect is particularly important for the polar model, where the regolith can remain at low temperature for long periods. In those conditions, $k(T)$ is lower and the coupling between surface and subsurface becomes weaker. This affects the cold-case ground temperature and therefore the minimum temperature predicted for the rover.

8.8 Two Regolith Optical Models

The optical properties define how the lunar surface interacts with radiation. They determine how much solar energy is absorbed, how much is reflected and how efficiently the surface emits infrared radiation. In the model, two optical descriptions are used:

- an equatorial/mid-latitude model, used up to 60°;

- a polar model, used from 70° to 90°.

This division is introduced because a single optical approximation does not represent all latitude ranges with the same accuracy. At low and mid latitudes, average optical properties are sufficient to reproduce the Apollo-like thermal behaviour. At high latitudes, the Sun remains close to the horizon and the incidence angle becomes a dominant variable in the absorbed solar flux.

8.8.1 Equatorial and Mid-Latitude Optical Model

For latitudes up to 60°, the regolith optical properties are treated as constant. The adopted solar absorptivity is:

$$\alpha_{\mathrm{eq}} = 0.87, \tag{8.19}$$

and the infrared emissivity is:

$$\varepsilon_{\mathrm{IR,eq}} = 0.97. \tag{8.20}$$

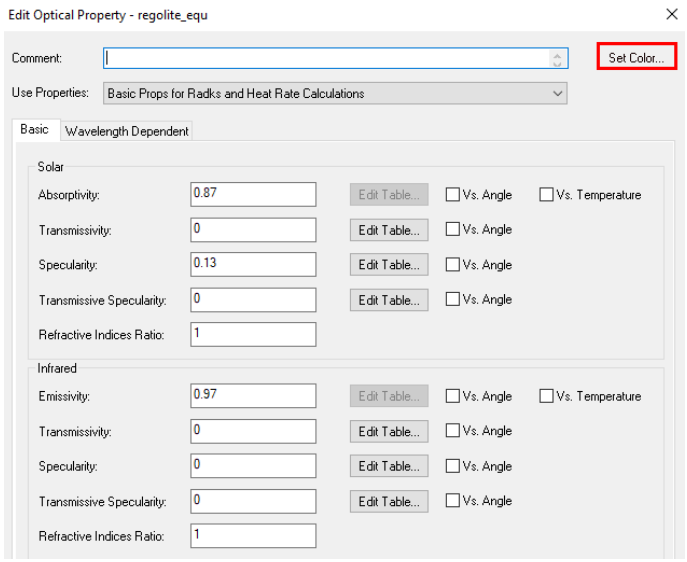


Figure 8.9: Thermo-optical properties assigned to the equatorial and mid-latitude regolith model.

This constant-property approximation is used only for the equatorial and mid-latitude branch of the present model. It represents an average lunar surface response in the range in which the Sun reaches appreciable elevation and the surface undergoes a strong day–night temperature cycle. The more detailed Diviner-based model used for the high-latitude branch is described in the following subsection.

8.8.2 Polar Optical Model

For latitudes from 70° to 90°, a polar optical model is adopted. The polar region is characterised by grazing solar illumination. Therefore, the absorbed solar flux must be reduced according to the incidence angle.

The albedo is modelled as a function of solar incidence angle following the empirical angular dependence used by Feng et al. [51]:

$$A_\theta = A_0 + \left[1 - \cos^{0.2752}(\theta)\right], \tag{8.21}$$

where θ is the solar incidence angle measured from the local normal. In the present Thermal Desktop implementation,

$$A_0 = 0.16, \tag{8.22}$$

which gives a normal-incidence absorptivity of $\alpha(0) = 0.84$, consistent with the first value of the angular table shown in Figure 8.10. The absorptivity is then

$$\alpha(\theta) = 1 - A_\theta. \tag{8.23}$$

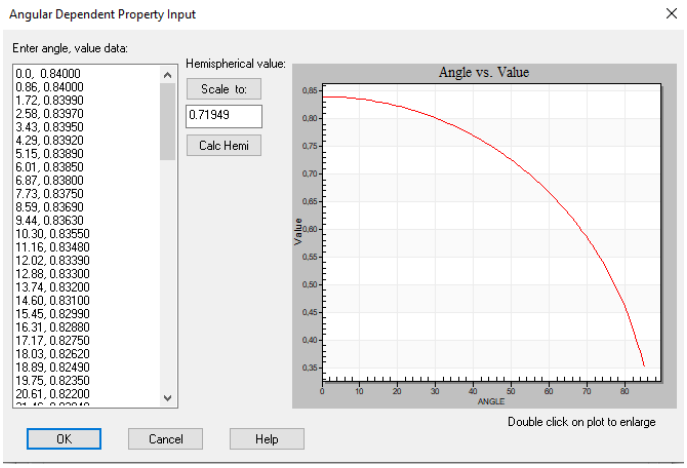


Figure 8.10: Angular-dependent solar absorptivity assigned to the polar regolith model.

In the final implementation, the thermo-physical properties, such as c_p and k, are temperature-dependent, while the optical absorbed fraction is varied with solar incidence angle. This distinction is important because temperature controls heat capacity and conduction, whereas incidence angle controls the amount of solar radiation absorbed by the surface.
The consequence is that the polar surface absorbs less solar energy than the equatorial surface. Therefore, even during illumination, the high-latitude regolith reaches lower maximum temperatures. A rover placed above this surface receives lower infrared radiation from the ground and is more exposed to cold-case criticality.

8.9 Latitude-Dependent Model Selection

The model used in the analysis is the union of two latitude-dependent regolith models:

1. from 0° to 60°, the equatorial/mid-latitude Apollo-based model is used;
2. from 70° to 90°, the polar variable-property model is used.

The first model is reliable for low and intermediate latitudes because it is based on the validated Apollo-type lunar surface thermal response. The second model is necessary at high latitudes because the south-pole environment is colder, the solar incidence angle is larger and the thermo-physical properties must remain valid over a lower temperature range.
The practical selection is reported in Table 8.2.

Table 8.2: Latitude-dependent selection of the lunar soil model.

Latitude range	**Model**	**Reason**
$0° \leq \lvert\varphi\rvert \leq 60°$	Equatorial/mid-latitude model	Apollo-like thermal behaviour
$60° < \lvert\varphi\rvert < 70°$	Transition interval	Not used as primary validated range
$70° \leq \lvert\varphi\rvert \leq 90°$	Polar variable-property model	Low Sun elevation and cold regolith

This modelling choice also defines the latitudes analysed in the parametric study:

$$\varphi = [0°, 30°, 45°, 60°, 70°, 80°, 85°, 89.999°]. \tag{8.24}$$

The values up to 60° belong to the first model, while values from 70° upward belong to the second model. The latitude 89.999° is used instead of exactly 90° to avoid numerical singularities that may occur at the pole in some coordinate definitions.

8.10 Pseudo-Orbit Implementation

Thermal Desktop is naturally designed to define orbital environments. In this work, however, the model represents a point fixed on the lunar surface. To reproduce the apparent motion of the Sun with respect to the local surface and to generate a complete environmental envelope, a pseudo-orbit is used.
The pseudo-orbit is defined with:

- fixed latitude;
- initial longitude;
- altitude equal to zero;
- orientation fixed with the lunar surface;
- one lunar day divided into 300 time intervals.

The altitude is set to zero because the model is placed on the surface. The local frame remains fixed to the lunar ground, while the Sun direction changes during the lunar day. The 300 intervals provide a compromise between temporal resolution and computational cost for the environmental model. These intervals are not intended to resolve the nominal three-hour rover sortie itself; they are used to reconstruct the slow regolith response over the complete lunar cycle and to extract representative boundary conditions for the rover analyses.

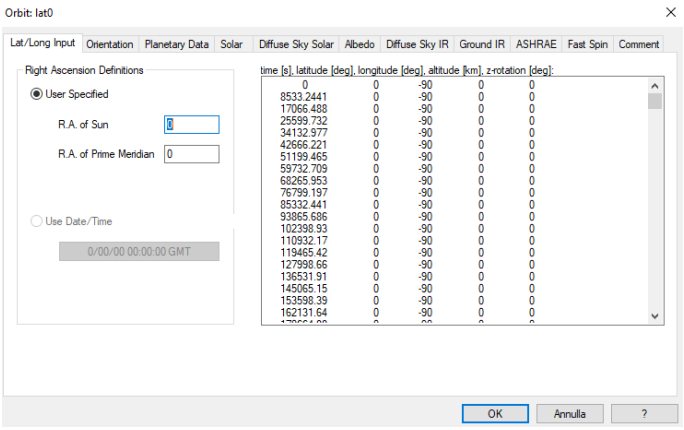


Figure 8.11: Pseudo-orbit definition used to reproduce the apparent solar motion over a complete lunar day.

The pseudo-orbit allows the model to compute the direct solar load on the surface, the time variation of the solar incidence angle, the surface temperature evolution during the lunar day and the different thermal response at each analysed latitude.

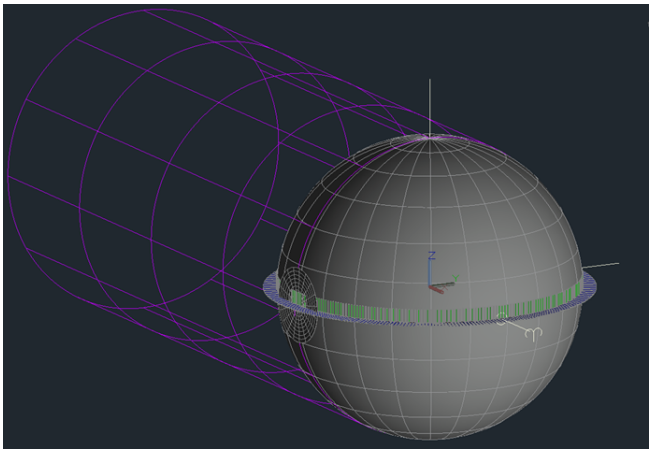


Figure 8.12: Thermal Desktop view of the surface-fixed pseudo-orbit environment.

8.11 Validation of the Soil Model

Before coupling the regolith to the rover, the predicted surface-temperature trends are compared with reference lunar temperature data. This comparison is essential because the rover analysis depends directly on the ground temperature and on the infrared radiation emitted by the regolith.
For the equatorial and mid-latitude branch, the reference behaviour is the large Apollo/Diviner day–night temperature excursion. For the high-latitude branch, the reference is the Diviner/LRO trend showing progressively lower daytime temperatures as latitude increases. The adopted temperature-dependent density, heat capacity and conductivity relations are based on Diviner-derived regolith models [50, 51].
The comparison shown in Figures 8.13 and 8.14 is used here as a trend- and order-of-magnitude consistency check. It verifies that the model reproduces the expected

decrease in peak surface temperature with latitude and the strong separation between equatorial and polar thermal regimes. No formal point-by-point correlation, residual metric or uncertainty fit is performed in this thesis; therefore, the term "validation" should be interpreted at the preliminary model level rather than as a flight-model correlation campaign.
If the surface model overestimates the temperature, the rover receives too much infrared radiation and the predicted hot case becomes too severe. If it underestimates the temperature, the rover appears colder than it would be in reality and the predicted cold case becomes more conservative. The consistency check is therefore required before using the regolith model as a boundary condition for the rover.

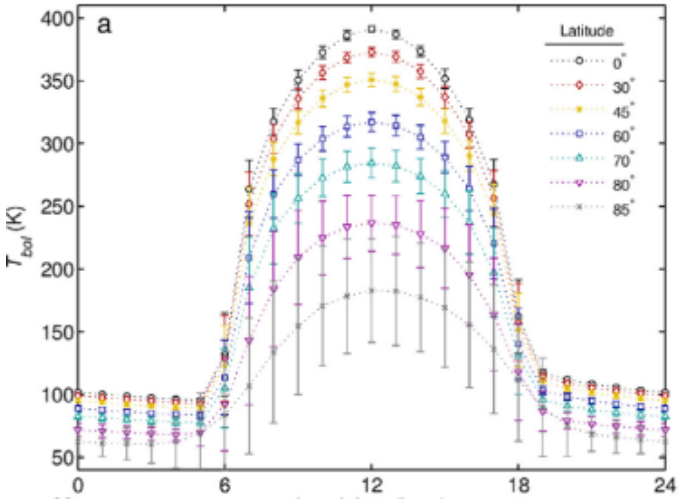


Figure 8.13: Reference lunar surface-temperature trends used for comparison with the numerical model. Credits: [43]

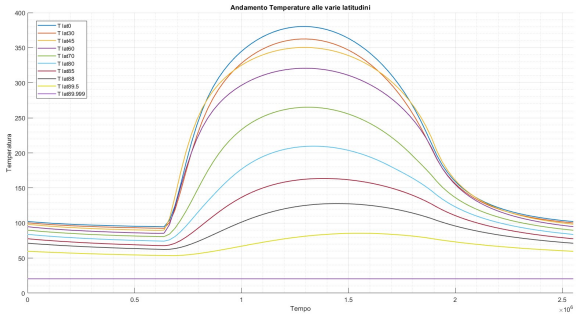


Figure 8.14: Simulated lunar surface-temperature histories at the analysed latitudes.

8.12 Chapter Summary

This chapter described the lunar surface thermal model used as environmental input for the mini rover analysis. The model represents the regolith as an active thermal system rather than as a fixed-temperature boundary. This is necessary because the ground temperature controls the infrared radiation received by the rover and changes

strongly with latitude, local time and regolith properties.
The lunar soil is represented by a layered model composed of a superficial dust layer and a deeper soil layer. The dust layer is thinner and more finely discretised because the largest temperature gradients occur close to the surface. The deeper soil provides thermal inertia, while a small upward heat flux at the lower boundary represents the contribution from deeper lunar layers. The temperature-dependent heat capacity and conductivity laws are based on Diviner-derived regolith formulations, while the polar branch also includes an incidence-angle-dependent solar absorptivity. The complete lunar-day transient is used to generate the environmental envelope; it is not interpreted as the duration of a nominal three-hour rover sortie.

Chapter 9

Rover and Thermal Control System Model

"Perfection is reached not when there is nothing left to add, but when there is nothing left to remove."

— Antoine de Saint-Exupéry
Terre des hommes

9.1 Modelling Philosophy and Chapter Logic

The objective of this chapter is to build the thermal model of the rechargeable lunar mini rover in a progressive and physically traceable way. The model is not introduced directly in its final configuration. Instead, it is constructed step by step, starting from the simplified rover body and then adding the elements that become necessary as the thermal behaviour is understood. This approach is useful because the thermal-control problem of a small lunar rover is not driven by a single parameter. It depends on the simultaneous effect of the lunar environment, the regolith temperature, the radiative coupling with the ground, the internal dissipated power, the insulation level and the heat-rejection path.

The logic followed in the chapter is the following. First, the internal rover box is created and the temperatures of its six faces are analysed at different latitudes. This first step is necessary to show that the rover panels do not experience the same thermal boundary condition. The top face, bottom face and side faces see different parts of the environment and therefore develop different thermal histories. The face-temperature plots are discussed by considering first the extreme latitude cases and then the intermediate ones, because the extremes reveal the dominant hot and cold tendencies of the model.

After this first observation, an external MLI-like shell is introduced. The purpose of the shell is to reduce the direct coupling between the internal protected compartment and the external lunar environment. The introduction of the MLI makes the internal temperature field more uniform and allows the internal box to be treated as a representative equipment compartment. However, the insulation also creates a classical thermal-control trade-off: it helps to retain heat in cold conditions, but it also traps internally generated heat in hot or high-power conditions.

The next step is therefore a sensitivity analysis on the effective coupling between the internal box and the MLI shell, together with the internal heat load. The results are again interpreted by considering first the two extreme insulation values and then the intermediate values. This order is adopted because the two extreme cases define the physical limits of the problem, while the intermediate cases indicate the possible compromise region.
Since the insulation alone cannot guarantee both heat retention and heat rejection, a radiator is then added on the top face of the rover. The radiator introduces an intentional heat-rejection path, separated from the global environmental leakage through the MLI. Several combinations of radiator conductance and insulation coupling are compared. The discussion follows the same logic: first the extreme radiator links are interpreted, and then the intermediate combinations are used to identify the design compromise.
Finally, representative hot and cold cases are evaluated. These cases show that a fixed radiator conductance cannot be optimal in both thermal extremes. In the hot case, the rover needs a strong thermal path to the radiator. In the cold case, the same thermal path becomes an unwanted heat leak. For this reason, the final part of the chapter introduces a variable radiator link, interpreted at preliminary level as the equivalent behaviour of a Loop Heat Pipe with a Thermal Control Valve.
It is important to distinguish the simulation time horizon used in this chapter from the nominal operational concept of the rover. The mission concept introduced in Chapter 3 is based on sorties of approximately three hours followed by return to the charging station. The simulations performed here over a complete lunar thermal cycle are therefore not intended to represent one continuous rover sortie. They are used as an environmental and design envelope to expose the rover model to the full range of boundary conditions associated with the selected latitude. A later mission-level model should superimpose the actual three-hour operational timeline and its time-dependent power profile on the environmental conditions identified here.

9.2 Temperature Limits and Result Classification

The internal rover temperature is compared with the allowable range selected for the protected equipment compartment. The lower and upper limits are

$$T_{\mathrm{min,req}} = 253.15\,\mathrm{K}, \qquad T_{\mathrm{max,req}} = 323.15\,\mathrm{K}, \tag{9.1}$$

corresponding approximately to $-20\,^{\circ}\mathrm{C}$ and $50\,^{\circ}\mathrm{C}$. These limits are used as preliminary requirements for the internal box, which represents the volume containing the battery, on-board computer, communication electronics, sensors and other temperature-sensitive equipment.
For each transient case, the minimum and maximum internal temperatures are extracted as

$$T_{\mathrm{min}} = \min_t T_{\mathrm{box}}(t), \qquad T_{\mathrm{max}} = \max_t T_{\mathrm{box}}(t). \tag{9.2}$$

A case is acceptable only if

$$T_{\mathrm{min,req}} \leq T_{\mathrm{box}}(t) \leq T_{\mathrm{max,req}} \qquad \forall t. \tag{9.3}$$

If the internal temperature falls below the lower limit, the case is classified as cold-critical. If the internal temperature exceeds the upper limit, the case is classified as hot-critical. If the whole transient response remains between the two limits, the case is considered acceptable.
This classification is deliberately simple. It does not yet include component-specific qualification limits, operational margins, heater dead bands or battery charge/discharge restrictions. However, it is adequate for the objective of this chapter, which is to compare different preliminary thermal-control configurations and identify the main design drivers.

9.3 Simplified Internal Rover Box

9.3.1 Purpose of the Simplified Rover Geometry

The first rover model is a simplified rectangular box. This approximation is adopted because the aim of the analysis is to understand the global thermal behaviour of the protected internal compartment, not to predict the detailed temperature of every individual unit. At this stage, the final layout of the rover is not fixed. The exact positions of the battery, on-board computer, communication unit, navigation sensors, payload, harnesses, brackets, screws, inserts, motor drivers and local mounting interfaces are still design-dependent. Introducing a detailed component-level model too early would therefore create a model that appears more realistic but is not necessarily more reliable. The simplified box is instead used to isolate the dominant heat-transfer mechanisms. The model must show how the rover exchanges heat with the lunar surface, how the external faces respond to different latitude conditions, how insulation changes the internal temperature field, how internal power affects the global temperature and why a radiator becomes necessary. Once these effects are understood, the model can be refined in a later phase by adding detailed equipment nodes and real mechanical interfaces.
This approach is also consistent with the mission concept of a rechargeable mini rover operating near an astronaut base. The rover is not designed as a large long-duration vehicle with abundant thermal-control resources. It is a compact robotic platform, with limited thermal inertia, limited area for radiators and limited power available for heaters or active control. For this reason, a preliminary thermal model is useful even before the final mechanical design is frozen.

9.3.2 Internal Box Geometry and Nodalisation

The internal rover body is modelled as a rectangular box made of six thin-shell surfaces. The adopted dimensions are

$$L_x = 0.40\,\mathrm{m}, \qquad L_y = 0.20\,\mathrm{m}, \qquad L_z = 0.20\,\mathrm{m}. \tag{9.4}$$

The wall thickness is

$$t_{\mathrm{box}} = 2\,\mathrm{mm}. \tag{9.5}$$

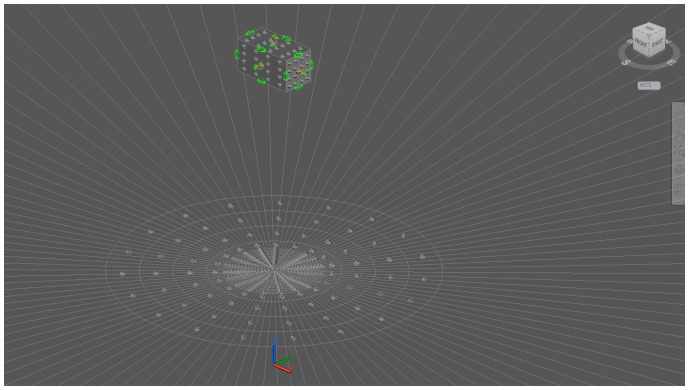


Figure 9.1: Simplified internal rover box used as the first thermal representation of the protected equipment compartment.

Figure 9.1 shows the starting geometry of the rover thermal model. The box represents the internal protected volume, while the external mechanical elements are not included in this first configuration. The use of a box is not intended to reproduce the final rover shape in detail. It is a controlled geometry that allows the effect of the main thermal paths to be studied clearly.
Each face is discretised with 16 nodes. This choice is a compromise between physical resolution and computational simplicity. A single node per face would impose an almost uniform panel temperature and would hide local gradients caused by radiation view factors and environmental exposure. A very fine discretisation would increase the computational cost without being justified by the preliminary level of the geometry. The adopted nodalisation therefore allows face-to-face and intra-face thermal differences to appear while keeping the model suitable for parametric analyses.
The rover body is placed at a representative height

$$h_{\text{rover}} = 1\,\text{m} \tag{9.6}$$

above the lunar surface. This value is used to compute the radiative interaction with the regolith. It does not define the final mechanical ground clearance of the rover, because the simplified model does not include wheels, suspension and deployment hardware. It is instead a numerical placement parameter for the preliminary radiation problem. Consequently, the results obtained with this simplified geometry are used primarily for comparative sensitivity studies; the more representative body–wheel–ground thermal paths are introduced in the following chapter.

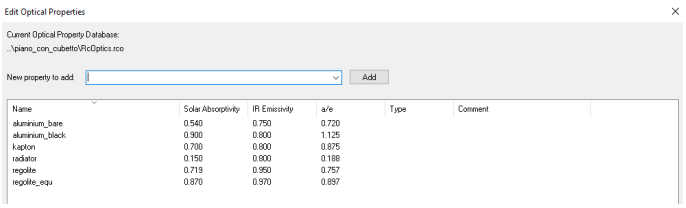


Figure 9.2: Thermo-optical properties assigned to the internal box surfaces in Thermal Desktop.

Figure 9.2 reports the optical settings used for the internal box. The internal side is treated with high emissivity, approximating a black aluminium cavity. This is useful

because the detailed internal equipment is not modelled explicitly. In a real rover, electronic boards, batteries, harnesses, brackets and structural supports would exchange heat by radiation inside the compartment. In the simplified model, using a high internal radiative coupling helps to distribute heat between panels and avoids an unrealistically isolated behaviour of individual walls.

9.3.3 Conductive Coupling Between Panels

At the beginning of the analysis, no arbitrary conductive connection is imposed between adjacent panels of the internal box unless a heat path is explicitly defined. This assumption may appear conservative, but it is useful because it keeps the model physically traceable. In the real rover, the panels would be connected through frames, joints, screws, inserts and brackets. These elements would conduct heat from one wall to another. However, their final geometry and thermal conductance depend on the mechanical design, which is not available at this stage.

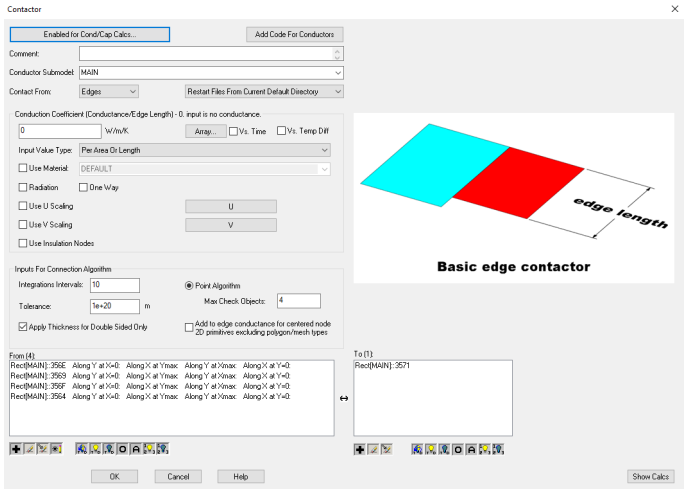


Figure 9.3: Initial modelling assumption for the internal panels: no arbitrary conductive connection is imposed between adjacent faces.

Figure 9.3 illustrates this assumption. The panels are not connected through artificial edge conductors. The temperature redistribution occurs through internal radiation and through the thermal paths introduced later, such as the MLI coupling and the radiator link. This choice avoids assigning uncertain conductances that would make the model appear detailed without improving its reliability.
The consequence is that the first bare-box results must be interpreted as a diagnostic step. They do not represent the final rover behaviour. Instead, they show how the different faces respond to the lunar thermal environment before the insulation and thermal-control system are introduced. This is useful because it highlights which panels are naturally hot or cold and why a dedicated insulation concept is required.

9.4 Face Temperature Behaviour Before the MLI Shell

The first set of plots shows the temperature evolution of the six box faces for different latitudes. These results are used to understand the raw environmental forcing on the rover. The bottom face is more coupled with the lunar ground, the top face has a stronger view to deep space, and the side faces are affected by solar direction and latitude. Therefore, the six faces do not behave as a single isothermal body.
The figures are discussed starting from the two extreme cases, 0° and 85°. This order is useful because the equatorial case represents the strongest hot tendency, while the high-latitude case represents the strongest cold tendency among the plotted cases. The intermediate latitudes are then used to show the transition between these two behaviours.

9.4.1 Extreme Latitude Cases

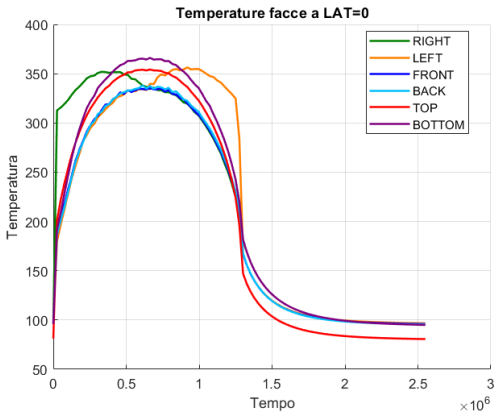


Figure 9.4: Temperature evolution of the internal box faces at the equator.

Figure 9.4 represents the equatorial case. This is the most severe hot reference among the analysed latitude plots. At low latitude, the Sun reaches a high elevation during the illuminated part of the lunar cycle and the regolith can reach high daytime temperatures. As a consequence, the rover receives heat not only from direct solar radiation and reflected solar radiation, but also from infrared emission from the warm ground.
The face temperatures differ because each panel sees a different radiative environment. The bottom face is more influenced by the ground infrared flux, while the top face sees more deep space. The lateral faces depend on their orientation with respect to the Sun and on the radiation reflected or emitted by the surrounding terrain. The important point is not only the absolute value of each curve, but the fact that the bare rover body does not naturally remain uniform. This confirms that the thermal model must account for face-dependent boundary conditions and not only for a single average environmental temperature.

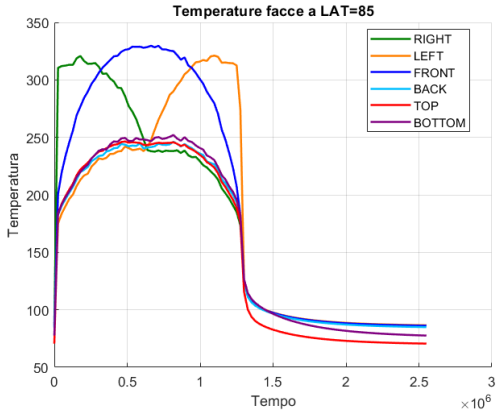


Figure 9.5: Temperature evolution of the internal box faces at high latitude.

Figure 9.5 represents the opposite extreme. At high latitude, the environmental heating is much weaker. The surface remains colder, the solar incidence is lower and the rover receives less infrared radiation from the regolith. The thermal problem therefore changes nature: instead of being dominated by overheating, it becomes dominated by heat retention and cold survival.
The comparison between Figure 9.4 and Figure 9.5 is one of the key motivations for the rest of the chapter. The same rover geometry cannot be judged from a single latitude. A configuration that is acceptable at high latitude may overheat at the equator, while a configuration designed to reject heat at the equator may become too cold near the pole. This is the first indication that the thermal-control system must be robust over a wide environmental range.

9.4.2 Intermediate Latitude Cases

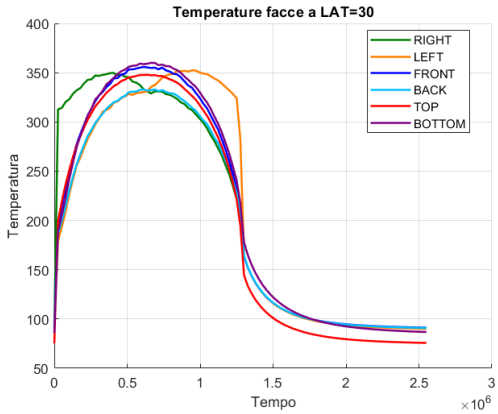


Figure 9.6: Temperature evolution of the internal box faces at 30° latitude.

Figure 9.6 shows the first intermediate case. The rover is still relatively close to the equatorial regime, so the lunar surface can provide a significant infrared contribution. However, the thermal forcing is already less severe than at 0°. This case shows the beginning of the transition from the hot-dominated equatorial behaviour toward the mid-latitude regime.

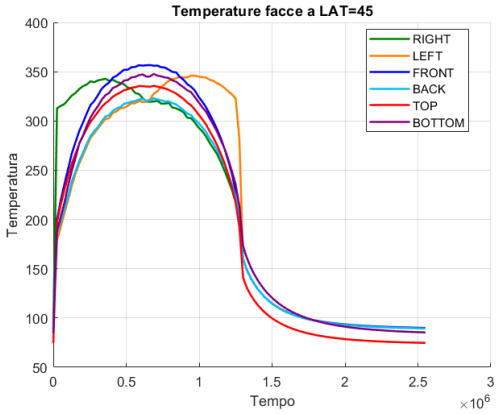


Figure 9.7: Temperature evolution of the internal box faces at 45° latitude.

Figure 9.7 represents a central latitude condition. The ground temperature and absorbed flux are lower than in the equatorial case, but the environment is not yet as cold as in the polar cases. This type of result is useful because it often corresponds to a transition region where neither the hot nor the cold extreme completely dominates. The thermal design must therefore preserve sufficient margin in both directions.

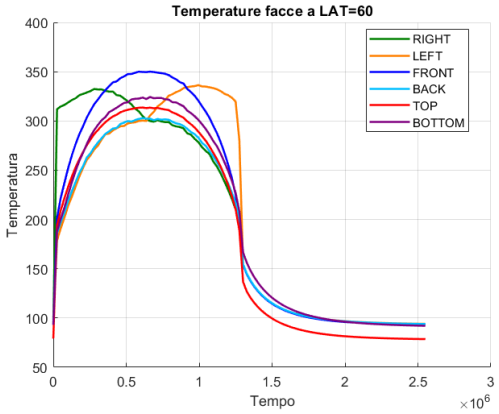


Figure 9.8: Temperature evolution of the internal box faces at 60° latitude.

Figure 9.8 shows that the rover response becomes increasingly sensitive to heat loss. At this latitude, the environmental heating is reduced, so the internal heat load and the insulation concept become more important. The plot therefore starts to reveal the cold-side design driver: the rover must avoid losing too much heat when the external environment is cold and the internal power is low.

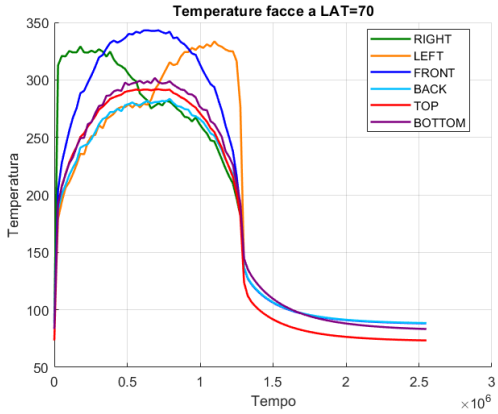


Figure 9.9: Temperature evolution of the internal box faces at 70° latitude.

Figure 9.9 confirms the shift toward cold-critical behaviour. The face temperatures are affected by the lower surface temperature and by the reduced solar contribution. This case is important because it shows that high-latitude operation cannot be treated simply as a colder version of the equatorial case. The relative importance of each heat path changes: environmental heat input decreases, while heat losses to space and through the radiator or insulation interfaces become more important.

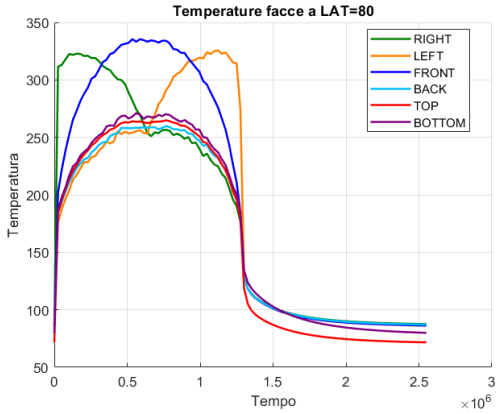


Figure 9.10: Temperature evolution of the internal box faces at 80° latitude.

Figure 9.10 is close to the polar regime. The external environment is colder and the role of internal dissipation becomes more evident. In this condition, the rover is more likely to require heat retention, survival power or a reduced coupling to the radiator. This result prepares the interpretation of the later hot and cold case maps, where high latitudes remain cold-critical even when some configurations are acceptable at lower latitudes.

The overall conclusion of the face-temperature study is that the bare internal box is not a satisfactory final model for the protected rover compartment. The individual panels are too directly affected by their local radiative boundary conditions. A layer that decouples the internal volume from the environment is therefore necessary. This motivates the introduction of the MLI-like shell.

9.5 MLI Shell Model

9.5.1 Purpose of the MLI-Like Shell

The external insulation is represented by an MLI-like shell surrounding the internal rover box. The purpose of the insulation is to reduce uncontrolled radiative heat exchange between the rover and the lunar environment. This is essential because the rover may experience very different boundary conditions depending on latitude and operation. In cold or high-latitude conditions, the rover must avoid excessive heat loss. In hot conditions, the insulation also reduces direct environmental heat input to the internal box.
The MLI-like shell performs four main functions:

- it reduces heat loss from the protected compartment in cold conditions;
- it reduces direct heating of the internal box by the external environment;
- it decouples the internal equipment from rapid external variations;
- it makes the internal temperature field more uniform and easier to interpret.

However, MLI is not a complete thermal-control system by itself. If the insulation is too effective, internal heat generated by electronics, mobility units, battery management or communication equipment cannot escape easily. Therefore, the MLI must later be combined with a controlled heat-rejection path.

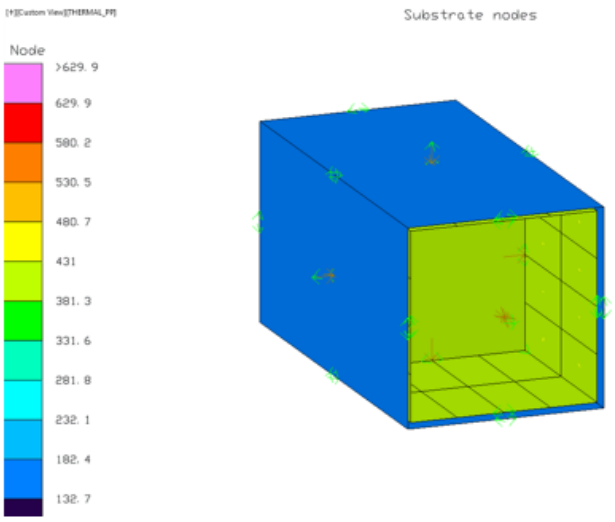


Figure 9.11: Example of the internal temperature field after introducing the surrounding MLI-like shell.

Figure 9.11 shows the effect of the external shell on the internal temperature field. Compared with the bare-box analysis, the internal compartment becomes more uniform. This behaviour is physically expected because the internal box no longer radiates directly to the lunar surface and to deep space. Instead, the external shell acts as an intermediate layer between the protected volume and the environment.
This result justifies the following modelling choice. Once the MLI shell is included, the internal box can be evaluated mainly through its global minimum and maximum

temperatures. The local differences between the six faces are reduced, so the model can focus on the overall temperature range of the protected equipment compartment.

9.5.2 MLI Geometry and Equivalent Representation

The insulation shell is represented by six thin-shell surfaces, one for each side of the rover. The adopted equivalent geometry is composed of:

- six Kapton thin-shell faces;
- numerical thin-shell thickness equal to 2 mm, used only for the equivalent shell representation;
- distance from the internal box equal to 5 mm;
- one node per external face;
- external radiation enabled on the outside of the shell.

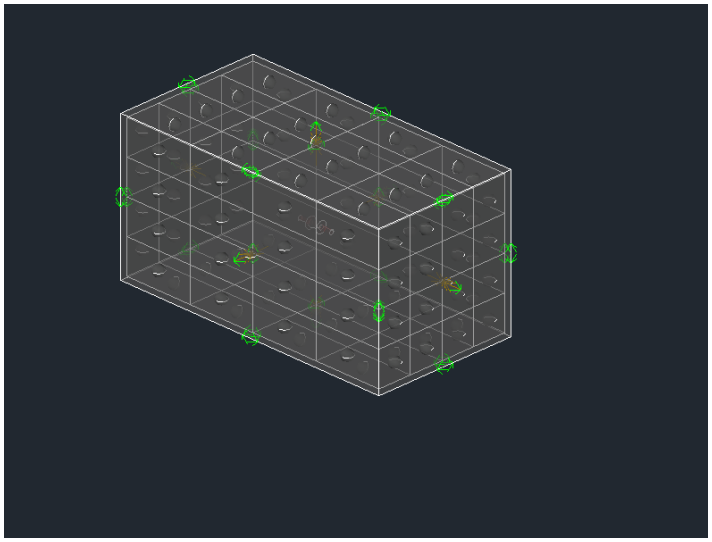


Figure 9.12: Complete simplified rover model composed of the internal equipment box and the external MLI-like shell.

Figure 9.12 shows the complete insulated rover model. The external shell is not intended to reproduce each physical layer of a real multi-layer blanket. A detailed MLI model would require the number of layers, spacer material, blanket compression, seams, penetrations, stitching, edge losses and local supports. These details are not available in the preliminary design phase. The shell is therefore treated as an equivalent insulation layer.
The 2 mm thin-shell thickness is a numerical modelling parameter and must not be interpreted as the physical thickness of the final MLI blanket. In the present model, the degree of insulation between the protected box and the external shell is controlled by the effective face-to-face area conductance defined in Section 9.5.3. The separation of 5 mm between the internal box and the shell represents the modelled gap between the protected structure and the external insulation. The use of one node per MLI

face is consistent with the purpose of the shell: it is not used to predict local blanket temperatures, but to represent the global thermal decoupling effect.

9.5.3 Effective Conductance Between Internal Box and MLI

The heat exchange between the internal box and the MLI shell is represented by an effective area conductance:

$$h_{\mathrm{box-MLI}} \qquad [\mathrm{W/(m^2\,K)}]. \tag{9.7}$$

The heat flow through this interface is

$$\dot{Q}_{\mathrm{box-MLI}} = h_{\mathrm{box-MLI}} A \left(T_{\mathrm{box}} - T_{\mathrm{MLI}}\right). \tag{9.8}$$

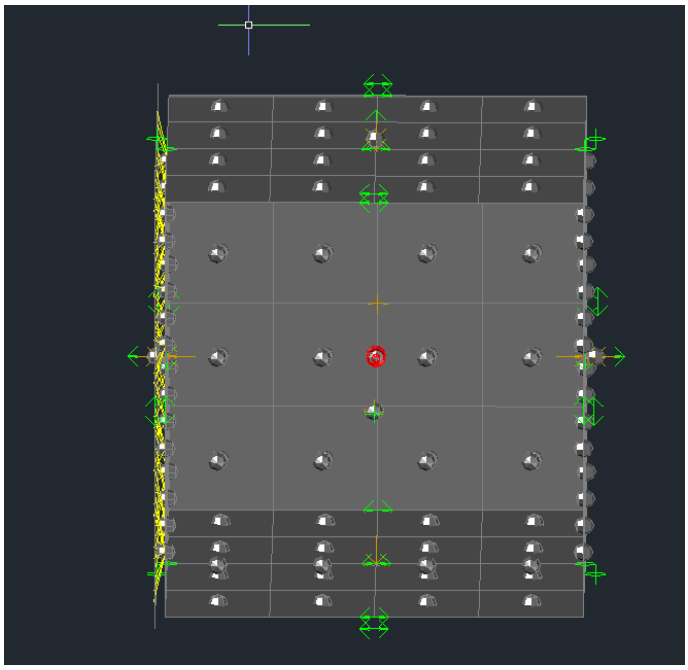


Figure 9.13: Effective face-to-face conductance used to couple the internal box to the MLI-like shell.

Figure 9.13 shows the conductance introduced between the internal box and the external shell. This parameter is one of the most important variables of the model because it controls how much the internal compartment follows the external shell temperature. A high value corresponds to a stronger thermal connection with the environment. A low value corresponds to better isolation.
The first analysed value is

$$h_{\mathrm{box-MLI}} = 0.08\,\mathrm{W/(m^2\,K)}. \tag{9.9}$$

The value is then reduced to

$$h_{\mathrm{box-MLI}} = 0.02\,\mathrm{W/(m^2\,K)} \tag{9.10}$$

to study a stronger insulation condition. Intermediate values such as $0.04\,\mathrm{W/(m^2\,K)}$, $0.05\,\mathrm{W/(m^2\,K)}$, $0.06\,\mathrm{W/(m^2\,K)}$, $0.08\,\mathrm{W/(m^2\,K)}$, $0.10\,\mathrm{W/(m^2\,K)}$ and $0.12\,\mathrm{W/(m^2\,K)}$ are

considered in the sensitivity maps. A still lower value of $0.012\,\mathrm{W/(m^2\,K)}$ is subsequently used for the dedicated cold-case study, whereas $1.0\,\mathrm{W/(m^2\,K)}$ is used only as a deliberately high-coupling reference in part of the radiator trade-off.
The physical interpretation is direct. A high conductance helps heat rejection because the internal box can transfer heat more easily to the external shell. However, it worsens cold survival because the internal box also loses heat more easily. A low conductance protects the internal box in cold conditions, but it also traps internal power and may cause overheating. This trade-off is the reason why the insulation sensitivity is not enough by itself to select the final thermal-control configuration.

9.6 Soil–Rover Radiative Coupling

The rover operates close to the lunar surface, so the regolith cannot be treated as a simple fixed-temperature boundary. The lunar soil absorbs direct solar radiation, reflects part of it as albedo, emits infrared radiation according to its local temperature and changes temperature during the lunar cycle. The rover exchanges radiation with this surface, especially through its lower and lateral external faces.
The surface affects the rover through:

- infrared radiation emitted by the regolith;
- reflected solar radiation from the ground;
- the view factor between the rover faces and the surface;
- the local surface temperature calculated by the regolith model;
- the latitude-dependent solar incidence and ground thermal response.

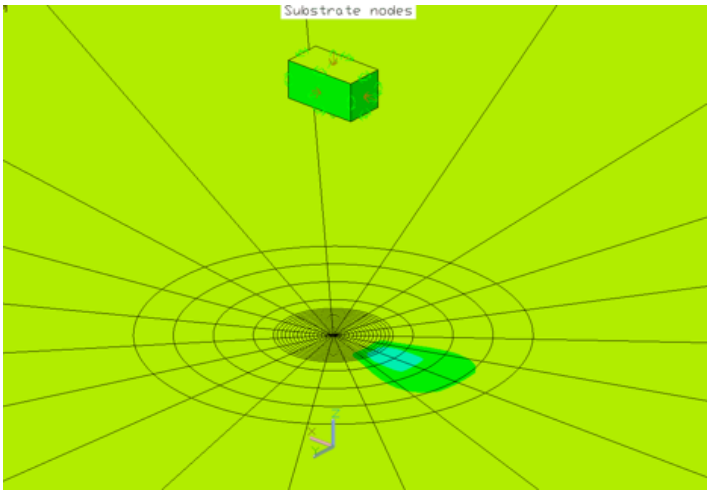


Figure 9.14: Radiative interaction between the rover and the lunar surface.

Figure 9.14 summarises the rover–soil radiative coupling. The bottom face has the highest view factor toward the ground and is therefore strongly affected by lunar infrared emission. The top face has a larger view toward deep space and is therefore a more favourable location for heat rejection. The side faces receive a combination of

direct solar input, reflected solar radiation and infrared emission from the surrounding terrain.
This coupling explains why latitude is a major design driver. At low latitude, the regolith becomes warmer and the rover receives more infrared heat. At high latitude, the ground is colder and the rover can radiate toward a colder surrounding environment. The same rover design can therefore become hot-critical in one latitude range and cold-critical in another. For this reason, all later sensitivity maps are presented as functions of both internal heat load and latitude.

9.7 Internal Heat Load

After the insulated geometry is defined, an internal heat load is applied to the rover box. This heat load represents the power dissipated by the rover subsystems. In a complete rover, the sources would include the on-board computer, navigation sensors, communication electronics, battery management system, motor drivers, actuators, payload electronics, heaters and possible recharge-related losses. In this preliminary model, these sources are not separated. A global internal power is applied to the internal box. This simplification is appropriate because the aim is to study the global thermal balance. The local temperature of each electronic unit would require information about its mass, position, mounting interface, dissipation profile and allowable limits. These details are not available at this stage. The global heat load is therefore used as a parametric driver of the rover thermal state.

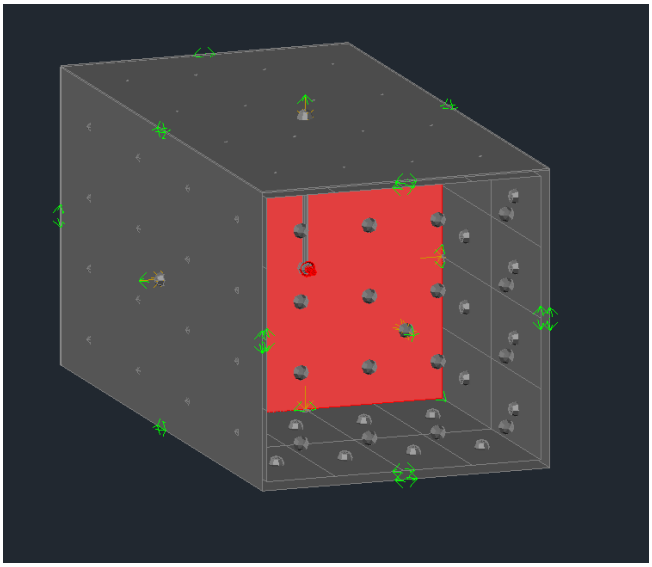


Figure 9.15: Definition of the internal panel where the distributed thermal load is applied.

Figure 9.15 indicates the internal panel used for the distributed thermal load. This represents a simplified heat source associated with the internal equipment mounted on the rover structure. The load is not intended to reproduce a single component. It is a system-level representation of the total dissipated power inside the protected compartment.

For the first insulation sensitivity analysis, the considered internal powers are

$$P_{\text{int}} = [0,\ 0.5,\ 1,\ 1.5,\ 2,\ 3,\ 4,\ 5,\ 6]\ \text{W}. \tag{9.11}$$

For the radiator hot- and cold-case study, the range is extended to

$$P_{\text{int,rad}} = [0,\ 1,\ 2,\ 3,\ 4,\ 5,\ 6,\ 7,\ 8,\ 9]\ \text{W}. \tag{9.12}$$

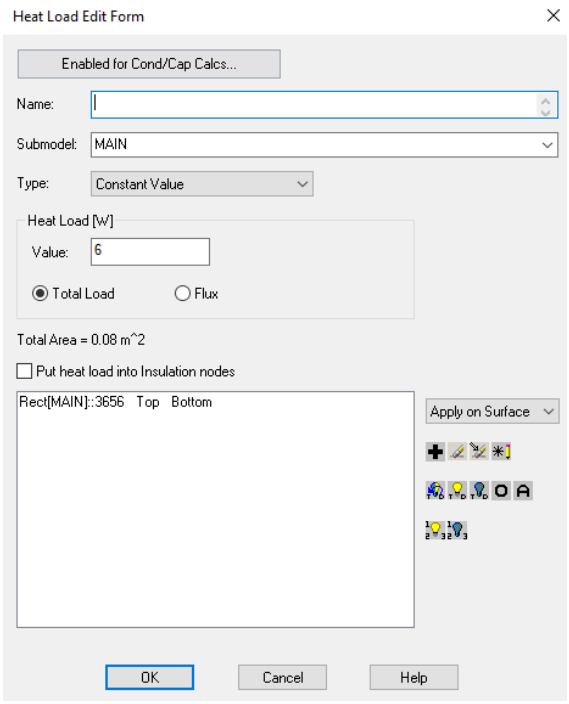


Figure 9.16: Example of the distributed thermal load applied to the internal panel.

Figure 9.16 shows the application of the distributed thermal load in Thermal Desktop. The parametric variation of this load is essential because the rover does not operate at a constant power level. A low value can represent standby, survival or low-power monitoring. Higher values represent active traverse, communication, payload operation, computation or battery-related dissipation. Increasing internal power improves the cold case because it warms the rover, but worsens the hot case because the additional heat must be rejected.

9.8 Sensitivity to MLI Coupling and Internal Power

The first complete parametric analysis is performed without a dedicated radiator. The objective is to verify whether the combination of MLI insulation and internal dissipated power can maintain the internal box inside the required temperature range. The parameters varied in this analysis are latitude, internal heat load and effective MLI coupling.
The interpretation is based on the following thermal balance. The internal box receives power from the equipment:

$$\dot{Q}_{\text{in}} = P_{\text{int}}. \tag{9.13}$$

It exchanges heat with the MLI shell through the effective conductance:

$$\dot{Q}_{\mathrm{box-MLI}} = h_{\mathrm{box-MLI}} A \left(T_{\mathrm{box}} - T_{\mathrm{MLI}}\right). \tag{9.14}$$

If $h_{\mathrm{box-MLI}}$ is small, the heat flow is limited. If $h_{\mathrm{box-MLI}}$ is large, the internal box is more strongly coupled to the external shell.
The maps are discussed by first considering the two extreme values, then the intermediate values. This order follows the physical logic of the design process: the extremes show the limiting behaviour, while the intermediate cases show the possible compromise.
For consistency, the insulation parameter is denoted throughout the text by $h_{\mathrm{box-MLI}}$ and expressed in $\mathrm{W/(m^2\,K)}$. Some of the MATLAB-generated figure titles retain the legacy symbol k_{MLI}; in those plots, k_{MLI} denotes the same effective face-to-face area conductance and must not be interpreted as an intrinsic material thermal conductivity in $\mathrm{W/(m\,K)}$.

9.8.1 Extreme MLI Coupling Cases

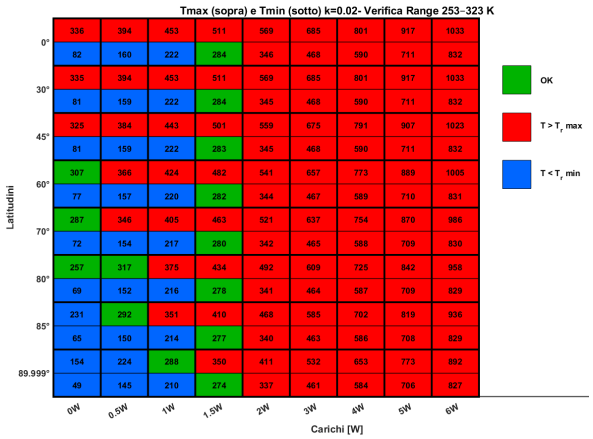


Figure 9.17: Sensitivity map for the strongest insulation case, $h_{\mathrm{box-MLI}} = 0.02\,\mathrm{W/(m^2\,K)}$.

Figure 9.17 represents the strongest insulation case among the analysed maps. The coupling between the internal box and the external shell is low. This means that the internal box exchanges little heat with the environment. The advantage is that the rover retains heat more effectively when the external environment is cold or when the internal power is small. The disadvantage is that, when the rover dissipates several watts, the heat has difficulty escaping.
This configuration is therefore favourable for cold survival but unfavourable for hot operation. If the internal power increases, the temperature tends to rise because the MLI prevents heat rejection. The map is useful because it identifies the upper limit of the insulation strategy: beyond a certain internal power, insulation alone becomes a problem rather than a solution.

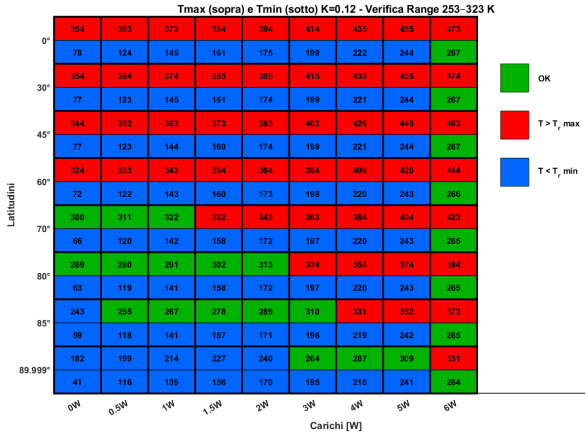


Figure 9.18: Sensitivity map for the weakest insulation case among the plotted values, $h_{\text{box}-\text{MLI}} = 0.12\,\text{W}/(\text{m}^2\,\text{K})$.

Figure 9.18 represents the opposite extreme. The coupling between the internal box and the external shell is higher, so the rover can exchange heat more easily with the external environment. This helps when internal power is high, because heat can be transferred out of the protected compartment more effectively. However, the same property worsens cold survival, because the internal box loses heat more easily when the shell and the surrounding environment are cold.
The comparison between Figures 9.17 and 9.18 shows the basic MLI trade-off. Strong insulation and weak insulation solve opposite parts of the problem. A low coupling protects the rover in cold conditions but can overheat at high power. A high coupling helps heat rejection but can make low-power or high-latitude conditions cold-critical. This means that the insulation parameter cannot be selected independently from the expected power level and the radiator concept.

9.8.2 Intermediate MLI Coupling Cases

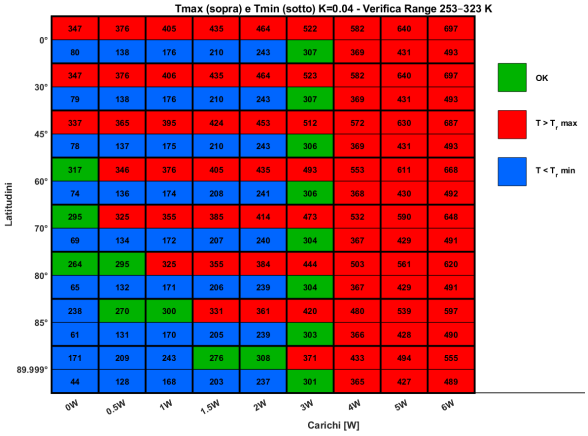


Figure 9.19: Sensitivity map for $h_{\text{box}-\text{MLI}} = 0.04\,\text{W}/(\text{m}^2\,\text{K})$.

Figure 9.19 is the first intermediate case after the strongest insulation configuration. The internal box is still significantly isolated, but the heat leakage is higher than in

the $h_{\mathrm{box-MLI}} = 0.02\,\mathrm{W/(m^2\,K)}$ case. As a result, the tendency to overheat at high power is reduced, while part of the cold-case protection is preserved. This map starts to show the transition from insulation-dominated behaviour toward a more balanced configuration.

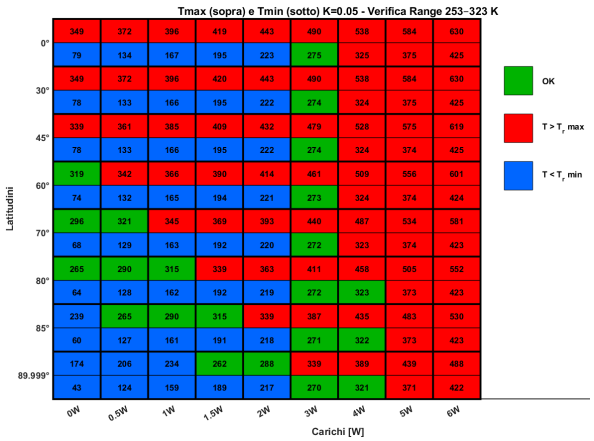


Figure 9.20: Sensitivity map for $h_{\mathrm{box-MLI}} = 0.05\,\mathrm{W/(m^2\,K)}$.

Figure 9.20 represents a central insulation value. This case is important because it is neither a very strong nor a very weak coupling. The map is therefore useful to identify a preliminary compromise and to prepare the later radiator analysis. The thermal response is controlled by both internal power and latitude, showing that no single MLI value can remove the need for a dedicated heat-rejection path.

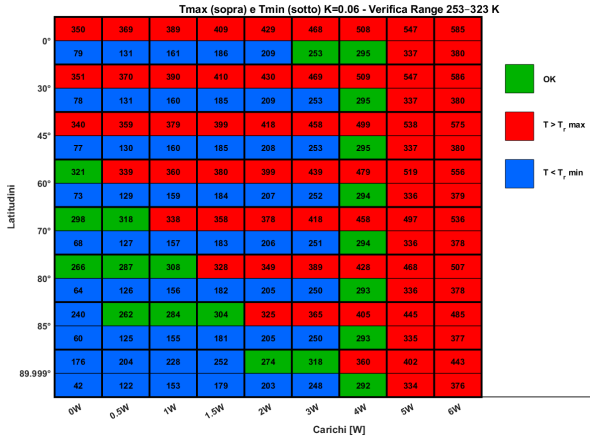


Figure 9.21: Sensitivity map for $h_{\mathrm{box-MLI}} = 0.06\,\mathrm{W/(m^2\,K)}$.

Figure 9.21 continues the transition toward a stronger thermal coupling with the external shell. Compared with the previous maps, heat rejection becomes easier, but cold protection is reduced. This confirms that the acceptable region is created by a balance between heat retention and heat rejection. It is not possible to improve all operating conditions by simply increasing or decreasing the insulation conductance.

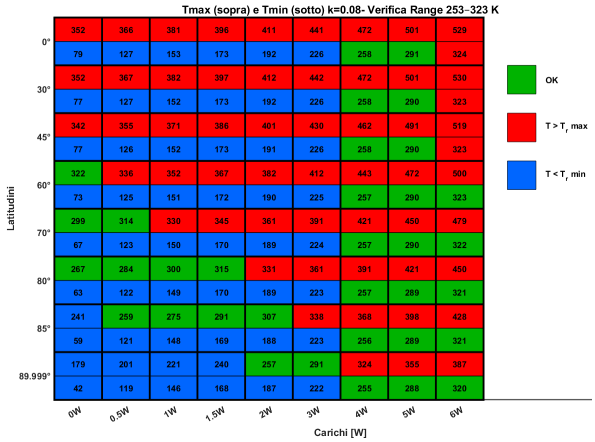


Figure 9.22: Sensitivity map for $h_{\text{box}-\text{MLI}} = 0.08\,\text{W}/(\text{m}^2\,\text{K})$.

Figure 9.22 is closer to the weak-insulation behaviour. The rover can reject internal heat more easily than in the previous cases, but it is also more exposed to external cold conditions. The map therefore shows that using the MLI shell itself as the main heat-rejection path is not an ideal design strategy. The whole surface becomes a heat leak, and this can be damaging in cold cases.

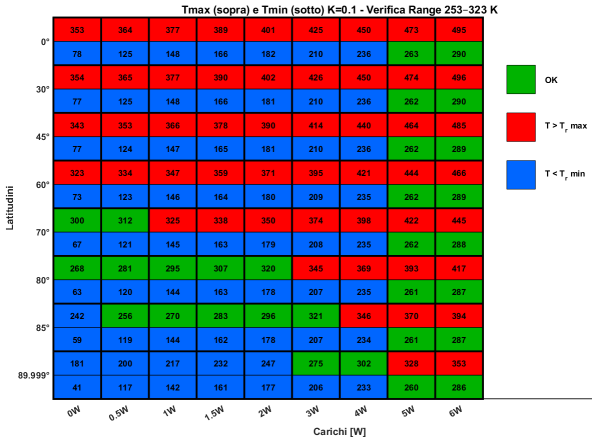


Figure 9.23: Sensitivity map for $h_{\text{box}-\text{MLI}} = 0.10\,\text{W}/(\text{m}^2\,\text{K})$.

Figure 9.23 is the last intermediate step before the weakest insulation case. The behaviour approaches the $h_{\text{box}-\text{MLI}} = 0.12\,\text{W}/(\text{m}^2\,\text{K})$ map. The internal box follows the external shell more closely, which helps to remove heat but reduces thermal isolation. This case reinforces the conclusion that the MLI must mainly act as an environmental decoupling layer, while a separate radiator should be used for intentional heat rejection. The combined conclusion of the MLI sensitivity study is that insulation is necessary but not sufficient. It improves temperature uniformity and reduces uncontrolled exchange with the lunar environment. However, it cannot by itself satisfy both cold and hot requirements over the complete range of internal powers and latitudes. This motivates the introduction of a radiator.

9.9 Need for a Dedicated Radiator

The radiator is introduced because the MLI shell alone cannot solve the thermal-control problem. The function of the MLI is to limit unwanted heat exchange with the environment. This is useful in cold conditions, but it becomes limiting when the rover dissipates heat during active operation. In that case, the heat generated by the equipment remains trapped inside the protected box unless an intentional rejection path is provided.
The radiator separates two functions that should be treated independently:

- the MLI provides environmental decoupling and heat retention;
- the radiator provides controlled heat rejection when the rover is warm or dissipating power.

This separation is important because increasing the global leakage through the MLI is not equivalent to adding a radiator. A leaky MLI exposes the entire rover to the environment and can worsen cold survival. A radiator instead concentrates heat rejection on a selected surface with a favourable view factor and suitable optical properties.

9.9.1 Radiator Geometry and Coupling

In the simplified model, the radiator area is chosen equal to the rover top face area:

$$A_{\mathrm{rad}} = A_{\mathrm{top}} = 0.40\,\mathrm{m} \times 0.20\,\mathrm{m} = 0.08\,\mathrm{m}^2. \tag{9.15}$$

The top face is selected because it has the most favourable view toward deep space. The bottom face sees mainly the lunar surface and would receive a stronger infrared contribution from the ground. A lateral radiator would be more sensitive to Sun direction and vehicle attitude. The upper face is therefore the most logical first candidate in the simplified box model.

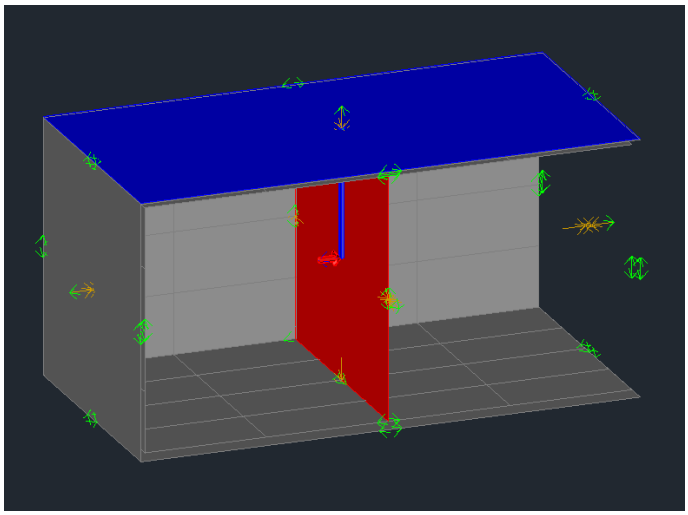


Figure 9.24: Top-face radiator added to the simplified rover model.

Figure 9.24 shows the radiator implemented on the upper side of the rover. The radiator is connected to the internal panel through an equivalent lumped conductor:

$$G_{\mathrm{rad}} \qquad [\mathrm{W/K}]. \tag{9.16}$$

The heat flow between the internal panel and the radiator is

$$\dot{Q}_{\mathrm{panel-rad}} = G_{\mathrm{rad}} \left(T_{\mathrm{panel}} - T_{\mathrm{rad}} \right). \tag{9.17}$$

At this level, G_{rad} represents the equivalent effect of the conductive or two-phase heat transport path between the internal equipment box and the radiator. Physically, it may correspond to a conductive interface, a thermal strap, a heat spreader, a heat pipe, a loop heat pipe or a combination of these elements.

9.9.2 Radiator Heat Balance

The radiator rejects heat mainly through infrared emission:

$$\dot{Q}_{\mathrm{emit}} = \varepsilon_{\mathrm{rad}} \sigma A_{\mathrm{rad}} \left(T_{\mathrm{rad}}^4 - T_{\mathrm{sink}}^4 \right). \tag{9.18}$$

At the same time, it can absorb external heat:

$$\dot{Q}_{\mathrm{abs}} = \alpha_{\mathrm{rad}} \dot{Q}_{\odot} + \alpha_{\mathrm{rad}} \dot{Q}_{\mathrm{alb}} + \varepsilon_{\mathrm{rad}} \dot{Q}_{\mathrm{IR,ground}}. \tag{9.19}$$

The net heat rejected by the radiator is therefore

$$\dot{Q}_{\mathrm{net,rad}} = \dot{Q}_{\mathrm{emit}} - \dot{Q}_{\mathrm{abs}}. \tag{9.20}$$

The radiator performance depends on emissivity, absorptivity, area, orientation, view factor to deep space, view factor to the lunar surface and conductive coupling to the internal box. For a good radiator, high infrared emissivity and low solar absorptivity are desirable. In a more detailed model, sun shields, louvers, variable-emittance coatings or thermal switches could also be considered.

9.10 Fixed Radiator Coupling Trade-Off

The radiator improves the hot case, but it can degrade the cold case. If the radiator is connected too weakly, the internal heat cannot reach the radiator and the rover overheats. If it is connected too strongly, the radiator removes heat even when the rover is cold. For this reason, the radiator conductance must not be selected only from the hot case.

The following maps compare different combinations of radiator conductance and effective box–MLI area conductance. The discussion starts from the two extreme radiator links, $G_{\mathrm{rad}} = 0.02\,\mathrm{W/K}$ and $G_{\mathrm{rad}} = 0.08\,\mathrm{W/K}$, and then considers the intermediate value $G_{\mathrm{rad}} = 0.05\,\mathrm{W/K}$. The value $h_{\mathrm{box-MLI}} = 1.0\,\mathrm{W/(m^2\,K)}$ is retained only as a high-coupling sensitivity reference and is not presented as the effective conductance of the selected insulation concept. This order shows why neither a very weak nor a very strong fixed radiator link is ideal.

9.10.1 Weak Radiator Link: $G_{\text{rad}} = 0.02\,\text{W/K}$

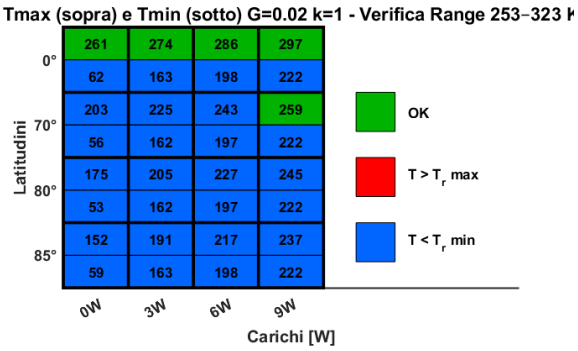


Figure 9.25: Radiator sensitivity map for $G_{\text{rad}} = 0.02\,\text{W/K}$ and $h_{\text{box-MLI}} = 1.0\,\text{W/(m}^2\,\text{K)}$.

Figure 9.25 shows a weak radiator link combined with a high MLI coupling. The radiator is present, but only a limited amount of heat can be transferred from the internal panel to the radiator. Therefore, the radiator does not dominate the thermal balance. The internal box still remains strongly affected by the global coupling through the shell and by the external environment.
This configuration can reduce the risk of overcooling through the radiator, because the radiator path is weak. However, it can be insufficient for hot operation, especially when the internal heat load increases. It is therefore more favourable to cold protection than to active heat rejection.

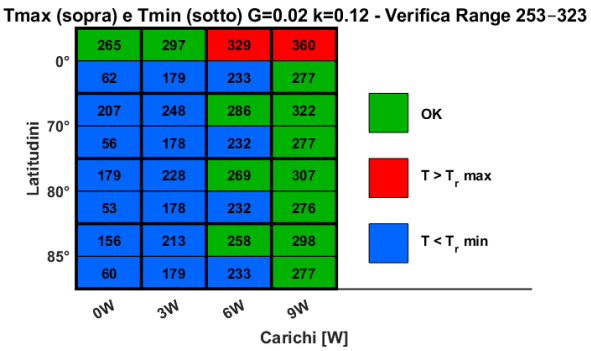


Figure 9.26: Radiator sensitivity map for $G_{\text{rad}} = 0.02\,\text{W/K}$ and $h_{\text{box-MLI}} = 0.12\,\text{W/(m}^2\,\text{K)}$.

Figure 9.26 keeps the same weak radiator link but changes the MLI coupling. In this case, the internal box is more protected from the environment than in the previous high-coupling configuration, but the weak radiator remains a limitation. If the rover dissipates several watts, the radiator cannot remove heat efficiently enough. This

case therefore shows the risk of combining strong insulation with an under-sized heat-rejection path.

9.10.2 Strong Radiator Link: $G_{\mathrm{rad}} = 0.08\,\mathrm{W/K}$

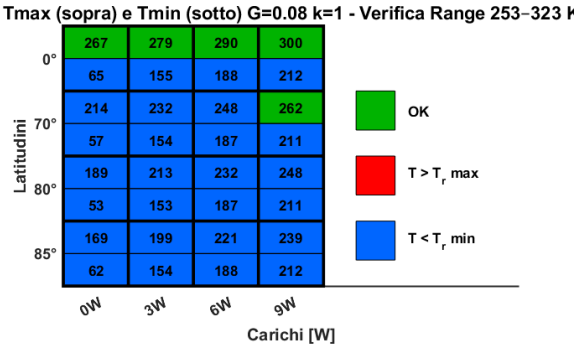


Figure 9.27: Radiator sensitivity map for $G_{\mathrm{rad}} = 0.08\,\mathrm{W/K}$ and $h_{\mathrm{box-MLI}} = 1.0\,\mathrm{W/(m^2\,K)}$.

Figure 9.27 represents the opposite radiator extreme. The conductance between the internal box and the radiator is higher, so heat can be transferred to the radiator more effectively. This is beneficial during hot operation because the internal temperature can be reduced. However, the same strong connection can remove too much heat during cold or low-power conditions.
This map therefore shows the second side of the radiator trade-off. A strong fixed radiator link may look attractive if only maximum temperatures are considered, but it is dangerous for survival and cold cases. In a lunar rover, heat rejection must be available when needed, but it should not remain fully active when the rover needs to conserve heat.

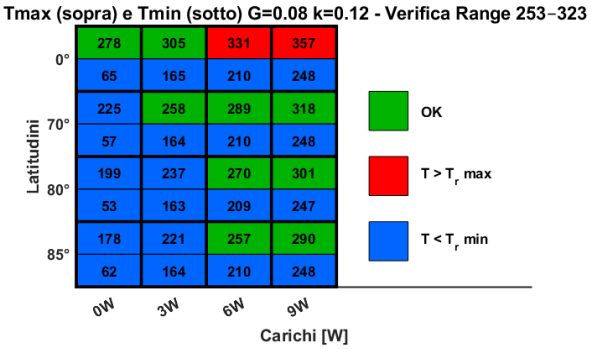


Figure 9.28: Radiator sensitivity map for $G_{\mathrm{rad}} = 0.08\,\mathrm{W/K}$ and $h_{\mathrm{box-MLI}} = 0.12\,\mathrm{W/(m^2\,K)}$.

Figure 9.28 combines a strong radiator link with a lower MLI coupling. The MLI

reduces uncontrolled environmental exchange, while the radiator provides the main intentional rejection path. This is physically coherent for hot cases, because the rover is insulated from the environment but still has a dedicated way to reject internal heat. The limitation is that, if the same radiator conductance remains active in cold conditions, the internal box may lose too much heat through the top radiator. This result supports the later introduction of variable conductance.

9.10.3 Intermediate Radiator Link: $G_{\mathrm{rad}} = 0.05\,\mathrm{W/K}$

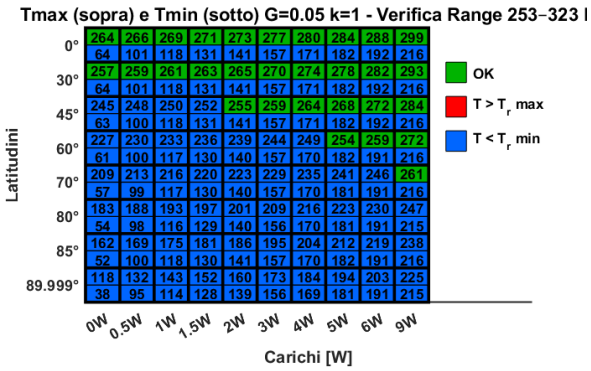


Figure 9.29: Radiator sensitivity map for $G_{\mathrm{rad}} = 0.05\,\mathrm{W/K}$ and $h_{\mathrm{box-MLI}} = 1.0\,\mathrm{W/(m^2\,K)}$.

Figure 9.29 shows the intermediate radiator conductance with a high MLI coupling. This configuration is less aggressive than the strong radiator case and rejects more heat than the weak radiator case. However, because the environmental coupling is still high, the internal box remains sensitive to the external shell and to latitude. This case is useful mainly as an intermediate reference, but it does not fully separate insulation and heat rejection.

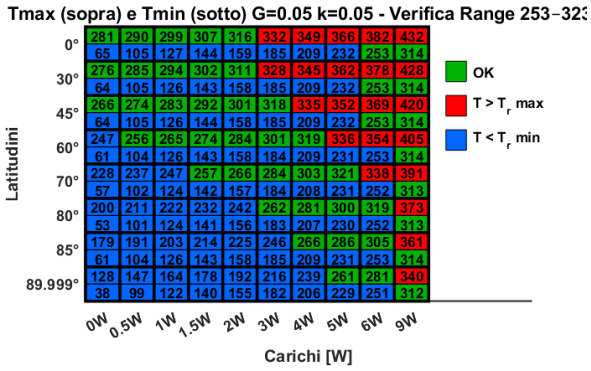


Figure 9.30: Radiator sensitivity map for $G_{\mathrm{rad}} = 0.05\,\mathrm{W/K}$ and $h_{\mathrm{box-MLI}} = 0.05\,\mathrm{W/(m^2\,K)}$.

Figure 9.30 is a balanced intermediate case. Both the insulation coupling and the

radiator conductance are moderate. The MLI reduces uncontrolled exchange with the environment, while the radiator provides a controlled heat-rejection path. This is one of the most useful configurations for preliminary interpretation because it is not located at either extreme of the design space.
Nevertheless, the fact that this case is a compromise does not mean that it is sufficient for all conditions. A fixed conductance can only be optimal for a limited range of internal powers and boundary conditions. When the latitude or operating mode changes, the same value can become too low for hot operation or too high for cold operation.

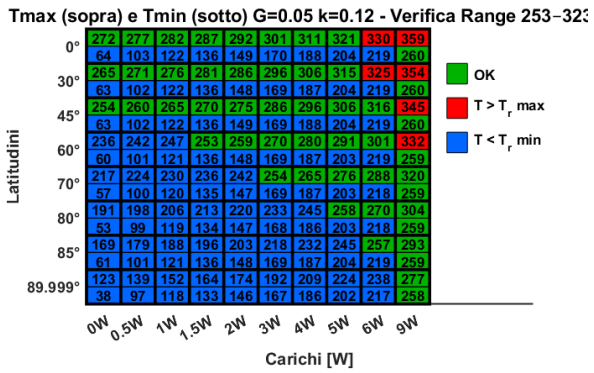


Figure 9.31: Radiator sensitivity map for $G_{\mathrm{rad}} = 0.05\,\mathrm{W/K}$ and $h_{\mathrm{box-MLI}} = 0.12\,\mathrm{W/(m^2\,K)}$.

Figure 9.31 shows the same intermediate radiator conductance with a different MLI coupling. Comparing it with Figure 9.30 demonstrates that the radiator cannot be sized independently from the insulation. The same radiator link produces a different internal temperature field when the global thermal leakage through the MLI changes. Therefore, the radiator and MLI must be designed as a coupled thermal-control system. The fixed-radiator trade-off can be summarised as follows. A weak link protects the rover from overcooling but may not reject enough heat. A strong link rejects heat efficiently but can overcool the rover. An intermediate link gives a better compromise, but it remains fixed. This is why hot and cold cases must be analysed next.

9.11 Hot and Cold Case Definitions

The hot and cold cases are used to test the thermal design under opposite conditions. The cold case checks whether the internal box remains above the minimum allowable temperature. It is critical when:

- internal power is low;
- latitude is high;
- the lunar surface is cold;
- the radiator removes too much heat;

- the conductance to the environment is too high;
- the rover is in standby or low-power mode.

The hot case checks whether the internal box remains below the maximum allowable temperature. It is critical when:

- internal power is high;
- latitude is low or intermediate;
- the lunar surface is warm;
- the rover receives significant environmental heat;
- the MLI traps internal heat;
- the radiator conductance is too low.

The two cases must always be interpreted together. A configuration that satisfies only the cold case may overheat during active operation. A configuration that satisfies only the hot case may become too cold during standby, shadowed operation or high-latitude operation. The purpose of the next sections is therefore not only to identify acceptable cells, but to understand why a single fixed configuration has a limited operating range.

9.12 Cold-Case Results With Fixed Radiator

The cold-case radiator analysis is performed with

$$G_{\mathrm{rad}} = 0.05\,\mathrm{W/K}, \qquad h_{\mathrm{box-MLI}} = 0.012\,\mathrm{W/(m^2\,K)}. \tag{9.21}$$

The result considered in the map is the minimum temperature of the internal box, T_{min}, for different latitudes and internal heat loads.

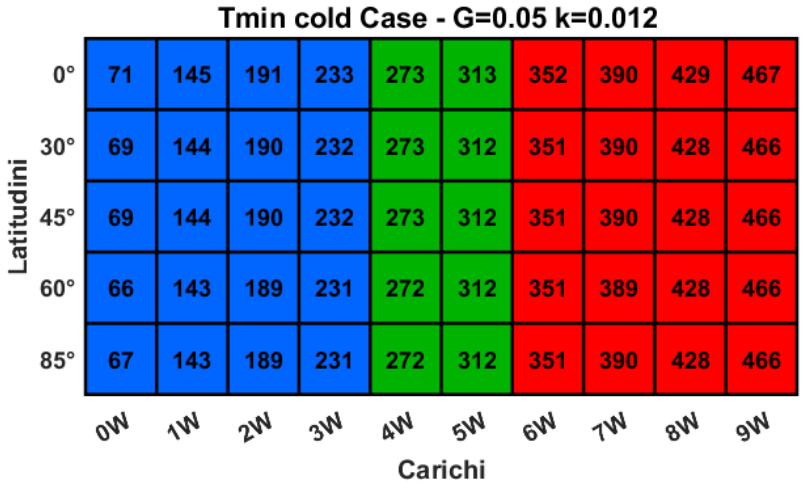


Figure 9.32: Cold-case map based on the minimum internal temperature of the rover box.

Figure 9.32 shows that the cold-case behaviour is dominated mainly by internal power. The latitude dependence is weaker than in the hot-case map because the minimum temperature is strongly controlled by the balance between internal dissipation, insulation and radiator heat leak.

For powers between 0 W and approximately 3 W, the minimum internal temperature remains below the lower requirement of 253.15 K. These cases are cold-critical. The rover does not generate enough internal heat to compensate for the thermal losses through the insulation and radiator paths. In practice, this means that low-power survival or standby modes would require either additional heaters, better isolation, lower radiator leakage or a thermally supported parking condition at the charging station.

For 4 W and 5 W, the minimum temperature lies inside the required range. The map indicates values of approximately 272 K–273 K around 4 W and approximately 312 K–313 K around 5 W. These cases are acceptable from the point of view of minimum temperature, because they remain above the lower limit and below the upper limit.

For powers from 6 W upward, the minimum temperature itself exceeds the upper allowable value. This means that the rover is not merely safe from cold; it is already too hot throughout the cold-case simulation. These cases are therefore hot-critical even in the cold-case table. This is an important result because it shows that internal power can dominate the thermal state even when the external condition is defined as cold.

The main conclusion from Figure 9.32 is that the acceptable power range is narrow for this fixed radiator configuration. The rover is too cold below roughly 4 W, acceptable around 4 W–5 W, and too hot from roughly 6 W upward. A fixed passive thermal configuration therefore cannot easily support all possible operating modes.

9.13 Hot-Case Results With Fixed Radiator

The hot-case radiator analysis is performed with

$$G_{\mathrm{rad}} = 0.05\,\mathrm{W/K}, \qquad h_{\mathrm{box-MLI}} = 0.12\,\mathrm{W/(m^2\,K)}. \tag{9.22}$$

The result considered in the map is the maximum internal temperature, $T_{\max}$, for different latitudes and internal heat loads.

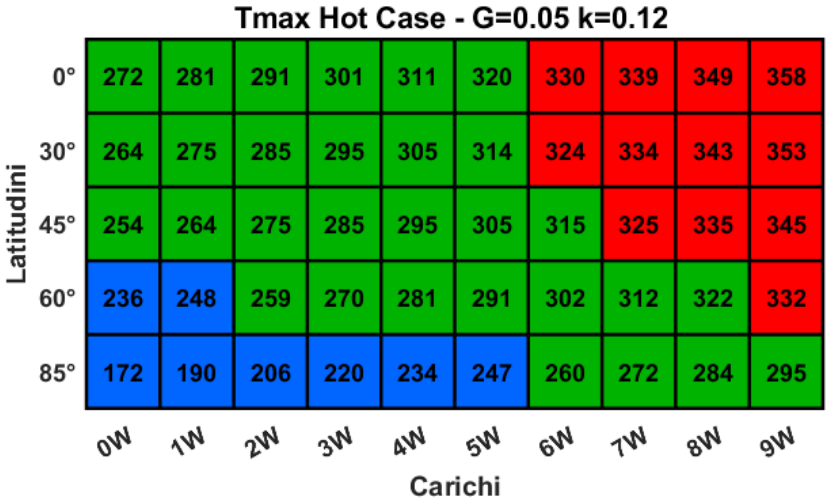


Figure 9.33: Hot-case map based on the maximum internal temperature of the rover box.

Figure 9.33 shows a clear latitude effect. At low latitude, the maximum temperature is higher because the lunar surface is warmer and the rover receives more environmental heat. At high latitude, the maximum temperature is lower because the surface remains colder and the solar contribution is reduced.
At 0°, the rover remains within the upper temperature limit up to about 5 W. At 6 W, the maximum temperature reaches approximately 330 K, exceeding the 323.15 K requirement. Therefore, near the equator, the hot-case internal power is limited to approximately 5 W for this fixed configuration.
At 30°, the same general trend is observed, with slightly lower temperatures. The case is acceptable up to about 5 W. At 6 W, the maximum temperature is approximately 324 K, just above the upper limit. At 45°, the acceptable range extends to about 6 W, while 7 W becomes slightly hot-critical, with a temperature around 325 K.
At 60°, the hot case becomes colder. Low powers such as 0 W and 1 W produce maximum temperatures below the lower requirement, meaning that the rover never becomes warm enough even in the hot case. From approximately 2 W to 8 W, the temperatures remain inside the allowable range. At 9 W, the temperature reaches about 332 K, exceeding the upper limit.
At 85°, the hot case is dominated by the cold polar environment. From 0 W to 5 W, the maximum temperature remains below the lower requirement. From 6 W to 9 W, the temperature becomes acceptable and remains below the upper limit. This means that, at high latitude, internal dissipation is necessary not only for operation but also for thermal survival.
The hot-case map therefore shows that the acceptable internal power range shifts with latitude. Low latitudes are limited by overheating at high power, while high latitudes are limited by insufficient heating at low power. This confirms that latitude must be included as a parameter in the thermal design of the rover.

9.14 Combined Interpretation of Hot and Cold Cases

The hot and cold case maps must be interpreted together. The cold-case map shows that, for the analysed fixed radiator configuration, powers below 4 W are too cold and powers above 5 W become too hot. The hot-case map shows that low latitudes overheat at high power, while high latitudes can remain too cold at low power even in the hot case.
The combined interpretation is:

- low latitude is hot-critical because the regolith is warmer and the rover receives more environmental heat;
- high latitude is cold-critical because the environment is colder and the absorbed heat is lower;
- the radiator helps the hot case but can worsen the cold case;
- the MLI helps cold survival but can trap heat during high-power operation;
- the acceptable internal power range depends on latitude and thermal-control configuration;
- a single fixed passive configuration is unlikely to cover all latitudes and operating modes.

This conclusion is central for the rover thermal-control strategy. The thermal design cannot be based only on selecting a fixed MLI conductance and a fixed radiator conductance. Such a solution may work for a narrow combination of latitude and internal power, but it does not provide enough flexibility for the complete mission envelope.

9.15 Physical Interpretation of the Results

The results can be interpreted by considering the heat paths connected to the internal box. The internal heat input is

$$\dot{Q}_{\text{in}} = P_{\text{int}}. \tag{9.23}$$

The main heat losses are through the MLI coupling and through the radiator:

$$\dot{Q}_{\text{out}} = \dot{Q}_{\text{box-MLI}} + \dot{Q}_{\text{panel-rad}}. \tag{9.24}$$

When P_{int} is low, the internal source is small. If the environment is cold or if the radiator remains connected, the internal temperature decreases and the case becomes cold-critical. This occurs in the cold-case map at low powers and in the hot-case map at high latitudes.
When P_{int} is high, the internal source is large. If the radiator and the insulation cannot reject the generated heat, the internal temperature increases and the case becomes hot-critical. This occurs at low latitudes for high powers and also in the cold-case map when the dissipated power is high enough that even the minimum temperature exceeds the upper limit.

The role of latitude is mainly related to the external boundary condition. At low latitude, the lunar surface becomes warmer and emits more infrared radiation toward the rover. At high latitude, the surface remains colder and the rover receives less environmental heat. Therefore, the same internal power produces a higher temperature at low latitude and a lower temperature at high latitude.
The radiator has a double effect. It is beneficial when the rover is hot because it provides heat rejection. It is harmful when the rover is cold because it continues to remove heat. The correct thermal-control strategy is therefore not simply to maximise the radiator size or conductance, but to control the heat path to the radiator.

9.16 Loop Heat Pipe as a Variable Radiator Link

9.16.1 Need for Variable Conductance

The fixed-radiator analysis shows the main contradiction of the rover thermal design. During hot operation, the rover requires a strong thermal path to the radiator in order to reject the heat generated by internal equipment. During cold or survival operation, the rover requires a weak thermal path to the radiator in order to retain heat. Within the range of cases analysed here, none of the investigated fixed conductance values provides the required behaviour over the complete hot–cold design envelope.
In the simplified model, the required behaviour is represented by two equivalent conductance values:

$$G_{\mathrm{rad,day}} = 0.12\,\mathrm{W/K} \tag{9.25}$$

for heat-rejection mode, and

$$G_{\mathrm{rad,night}} = 0.012\,\mathrm{W/K} \simeq 0.01\,\mathrm{W/K} \tag{9.26}$$

for heat-conservation mode. The ratio between the two states is

$$\frac{G_{\mathrm{rad,day}}}{G_{\mathrm{rad,night}}} = \frac{0.12}{0.012} = 10. \tag{9.27}$$

This means that the thermal link to the radiator is reduced by approximately one order of magnitude when the rover must conserve heat. The subscripts “day” and “night” are retained as shorthand for the high- and low-conductance states used in the numerical model; physically, the switching criterion should be linked to the thermal state or operating mode of the rover rather than to a universal lunar day–night boundary.
The radiator area does not change. What changes is the effective heat transport path between the internal panel and the radiator. In hot conditions, the link is open or active and heat reaches the radiator. In cold conditions, the link is strongly reduced and the radiator is almost thermally disconnected from the internal box.

9.16.2 General Function of a Loop Heat Pipe

A Loop Heat Pipe is a passive two-phase heat transport device. It transfers heat from a heat source to a heat sink by evaporation and condensation of a working fluid. In

the rover application, the heat source is the internal panel or heat spreader connected to the equipment box, while the heat sink is the external radiator.
The main components of a LHP are:

- an evaporator connected to the heat source;
- a porous wick inside the evaporator;
- a compensation chamber;
- a vapour line;
- a condenser connected to the radiator;
- a liquid return line;
- the working fluid.

The operating cycle starts when heat generated inside the rover reaches the evaporator. The liquid working fluid absorbs this heat and evaporates. The heat is transported as latent heat:

$$\dot{Q}_{\text{evap}} = \dot{m} h_{fg}, \tag{9.28}$$

where $\dot{m}$ is the mass flow rate and h_{fg} is the latent heat of vaporisation of the working fluid.
The vapour flows through the vapour line toward the condenser, where it rejects heat to the radiator and condenses back to liquid. The liquid then returns to the evaporator through the liquid line. The circulation is driven by the capillary pressure generated by the porous wick, so a mechanical pump is not required. The capillary pressure must be high enough to overcome the total pressure losses in the loop:

$$\Delta P_{\text{cap}} \geq \Delta P_{\text{vapour}} + \Delta P_{\text{liquid}} + \Delta P_{\text{condenser}} + \Delta P_{\text{gravity}} + \Delta P_{\text{minor}}. \tag{9.29}$$

9.16.3 Difference Between Heat Pipe and Loop Heat Pipe

A conventional heat pipe and a Loop Heat Pipe are both two-phase devices, but their architecture is different. In a conventional heat pipe, the wick usually extends along most of the pipe and returns liquid from the condenser to the evaporator. In a LHP, the main wick is concentrated in the evaporator, while the vapour and liquid are transported through separate lines.
This architecture is useful for a mini rover because the heat source and the radiator may not be close to each other. The electronics and battery are located inside the protected compartment, while the radiator should be placed on an external surface with a favourable view to deep space. A LHP can transport heat over a distance, can be routed through the rover structure and can be combined with valves to obtain variable conductance or shut-off behaviour.

9.16.4 Thermal Control Valve and Variable Conductance Logic

A standard LHP transports heat efficiently, but it may remain too strongly coupled to the radiator when the sink is cold. For this reason, a Thermal Control Valve can be used to provide heat-switching behaviour. The qualitative operating logic is:

- when the evaporator or internal panel temperature is high, the valve allows heat transport toward the condenser and radiator;
- when the evaporator or internal panel temperature is low, the valve reduces or stops the heat flow toward the radiator;
- the radiator is therefore strongly connected in hot conditions and weakly connected in cold conditions.

In Thermal Desktop, this behaviour can be represented by a two-state conductor:

$$G_{\mathrm{rad}}(t) = \begin{cases} G_{\mathrm{rad,day}}, & \text{heat-rejection mode,} \\ G_{\mathrm{rad,night}}, & \text{heat-conservation mode.} \end{cases} \tag{9.30}$$

A more realistic implementation can depend on the evaporator temperature:

$$G_{\mathrm{rad}}(T_{\mathrm{evap}}) = \begin{cases} G_{\mathrm{rad,day}}, & T_{\mathrm{evap}} \geq T_{\mathrm{set}} + \Delta T, \\ G_{\mathrm{rad,night}}, & T_{\mathrm{evap}} \leq T_{\mathrm{set}}, \\ G_{\mathrm{transition}}(T_{\mathrm{evap}}), & T_{\mathrm{set}} < T_{\mathrm{evap}} < T_{\mathrm{set}} + \Delta T. \end{cases} \tag{9.31}$$

Here T_{evap} can be represented, in the simplified model, by the temperature of the internal panel connected to the radiator. The parameter T_{set} is the activation threshold, while ΔT can represent a transition or hysteresis interval.

9.16.5 Physical Meaning of the Conductance Reduction

The heat transferred through the equivalent radiator link is

$$\dot{Q}_{\mathrm{rad-link}} = G_{\mathrm{rad}} \left(T_{\mathrm{panel}} - T_{\mathrm{rad}} \right). \tag{9.32}$$

For a representative temperature difference of 50 K, the heat transferred in high-conductance mode is

$$\dot{Q}_{\mathrm{day}} = 0.12 \times 50 = 6\,\mathrm{W}. \tag{9.33}$$

In low-conductance mode, the heat transferred becomes

$$\dot{Q}_{\mathrm{night}} = 0.012 \times 50 = 0.6\,\mathrm{W}. \tag{9.34}$$

Therefore, for the same temperature difference, the heat leak to the radiator is reduced by a factor of ten. This reduction is the key thermal-control function. It allows the radiator to reject several watts when the rover is hot, while limiting parasitic heat loss when the rover is cold.

The low-conductance state is not set to zero because real hardware always has residual heat paths. Heat can still leak through evaporator walls, fluid lines, mounting brackets, supports, valve bodies and nearby structural interfaces. The value 0.012 W/K therefore represents a reduced but non-zero thermal connection.

9.16.6 Variable Radiator Example

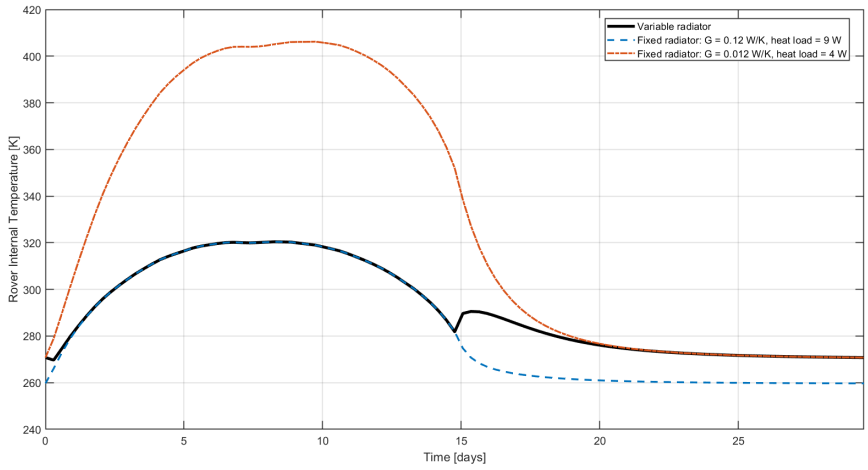


Figure 9.34: Example of variable radiator activation through the equivalent Loop Heat Pipe conductance for a high-latitude case with 9 W internal load.

Figure 9.34 shows the final modelling idea. The radiator is no longer treated as a permanently fixed heat sink. Instead, its equivalent conductance is increased when heat must be rejected and reduced when heat must be preserved. In heat-rejection mode, the conductance approaches 0.12 W/K. In heat-conservation mode, it is reduced toward 0.012 W/K or approximately 0.01 W/K.
This example closes the modelling chain developed in the chapter. The bare rover shows different panel temperatures. The MLI shell improves internal uniformity and reduces uncontrolled environmental exchange. The heat-load sensitivity shows that insulation alone is insufficient. The fixed radiator improves heat rejection but creates a cold-case penalty. The variable radiator link mitigates this conflict at preliminary level by providing a high conductance when heat rejection is required and a reduced conductance when heat must be conserved.

9.17 Design Implications

Several design implications follow from the analysis.
First, the rover cannot be designed using only one thermal extreme. The equatorial case and the high-latitude case lead to different critical conditions. At low latitude, the rover is more likely to overheat during high-power operation. At high latitude, the rover is more likely to become too cold during low-power operation. Therefore, the final thermal-control system must be evaluated over the expected latitude and operational range.
Second, MLI is necessary but not sufficient. It reduces uncontrolled exchange with the lunar environment and improves internal temperature uniformity, but it also reduces the ability of the rover to reject heat. The MLI must therefore be coupled with a dedicated heat-rejection device.
Third, a radiator is necessary but cannot remain fully fixed. A weak radiator link

is not sufficient in hot cases, while a strong fixed link can overcool the rover in cold cases. The radiator should therefore be connected through a variable thermal link, a thermal switch, a controlled conductance path, a LHP/TCV system or an equivalent heat-switching device.
Fourth, internal power is part of the thermal-control strategy. At high latitude, a minimum dissipated power can help maintain the rover above the lower temperature limit. At low latitude, the maximum allowable power is limited by overheating. Therefore, the rover power modes, sortie duration, communication phases, payload operations and battery charge/discharge periods should be linked to the thermal model.
Fifth, the charging station can become part of the thermal architecture. Since the rover is rechargeable and operates near a base, the station may provide a more favourable boundary condition, partial shielding, a conductive thermal interface or active thermal conditioning. This aspect is not included in the present simplified model, but it is important for the complete system design.

9.18 Possible Improvements to the Model

The model developed in this chapter is suitable for preliminary body-level thermal design, but it can be improved in several directions. The wheel, hub, wheel–ground and deployable-support paths are intentionally not included in the architecture summarised here because they are developed explicitly in the following chapter.
At component and structure level, the rover model can be refined by adding:

- real structural panels and mechanical frames;
- separate nodes for battery, electronics, sensors, payload and communication units;
- component-level heat capacities and dissipations;
- conductive paths through screws, brackets, inserts and harnesses;
- thermal straps between high-power components and the heat-rejection system;
- the mechanical and thermal interface with the charging station.

The insulation model can be improved by including:

- effective MLI emissivity;
- edge losses;
- seams, holes and blanket penetrations;
- compression effects;
- dust contamination and degradation of optical properties.

The radiator model can be refined by adding:

- detailed radiator coating properties;

- solar exposure and shadowing analysis;
- local view factors to ground and space;
- heat spreaders or thermal straps;
- a detailed LHP/FloCAD representation;
- thermal switch or valve control laws;
- heater logic for cold survival.

Finally, the operational model should include a realistic three-hour sortie timeline, with standby, traverse, communication, payload activity, return and recharge phases. The power profile should be time-dependent, and the thermal interaction with the base station should be included.

9.19 Baseline Modelling Architecture Before Wheel-System Extension

At the end of the present chapter, the baseline body-level thermal-control architecture is based on four coupled elements:

1. the lunar surface model, which provides ground temperature, albedo and infrared boundary conditions;
2. the internal rover box, which represents the protected equipment compartment;
3. the external MLI-like shell, which limits uncontrolled heat exchange with the environment;
4. the top-face radiator with a variable conductance link, which rejects heat when required.

The main heat paths included in the model are:

- radiation between the lunar surface and the external rover shell;
- radiation from the external shell and radiator to deep space;
- effective conduction between the internal box and the MLI shell;
- internal radiation inside the box;
- distributed internal heat dissipation;
- equivalent conductive coupling between the internal top panel and the radiator;
- infrared emission from the radiator.

This baseline architecture separates insulation and heat rejection. The MLI-like shell is used to reduce unwanted exchange with the environment, while the radiator provides the intentional heat-rejection surface. The radiator link is interpreted as a variable-conductance system, represented by the equivalent action of a Loop Heat Pipe combined with a Thermal Control Valve. This is not yet the complete final rover architecture: the thermal paths associated with the wheels, hubs, ground contact and deployable support rods are added and assessed in the following chapter.

9.20 Chapter Summary

This chapter presented the preliminary thermal model of the rechargeable lunar mini rover and its thermal-control system. The analysis started from a simplified rectangular internal box with dimensions $0.40\,\mathrm{m}\times0.20\,\mathrm{m}\times0.20\,\mathrm{m}$, wall thickness 2 mm and 16 nodes per face. The first face-temperature plots showed that the rover panels do not experience the same thermal boundary condition. At the equator, the rover is more affected by the warm lunar surface and by stronger environmental heat input. At high latitude, the colder environment makes heat retention more critical.
An external MLI-like shell was then introduced around the internal box. The shell improves the internal temperature uniformity and reduces direct environmental coupling. The sensitivity analysis on MLI coupling and internal power showed that insulation creates a trade-off. Strong insulation improves cold survival but can cause overheating when internal power is high. Weak insulation helps heat rejection but can make low-power or high-latitude conditions cold-critical.
A radiator was then added on the top face, with an area of $0.08\,\mathrm{m}^2$. The fixed-radiator sensitivity maps showed that the radiator conductance must be selected carefully. A weak link may not reject enough heat, while a strong fixed link can overcool the rover. The intermediate cases improve the compromise but do not remove the fundamental limitation of a fixed passive connection.
The cold-case results with $G_{\mathrm{rad}} = 0.05\,\mathrm{W/K}$ and $h_{\mathrm{box-MLI}} = 0.012\,\mathrm{W/(m^2\,K)}$ showed that powers from 0 W to about 3 W are cold-critical, powers around 4 W–5 W are acceptable and powers from 6 W upward become too hot. The hot-case results with $G_{\mathrm{rad}} = 0.05\,\mathrm{W/K}$ and $h_{\mathrm{box-MLI}} = 0.12\,\mathrm{W/(m^2\,K)}$ showed that low latitudes are hot-critical at high powers, while high latitudes can remain cold-critical at low powers.
The main conclusion is that, for the analysed cases, a fixed radiator link is not sufficient to cover the full range of hot and cold conditions. The radiator link should therefore provide a variable effective conductance. In the preliminary model, this function is represented by the equivalent action of a Loop Heat Pipe combined with a Thermal Control Valve, using a high-conductance state of $0.12\,\mathrm{W/K}$ for heat rejection and a low-conductance state of $0.012\,\mathrm{W/K}$, approximately $0.01\,\mathrm{W/K}$, for heat conservation. This variable conductance provides the required system-level thermal-control logic: reject heat during hot operation and preserve heat during cold or low-power conditions. The architecture obtained in this chapter is the baseline body-level solution; the following chapter extends it by introducing the wheel, hub, wheel–ground and deployable-support thermal paths.

Chapter 10

Thermal Modelling and Thermo-Structural Design of the Wheel and Support System

"Rota tu volubilis."

— *Carmina Burana*, "O Fortuna"
Medieval Latin poem

10.1 Modelling Rationale and Design Sequence

In the first version of the rover thermal model, the wheels were represented only as external radiating surfaces. They absorbed direct solar radiation, received infrared radiation from the lunar regolith, exchanged radiation with the rover external surfaces and rejected heat towards deep space. No conductive connection was initially introduced between the wheel assembly and the rover body. From a thermal point of view, the wheels therefore behaved as independent components and the initial condition could be idealised as

$$G_{\text{wheel}-\text{body}} = 0. \tag{10.1}$$

The corresponding simplified wheel energy balance was

$$C_{\text{wheel}} \frac{dT_{\text{wheel}}}{dt} = \dot{Q}_{\text{solar}} + \dot{Q}_{\text{IR,ground}} + \dot{Q}_{\text{rad,rover}} - \dot{Q}_{\text{rad,space}}. \tag{10.2}$$

This representation was useful as a first step because it isolated the radiative response of the wheels. It was nevertheless incomplete for the final rover model. A real wheel is mechanically connected to a hub and to the rover structure and, while resting on the lunar surface, it is also thermally coupled to the regolith. Once these paths are introduced, the wheel becomes part of the thermal network of the complete vehicle and can influence the temperature of the protected internal region.

The development of the wheel model was therefore carried out following a progressive design logic. First, the wheel geometry and its contact sector were constructed. A central hub and the conductive links required to connect the wheel assembly to the

rover were then introduced. The next step was not to assume a final value for the hub–body conductance, but to investigate its influence on the minimum temperature of the internal panel. This sensitivity study showed that a conductance of the order of

$$G_{\text{isolation}} \simeq 0.003 \text{ W/K} \tag{10.3}$$

was required to obtain the desired level of thermal isolation in the cold cases with a limited internal heat load.

At that point, two possible design directions were available. The first was to introduce a thermal switch or another variable-conductance element directly in the hub–body path. The second was to retain a simple fixed mechanical connection and modify the way in which the rover interacted with the ground during the cold phase. The second solution was selected. Four deployable hollow rods were therefore introduced to support and lift the rover, removing the strong wheel–regolith conductive contact when the wheels would otherwise behave as an important cold sink.

The rods were not selected only from a thermal point of view. Their material and geometry were chosen through a dedicated MATLAB thermo-structural search in which thermal conductance, structural stresses, Euler buckling, deflection and mass were evaluated simultaneously. The selected support was then implemented in Thermal Desktop and combined with time-dependent wheel–ground and rod–ground contact conditions.

The final development sequence can therefore be summarised as follows:

1. construction and discretisation of the wheel geometry;
2. introduction of the hub and of the wheel–hub, hub–hub and hub–body conductive paths;
3. sensitivity analysis of the minimum internal-panel temperature as a function of the hub–body conductance;
4. identification of approximately 0.003 W/K as the reference isolation level;
5. comparison between a thermal-switch approach and an alternative mechanical support strategy;
6. selection of deployable hollow support rods through a MATLAB thermo-structural trade-off;
7. implementation of the selected rods in the Thermal Desktop model;
8. removal of the wheel–ground contact and activation of the rod–ground path during the cold phase;
9. final verification at 70°, 80° and 85° latitude.

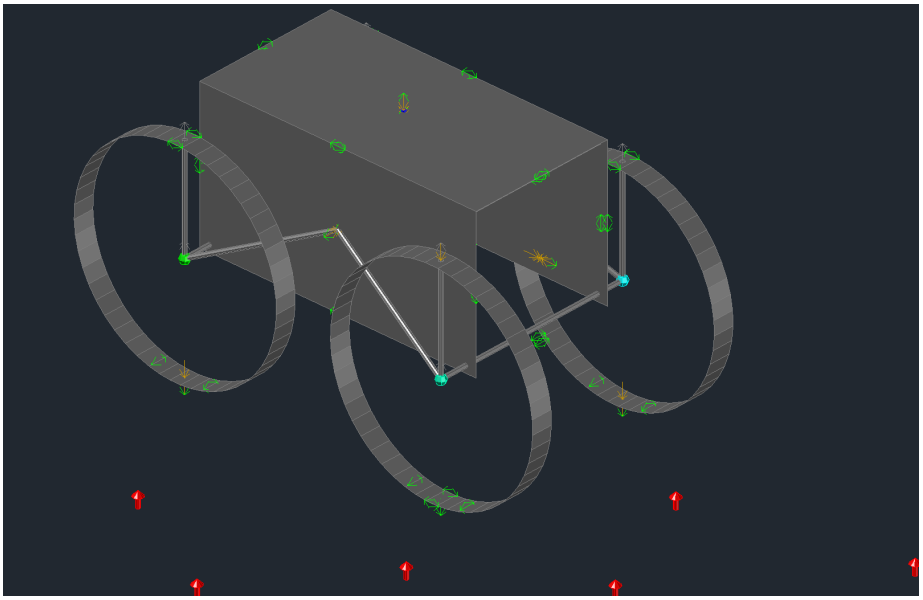


Figure 10.1: Baseline rover geometry during the first stage of the wheel-model development.

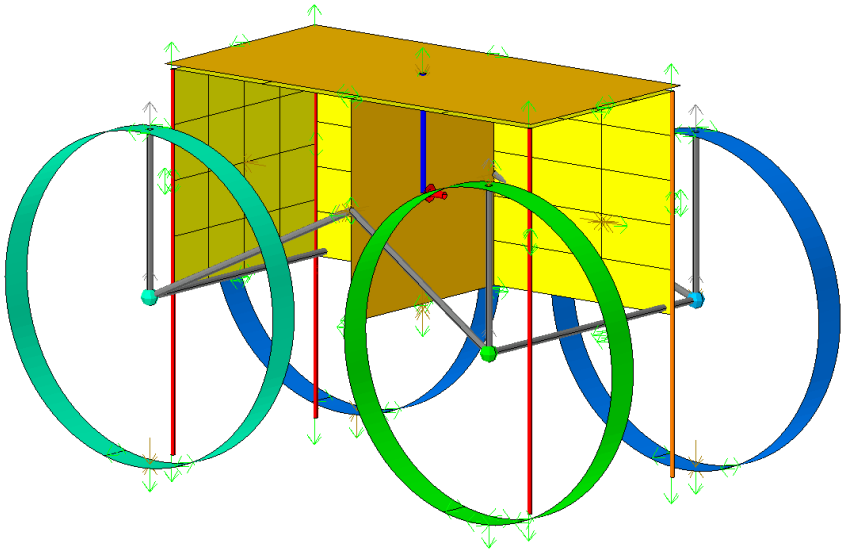


Figure 10.2: Final Thermal Desktop configuration including wheels, hubs and deployable support rods.

10.2 Construction of the Wheel Assembly

10.2.1 Wheel geometry and material definition

Each wheel was represented as a cylindrical surface with radius

$$R_{\text{wheel}} = 0.15 \text{ m} \tag{10.4}$$

and axial width

$$b_{\text{wheel}} = 0.03 \text{ m}. \tag{10.5}$$

The circumferential surface was discretised so that different regions could interact independently with the Sun, the lunar surface, deep space and the rover body. The lower sector was treated separately because it represents the portion that can establish direct contact with the regolith. The angular definition shown in Figure 10.3 isolates a 30° ground-contact sector and leaves a complementary 330° external surface.
The complete cylindrical lateral area is

$$A_{\text{full}} = 2\pi R_{\text{wheel}} b_{\text{wheel}} = 2.8274 \times 10^{-2} \text{ m}^2. \tag{10.6}$$

The apparent area associated with the 30° sector is

$$A_{\text{wheel,contact}} = R_{\text{wheel}} \left(\frac{30\pi}{180} \right) b_{\text{wheel}} = 2.3562 \times 10^{-3} \text{ m}^2, \tag{10.7}$$

while the remaining 330° surface is

$$A_{330^\circ} = A_{\text{full}} - A_{\text{wheel,contact}} = 2.5918 \times 10^{-2} \text{ m}^2. \tag{10.8}$$

The separation of the lower sector is essential for the subsequent operational strategy because it makes it possible to activate or remove the wheel–regolith conductive path without changing the remaining radiative surface of the wheel. The selected sector is an apparent geometrical contact area; the real microscopic area of contact with granular regolith would depend on local pressure, roughness and soil compaction.
The wheel was assigned aluminium as the structural material in the Cond/Cap definition, with a modelled thickness of

$$t_{\text{wheel}} = 0.004 \text{ m}. \tag{10.9}$$

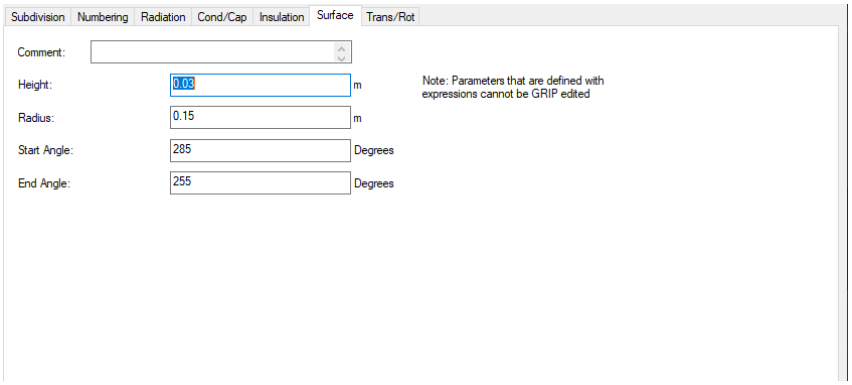


Figure 10.3: Thermal Desktop definition of the wheel geometry, with radius 0.15 m, axial width 0.03 m and the angular sector used for the ground contact.

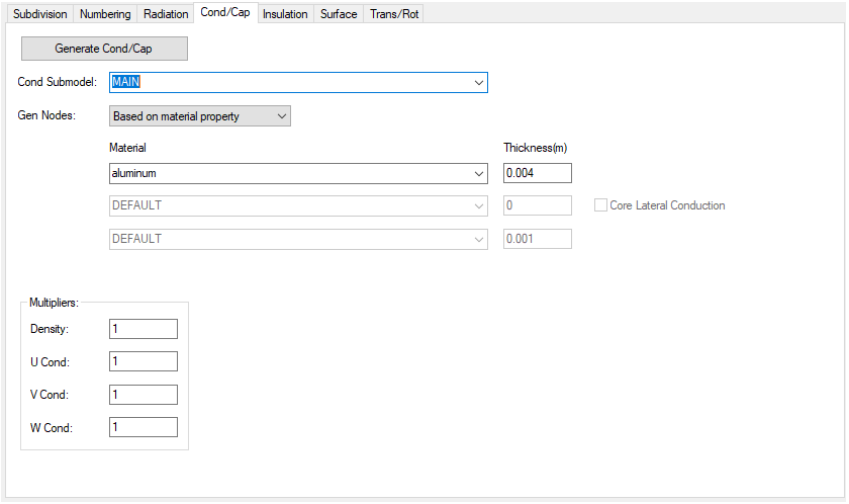


Figure 10.4: Wheel Cond/Cap definition with aluminium material and 4 mm modelled thickness.

Adjacent wheel sectors were connected through an edge contactor. In the implemented model, the input is defined per unit edge length and the value shown in Figure 10.5 is

$$g_{\text{edge}} = 167\ \text{W}\,\text{m}^{-1}\,\text{K}^{-1}. \tag{10.10}$$

This connection maintains conductive continuity around the discretised rim while preserving the subdivision required for the radiative and ground-contact calculations.

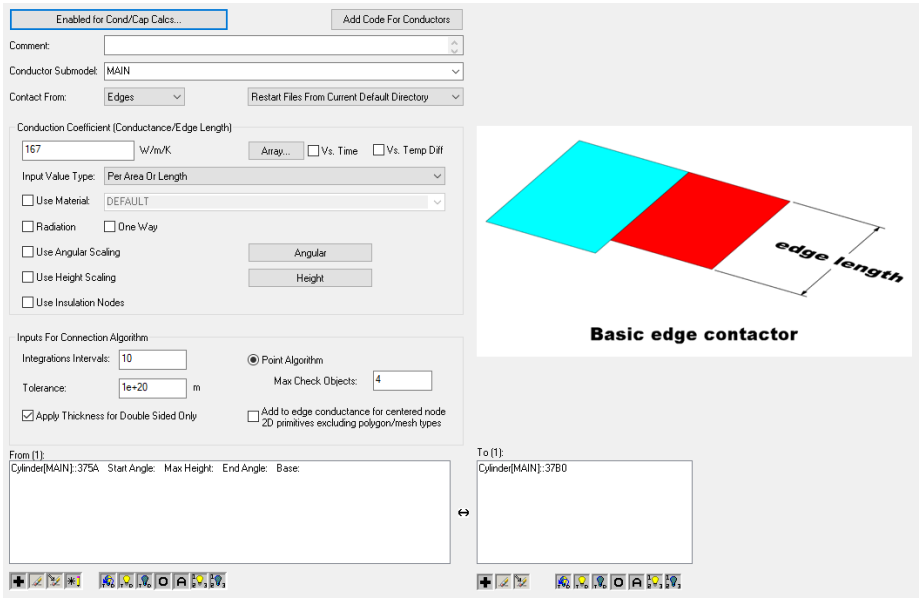


Figure 10.5: Edge contactor used to maintain conductive continuity between adjacent discretised wheel sectors.

10.2.2 Hub and conductive connections

After the wheel geometry had been defined, the central hub and the conductive connections required to couple the wheel assembly to the rover were introduced. Figure 10.6

shows the generic conductor used between the wheel and the hub. The implemented value is

$$G_{\text{wheel}-\text{hub}} = 0.15 \text{ W/K}. \tag{10.11}$$

The *Per Area* option is not enabled. Therefore, the value is a total conductance and is not multiplied by the area displayed in the conductor window. The selected surface only identifies the geometrical target of the connection.

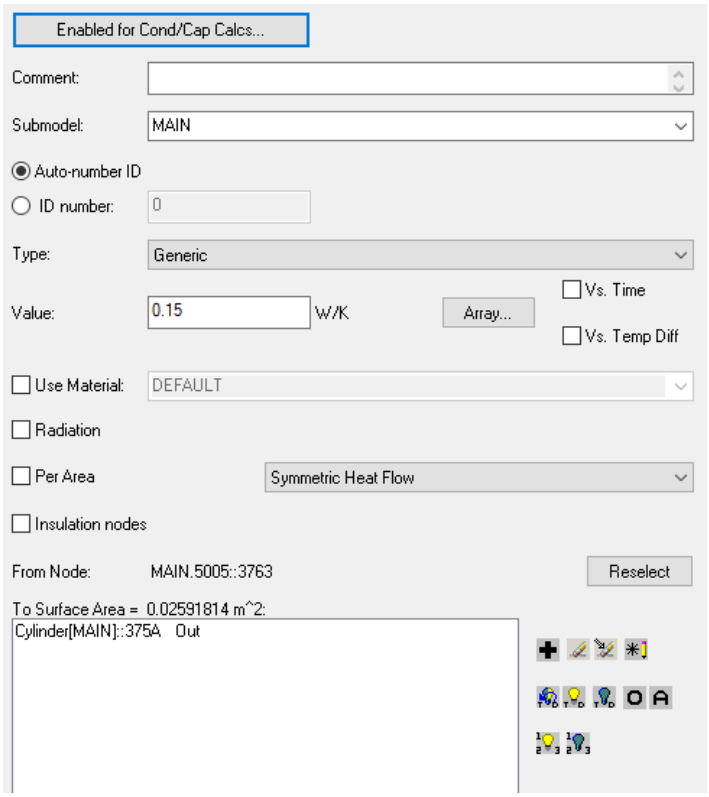


Figure 10.6: Generic conductor used for the wheel–hub thermal connection, with a total conductance of 0.15 W/K.

The internal hub–hub connection was implemented as a generic conductor with a time-dependent array and a scaling factor of 0.02, as shown in Figure 10.7. Its instantaneous value is therefore defined by the prescribed array and the scaling factor. This internal connection was kept as part of the wheel assembly and was not the parameter used in the following sensitivity study.
The key connection for the thermal trade-off is the path between the hub and the rover body. In the final mechanical configuration, this connection was represented by a fixed generic conductor with

$$G_{\text{hub}-\text{body,final}} = 0.02 \text{ W/K}. \tag{10.12}$$

As for the wheel–hub link, the *Per Area* option is disabled and the value is therefore the total conductance between the selected nodes.
For a generic conductive link, the transferred heat rate is

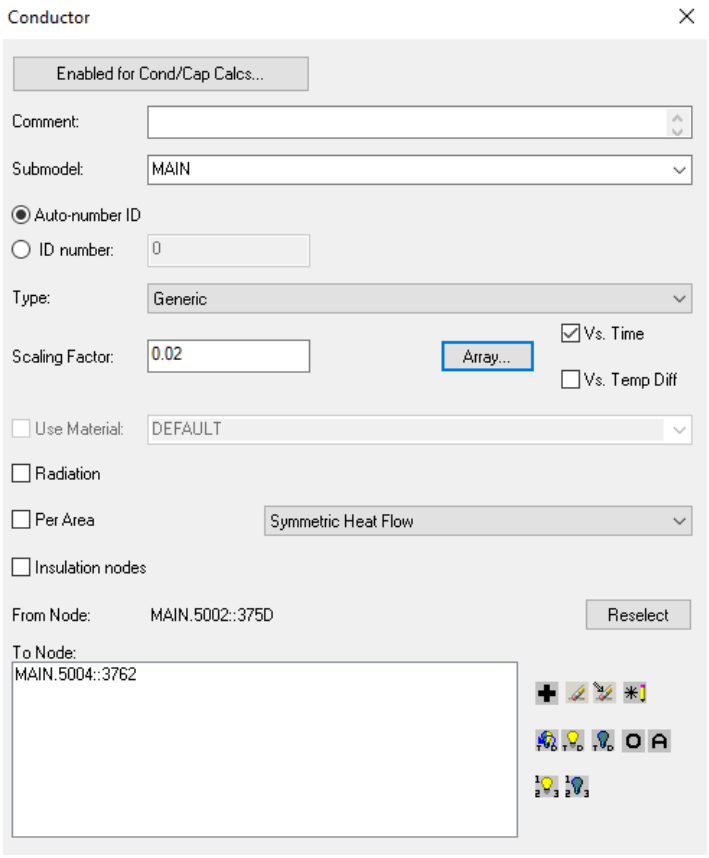


Figure 10.7: Thermal Desktop definition of the internal hub–hub conductor, implemented with a time-dependent array and a scaling factor of 0.02.

$$\dot{Q}_{ij} = G_{ij}\,(T_i - T_j)\,. \tag{10.13}$$

Consequently, even a conductance of only a few hundredths of a watt per kelvin can be important for a mini rover whose cold-case internal power is of the order of a few watts. For example, the final 0.02 W/K hub–body link transfers

$$\dot{Q}_{\mathrm{hub-body}} = 0.02 \times 100 = 2 \text{ W} \tag{10.14}$$

for a temperature difference of 100 K. This observation motivated a direct sensitivity analysis rather than an arbitrary choice of the hub–body conductance.

10.3 Hub-to-Body Conductance Sensitivity Analysis

The hub–body conductance was varied to determine the degree of thermal isolation required to prevent the wheel assembly from excessively reducing the minimum temperature of the internal rover panel. The quantity used to compare the configurations was therefore the minimum internal-panel temperature, $T_{\min}$, rather than the wheel temperature itself.
The three conductance levels represented in the final comparison are

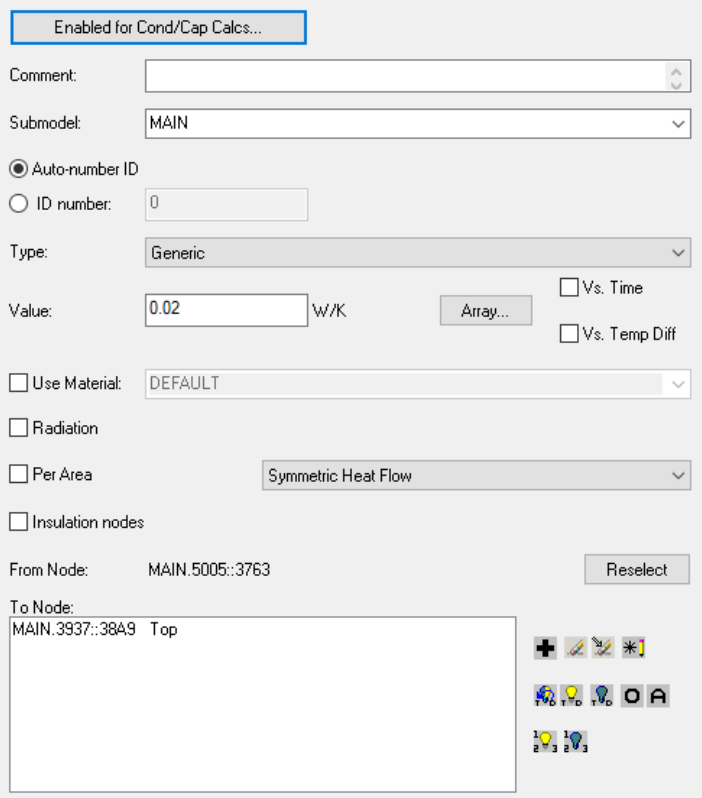


Figure 10.8: Final fixed generic conductor between the wheel hub and the rover body, with $G_{\text{hub-body}} = 0.02$ W/K.

$$G_{\text{hub-body}} = 0.03, \qquad 0.01, \qquad 0.003 \text{ W/K}. \tag{10.15}$$

The simulations were evaluated at the high latitudes of 70°, 80° and 85° because these cases are the most relevant for the final cold-case design. The matrix plots use the same temperature classification adopted for the rover internal region:

$$253.15 \text{ K} \leq T \leq 323.15 \text{ K}. \tag{10.16}$$

Since the present trade-off is driven by the cold condition, only T_{min} is reported in each matrix cell.

10.3.1 Case $G_{\text{hub-body}} = 0.03$ W/K

For the 0.03 W/K case, the minimum internal-panel temperatures were taken directly from the three latitude-specific Thermal Desktop result files. The considered internal heat loads are 0, 4, 8 and 12 W.
The matrix shows that the 8 W cases remain close to, but slightly below, the lower temperature requirement at all three latitudes, with minimum temperatures of approximately 251–252 K. Increasing the internal load to 12 W raises the minimum temperature well above the lower limit. The 0.03 W/K connection therefore still represents a significant thermal leak during the cold phase.

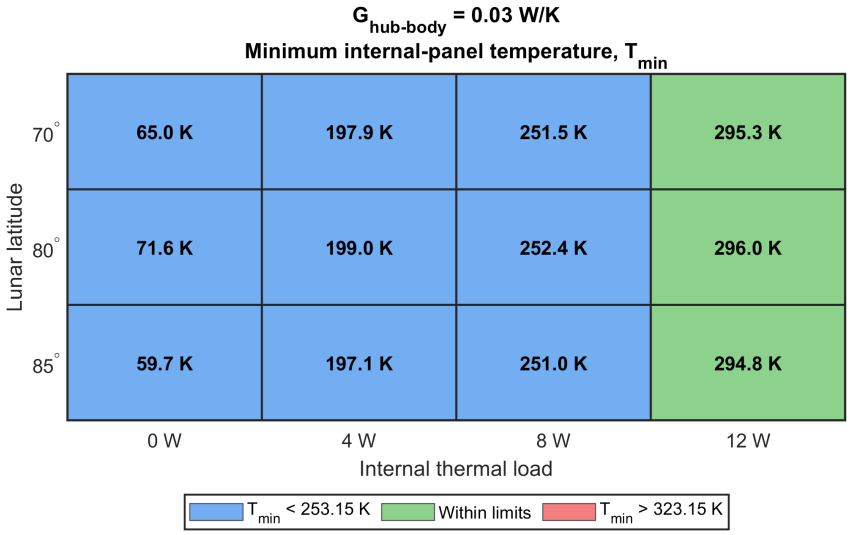


Figure 10.9: Minimum internal-panel temperature as a function of latitude and internal heat load for $G_{\mathrm{hub-body}} = 0.03$ W/K.

10.3.2 Case $G_{\mathrm{hub-body}} = 0.01$ W/K

Reducing the conductance to 0.01 W/K decreases the thermal interaction between the wheel assembly and the protected rover body. In this case, the 6 W minimum temperatures remain below the 253.15 K limit, while the 8 W cases are above it.
To identify the transition more clearly, a 7 W column was added to the matrix by linear interpolation between the corresponding 6 W and 8 W results:

$$T_{\mathrm{min},7W} = \frac{T_{\mathrm{min},6W} + T_{\mathrm{min},8W}}{2}. \tag{10.17}$$

For this conductance level, the 80° row was also obtained by interpolation between the corresponding 70° and 85° values:

$$T_{\mathrm{min},80^\circ} = \frac{T_{\mathrm{min},70^\circ} + T_{\mathrm{min},85^\circ}}{2}. \tag{10.18}$$

These interpolated values are used only to complete the comparison matrix and do not represent additional Thermal Desktop simulation runs. The resulting trend indicates that approximately 7 W of internal power is required to remain above the lower temperature limit for the analysed cold cases.

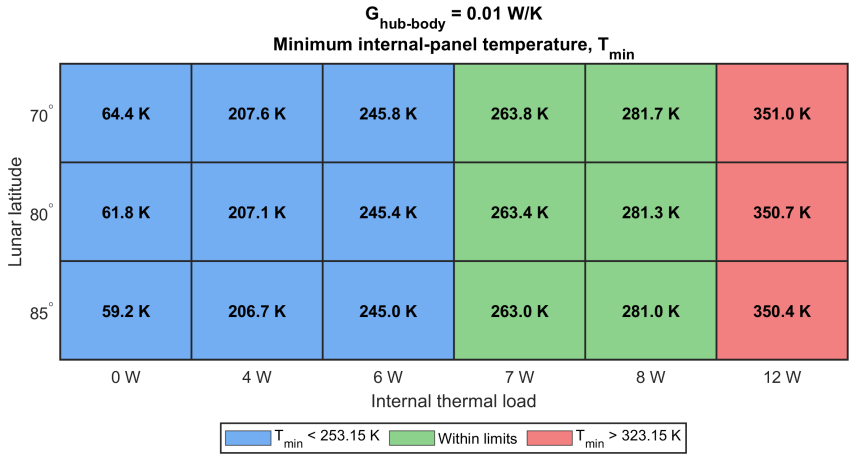


Figure 10.10: Minimum internal-panel temperature for $G_{\mathrm{hub-body}} = 0.01$ W/K. The 7 W cases and the 80° row are obtained by linear interpolation as described in the text.

10.3.3 Case $G_{\mathrm{hub-body}} = 0.003$ W/K

The lowest investigated conductance was 0.003 W/K. With this value, the 4 W cases remain below the required minimum temperature, whereas the transition to an acceptable cold condition occurs at approximately 5 W.
The 5 W column was obtained from the 4 W and 6 W cases according to

$$T_{\mathrm{min},5W} = \frac{T_{\mathrm{min},4W} + T_{\mathrm{min},6W}}{2}. \tag{10.19}$$

As for the 0.01 W/K matrix, the 80° values were obtained from the arithmetic mean of the 70° and 85° results. These interpolated points are displayed to make the conductance trade-off easier to compare and are not independent simulation cases.
The matrix shows that a hub–body conductance of approximately 0.003 W/K reduces the cold-case thermal leak sufficiently for the internal panel to remain above the lower limit with an internal load of approximately 5 W. This value was therefore retained as the reference isolation level for the subsequent design decision.

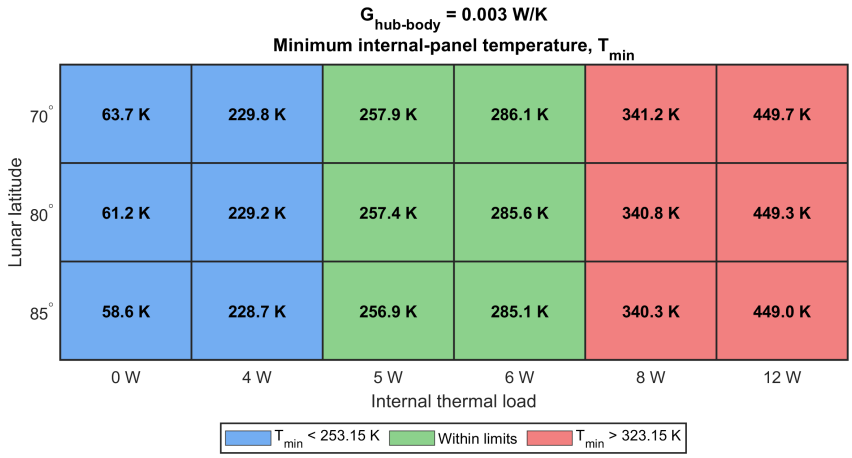


Figure 10.11: Minimum internal-panel temperature for $G_{\mathrm{hub-body}} = 0.003$ W/K. The 5 W cases and the 80° row are obtained by linear interpolation as described in the text.

10.3.4 Interpretation of the sensitivity study

The three matrices provide the main design result of the wheel–body sensitivity study. As the hub–body conductance decreases, the internal power required to satisfy the cold temperature requirement is reduced. The approximate transition moves from more than 8 W for 0.03 W/K, to approximately 7 W for 0.01 W/K, and finally to approximately 5 W for 0.003 W/K.
The physical meaning can also be illustrated by considering a representative temperature difference of 100 K:

$$\dot{Q} = G\Delta T. \tag{10.20}$$

For the three investigated conductances, the corresponding heat-transfer levels are

$$\dot{Q} = 3, \qquad 1, \qquad 0.3 \text{ W}, \tag{10.21}$$

respectively. A heat leak of a few watts is comparable with the complete cold-case internal power budget of the rover, which explains the strong influence of the hub–body path.
The result of this analysis should not be interpreted as a requirement to manufacture a conventional rigid hub connection with exactly 0.003 W/K. Instead, 0.003 W/K was used as a system-level isolation benchmark: the final architecture had to prevent the wheel and the terrain from extracting more heat from the rover than a path of this order would permit.

10.4 Design Decision: Thermal Switch or Alternative Support Strategy

Once the required isolation level had been identified, a variable hub–body connection represented the most direct solution. A preliminary thermal-switch-like profile was therefore considered in Thermal Desktop. The idealised profile shown in Figure 10.12 uses a high-conductance state during the first half of the cycle and a low-conductance state during the second half:

$$G_{\text{hub}-\text{body}}(t) = \begin{cases} 0.3 \text{ W/K}, & 0 \le t \le 1\,275\,720 \text{ s}, \\ 0.003 \text{ W/K}, & 1\,275\,720 < t \le 2\,551\,440 \text{ s}. \end{cases} \tag{10.22}$$

The low state corresponds directly to the isolation level identified by the previous sensitivity study. The high state was used as an idealised representation of a strongly conducting connection during the illuminated and operational phase.

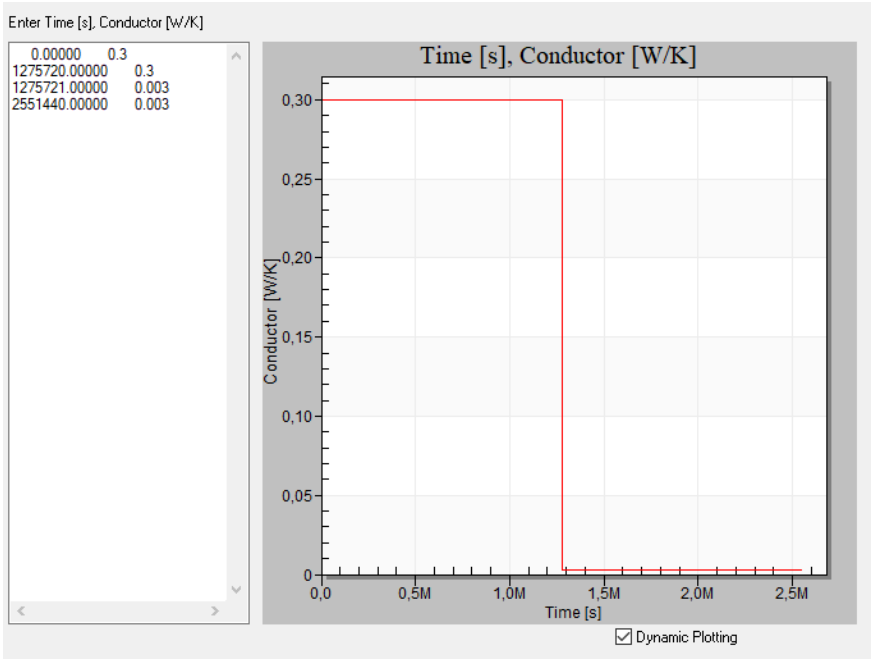


Figure 10.12: Idealised hub–body variable-conductance profile considered as a thermal-switch-like solution: 0.3 W/K during the first half-cycle and 0.003 W/K during the second half-cycle.

Although thermally effective, this solution was not retained for the final rover. A dedicated thermal switch at each wheel would add interfaces, attachment hardware and a temperature-dependent or actuated mechanism in a mechanically loaded region. The implementation would have to be repeated for all four wheel assemblies and would be exposed to lunar dust, wheel reactions, launch loads and large temperature excursions. The mass and qualification effort of four dedicated devices were therefore considered disproportionate for the present small-rover concept.

A second consideration is that the hub–body link is not the only cold-case thermal path. As long as the rover rests on its wheels, each wheel is also strongly coupled to the regolith. Therefore, lowering the hub–body conductance alone does not remove the wheel–ground interaction.

For these reasons, the final concept retains the fixed hub–body mechanical link of 0.02 W/K shown in Figure 10.8, but modifies the ground-support condition during the cold phase. The wheels are lifted from the lunar surface by four deployable rods. The direct wheel–regolith contact is consequently removed and replaced by a much weaker terrain–rod–rover path.

This distinction is important for the interpretation of the design. The value 0.003 W/K obtained from the sensitivity study is the target isolation level that motivated the alternative architecture, whereas 0.02 W/K is the fixed mechanical hub–body conductance retained in the final Thermal Desktop model.

10.5 Thermo-Structural Selection of the Deployable Support Rods

10.5.1 Design requirements and MATLAB search

The alternative support strategy is useful only if the rods are simultaneously able to support the rover and to provide a sufficiently small thermal leak. Their design was therefore treated as a combined thermo-structural problem rather than as a purely geometrical addition to the Thermal Desktop model.
A dedicated MATLAB script automatically evaluated hollow cylindrical rods with external diameters from 2 to 12 mm in 1 mm increments and wall thicknesses of 1 and 2 mm. Three candidate materials were considered:

- aluminium 6061-T6;
- AISI 304 stainless steel;
- titanium Ti-6Al-4V.

The material properties used in the search are summarised in Table 10.1.

Table 10.1: Material properties used in the MATLAB thermo-structural search.

Material	E [GPa]	σ_y [MPa]	ρ [kg/m^3]	k [W/(m K)]
Aluminium 6061-T6	68.9	276	2700	167
AISI 304 stainless steel	193	215	8000	16.2
Titanium Ti-6Al-4V	113.8	880	4430	6.7

The baseline geometrical and loading inputs were

$$L_{\text{thermal}} = 0.35 \text{ m}, \qquad L_{\text{free}} = 0.15 \text{ m}, \tag{10.23}$$

and

$$F = 2 \text{ N per rod}, \qquad \theta = 10^\circ, \qquad N_{\text{rods}} = 4. \tag{10.24}$$

The thermal length represents the complete conduction path considered between the ground contact and the rover attachment. The free length is the unsupported length used in the simplified bending and Euler-buckling verification.
The force was decomposed into axial and transverse components:

$$F_{\text{axial}} = F\cos\theta, \qquad F_{\text{transverse}} = F\sin\theta. \tag{10.25}$$

For each combination of material and geometry, the script calculated the annular cross-sectional area, second moment of area, axial stress, bending stress, combined normal stress, Euler critical load, transverse displacement, mass and thermal conductance.
For a hollow circular section,

$$A = \frac{\pi}{4}\left(D_{\text{e}}^2 - D_{\text{i}}^2\right) \tag{10.26}$$

and

$$I = \frac{\pi}{64}\left(D_{\mathrm{e}}^4 - D_{\mathrm{i}}^4\right). \tag{10.27}$$

The section modulus is

$$W = \frac{I}{D_{\mathrm{e}}/2}, \tag{10.28}$$

and the maximum normal stress was evaluated as

$$\sigma_{\max} = \frac{F_{\mathrm{axial}}}{A} + \frac{F_{\mathrm{transverse}} L_{\mathrm{free}}}{W}. \tag{10.29}$$

Euler buckling was checked through

$$P_{\mathrm{cr}} = \frac{\pi^2 E I}{\left(K L_{\mathrm{free}}\right)^2}, \tag{10.30}$$

with $K = 2$, corresponding to the conservative fixed–free idealisation adopted in the script. The transverse displacement was estimated as

$$\delta = \frac{F_{\mathrm{transverse}} L_{\mathrm{free}}^3}{3EI}. \tag{10.31}$$

The thermal conductance of a candidate rod was calculated from

$$G_{\mathrm{rod}} = \frac{kA}{L_{\mathrm{thermal}}}. \tag{10.32}$$

A configuration was retained only if the following requirements were satisfied:

$$FS_{\mathrm{yield}} \geq 2, \qquad FS_{\mathrm{Euler}} \geq 2, \tag{10.33}$$

$$m_4 \leq 0.8 \text{ kg}, \qquad G_{\text{single rod}} \leq 0.003 \text{ W/K}. \tag{10.34}$$

Configurations with a total mass of the four rods below 0.5 kg were classified as preferable. The 0.003 W/K value obtained from the hub–body sensitivity study was used here as a conservative order-of-magnitude upper limit for each candidate low-conductance support path. It should not be interpreted as an exact equality between the original hub–body path and the complete four-rod network. The finally selected titanium geometry is more insulating than this limit, and the four rods combined remain below 0.003 W/K in the simplified thermal network.

10.5.2 Material and geometry trade-off

The final selected geometry has external and internal diameters

$$D_{\mathrm{e}} = 4 \text{ mm}, \qquad D_{\mathrm{i}} = 2 \text{ mm}, \tag{10.35}$$

corresponding to a wall thickness of

$$t = 1 \text{ mm}. \tag{10.36}$$

The comparison between the three candidate materials for this geometry is reported in Table 10.2.

Table 10.2: Comparison of four hollow rods with $D_e = 4$ mm and $D_i = 2$ mm.

Material	m_4 [kg]	G_1 [W/K]	G_4 [W/K]	FS_y
Aluminium 6061-T6	0.0356	0.004497	0.01799	30.49
AISI 304 stainless steel	0.1056	0.000436	0.001745	23.75
Titanium Ti-6Al-4V	0.0585	0.000180	0.000722	97.21

Aluminium is the lightest candidate, but its high thermal conductivity causes the conductance of the selected 4/2 mm rod to exceed the 0.003 W/K thermal limit. Stainless steel satisfies the thermal requirement but produces the highest mass. Ti-6Al-4V provides the smallest thermal conductance of the three materials while retaining a moderate mass and a large preliminary structural margin. It was therefore selected for the support system.
For the selected titanium rod, the calculated structural quantities are

$$\sigma_{\max} \approx 9.05 \text{ MPa}, \qquad FS_{\text{yield}} \approx 97.2, \tag{10.37}$$

$$P_{\text{cr}} \approx 147 \text{ N}, \qquad FS_{\text{Euler}} \approx 74.6, \tag{10.38}$$

and

$$\delta \approx 0.291 \text{ mm}, \qquad m_4 \approx 0.0585 \text{ kg}. \tag{10.39}$$

These large margins are partly a consequence of the low nominal load used in the preliminary analytical model. The calculation does not include local joint stresses, deployment loads, impact with uneven terrain, launch vibration, fatigue or manufacturing defects. The selected geometry must therefore be interpreted as a preliminary baseline rather than as a flight-qualified structural design.

10.5.3 Thermal Desktop implementation of the selected rod

The selected support was modelled as a hollow cylindrical rod with height

$$L_{\text{rod}} = 0.345 \text{ m}, \tag{10.40}$$

external radius

$$R_e = 0.002 \text{ m}, \tag{10.41}$$

and internal radius

$$R_i = 0.001 \text{ m}. \tag{10.42}$$

The corresponding annular area is

$$A_{\text{rod}} = \frac{\pi}{4}\left(D_e^2 - D_i^2\right) = 9.425 \times 10^{-6} \text{ m}^2, \tag{10.43}$$

while the second moment of area is

$$I_{\mathrm{rod}} = \frac{\pi}{64}\left(D_{\mathrm{e}}^4 - D_{\mathrm{i}}^4\right) = 1.178 \times 10^{-11}\ \mathrm{m}^4. \tag{10.44}$$

Using the Ti-6Al-4V thermal conductivity adopted in the MATLAB script,

$$k_{\mathrm{Ti}} = 6.7\ \mathrm{W\,m^{-1}\,K^{-1}}, \tag{10.45}$$

and $L_{\mathrm{thermal}} = 0.35$ m, the axial conductance of one rod is

$$G_{\mathrm{rod}} = \frac{k_{\mathrm{Ti}} A_{\mathrm{rod}}}{L_{\mathrm{thermal}}} = 1.80 \times 10^{-4}\ \mathrm{W/K}. \tag{10.46}$$



Figure 10.13: Hollow cylindrical support used for the final deployable-rod concept.

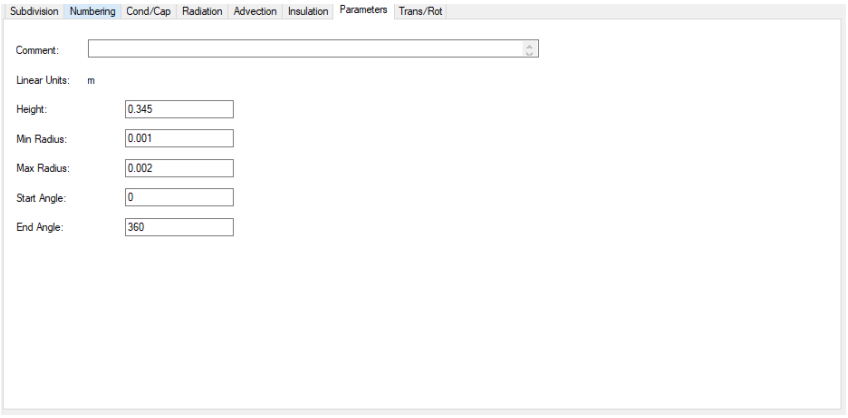


Figure 10.14: Thermal Desktop geometrical definition of the selected titanium support rod, with $R_{\mathrm{e}} = 2$ mm, $R_{\mathrm{i}} = 1$ mm and height 0.345 m.

10.6 Operational Wheel–Ground and Rod–Ground Contact Strategy

The selected rods provide the required structural support, but the thermal benefit is obtained only when they are combined with a change in the rover ground-contact condition. During the illuminated part of the environmental design cycle, the rover is represented as resting on its wheels and the rods are inactive. Before the cold part of the design cycle, the rods are deployed, the rover body is raised and the direct wheel–regolith contact is removed. This complete-cycle switching law is a bounding thermal-analysis scenario and does not represent the nominal approximately three-hour sortie timeline introduced in Chapter 3.
The transition was implemented over a complete simulated lunar cycle of

$$t_{\text{cycle}} = 2\,551\,440 \text{ s} \tag{10.47}$$

with the change of support condition imposed at

$$t_{\text{switch}} = 1\,275\,720 \text{ s}. \tag{10.48}$$

10.6.1 Wheel–regolith contact

When the rover rests on its wheels, the selected 30° lower sector is connected to the regolith through a face contactor. The wheel-side contact area is

$$A_{\text{wheel,contact}} = 2.356194 \times 10^{-3} \text{ m}^2. \tag{10.49}$$

The wheel–regolith interface was defined starting from the range of total thermal contact conductance adopted from the NASA Lunar Terrain Vehicle wheel thermal-sensitivity study by Birmingham [52]. That study specifically investigates heat leak through the wheels and the sensitivity of wheel–surface thermal interactions under lunar operating conditions. The conductance range adopted in the present model is

$$0.5 \leq G_{\text{wheel}-\text{ground}} \leq 100 \qquad \text{W/K}. \tag{10.50}$$

Thermal Desktop requires the face-contactor input in the form of conductance per unit area. Therefore, the total conductance range must be converted using the geometrical contact area of the selected wheel sector:

$$h_{\text{wheel}-\text{ground}} = \frac{G_{\text{wheel}-\text{ground}}}{A_{\text{wheel,contact}}}. \tag{10.51}$$

With

$$A_{\text{wheel,contact}} = 2.356194 \times 10^{-3} \text{ m}^2, \tag{10.52}$$

the reference conductance interval corresponds approximately to

$$2.12 \times 10^2 h_{\text{wheel}-\text{ground}} 4.24 \times 10^4 \qquad \text{W m}^{-2} \text{ K}^{-1}. \tag{10.53}$$

A representative value inside this converted interval was selected and rounded to

$$h_{\mathrm{wheel-ground}} = 10\,000\ \mathrm{W\,m^{-2}\,K^{-1}}. \tag{10.54}$$

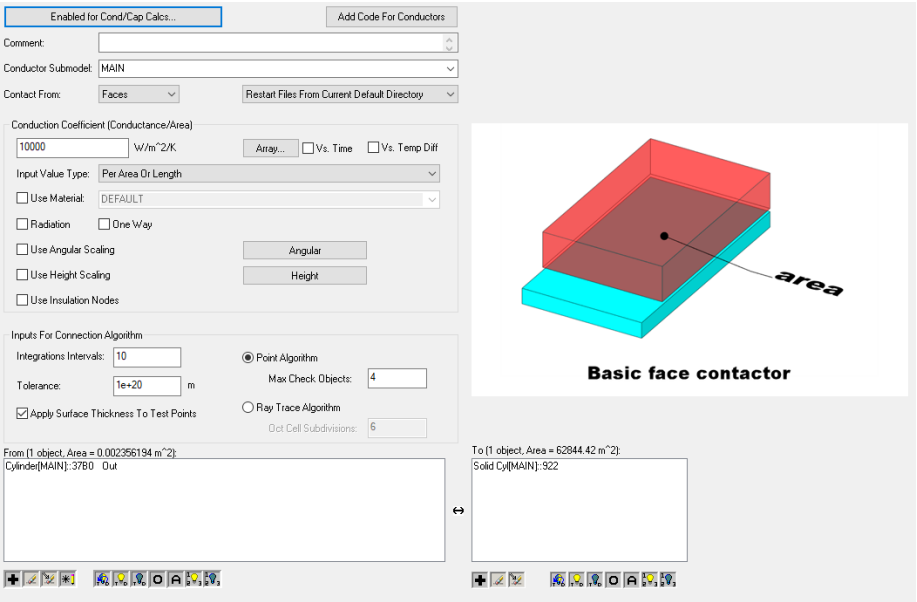


Figure 10.15: Face contactor used to represent the active wheel–regolith contact over the selected wheel sector. The Thermal Desktop input is expressed per unit contact area.

The corresponding total conductance represented by the selected contactor is therefore

$$G_{\mathrm{wheel-ground}} = h_{\mathrm{wheel-ground}} A_{\mathrm{wheel,contact}} = 10\,000\left(2.356194 \times 10^{-3}\right) \approx 23.56\ \mathrm{W/K}. \tag{10.55}$$

The value of approximately 23.56 W/K lies inside the adopted 0.5–100 W/K reference interval. Consequently, the value $10\,000\ \mathrm{W\,m^{-2}\,K^{-1}}$ should not be interpreted as the intrinsic thermal conductivity of lunar regolith, nor as an arbitrarily imposed "perfect" contact. It is the area-normalised Thermal Desktop representation of a wheel–regolith contact conductance selected within the reference range for the apparent geometrical contact sector used in the model. The actual interface conductance would depend on wheel load, sinkage, contact pressure, regolith compaction, surface roughness and the true microscopic contact area.
The time law applied to the wheel–ground contact is

$$h_{\mathrm{wheel-ground}}(t) = \begin{cases} 10\,000\ \mathrm{W\,m^{-2}\,K^{-1}}, & 0 \le t \le 1\,275\,720\ \mathrm{s}, \\ 0, & 1\,275\,720 < t \le 2\,551\,440\ \mathrm{s}. \end{cases} \tag{10.56}$$

The zero value in the second half-cycle represents the physical lifting of the wheels from the lunar surface. During the first half-cycle, the imposed coefficient of $10\,000\ \mathrm{W\,m^{-2}\,K^{-1}}$ corresponds to a total wheel–ground conductance of approximately 23.56 W/K over the selected contact sector.

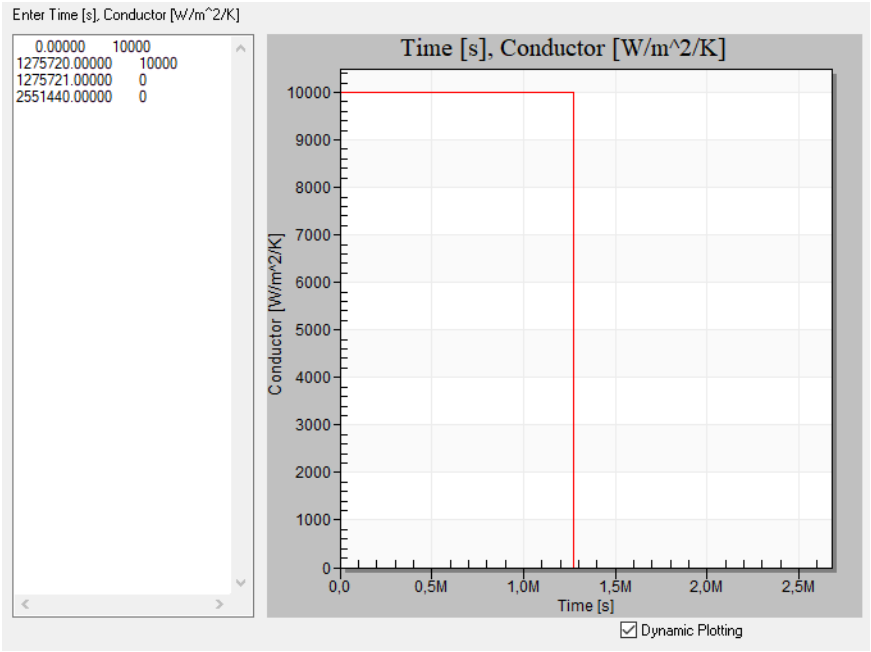


Figure 10.16: Time-dependent wheel–ground contact coefficient: the contact is active during the first half-cycle and removed after deployment of the support rods.

10.6.2 Rod–regolith contact

The rod contact follows the opposite schedule. It is inactive while the rover is supported by the wheels and becomes active when the rover is raised.
The adopted rod–ground contact coefficient is

$$h_{\mathrm{rod-ground}} = 318\ \mathrm{W\,m^{-2}\,K^{-1}}. \tag{10.57}$$

Applied to the annular rod-end area, this coefficient corresponds to an interface conductance of approximately

$$G_{\mathrm{contact,rod}} = 318 A_{\mathrm{rod}} \approx 2.997 \times 10^{-3}\ \mathrm{W/K}. \tag{10.58}$$

The time law is

$$h_{\mathrm{rod-ground}}(t) = \begin{cases} 0, & 0 \le t \le 1\,275\,720\ \mathrm{s}, \\ 318\ \mathrm{W\,m^{-2}\,K^{-1}}, & 1\,275\,720 < t \le 2\,551\,440\ \mathrm{s}. \end{cases} \tag{10.59}$$

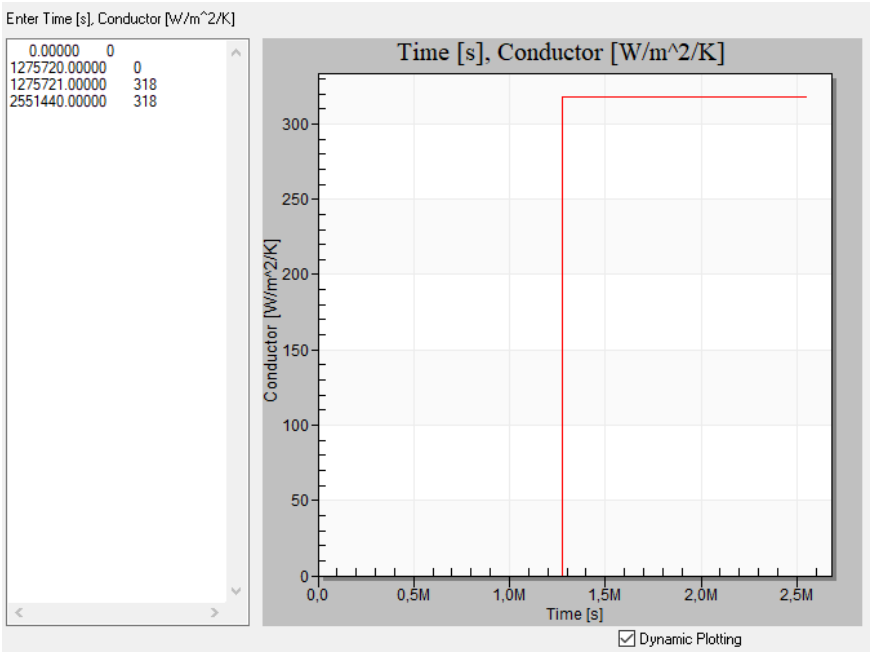


Figure 10.17: Time-dependent rod–ground contact coefficient, activated when the wheel–ground contact is removed.

The contact resistance and the thermal resistance of the titanium rod act approximately in series. Neglecting the body-side joint resistance,

$$G_{\mathrm{eq},1} = \left(\frac{1}{G_{\mathrm{contact,rod}}} + \frac{1}{G_{\mathrm{rod}}} \right)^{-1} \approx 1.70 \times 10^{-4}\ \mathrm{W/K}. \tag{10.60}$$

For four identical rods acting in parallel,

$$G_{\mathrm{eq},4} = 4G_{\mathrm{eq},1} \approx 6.81 \times 10^{-4}\ \mathrm{W/K}. \tag{10.61}$$

The complete terrain–rod–rover conductive path is therefore well below the 0.003 W/K isolation benchmark identified in the hub–body sensitivity analysis. At a representative temperature difference of 100 K, the total heat transfer through the four rods is only

$$\dot{Q}_{\mathrm{rods}} = G_{\mathrm{eq},4}\Delta T \approx 0.068\ \mathrm{W}. \tag{10.62}$$

The comparison between the active wheel–ground path, represented by approximately 23.56 W/K for the selected wheel contact sector, and the much weaker four-rod conductive path, approximately 6.8×10^{-4} W/K in the present simplified model, illustrates the thermal purpose of the lifting strategy. These two values describe different physical interfaces and should therefore be interpreted as system-level model conductances rather than as intrinsic material properties.
The instantaneous exchange of contact conditions at t_{switch} is a simplified representation of the deployment process. A real mechanism would require a finite interval during which the rods are deployed and the wheels progressively lose contact with the ground. The step function is retained here because the objective is to evaluate the preliminary thermal benefit of the two limiting configurations.

10.7 Thermo-Optical Properties of Wheels and Rods

The external wheel surface and the titanium support rods were assigned separate thermo-optical properties. The implemented values are reported in Table 10.3.

Table 10.3: Thermo-optical properties implemented for the wheel and support rods.

Surface	α	ε	α/ε
Titanium support rods	0.16	0.15	1.067
Wheel external surface	0.20	0.19	1.053

The low emissivity limits radiative heat rejection during the cold phase. This is beneficial once the rover is raised because the wheels and rods remain radiatively exposed even though the direct wheel–ground conductive contact has been removed. The same low emissivity also reduces heat rejection during illumination, and therefore introduces a hot–cold trade-off that must be checked in the final simulations.
The values used here represent the selected numerical surface properties. They should not be interpreted as universal properties of bulk titanium or of every possible wheel surface finish. Dust contamination, oxidation, roughness and ageing can modify both absorptivity and emissivity.

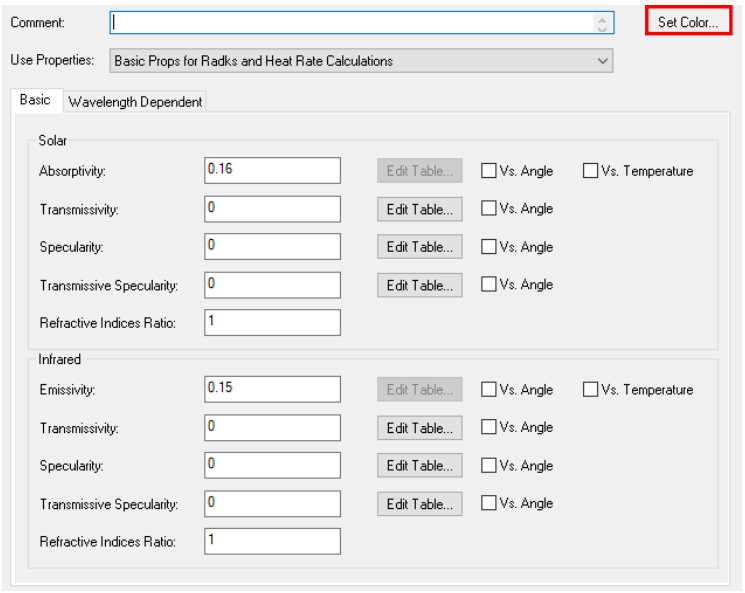


Figure 10.18: Thermo-optical properties assigned to the titanium support rods.

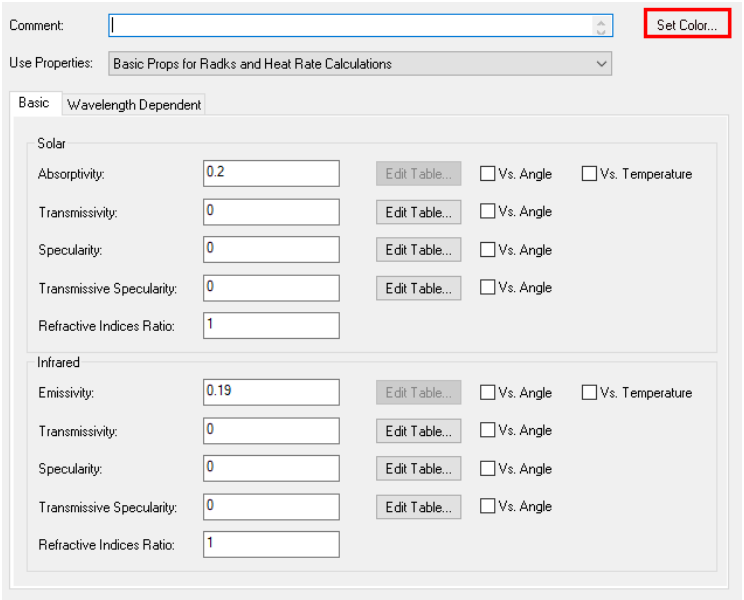


Figure 10.19: Thermo-optical properties assigned to the external wheel surface.

10.8 Final High-Latitude Thermal Verification

The complete configuration was evaluated at 70°, 80° and 85° latitude. During the first half-cycle, the wheels are in contact with the regolith and the rods are thermally inactive. At the switching time, the wheel contact is removed and the rod contact is activated. The hub–body connection remains fixed at 0.02 W/K throughout the complete simulation.
The internal temperature objective is

$$253.15\ \text{K} \leq T \leq 323.15\ \text{K}, \tag{10.63}$$

corresponding to −20°C and +50°C.
The final simulations use the load combinations identified as 12 W/5 W at 70° and 80° and 14 W/5 W at 85°.

10.8.1 Result at 70°

The 70° case begins close to 258 K and warms during the first part of the cycle. The temperature reaches approximately 320–321 K and remains close to the upper part of the allowable range for a significant interval.
At the switching time, the change from wheel support to rod support produces a rapid local variation. A short dip followed by a recovery to approximately 286 K is visible before the long cold-phase decrease. This feature is consistent with the instantaneous exchange of contact boundary conditions and should therefore be interpreted partly as a switching transient of the simplified model.
The final temperature remains close to 258 K. The nominal case is therefore inside the adopted operating interval, with a small hot margin but a more comfortable cold margin.

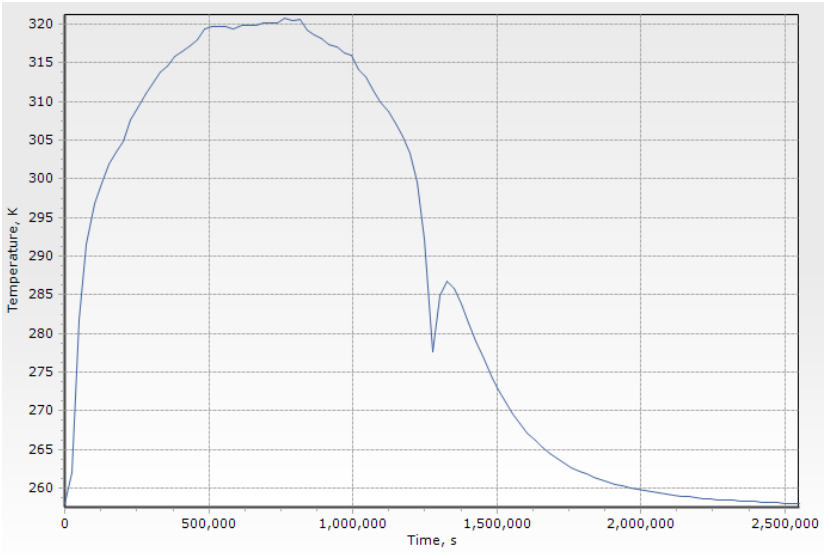


Figure 10.20: Internal temperature history at 70° latitude for the 12 W/5 W final wheel/support configuration.

10.8.2 Result at 80°

The 80° case starts near 258 K and reaches a maximum of approximately 318–319 K. The first half-cycle remains comparatively stable near the upper plateau.
After the switch to the rod-supported configuration, the temperature decreases smoothly and approaches approximately 256 K at the end of the simulation. The hot peak is lower than in the 70° case, while the final cold temperature is also slightly lower. The nominal curve remains within the selected temperature interval.

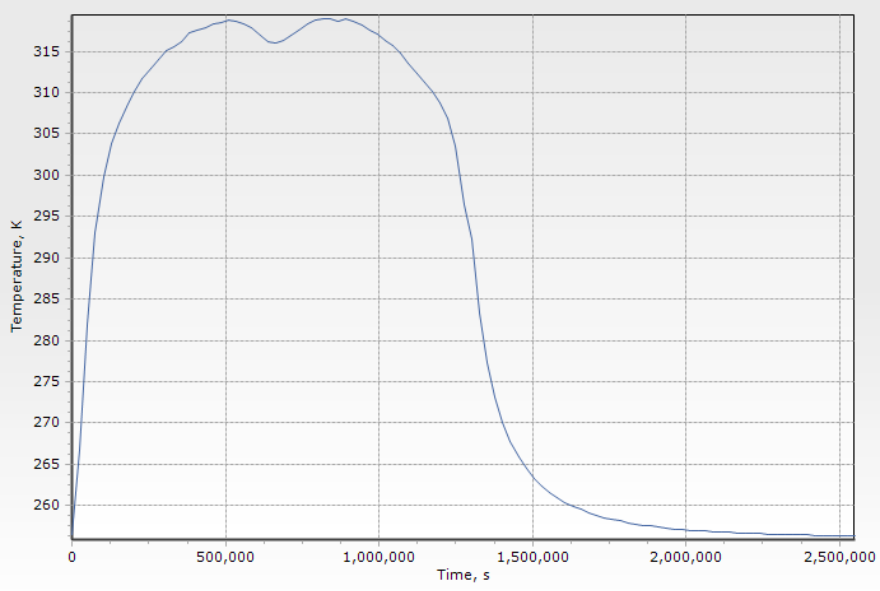


Figure 10.21: Internal temperature history at 80° latitude for the 12 W/5 W final wheel/support configuration.

10.8.3 Result at 85°

The 85° case uses the higher 14 W/5 W load combination. The temperature reaches approximately 321–322 K during the first half-cycle. After deployment of the support rods, it decreases rapidly and then continues to fall more gradually until it approaches approximately 254–255 K.
This is the most constrained of the three final cases. The hot peak is close to the upper allowable limit and the final cold temperature is only slightly above the lower limit. The nominal result remains acceptable, but the small margin makes this case particularly sensitive to uncertainties in internal power, surface properties, contact conductance, terrain temperature and model correlation.

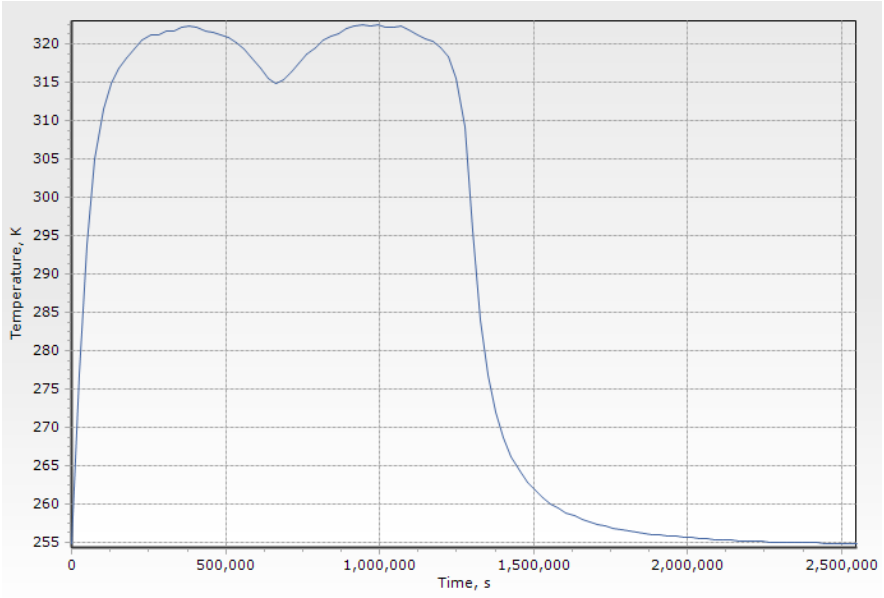


Figure 10.22: Internal temperature history at 85° latitude for the 14 W/5 W final wheel/support configuration.

10.8.4 Interpretation of the final cases

The three final simulations complete the design sequence that started from the hub–body sensitivity analysis. The original problem was the excessive thermal coupling between the cold external wheel/terrain system and the internal rover region. The sensitivity matrices showed that an equivalent isolation level of approximately 0.003 W/K was desirable. Rather than introducing a dedicated thermal switch at every hub, the final architecture keeps the fixed hub–body connection and removes the much stronger wheel–regolith conductive path during the cold phase.
The deployed Ti-6Al-4V supports introduce a terrain–rod–rover conductive path of only approximately 6.8×10^{-4} W/K for all four rods combined. In the nominal final simulations, this strategy is sufficient to maintain the internal temperature inside the adopted limits at 70°, 80° and 85°.
The result should therefore be interpreted as a combined thermo-structural design choice. The rods are not only mechanical supports and they are not only thermal insulators. Their geometry and material were selected to satisfy structural and mass

constraints while simultaneously providing the low-conductance support path required by the thermal analysis.

10.9 Model Limitations and Required Refinements

The present model is appropriate for a preliminary system-level analysis, but several simplifications must be retained when interpreting the results.

The wheel–ground contact used in the present model is an equivalent system-level representation. The selected value of $10\,000\ \mathrm{W\,m^{-2}\,K^{-1}}$ corresponds to approximately 23.56 W/K over the modelled contact sector and lies within the adopted 0.5–100 W/K reference range. Nevertheless, a more detailed model should make the contact conductance dependent on wheel load, sinkage, pressure, regolith compaction, roughness and temperature, and should distinguish the apparent geometrical sector from the smaller real microscopic contact area.

The deployment is represented by an instantaneous exchange of contact boundary conditions. A physical mechanism would require a finite deployment interval, during which both the wheel and rod paths could be partially active. A later transient model should therefore include a deployment sequence and smaller time steps around the transition.

The switch is imposed at one half of the simulated cycle. This is an operational modelling assumption rather than a universal day–night boundary for every high-latitude lunar site. The optimum deployment time should ultimately be linked to the actual illumination and ground-temperature history of the selected landing region.

The structural rod model uses homogeneous material properties and simplified boundary conditions. Local stresses in the deployment joints, locks, contact tips and rover attachments are not included. The analysis also neglects launch vibration, fatigue, accidental lateral loads and unequal load sharing between the supports.

The thermo-optical properties are fixed during each simulation. Lunar dust contamination and long-term degradation may change α and ε, and temperature-dependent material properties may modify the rod conductance.

Finally, the final temperature curves demonstrate the feasibility of the selected support concept but do not by themselves provide a full uncertainty margin. Hot- and cold-case optical-property variations, contact-conductance tolerances and heater-power margins should be included in a later design phase, especially for the 85° case.

10.10 Chapter Summary

This chapter presented the progressive development of the wheel and support thermal model, from the initial radiative-only representation to the final thermo-structural configuration. The initial radiative-only wheels were first replaced by a geometrically and conductively coupled wheel–hub–body model. This made it possible to quantify the effect of the wheel assembly on the temperature of the internal rover panel.

The central trade-off was performed by varying the hub–body conductance and evaluating the minimum internal-panel temperature. The comparison of 0.03, 0.01 and 0.003 W/K showed that decreasing this connection substantially reduces the cold-case

internal power required to remain above 253.15 K. The 0.003 W/K case was therefore retained as the reference isolation level for the subsequent design.

A thermal-switch-like hub–body profile was considered as the most direct means of reaching this conductance during the cold phase, but the final concept avoided the additional complexity of installing a dedicated variable-conductance device at each wheel. The hub–body mechanical connection was instead kept fixed at 0.02 W/K, while the external boundary condition was modified by lifting the rover from the regolith.

Four hollow support rods were then selected through a MATLAB thermo-structural analysis that simultaneously considered material properties, diameter, wall thickness, thermal conductance, mass, yield stress, Euler buckling and transverse displacement. The selected Ti-6Al-4V geometry has an external diameter of 4 mm, an internal diameter of 2 mm and a mass of approximately 0.0585 kg for four rods.

In the final Thermal Desktop implementation, the wheel–ground path is active only during the first half-cycle. Its area-normalised coefficient of $10\,000\ \mathrm{W\,m^{-2}\,K^{-1}}$ corresponds to approximately 23.56 W/K over the selected wheel contact sector, a value inside the adopted 0.5–100 W/K reference interval. During the cold phase, the wheels are lifted and the rover is supported by the titanium rods. The estimated total conductance of the four terrain–rod–rover paths is approximately 6.8×10^{-4} W/K, below the 0.003 W/K isolation benchmark derived from the sensitivity analysis.

The final simulations at 70°, 80° and 85° indicate that the resulting architecture can maintain the nominal internal temperature within the adopted 253.15–323.15 K interval. The 85° case remains the most critical because both hot and cold margins are small. Overall, the chapter shows how the wheel thermal analysis led directly to a combined thermal and structural support solution, linking the sensitivity study, the isolation requirement, the MATLAB sizing process and the final Thermal Desktop verification.

Chapter 11

Conclusions

"Per aspera ad astra."

— Latin proverb

11.1 Overall Conclusions

The objective of this thesis was to develop a consistent preliminary thermal-analysis framework and a first thermal-control architecture for a rechargeable lunar mini rover. The work was developed at system level: the aim was not to define a flight-qualified thermal-control system, but to identify the mechanisms and design parameters that most strongly determine the thermal behaviour of a compact rover on the lunar surface.
A first important result concerns the environment itself. The lunar surface cannot be treated simply as a fixed-temperature boundary. The regolith stores and releases heat, emits infrared radiation toward the rover and experiences a thermal response that changes strongly with latitude and illumination. The soil was therefore represented through a layered model, using an equatorial/mid-latitude description and a high-latitude representation with temperature-dependent thermo-physical properties and incidence-dependent absorbed solar fraction. The comparison with reference lunar trends was used as a consistency check of the predicted temperature level and latitude dependence before coupling the surface model to the rover.
The rover model was then developed progressively, starting from a simplified internal aluminium box with dimensions $0.40 \times 0.20 \times 0.20$ m. The initial simulations showed that the different faces of the rover are exposed to different radiative conditions. The lower region is strongly influenced by the lunar surface, the upper face has a more favourable view toward deep space, and the lateral faces depend on solar direction and latitude. An external MLI-like shell was therefore introduced to reduce uncontrolled exchange with the environment and to improve the thermal uniformity of the protected internal region.
The sensitivity analysis also demonstrated that insulation cannot be considered independently from internal power. A very low coupling to the external shell improves heat retention during cold conditions, but it can trap the heat generated by the equipment and produce overheating. Conversely, a stronger thermal coupling can improve heat rejection while making low-power and high-latitude cases more vulnerable to cold conditions. Internal dissipation is therefore not only an input to the thermal model but

also part of the thermal-control problem: the acceptable operating range depends on the combination of latitude, insulation and rover power mode.
The introduction of the radiator led to the same general conclusion. A top-face radiator with an area of approximately 0.08 m^2 provides a dedicated heat-rejection surface, but a fixed thermal connection cannot cover the complete set of analysed hot and cold conditions. With a weak link, the rover is protected against excessive heat loss but can become too hot; with a strong link, internal heat is rejected effectively but the radiator can become an important cold sink. The hot- and cold-case maps therefore indicated the need for a variable heat-rejection path. In the preliminary model this behaviour was represented through the equivalent action of a Loop Heat Pipe combined with a Thermal Control Valve, with a high-conductance state of approximately 0.12 W/K for heat rejection and a low-conductance state of approximately 0.012 W/K for heat conservation. The relevant result is not the detailed sizing of the LHP, which was outside the scope of the work, but the identification of variable conductance as a required system-level function.
The final part of the work extended the same design logic to the wheels and to the mechanical contact with the lunar surface. The wheels were initially radiative-only components, but the introduction of the hub, the body connection and the wheel–regolith contact showed that the mobility system can create an additional thermal path between the external environment and the protected rover body. A sensitivity analysis of the hub–body conductance was therefore carried out using the minimum internal-panel temperature as the principal cold-case indicator. The comparison of 0.03, 0.01 and 0.003 W/K showed that a conductance of the order of 0.003 W/K provides the level of isolation required to reduce the cold-case power demand significantly.
Rather than implementing a dedicated thermal switch at every wheel, the final concept retained a fixed hub–body connection and changed the mechanical support condition during the cold part of the design cycle. The active wheel–regolith contact was derived from the NASA Lunar Terrain Vehicle wheel thermal-sensitivity conductance range used in Chapter 10 and converted to the Thermal Desktop per-area input; the selected coefficient corresponds to a total conductance of approximately 23.56 W/K over the modelled contact sector. Four deployable hollow rods were then introduced to lift the wheels from the regolith and replace this path with a much weaker conductive route. A MATLAB trade-off selected Ti-6Al-4V hollow rods with 4 mm external and 2 mm internal diameter. For the four supports, the simplified terrain–rod–rover conductance is approximately 6.8×10^{-4} W/K, below the 0.003 W/K isolation benchmark.
The final high-latitude simulations at 70°, 80° and 85° showed that the complete preliminary strategy can maintain the nominal internal temperature inside the adopted system-level interval of 253.15–323.15 K for the analysed load combinations. This interval is a preliminary design envelope rather than the qualification range of a specific battery or electronic unit. The 85° case remains the most constrained because both hot and cold margins are small. These results demonstrate nominal feasibility, not qualification compliance.
The complete-lunar-cycle simulations and the half-cycle change between wheel and rod support are environmental design-envelope assumptions. They do not represent a continuous month-long rover mission. The nominal mission concept remains based on approximately three-hour sorties followed by return to the charging station; a future

operational model should map these shorter sorties onto the bounding environmental states identified by the longer parametric simulations.
Taken together, the main conclusion of the thesis is that the thermal control of a rechargeable lunar mini rover cannot be reduced to a single passive element or to a single worst-case temperature. The environment, regolith, insulation, internal power, radiator and wheel–ground interaction form one coupled problem. The most effective preliminary architecture therefore separates the different thermal functions: the MLI-like shell limits uncontrolled environmental coupling, the radiator provides intentional heat rejection through a variable thermal link, and the deployable supports reduce parasitic heat loss toward the regolith during the cold phase. The thermal solution is consequently linked directly to the rover operating mode and mechanical configuration.

11.2 Limitations and Future Development

The model developed in this thesis remains preliminary. The rover body is represented through a simplified geometry and the internal dissipation is mainly applied as an equivalent distributed load rather than through a complete component-level network. The MLI is represented by an equivalent shell and does not explicitly include seams, edges, penetrations, blanket compression or local degradation. Similarly, the Loop Heat Pipe is represented through its equivalent variable conductance rather than through a complete two-phase fluid model.
The wheel and support system also contains modelling assumptions. The selected wheel–regolith contact lies within the adopted NASA reference conductance range after conversion to the modelled contact area, but the real interface would still depend on wheel load, sinkage, soil compaction, roughness, temperature and microscopic contact area. Rod deployment is represented as an instantaneous exchange between wheel and support contact conditions. The structural verification uses simplified static loading and does not include deployment dynamics, joint stresses, launch vibration, impact, fatigue or unequal load distribution.
The next development step should move from the present system-level model toward a correlated component-level thermal network once the actual equipment is selected. Battery, avionics, communication hardware, sensors, motor drives and payload can then be introduced as separate nodes with realistic heat capacities, power profiles and allowable temperature ranges. Conductive paths through brackets, fasteners, harnesses, bearings and joints should be derived from the mechanical design, while the wheel–ground and rod–ground interfaces should be refined with load-, pressure-, temperature- and terrain-dependent contact models. Dust contamination and ageing should also be included in the thermo-optical uncertainty ranges.
The radiator and variable thermal link should also be refined. A more physical LHP/TCV representation, potentially using SINDA/FLUINT or FloCAD, would allow start-up behaviour, compensation-chamber dynamics, capillary limits and valve response to be evaluated. The final analysis should include hot- and cold-case property dispersions, conductance tolerances and heater-power margins rather than relying only on nominal curves.
Finally, the thermal model should be coupled to a realistic operational timeline. Departure from the charging station, traverse, payload operation, communication, return,

docking and recharge should be represented by different time-dependent power profiles and boundary conditions. Since the rover is rechargeable, the charging station itself can become part of the thermal-control architecture through shielding, conductive coupling or active conditioning. Including this interaction would make it possible to evaluate not only survival over an idealised lunar cycle, but the complete thermal feasibility of the intended operational concept.

Overall, the model provides a coherent basis for the next design phase and identifies the dominant thermal trade-offs and control functions. The central result is that insulation, variable heat rejection, internal power and ground-contact paths must be designed as one coupled thermal architecture rather than as independent subsystems.

Bibliography

[1] NASA, "Moon to mars architecture," NASA, 2026, accessed August 2026. [Online]. Available: https://www.nasa.gov/moontomarsarchitecture/

[2] ——, "Moon base systems," NASA, 2026, accessed August 2026. [Online]. Available: https://www.nasa.gov/moonbase-systems/

[3] European Cooperation for Space Standardization, "ECSS-E-ST-31C: Thermal Control General Requirements," European Cooperation for Space Standardization, Tech. Rep., 2008.

[4] D. G. Gilmore, Ed., *Spacecraft Thermal Control Handbook, Volume I: Fundamental Technologies*, 2nd ed. El Segundo, California and Reston, Virginia: The Aerospace Press and American Institute of Aeronautics and Astronautics, 2002.

[5] NASA, "Cooperative Autonomous Distributed Robotic Exploration (CADRE)," NASA Space Technology Mission Directorate, 2025, accessed August 2026. [Online]. Available: https://www.nasa.gov/cooperative-autonomous-distributed-robotic-exploration-cadre/

[6] Astrobotic, "Spacefarer & CubeRover Joint Lunar Rover Demonstration on Griffin-1," Astrobotic Press Release, Apr. 2024, image credit: Astrobotic/Mission Control; accessed September 2026.

[7] NASA, "Moon base development," NASA, 2026, accessed August 2026. [Online]. Available: https://www.nasa.gov/moonbase-phases/

[8] R. Greeley, "Lava tubes and channels in the lunar marius hills," *The Moon*, vol. 3, no. 3, pp. 289–314, 1971.

[9] NASA, "Marius hills pit — lava tube skylight?" NASA Science Photojournal, Lunar Reconnaissance Orbiter, 2010, PIA12954; page updated September 2025. [Online]. Available: https://science.nasa.gov/photojournal/marius-hills-pit-lava-tube-skylight/

[10] ——, "New views of lunar pits," NASA Science Photojournal, Lunar Reconnaissance Orbiter, 2010, PIA13518; LROC NAC image M126710873R; accessed September 2026.

[11] Silvercat, "Location of mare tranquillitatis," Wikimedia Commons, 2007, CC BY-SA; accessed September 2026.

[12] NASA, "Marius Hills (LROC-WAC Nearside Mosaic)," Wikimedia Commons; LROC-WAC global mosaic via JMARS, 2019, public domain; accessed September 2026.

[13] ——, "The harsh environment of the lunar south pole," NASA Moon Base, 2026, accessed August 2026. [Online]. Available: https://www.nasa.gov/reference/moonbase-environment/

[14] ——, "Shadows near the moon's south pole," NASA Science / Scientific Visualization Studio, 2021, accessed August 2026. [Online]. Available: https://science.nasa.gov/resource/shadows-near-the-moons-south-pole/

[15] ——, "The lunar south pole," NASA Science Photojournal, Lunar Reconnaissance Orbiter, 2010, PIA13523; LROC WAC mosaic; accessed September 2026.

[16] J. Meseguer, I. Pérez-Grande, and A. Sanz-Andrés, *Spacecraft Thermal Control*. Woodhead Publishing, 2012.

[17] NASA, "Dust-Repelling Coating for Thermal Radiators (KSC-TOPS-105)," NASA Technology Transfer Program, reference No. KSC-TOPS-105; Case No. KSC-14698; accessed September 2026. [Online]. Available: https://technology.nasa.gov/patent/KSC-TOPS-105

[18] European Space Agency, "Multi-layer insulation blankets," ESA Multimedia, Aug. 2016, image credit: ESA–G. Porter; ESA Standard Licence; accessed September 2026. [Online]. Available: https://www.esa.int/ESA_Multimedia/Images/2016/08/Multi-layer_insulation_blankets

[19] NASA, "State-of-the-art small spacecraft technology report," National Aeronautics and Space Administration, Tech. Rep., 2024, thermal Control chapter, Figure 7.4; image credit: Space Dynamics Laboratory (SDL); accessed September 2026. [Online]. Available: https://www.nasa.gov/wp-content/uploads/2025/02/soa-2024.pdf

[20] Redwire Space, "Q-Rad Deployable Radiator," Product Datasheet, Version 2, Jul. 2021, accessed September 2026. [Online]. Available: https://redwirespace.com/wp-content/uploads/2023/06/redwire-qrad-flysheet.pdf

[21] H. Peabody, "Thermal design for spaceflight," Spacecraft Thermal Engineering Course, NASA Goddard Space Flight Center, 2022, accessed March 2025.

[22] European Space Agency, "Rosetta thermal louvres," ESA Multimedia, Aug. 2015, image credit: ESA–A. Le Floc'h; ESA Standard Licence; accessed September 2026. [Online]. Available: https://www.esa.int/ESA_Multimedia/Images/2015/08/Rosetta_thermal_louvres

[23] NASA, "Passive PCB-Mounted Thermal Switch (MFS-TOPS-134)," NASA Technology Transfer Program, Marshall Space Flight Center, reference No. MFS-TOPS-134; Case No. MFS-34499-1; accessed September 2026. [Online]. Available: https://technology.nasa.gov/patent/MFS-TOPS-134

[24] W. E. Johnson, K. E. Daniel, K. A. Roberts, R. G. Schunk, and J. T. Farmer, "Hybrid Thermal Control System for Extreme Thermal Environments," in *52nd International Conference on Environmental Systems*, no. ICES-2023-338, Calgary, Canada, Jul. 2023.

[25] J. R. Wertz and W. J. Larson, Eds., *Space Mission Analysis and Design*, ser. Space Technology Library. Dordrecht, The Netherlands: Kluwer Academic Publishers, 1991, vol. 2.

[26] European Cooperation for Space Standardization, "ECSS-E-HB-31-03A: Thermal Analysis Handbook," European Cooperation for Space Standardization, Tech. Rep., 2016.

[27] American Bureau of Shipping, "Guidance notes on thermal analysis of vessels with tanks for liquefied gas," American Bureau of Shipping, Tech. Rep., 2019.

[28] J. R. Howell, M. P. Mengüç, K. Daun, and R. Siegel, *Thermal Radiation Heat Transfer*, 7th ed. CRC Press, 2020.

[29] T. Walker, S.-C. Xue, and G. W. Barton, "Numerical determination of radiative view factors using ray tracing," *Journal of Heat Transfer*, vol. 132, no. 7, p. 072702, 2010.

[30] R. R. McMurchy, R. G. Payne, and R. L. Dotts, "Thermal Network Modeling Handbook," TRW Systems Group, Tech. Rep. 14690-H003-R0-00, Jan. 1972, prepared for NASA under Contract NAS 9-10435; NASA CR-144418.

[31] H. Peabody, "Thermal Modeling and Analysis at GSFC," NASA Goddard Space Flight Center, Code 545, course material, 2022.

[32] G. Marraffa, "Thermal Analysis of 6U CubeSats," Master's thesis, Politecnico di Torino, 2019.

[33] Astrobotic, *Astrobotic Lunar Landers Payload User's Guide*, 2022. [Online]. Available: https://www.astrobotic.com/wp-content/uploads/2022/01/PUGLanders_011222.pdf

[34] P. Fortescue, G. Swinerd, and J. Stark, Eds., *Spacecraft Systems Engineering*, 4th ed. Chichester, UK: John Wiley & Sons, 2011.

[35] United Launch Alliance, *Atlas V Launch Services User's Guide*, 2010, revision 11.

[36] NASA, "HLS-UG-001 – Human Landing System Lunar Thermal Analysis Guidebook," National Aeronautics and Space Administration, Tech. Rep. HLS-UG-001, 2021. [Online]. Available: https://ntrs.nasa.gov/citations/20210010030

[37] D. A. Paige *et al.*, "The Lunar Reconnaissance Orbiter Diviner Lunar Radiometer Experiment," *Space Science Reviews*, vol. 150, pp. 125–160, 2010.

[38] NASA, "SLS-SPEC-159 – Cross-Program Design Specifications for Natural Environments (DSNE)," National Aeronautics and Space Administration, Tech. Rep. SLS-SPEC-159, 2020.

[39] T.-Y. Park, J.-J. Lee, J.-H. Kim, and H.-U. Oh, "Preliminary thermal design and analysis of lunar lander for night survival," *International Journal of Aerospace Engineering*, p. 4236396, 2018.

[40] A. Dollfus, J. E. Geake, and C. Titulaer, "Polarimetric properties of the lunar surface and its interpretation. part 3: Apollo 11 and apollo 12 lunar samples," in *Proceedings of the Lunar Science Conference 2*, 1971.

[41] S. L. Lawson and B. M. Jakosky, "Lunar surface thermophysical properties derived from Clementine LWIR and UVVIS images," *Journal of Geophysical Research: Planets*, vol. 106, 2001.

[42] M. Formisano, M. C. De Sanctis, S. Boazman, A. Frigeri, D. Heather, G. Magni, M. Teodori, S. De Angelis, and M. Ferrari, "Thermal modeling of the lunar south pole: Application to the PROSPECT landing site," *Planetary and Space Science*, vol. 251, p. 105969, 2024.

[43] J.-P. Williams, D. A. Paige, B. T. Greenhagen, and E. Sefton-Nash, "The global surface temperatures of the moon as measured by the Diviner lunar radiometer experiment," *Icarus*, vol. 283, pp. 300–325, 2017.

[44] A. Szerszen, "Thermal environment modeling practices for the descent trajectory of lunar landers," in *Thermal and Fluids Analysis Workshop (TFAWS)*, no. 20190030703. Newport News, Virginia, USA: NASA Marshall Space Flight Center, Aug. 2019. [Online]. Available: https://ntrs.nasa.gov/citations/20190030703

[45] J. I. Minow, W. C. Blackwell, Jr., V. N. Coffey, W. B. Cooke, J. W. Howard, L. N. Parker, J. Sharp, G. Schunck, R. W. Suggs, and J. W. Wang, "Environment challenges for exploration of the moon," NASA Technical Reports Server, Jan. 2008, conference paper; Document ID 20080013552; accessed September 2026. [Online]. Available: https://ntrs.nasa.gov/citations/20080013552

[46] E. Mazarico, G. A. Neumann, D. E. Smith, M. T. Zuber, and M. H. Torrence, "Illumination conditions of the lunar polar regions using LOLA topography," *Icarus*, vol. 211, pp. 1066–1081, 2011.

[47] J. Uri, "50 years ago: Nasa selects landing site for apollo 17," NASA Johnson Space Center, Feb. 2022, apollo 17 landing-site image with earlier Apollo landing sites shown for reference; accessed September 2026. [Online]. Available: https://www.nasa.gov/history/50-years-ago-nasa-selects-landing-site-for-apollo-17/

[48] NASA/JPL/USGS, "South pole region of the moon as seen by clementine," NASA Science Photojournal, Jun. 1996, PIA00001; Clementine UV/Visible Camera; orthographic mosaic of the lunar south polar region; accessed September

2026. [Online]. Available: https://science.nasa.gov/photojournal/south-pole-region-of-the-moon-as-seen-by-clementine/

[49] T. Horvath, P. O. Hayne, and D. A. Paige, "Thermal and illumination environments of lunar pits and caves: Models and observations from the Diviner Lunar Radiometer Experiment," *Geophysical Research Letters*, vol. 49, 2022.

[50] P. O. Hayne, J. L. Bandfield, M. A. Siegler, A. R. Vasavada, R. R. Ghent, J.-P. Williams, B. T. Greenhagen, O. Aharonson, C. M. Elder, P. G. Lucey, and D. A. Paige, "Global regolith thermophysical properties of the moon from the Diviner Lunar Radiometer Experiment," *Journal of Geophysical Research: Planets*, vol. 122, no. 12, pp. 2371–2400, 2017.

[51] J. Feng, M. A. Siegler, and P. O. Hayne, "New constraints on thermal and dielectric properties of lunar regolith from LRO Diviner and CE-2 microwave radiometer," *Journal of Geophysical Research: Planets*, vol. 125, no. 1, p. e2019JE006130, 2020.

[52] W. Birmingham, "Thermal Sensitivity Study of Lunar Terrain Vehicle Wheels," NASA Johnson Space Center, NASA Technical Reports Server White Paper 20240006096, May 2024. [Online]. Available: https://ntrs.nasa.gov/citations/20240006096